

DEVELOPMENT OF STANDARDIZATION STRATEGIES FOR REPRODUCIBLE
EXTRUSION-BASED 3D BIOPRINTING PROCESSES

Zur Erlangung des akademischen Grades einer
DOKTORIN DER INGENIEURWISSENSCHAFTEN (Dr.-Ing.)

von der KIT-Fakultät für Chemieingenieurwesen und Verfahrenstechnik des
Karlsruher Instituts für Technologie (KIT)
genehmigte

DISSERTATION

von
Svenja Strauß, M. Sc.
aus Speyer

Tag der mündlichen Prüfung: 08.02.2024

Erstgutachter: Prof. Dr. Jürgen Hubbuch
Zweitgutachter: Prof. Dr.-Ing. Christoph Klahn

Unless otherwise noted, this work is licensed under



Attribution-NonCommercial-NoDerivatives 4.0 International License (CC BY-NC-ND 4.0):
<https://creativecommons.org/licenses/by-nc-nd/4.0/deed.en>

*„Only if we understand can we care. Only if we care will we help.
Only if we help shall they be saved.“*

— JANE GOODALL

Acknowledgements

Während der Promotion gab es viele Personen, die mich unterstützt haben und stark zum Gelingen dieser Arbeit beigetragen haben.

Zuallererst möchte ich mich bei Prof. Dr. Jürgen Hubbuch bedanken für die Möglichkeit, am Institut für Molekulare Aufarbeitung von Bioprodukten (MAB) und Institut für Funktionelle Grenzflächen (IFG) die Doktorarbeit anzufertigen. Die stete Neugier und Begeisterung für neue Forschungsfragen sind einzigartig und ich habe gelernt, Problemstellungen auch aus einem anderen Blickwinkel zu betrachten. Das entgegengebrachte Vertrauen und die Freiheiten habe ich immer sehr geschätzt.

Vielen Dank an Prof. Dr. Matthias Franzreb mit seiner Abteilung für die Offenheit in der Arbeitsgruppe und für die Verfügungsstellung von den Laboren.

Ebenfalls möchte ich mich bei Prof. Dr.-Ing Klahn für das entgegengebrachte Interesse an meiner Arbeit und die Übernahmen des Koreferats bedanken.

Mein besonderer Dank gilt allen Kooperationspartnern Dr.-Ing. Lukas Wenger, David Grijalva, Dr.-Ing. Sarah Gretzinger und Dr.-Ing. Barbara Schmiege. Vielen Dank für die wertvollen Diskussionsrunden und zielgerichtete Zusammenarbeit, die auch immer Spaß bereitet hat.

Nicht zu vergessen sind meine Studenten Lena Enghauser, Rafaela Meutelet, Luka Radosevic, Bianca Schroth und Christian Lachmuth. In den jeweiligen Projekten trugen sie mit ihrem Einsatz im Labor, ihrem Intellekt in den Besprechungen und ihren Auswertungen maßgeblich zum Erfolg bei. Ein besonderer Dank gilt allen Kollegen am MAB. Vielen Dank für die hilfsbereite Atmosphäre, eine unvergessliche Konferenzzeit, ersehnte Kaffeepausen, einzigartige Seminarfahrten und die Schnabelhausparties. Auch die Unterstützung in der administrativen und IT-Infrastruktur war immer vorbildlich.

Natürlich möchte ich mich auch bei all meinen Freunden bedanken, die mir geholfen haben, in der Freizeit beim Sport, in Urlauben, bei Ausflügen oder gemeinsamen Filmabenden den Kopf freizubekommen.

Zuletzt möchte ich mich bei meiner Familie bedanken. Vielen Dank, dass ihr mich schon immer bedingungslos unterstützt.

Abstract

Additive manufacturing (AM) and three-dimensional (3D) printing are now well-established manufacturing methods in many areas of research and industry. One advantage is that complex or highly customized geometries can be produced from materials such as metals, ceramics and polymers. In addition to an already existing large variety of printable materials, bioinks are emerging. The number and diversity of bioinks are increasing continuously. Generally, a bioink consists of biological cells brought in a soft matrix. With regard to this, the so-called extrusion-based bioprinting (EBB) method is currently being of particular interest in research. Ultimately, artificially manufactured tissues are envisioned to be used as patient-specific implants or as models for pharmaceutical studies.

From a bioengineering point of view, the goal is to enable a safe, effective, and large-scale employment of 3D-printed tissues in customized human medical applications. This goal implies a series of technical challenges to be tackled. In order to achieve this, it requires the development of robust, reproducible, and automated processes covering the mixing, printing, and evaluation steps, where the evaluation comprises both geometry and cell viability analysis. Throughout the entire process, requirements for tissue sterility, biocompatibility and right geometrical accuracy pose major constraints with respect to a safe use of the implant or model. Moreover, a high viability of brought in cells as well as flexible tissue geometries are key drivers for effective medical treatments. This thesis characterizes feasible approaches and methodologies that offer solutions to the above named technical challenges. For this purpose, five specific studies were carried out and are presented in the following.

In the first study (Chapter 3), the general applicability of image analysis (IA) for geometry accuracy analysis is investigated. This includes an image capturing step that can be challenging for low contrast bioinks, followed by the image analysis that uses algorithms to extract the characteristics of interest. Image processing can be implemented as process analytical technology (PAT)-tool and offers multiple advantages. The method is objective, reproducible, non-invasive, and generates data suitable for long-time storage. The storage can be particularly challenging for high water content biomaterials of the printed object itself. As a starting point, this study focused on the analysis of a line consisting of one layer. Later on, all complex geometries can be broken down to simple structures and the integrity of that base is important to build up a complete object. As an image capturing step, cell confluency measurements of a plate reader were used and the images were subsequently analyzed by the line analysis tool with regard to the width, area as well as the length. After

having finished the tool development, limitations have been tested by screening several materials of varying transparencies. It was shown that image quality of complete transparent materials, such as Kolliphor, is not sufficient for the line analysis tool. In contrast, more opaque materials, such as the commercially available bioinks BiogelxTM-ink-RGD and Cellink[®] Bioink, are analyzable. In summary, for a wide range of biomaterials IA is a proper analysis method. With regard to the analysis of transparent materials, a suitable illumination setup is needed. Afterwards, the line analysis tool was used to determine shrinkage behavior of bioinks over a period of 10 min. The tool was able to characterize the changes and shrinkage was identified as a critical process parameter.

In the second study (Chapter 4), the increase of bioprinting process reproducibility by providing a constant flow rate was verified. Reproducible means producing the identical result under the same conditions. In general, automation increases process reproducibility. Hence, proper process parameters have to be monitored and controlled. It was assumed that a constant flow rate instead of the currently mostly constantly set printing parameters (extrusion pressure, printhead speed, distance to substrate) fosters reproducibility. Basic principle is that the network of all influencing parameters results in one flow rate. For a proof of concept, a liquid flow meter was incorporated into the bioprinter and two different processing modes (set pressure vs. set flow rate) were compared. Reproducibility was investigated by comparing volumes of printed cylinders for both approaches. In the set pressure mode, the same extrusion pressure was applied during all experiments and in the set flow rate approach, the flow sensor was used as calibration tool beforehand to adjust the pressure to the target flow rate. The set flow rate-based approach was proven to be more reliable in comparison to the set pressure mode. The set up with the flow meter could also be used to monitor the influence of the filling level in the cartridge on the flow rate. At the same time, the transferability of printing parameters between two devices was investigated. For this purpose, the flow sensor was incorporated in two different printing devices and monitored the flow rate while the cartridge was totally emptied after filling. It could be demonstrated that printing parameters cannot be directly transferred one-to-one, resulting in differing flow rates due to the system configuration properties. Another relevant conclusion was that the filling level in both tested bioprinters also effected the flow rate.

In the third study (Chapter 5), an automated pressure control for a constant flow rate generation was implemented in a pneumatically driven bioprinter. Hitherto, most extrusion-based printing processes are controlled pneumatically and are consequently not adaptable to disturbing factors caused by the printer system or by the ink. This is not sufficient with respect to process robustness and a later safe, medical production. From a process engineering point of view, the next logical step is to implement a closed loop control to adapt automatically the pressure to generate a set flow rate. As shown in the previous study, the flow rate changes during the course of a printing process and therefore it is advantageous to adjust the pressure based on real-time data rather than at the beginning of a printing process. A proportional-integral-derivative (PID) feedback loop was developed to process automatically the sensor data and to control the pressure adjustment in the printer software. To assess the applicability of the pressure control, three case studies were conducted using this setup: a) Continuous dispensing: Multiple runs of continuous dispensing proved an automated pressure adjustment to ensure a constant flow rate more consistently than in a constant pressure configuration. Even a nozzle clogging could be solved. b) Adaption to ink inhomogeneities: To simulate ink inhomogeneities, cylinders were printed out of a cartridge filled with layers of differently concentrated Kolliphor. During the transition to the next layer, the control was able to adjust the pressure so the cylinders could be printed intact. In contrast, the cylinders printed

in the constant pressure setup were not intact. c) Process transfer to other nozzle types: These experiments affirmed that the established control facilitates a process transfer without the need of time and cost consuming screenings which are simultaneously based on subjective impressions of an operator. Such a closed loop control demands for adapted flow meters specially developed for a wide range of different highly viscous materials with differing material characteristics. Another requirement is that the design is as small as possible so that it fits into the installation space of the bioprinter. In any case, they represent additional installation parts, which also increase the complexity of the system.

In the fourth study (Chapter 6), standardized methods were developed to compare bioink performance and the process effect on cell viability was investigated. Here, the extrusion pressure for a target flow rate was calculated based on the ink specific flow behavior and nozzle design. The standardization to one flow rate allows for a comparability between bioinks and accelerates development of new bioinks. This workflow was applied for two in-house produced bioinks based on alginate and gelatin, differing in 1%(w/v) alginate content. The polymeric solutions were extruded one time with and one time without cells at the same flow rate. Printing performance was assessed for all four formulations. For this purpose, the image acquisition setup was further developed in both, hardware and software. A fast image acquisition using a monochrome camera with proper illumination was possible and additional to the lines, circles as well as angles were automatically analyzed. Besides a high shape fidelity, cell viability is of great importance for the functionality of artificial tissues during and after the manufacturing process. One factor contributing to the cell viability of the whole bioprinting process is the preparation step of mixing the cells with the matrix material and the extrusion during the printing process. As a model system NIH 3T3 fibroblasts are distributed within the polymeric solutions and extruded. Flow cytometry as analysis method was conducted at several points of the process, namely after cell harvest, after the mixing step and after the extrusion process. Hereby, cells from the sample were stained using live/dead stains and analyzed via a flow cytometer allowing for an evaluation in a statistically meaningful number compared to individual microscope images. It was determined that a 1% (w/v) increase in alginate concentration resulted in little differing printing accuracy, but effected cell viability noticeably after both processing steps.

In the fifth study (Chapter 7), in a round robin test, it was investigated whether the current standards are sufficient to have a robust process and to reach comparable results. All previously performed experiments were carried out in one individual laboratory. However, meeting quality and safety standards at several locations is important and will be most likely demanded by regulatory agencies. Therefore, empirical data were gathered in the framework of a round robin test for extrusion-based bioprinting in twelve independent academic laboratories. Four different structures were printed with three bioinks and subsequently analyzed with IA. Beforehand, the workflow and design of this study were standardized as best as possible under current circumstances. This included among other, use of labware from same manufacturer, bioink material from same batches, and identical geometry models. Furthermore, standard operating procedures (SOPs) were written, e.g. the bioink preparation and the printing process including specified printing windows. A research data management system was specially created for central data exchange and storage which at the same time took over the function of an electronic laboratory notebook (ELN). The image acquisition was standardized by an imaging system which was specially developed in the course of this project by the Laboratory for MEMS Applications, Department of Microsystems Engineering of

the University of Freiburg (Freiburg, Germany) and Hahn-Schickard-Gesellschaft für Angewandte Forschung e.V. (Villingen-Schwenningen, Germany). It was adjusted for the imaging of hydrogels, since they often have little contrast. Afterwards, the entire collection of raw image data was screened in the course of a visual inspection in a qualitative analysis. Hereby, a closer look was taken to what extent deviations occurred and classified into categories which could be problematic with regard to automated image analysis. Found variations were offset position, orientation of structure, additional paths, non-continuous filaments, material excess, off focus, and weak contrast. Following this, the printed structures were analyzed in a quantitative assessment by three independent image analysis groups. All three groups achieved similar results. In conclusion, it can be said that under current standardization there is still a considerable potential for further development due to a lack of automation and standardization. The influences of the bioprinter equipment and individual operators are still significant. However, automated image processing was demonstrated as a suitable methodology, since the results of all three IA groups were comparable. This study revealed some challenges which still have to be overcome when taking the leap from research to medical applications. Besides, infrastructures for material and method distribution, data exchange and storage were established which are useful for future studies.

To put it all in a nutshell, in the present work IA has been verified as a feasible non-invasive method for automated printing performance evaluation. IA facilitates the comparison of newly developed bioinks, printing systems or process transfers. A constant flow rate was identified to be a key element for reliable and reproducible extrusion processes. It is not yet possible to print independent of location and person, but being aware of these identified parameters, countermeasures can be taken. This includes to advance automated and robust printer designs, the preparation of SOPs for bioprinting procedures and staff training.

Zusammenfassung

Die additive Fertigung (AM) und der dreidimensionale (3D-) Druck sind heute in vielen Bereichen der Forschung und Industrie etablierte Fertigungsverfahren. Ein großer Vorteil besteht darin, dass komplexe oder kundenspezifische Geometrien hergestellt werden können aus Materialien wie Metallen, Keramiken und Polymeren. Neben einer bereits bestehenden großen Vielfalt an druckbaren Materialien werden zunehmend auch sogenannte Biotinten entwickelt, deren Anzahl ständig zunimmt. Im Allgemeinen besteht eine Biotinte aus biologischen Zellen, die in eine weiche Matrix eingebracht werden. In diesem Zusammenhang ist das so genannte extrusionsbasierte Bioprinting (EBB) derzeit von besonderem Interesse für die Forschung. Letztlich sollen die künstlich hergestellten Gewebe als patientenspezifische Implantate oder als Modelle für pharmazeutische Studien eingesetzt werden.

Aus biotechnologischer Sicht besteht das Ziel darin, einen sicheren, effektiven und zuverlässigen großtechnischen Einsatz von 3D-gedruckten Geweben in personenspezifischen, humanmedizinischen Anwendungen zu ermöglichen. Dieses Ziel impliziert eine Reihe von technischen Herausforderungen. Um dies zu erreichen, müssen robuste, reproduzierbare und automatisierte Prozesse entwickelt werden, die die Schritte Mischen, Drucken und Auswerten umfassen. Hierbei umfasst die Auswertung zum einen die Geometrie und zum anderen die Analyse der Zellebensfähigkeit. Während des gesamten Prozesses stellen die Sterilität des Gewebes, die Biokompatibilität und die nötige geometrische Genauigkeit wichtige Herausforderungen für eine sichere Verwendung des Implantats oder des Modells dar. Darüber hinaus sind eine hohe Lebensfähigkeit der eingebrachten Zellen sowie flexible Gewebegeometrien Schlüsselfaktoren für effektive medizinische Behandlungen. In dieser Arbeit werden praktikable Ansätze und Methoden beschrieben, die Lösungen für die oben genannten technischen Herausforderungen bieten. Zu diesem Zweck wurden fünf spezifische Studien durchgeführt, die im Folgenden vorgestellt werden.

In der ersten Studie (Kapitel 3) wird die allgemeine Anwendbarkeit der Bildanalyse (IA) für die Analyse der Geometriegenauigkeit untersucht. Dazu gehört ein Schritt zur Bilderfassung, die bei optisch kontrastarmen Biotinten eine Herausforderung darstellen kann, gefolgt vom Schritt der Bildanalyse, bei der Algorithmen zur Extraktion der zu untersuchenden Merkmale eingesetzt werden. Die Bildverarbeitung kann als prozessanalytische Technologie (PAT) eingesetzt werden und bietet mehrere Vorteile. Die Methode ist objektiv, reproduzierbar, nicht invasiv und erzeugt Daten, die sich für eine Langzeitspeicherung eignen. Die Lagerung des gedruckten Objekts selbst aus Biomaterialien mit hohem Wassergehalt kann eine besondere Herausforderung darstellen. Als

Ausgangspunkt konzentrierte sich diese Studie auf die Analyse einer aus einer Schicht bestehenden Linie. Später können alle komplexen Geometrien auf einfache Strukturen heruntergebrochen werden, und die Integrität dieser Basis ist wichtig für den Aufbau eines vollständigen Objekts. Als Erfassungsschritt wurden Zellkonfluenzmessungen eines Mikrotiterplatten-Lesegerät verwendet und die Bilder anschließend mit dem Linienanalysetool hinsichtlich der Breite, Fläche sowie der Länge analysiert. Nachdem die Entwicklung des Tools abgeschlossen war, wurden die Detektionsgrenzen durch das Screening verschiedener Materialien mit unterschiedlicher Transparenz getestet. Es zeigte sich, dass die Bildqualität von vollständig transparentem Material, z.B. Kolliphor, für das Linienanalysetool nicht ausreichend ist. Im Gegensatz dazu können opake Materialien wie die kommerziell erhältlichen Biotinten BiogelxTM-ink-RGD und Cellink[®] Bioink analysiert werden. Zusammenfassend lässt sich sagen, dass IA für ein breites Spektrum von Biomaterialien eine geeignete Analysemethode darstellt. Für die Analyse von transparenten Materialien ist ein geeigneter Beleuchtungsaufbau erforderlich. Anschließend wurde das Linienanalysetool verwendet, um das Schrumpfungsverhalten von Biotinten über einen Zeitraum von 10 min zu bestimmen. Das Tool war in der Lage, die Veränderungen zu charakterisieren und die Schrumpfung wurde als kritischer Prozessparameter identifiziert.

In der zweiten Studie (Kapitel 4) wurde die Erhöhung der Reproduzierbarkeit des Bioprinting-Prozesses durch die Sicherstellung einer konstanten Durchflussrate überprüft. Reproduzierbar bedeutet, dass unter gleichen Bedingungen das gleiche Ergebnis erzielt wird. Im Allgemeinen erhöht Automatisierung die Reproduzierbarkeit eines Prozesses. Daher müssen die richtigen Prozessparameter überwacht und geregelt werden. Es wurde davon ausgegangen, dass eine konstante Durchflussrate anstelle der derzeit meist konstant eingestellten Druckparameter (Extrusionsdruck, Druckkopfgeschwindigkeit, Abstand zum Substrat) die Reproduzierbarkeit begünstigt. Grundprinzip ist, dass die Vernetzung aller Einflussparameter zu einer Durchflussrate führt. Für einen Proof of Concept wurde ein Flüssigkeitsdurchflussmesser in den Bioprinter eingebaut und zwei verschiedene Prozessführungsmodi (eingestellter Druck vs. eingestellte Durchflussrate) verglichen. Die Reproduzierbarkeit wurde untersucht, indem die Volumina der gedruckten Zylinder für beide Ansätze verglichen wurden. Im Modus des eingestellten Drucks wurde bei allen Versuchen derselbe Extrusionsdruck eingestellt, während beim Ansatz der eingestellten Durchflussrate der Durchflusssensor zuvor als Kalibrierungsinstrument verwendet wurde, um den Druck an die Zieldurchflussrate anzupassen. Der auf der eingestellten Durchflussrate basierende Ansatz erwies sich im Vergleich zum Modus des eingestellten Drucks als zuverlässiger. Die Einrichtung mit dem Durchflussmesser konnte auch genutzt werden, um den Einfluss des Füllstands in der Kartusche auf die Durchflussrate zu überwachen. Zugleich wurde die Übertragbarkeit von Druckparametern zwischen zwei Geräten untersucht. Dazu wurde der Durchflusssensor in zwei verschiedene Bioprinter eingebaut und die Durchflussmenge überwacht, während die Kartusche nach dem Befüllen vollständig entleert wurde. Es konnte gezeigt werden, dass die Druckparameter nicht direkt eins-zu-eins übertragen werden können, weil die jeweiligen Eigenschaften der Systemkonfiguration zu unterschiedlichen Durchflussraten führen. Eine weitere relevante Schlussfolgerung war, dass der Füllstand in beiden getesteten Bioprintern auch die Durchflussrate beeinflusst.

In der dritten Studie (Kapitel 5) wurde eine automatische Druckregelung zur Erzeugung einer konstanten Durchflussrate in einem pneumatisch betriebenen Bioprinter implementiert. Bisher werden die meisten extrusionsbasierten Druckverfahren pneumatisch gesteuert und sind somit empfindlich gegen Störfaktoren, die durch das Drucksystem oder die Tinte verursacht werden. Dies ist im Hinblick auf die Prozessrobustheit und eine spätere sichere, medizinische Produktion nicht

tolerierbar. Aus verfahrenstechnischer Sicht ist der nächste logische Schritt die Implementierung eines geschlossenen Regelkreises zur automatischen Anpassung des Drucks, um eine bestimmte Durchflussrate zu erzeugen. Wie in der vorangegangenen Studie gezeigt wurde, ändert sich die Durchflussmenge im Laufe eines Druckprozesses, weshalb es von Vorteil ist, den Druck auf der Grundlage von Echtzeitdaten und nicht zu Beginn eines Druckprozesses anzupassen. Es wurde eine proportional-integral-derivative (PID) Rückkopplungsschleife entwickelt, um die Sensordaten automatisch zu verarbeiten und die Druckeinstellung in der Druckersoftware zu steuern. Um die Anwendbarkeit der Druckregelung zu bewerten, wurden drei Fallstudien mit diesem Aufbau durchgeführt: a) Kontinuierliches Extrudieren: In mehreren Durchläufen mit kontinuierlicher Extrusion wurde bewiesen, dass eine automatische Druckanpassung eine konstante Durchflussrate besser gewährleistet als bei einer Konfiguration mit konstantem Druck. Selbst eine Düsenverstopfung konnte gelöst werden. b) Anpassung an Tinteninhomogenitäten: Um Tinteninhomogenitäten zu simulieren, wurden Zylinder aus einer Kartusche gedruckt, die mit Schichten unterschiedlich konzentrierten Kolliphors gefüllt war. Beim Übergang zur nächsten Schicht konnte die Steuerung den Druck so anpassen, dass die Zylinder unversehrt gedruckt werden konnten. Im Gegensatz dazu waren die bei konstantem Druck gedruckten Zylinder nicht intakt. c) Übertragung des Prozesses auf andere Düsentypen: Diese Versuche bestätigten, dass die etablierte Regelung eine Prozessübertragung ohne zeit- und kostenintensive Screenings, die gleichzeitig auf subjektiven Eindrücken eines Bedieners beruhen, ermöglicht. Eine solche Regelung erfordert angepasste Durchflussmessgeräte, die speziell für ein breites Spektrum verschiedener hochviskoser Materialien mit unterschiedlichen Materialeigenschaften entwickelt wurden. Eine weitere Anforderung ist eine möglichst kleine Bauform, damit sie in den Bauraum des Bioprinters passen. In jedem Fall stellen sie zusätzliche Einbauteile dar, die auch die Komplexität des Systems erhöhen.

In der vierten Studie (Kapitel 6) wurden standardisierte Methoden zum Vergleich der Biotinteneigenschaften entwickelt und der Prozesseffekt auf die Zellviabilität untersucht. Hier wurde der Extrusionsdruck für eine Zieldurchflussrate auf der Grundlage des spezifischen Fließverhaltens der Tinte und des Düsendesigns berechnet. Die Standardisierung auf eine Durchflussrate ermöglicht eine Vergleichbarkeit zwischen Biotinten und beschleunigt die Entwicklung neuer Biotinten. Dieser Arbeitsablauf wurde für zwei selbst hergestellte Biotinten auf der Basis von Alginat und Gelatine angewandt, die sich durch einen Alginatgehalt von 1% (w/v) unterscheiden. Die Polymerlösungen wurden einmal mit und einmal ohne Zellen bei gleicher Fließgeschwindigkeit extrudiert. Die Druckgenauigkeit wurde für alle vier Formulierungen bewertet. Zu diesem Zweck wurde die Bildaufnahmeeinrichtung sowohl in Bezug auf die Hardware als auch auf die Software weiterentwickelt. Eine schnelle Bildaufnahme mit einer Monochrom-Kamera bei geeigneter Beleuchtung war möglich und zusätzlich zu den Linien wurden Kreise und Winkel automatisch analysiert. Neben einer hohen Formtreue ist die Lebensfähigkeit der Zellen während und nach dem Herstellungsprozess von großer Bedeutung für die Funktionalität des künstlichen Gewebes. Ein Faktor, der die Lebensfähigkeit der Zellen beeinflusst, ist der Vorbereitungsschritt des Mischens der Zellen mit dem Matrixmaterial und die Extrusion während des Druckprozesses. Als Modellsystem werden NIH 3T3 Fibroblasten in den Polymerlösungen verteilt und extrudiert. Die Durchflusszytometrie als Analysemethode wurde an mehreren Stellen des Prozesses durchgeführt, nämlich nach der Zellernte, nach dem Mischschritt und nach dem Extrusionsprozess. Dabei wurden Zellen aus der Probe mit einem Lebend-/Tot-Farbstoff angefärbt und mit einem Durchflusszytometer analysiert, was eine statistisch aussagekräftige Auswertung im Vergleich zu einzelnen Mikroskopbildern ermöglichte. Es wurde festgestellt, dass eine Erhöhung der Alginatkonzentration um 1% (w/v) nur geringe Unterschiede in der Druckgenauigkeit

zur Folge hatte, aber die Lebensfähigkeit der Zellen nach beiden Verarbeitungsschritten merklich beeinflusste.

In der fünften Studie (Kapitel 7) wurde ein Ringversuch durchgeführt zur Untersuchung, ob die derzeitigen Standards ausreichen, um ein robustes Verfahren und vergleichbare Ergebnisse zu erhalten. Alle bisher durchgeführten Versuche wurden in einem einzigen Labor durchgeführt. Die Einhaltung von Qualitäts- und Sicherheitsstandards an mehreren Standorten ist jedoch wichtig und wird höchstwahrscheinlich von den Aufsichtsbehörden gefordert werden. Daher wurden im Rahmen eines Ringversuchs zum extrusionsbasierten Bioprinting empirische Daten in zwölf unabhängigen, akademischen Laboren gesammelt. Vier verschiedene Strukturen wurden jeweils mit drei Biotinten gedruckt und anschließend mit IA analysiert. Im Vorfeld wurden der Arbeitsablauf und das Design dieser Studie so gut wie unter den gegebenen Umständen möglich standardisiert. Dazu gehörten unter anderem die Verwendung von Laborgeräten desselben Herstellers, Biotintenmaterialien aus denselben Chargen und Modelle mit identischer Geometrie. Darüber hinaus wurden Standardarbeitsanweisungen (SOPs) verfasst, z.B. für die Herstellung der Biotinten und den Druckprozess durch die Festlegung bestimmter Fenster für einzelne Druckparameter. Speziell für den zentralen Datenaustausch und die Datenspeicherung wurde ein Forschungsdatenmanagementsystem geschaffen, das auch die Funktion eines elektronischen Laborjournals (ELN) übernahm. Die Bildaufnahme wurde durch ein Bildgebungssystem standardisiert, das im Rahmen dieses Projekts vom Labor für MEMS-Anwendungen, Abteilung Mikrosystemtechnik der Universität Freiburg (Freiburg, Deutschland) und der Hahn-Schickard-Gesellschaft für Angewandte Forschung e.V. (Villingen-Schwenningen, Deutschland) speziell entwickelt wurde. Es wurde für die Abbildung von Hydrogelen angepasst, da diese oft wenig Kontrast aufweisen. Anschließend wurde die gesamte Sammlung von Rohbilddaten im Rahmen einer visuellen Inspektion in einer qualitativen Analyse beurteilt. Dabei wurde genauer betrachtet, inwieweit Abweichungen auftraten und diese in Kategorien eingeteilt, die im Hinblick auf eine automatisierte Bildauswertung problematisch sein könnten. Gefundene Abweichungen waren Offset-Position, in der Ausrichtung der Struktur, zusätzliche Pfade, nicht durchgängige Filamente, Materialüberschuss, außerhalb der Fokusebene und schwacher Kontrast. Anschließend wurden die gedruckten Strukturen in einer quantitativen Bewertung von drei unabhängigen Bildanalysegruppen analysiert. Alle drei Gruppen erzielten ähnliche Ergebnisse. Zusammenfassend lässt sich sagen, dass bei der derzeitigen Standardisierung aufgrund der fehlenden Automatisierung und Standardisierung noch ein erhebliches Entwicklungspotenzial vorhanden ist. Die Einflüsse der Bioprintergeräte und der einzelnen Bediener sind immer noch erheblich. Die automatisierte Bildverarbeitung hat sich jedoch als geeignete Methode erwiesen, da die Ergebnisse aller drei IA-Gruppen vergleichbar waren. Diese Studie zeigte einige Herausforderungen auf, die beim Sprung von der Forschung zur medizinischen Anwendung noch zu bewältigen sind. Außerdem wurden Infrastrukturen für die Material- und Methodenverteilung, den Datenaustausch und die Speicherung geschaffen, die für künftige Studien nützlich sind.

Zusammenfassend lässt sich sagen, dass sich die IA in der vorliegenden Arbeit als praktikable, nicht-invasive Methode zur automatisierten Bewertung der Druckleistung erwiesen hat. IA erleichtert den Vergleich von neu entwickelten Biotinten, Drucksystemen oder Prozesstransfers. Es wurde festgestellt, dass eine konstante Durchflussrate ein Schlüsselement für zuverlässige und reproduzierbare Extrusionsprozesse ist. Es ist noch nicht möglich, orts- und personenunabhängig zu drucken, aber wissend, welche identifizierten Quellen für Abweichungen vorhanden sind, können Gegenmaßnahmen

ergriffen werden. Dazu gehören die Weiterentwicklung von automatisierten und robusten Druckern, die Erstellung von SOPs für Bioprinting-Verfahren und die Schulung von Mitarbeitern.

Contents

Acknowledgements	iii
Abstract	v
Zusammenfassung	ix
Contents	xv
1 Introduction	1
1.1 Additive manufacturing and 3D printing	2
1.2 Bioprinting	4
1.2.1 Hydrogels and bioinks	6
1.2.2 Analytics	8
2 Thesis outline	19
2.1 Research proposal	19
2.2 Manuscript overview	22
3 Image Analysis as PAT-Tool for Use in Extrusion-Based Bioprinting	33
Svenja Strauß, Rafaela Meutelet, Luka Radosevis, Sarah Gretzinger, and Jürgen Hubbuch	
3.1 Abstract	34
3.2 Introduction	34
3.3 Materials and Methods	35
3.3.1 Bioprint substances and bioink preparation	35
3.3.2 Bioprinting process	36
3.3.3 Image processing	36
3.3.4 Shrinkage study	38
3.3.5 Data analysis and statistical analysis	39
3.4 Results	39
3.4.1 Line analysis tool	39
3.4.2 Shrinkage study	40
3.5 Discussion	45
	xv

3.6	Conclusion	47
4	Evaluation of the Reproducibility and Robustness of Extrusion-based Bioprinting Processes applying a Flow Sensor	51
	Svenja Strauß, Bianca Schroth, and Jürgen Hubbuch	
4.1	Introduction	52
4.2	Materials and methods	54
4.2.1	Ink preparation and printing systems	55
4.2.2	Density calibration	55
4.2.3	SLI liquid flow meter	55
4.2.4	Investigation of cartridge filling level influence	58
4.2.5	Reproducibility experiments	58
4.2.6	Data analysis	60
4.3	Results	60
4.3.1	Sensor calibration	60
4.3.2	Printing accuracy	60
4.3.3	Influence of cartridge filling level	61
4.3.4	Reproducibility experiments	65
4.4	Discussion	70
4.5	Conclusion	71
5	Automated and Dynamic Extrusion Pressure Adjustment Based on Real-Time Flow Rate Measurements for Precise Ink Dispensing in 3D Bioprinting	75
	Lukas Wenger, Svenja Strauß and Jürgen Hubbuch	
5.1	Introduction	76
5.2	Materials and methods	79
5.2.1	Ink preparation	79
5.2.2	Rheology	80
5.2.3	Adaptive PID pressure control: hardware and software setup	80
5.2.4	Application of the adaptive pressure control	85
5.3	Results and discussion	86
5.3.1	Implementation of the experimental setup	86
5.3.2	Rheology	87
5.3.3	Application of the adaptive pressure control	87
5.3.4	Potential challenges of working with complex cell-laden bioinks	95
5.3.5	Implications for process development, monitoring and control	96
5.4	Conclusion	96
6	Analytics in Extrusion-Based Bioprinting: Standardized Methods improving Quantification and Comparability of the Performance of Bioinks	103
	Svenja Strauß, David Grijalva Garces and Jürgen Hubbuch	
6.1	Introduction	104
6.2	Materials and methods	105
6.2.1	Cell culture	105
6.2.2	Biomaterial ink and bioink preparation	106

6.2.3	Rheological characterization	106
6.2.4	Printing performance evaluation	107
6.2.5	Data handling and statistical analysis	111
6.3	Results and discussion	112
6.3.1	Rheological characterization	112
6.3.2	Printing performance	113
6.4	Conclusion	120
7	On the Reproducibility of extrusion-based Bioprinting: Round Robin Study on Standardization in the Field	125
	Svenja Strauß, David Grijalva Garces and Jürgen Hubbuch	
7.1	Introduction	127
7.2	Materials and methods	129
7.2.1	Round robin workflow and design	129
7.2.2	Biomaterials, labware, and geometries	130
7.2.3	Round robin - 3D printing	131
7.2.4	Central data exchange and storage	134
7.2.5	Round robin - Image analysis	134
7.2.6	Data handling and visualization	137
7.3	Results and discussion	137
7.3.1	Round robin - 3D printing	137
7.3.2	Round robin - Image analysis: qualitative	137
7.3.3	Round robin - Image analysis: quantitative	140
7.3.4	Assessment of the reproducibility in 3D bioprinting	142
7.4	Conclusion	148
8	Conclusion	153
9	Outlook	157
	References	159
	List of Figures	177
	List of Tables	179
	Appendices	184
C	Image Analysis as PAT-Tool for Use in Extrusion-Based Bioprinting	185
	Svenja Strauß, Rafaela Meutelet, Luka Radosevis, Sarah Gretzinger, and Jürgen Hubbuch	
C.1	186
D	Evaluation of the Reproducibility and Robustness of Extrusion-based Bioprinting Processes applying a Flow Sensor	189
	Svenja Strauß, Bianca Schroth, and Jürgen Hubbuch	
D.1	Density calibration curves	190

D.2	Flow sensor calibration curves	190
E	Automated and Dynamic Extrusion Pressure Adjustment Based on Real-Time Flow Rate Measurements for Precise Ink Dispensing in 3D Bioprinting	195
E.1	Sensor calibration curves	196
E.2	Experimental setup	197
E.3	Continuous dispensing P25	198
E.4	Continuous dispensing A2L7	199
G	On the Reproducibility of extrusion-based Bioprinting: Round Robin Study on Standardization in the Field	201
	Svenja Strauß, David Grijalva Garces and Jürgen Hubbuch	
G.1	CAD models used during the Round robin - 3D printing test	203
G.2	Schematic draft of line and circle width	203
G.3	Exemplary raw images	204

Introduction

A considerable trend in the biopharmaceutical industry is towards personalized regenerative medicine (RM), a curative approach in which diseased tissue is to be healed or replaced. In particular, gene therapy and cell therapy are highly regarded for the new possibilities they offer [1, 2]. Advancing from suspension cell infusions to solid tissues, 3D bioprinting is a suitable manufacturing technique to fabricate personalized tissues. For this purpose, artificial tissues are designed patient-specific in advance and then manufactured in the laboratory [3]. Artificial tissues cannot only be employed as implants, but also as testing systems for the effectiveness of drug candidates, as drug delivery systems and for organ-on-chip applications [4–6]. It is currently possible to print relatively simple tissue structures such as skin, cartilage, muscle, parts of the liver and parts of the kidney. A current obstacle is still the incorporation of vascularized structures in order to guarantee the supply of complex organs [7, 8]. Manufacturing requires expertise from various disciplines, such as cell biology, materials science and process engineering. The structures are built by depositing layers of bioink, a soft material that contains cells. This scaffold material functions as structure which is needed to get into the third dimension [9]. In most cases, the supporting structure consists of a hydrogel offering mild conditions and mimicking the extracellular matrix (ECM). Finding suitable hydrogel formulations remains one of the greatest challenges, as they must be application-specific, cell compatible, dimensionally stable, and ideally crosslinkable after printing [10, 11]. Great successes have already been achieved by individual research groups. However, in order for these to be translated into medical applications, standardized production methods including quality control are required. Results become comparable and process development is accelerated with a higher degree of standardization and associated automation. With regard to a safe use in multiple locations independent of the operator, robust and reproducible processes play an important role [12, 13]. In this work, the focus lies on extrusion-based bioprinting operating with a pneumatic extrusion system. Here, the success consists of the interplay of cell-loaded bioink, printing process and printer equipment. This already starts by choosing the printer system with optional equipment, such as temperature control or coordination calibration, and is followed by the material properties

particularly by the rheological behavior of the bioink [14]. The viscosity as a part of rheology again is particularly influenced by temperature, polymer concentration, pH, ionic strength, UV radiation for UV-responsive polymers, and environmental pressure [15]. It becomes obvious that there is a large network of parameters which cannot always be considered individually, as they strongly influence each other. It is common practice to use laborious parameter screenings to determine printing parameters that are based on a person's individual impressions. Since all influences ultimately result in a flow rate, a much more general approach would be to implement a constant flow rate that also allows for objective description and process transfers. A robust and reliable process is a prerequisite for regulatory approval, and implementing Process Analytical Technology (PAT) is an appropriate strategy. However, as the products of the bioprinting process are solids, typical process analytical technologies like spectroscopy do not work. Image analysis is a promising evaluation procedure, as vision systems are already established in other complex fields, such as for pick and place tasks and as automated agricultural support systems [16, 17]. Image Analysis (IA) affords the advantages of being a fast and non-invasive methodology, being predestined for automation, being able of evaluating real-time data, and the data are long time storable. The aim of this thesis is to investigate, how far standardization in bioprinting has progressed and can be improved so that material characterization and process development can be accelerated by increased comparability. In the following sections theoretical fundamentals of additive manufacturing processes, materials and analytical methods are explained.

1.1 Additive manufacturing and 3D printing

Additive manufacturing (AM), also often referred to as 3D printing, is defined as "a process of joining materials to make objects from 3D model data, usually layer upon layer, as opposed to subtractive manufacturing methodologies" [18]. Various materials can be used, primarily polymers, metals, ceramics and composites [19]. The main objective is the generation of a three-dimensional structure based on a previously created virtual model. The general workflow includes multiple steps. At first, the virtual model has to be created either by 3D scanning of physical objects or by designing a 3D model via computer aided design (CAD). Depending on the method and model, it might be necessary to implement support structures. This data can be exported to different formats, such as STL (standard triangle language as well as standard tessellation language) files in which the object surface is approximated by triangles. In the next step, the model is exported in a machine-specific software in which the object scale, positioning, and printing parameters are defined. The model is then sliced to allow a layer-by-layer construction and exported in a machine-specific file format. For extrusion processes this is often G-code. The Additive Manufacturing File Format (AMF) depends on the AM process, as some processes also require control of mirrors and exposure, for example [20, 21]. After the manufacturing process, a post-processing step is most of the time needed, e.g. to modify the surface or to remove the supporting structures [18]. The original application of this technology was for rapid prototyping to build and analyze newly developed models. 3D printing offers a high degree of flexibility and can be adapted relatively easily for further developments. Especially for polymers, it is still often used for rapid prototyping. According to that, 3D printing is profitable when small customized batches are to be produced as the design can be modified quickly. In the interest of environment and sustainability, it is attractive that new geometries can be produced with reduced material waste in contrast to traditional subtractive methods. Furthermore, a more local production with short supply chains is possible and the product life can be extended

due to possible repairs and a close relationship between manufacturer and consumer [18, 21–23]. AM is widely employed in the production of light-weight structures in the aerospace or automotive industry [24–26]. Other application fields include biomedical engineering and consumer products [27, 28]. Unlike subtractive methods, which mainly use solids, AM can use liquids, powders and solids as starting materials for varying production techniques. One of the best-known methods is Material Extrusion (MEX), which also includes Fused Deposition Modeling (FDM), which is actually a brand name [29, 30]. Here, a thermoplastic filament is melted, extruded through a nozzle and solidifies after cooling. This method is popular for professionals, but also for do-it-yourselfers at home [31]. Other methodologies based on liquids are stereolithography (SLA) and polyjetting [32]. Vat photopolymerization (VPP) is an AM category consisting of all processes during which a liquid resin is cured in a resin bath via light-activated photopolymerization. Stereolithography is an exemplary process and was the first to be patented and commercialized. In this setup, coherent light sources such as lasers are used to start polymerization in a plane on the surface. Afterwards, the platform is moved in z-direction and the next layer can be added. This method allows for a spatial high-resolution [33]. Digital light processing (DLP) is closely related to SLA, but uses selectively masked light sources and exposes the entire plane to the light source to speed up the manufacturing process. An optimized version of this method is continuous liquid interface production (CLIP). Here an oxygen permeable film is close to the light source inhibiting the photopolymerization which makes an intermediate step to apply a new layer of resin redundant [28]. Material jetting (MJT) consists of an inkjet printer which deposits photopolymer droplets to build up the model. The results have a high resolution and several colours can be printed. However, the mechanical stability is lower in comparison to SLA [32]. A solid based AM manufacturing process and simultaneously making use of AM and subtractive methods is laminated object manufacturing (LOM). Thin sheets of material are stacked together and represent a relatively cheap and fast possibility for the production of large parts. The products can then be cut afterwards. Materials such as paper, metal sheets, composite sheets, ceramic tapes, and thermoplastic sheets can be processed [31]. The next class includes powders as raw materials which are either melted (Powder Bed Fusion (PBF)) or bound applying a liquid binder (Binder Jetting (BJT)) [30, 32]. When focused thermal energy is used to combine materials during deposition by melting, this is referred to as directed energy deposition (DED). Often, a laser is used to successively melt powder with spatial control and unaffected powder is preserved and supports the next layer so that overhangs can be printed [30, 33]. If the starting powder consists of a polymer, it is referred to as Selective Laser Sintering (SLS) and for metallic powders as Selective Laser Melting (SLM). Besides, oxidation must be prevented and therefore the process is executed in an inert gas atmosphere [30, 32, 34]. Similar to that, an electron laser can be used for melting of powder in electron beam melting (EBM). This process uses a high voltage laser beam and is intended to be used in outer space due to the fact that a vacuum chamber is needed. In binder jetting, a liquid binder is jetted in specific patterns and glues the powder together. Here again, no support structures are needed as the object is self-supporting in the powder bath. A wide range of materials can be used such as metals, polymers, ceramics and composites. The objects have a weak mechanical property and in order to increase density infiltration materials are used. In a post-processing step, the objects are sintered or heat-treated [21, 35].

1.2 Bioprinting

With the advancements in available additive manufacturing methods, 3D printing has entered the medical and biotechnological field. 3D printed models are used for surgery plannings, to train staff, to develop customized laboratory equipment, and to print chromatography column beds, to name but a few [36–40]. Research is also pursued for including bioactive molecules or cells. This research area is referred to as bioprinting and poses new challenges regarding material selection as well as manufacturing methods [41, 42]. To date, there is no official definition of bioprinting yet. A first definition for organ printing was published in 2003 by Mironov as "a rapid prototyping computer-aided 3D printing technology, based on using layer by layer deposition of cell and/or cell aggregates into a 3D gel with sequential maturation of the printed construct into perfused and vascularized living tissue or organs" [43]. In 2010 bioprinting was defined by Guillemot as "the use of computer-aided transfer processes for patterning and assembling living and non-living materials with a prescribed 2D or 3D organization in order to produce bio-engineered structures serving in regenerative medicine (RM), pharmacokinetic and basic cell biology studies" [44]. Bioprinting is understood as integral part of biofabrication which is defined as "the automated generation of biologically functional products with structural organization from living cells, bioactive molecules, biomaterials, cell aggregates such as micro-tissues, or hybrid cell-material constructs, through Bioprinting or Bioassembly and subsequent tissue maturation processes" [42]. Biofabrication is again part of the larger tissue engineering (TE) field which is defined as "an interdisciplinary field that applies the principles of engineering and life sciences towards the development of biological substitutes that restore, maintain, or improve biological tissue function or a whole organ" [45]. What is certain is that the preservation of sensitive biological activity is paramount and that mild production conditions are essential. This includes the selection of biocompatible materials and the use of no harsh manufacturing techniques. New materials have to be developed with regard to mimic the structure of native tissue. Hydrogels are often used as support material for this purpose [46]. A more detailed description of materials is given in Section 1.2.1. During printing, the required chemical and physical parameters must be selected in such a way that bioactivity is not restricted. For example, occurring temperature, shear stresses, and crosslinking conditions of the hydrogel must be taken into account. Finding the right combination for ensuring both, shape fidelity and cytocompatibility, was described by Malda et al. as the 'biofabrication window' [3]. Thus, three manufacturing techniques are prominent and are briefly described in the following. They are shown in Figure 1.1.

The first technique is the laser-induced forward transfer (LIFT) which was originally developed for metals and is not as common as the other two methods [9, 47]. The design includes a donor slide typically made from glass which is covered with an energy absorbing layer, usually made from gold or titanium. Above, there is a layer of suspended cells or biological material and this layer again is covered with an energy absorbing layer collector slide. Using a focusing system, a laser pulse is directed to the absorbing layer causing there a local evaporation and the cells are propelled by a high pressure toward the collector substrate. Consequently, the cells can be positioned relatively accurately in small 3D objects [3]. With this method very high resolutions within micron range are possible and the process is nozzle free. This means hat the possibility of nozzle clogging does not exist. However, the method has several limitations: a low speed and thus the method requires rapid gelation kinetics of hydrogels, metal residues may be present in the final product and the time consuming preparation [9].

The next category are inkjet printers which are also known as drop-on-demand. Here, droplets of

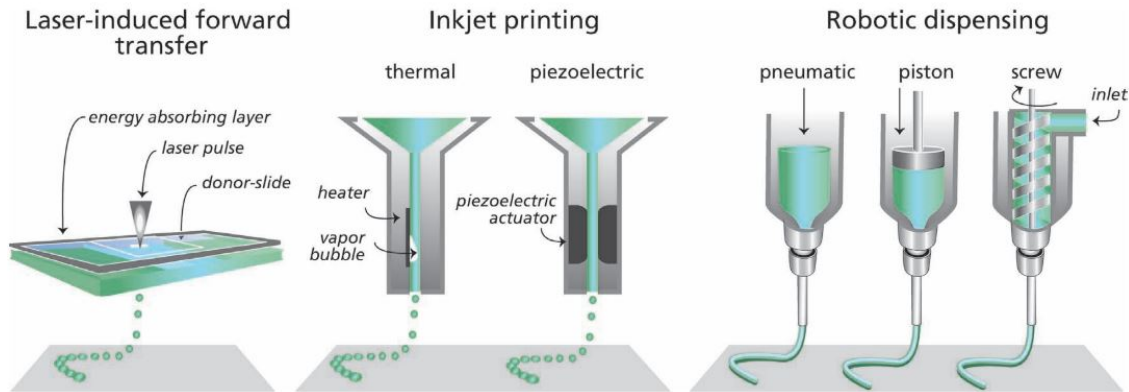


Figure 1.1 Different manufacturing techniques in bioprinting. Laser-induced forward transfer, inkjet printing and robotic dispensing are employed to deposit bioinks on substrate with spatial control. Illustration is taken from Malda et al. [3].

defined volumes are formed and deposited in control on the substrate. These droplets are generated by acoustic waves caused thermally by short heat pulses or by piezoelectric crystals. Materials can be printed with viscosities in the range from 3.5 to 12 mPa/s with a resolution from 10 to 50 μm . Under this method cell viability is with $>85\%$ high, whereas cell densities with $<10^6$ cells/mL are relatively low [9]. The gelation mechanism can be photopolymerization or chemical crosslinking. Concentration gradients can be introduced by changing the droplet size during printing process. Advantageous is that the process is nozzle-free and multiple printheads can be applied for multiple cell types [47]. As the channels and orifices dimensions are in the same range as cell sizes, there are challenges in maintaining a high cell viability causing that this approach has so far not yielded much success [3].

Robotic dispensing or extrusion-based bioprinting (EBB) is probably the most common used method. The underlying principle is the extrusion of a continuous filament of high viscosity material through a nozzle and to deposit it on the substrate with spatial control. The extrusion can be realized pneumatically or mechanically which again can be divided into piston or screw driven extrusion. Piston driven extruders are relatively simple systems with less components which is beneficial with regard to sterility. Moreover, the introduced shear stress on cells is lower in comparison to a screw-driven extrusion [48]. The extrusion rate is not only dependent on the applied pressure, but also on material properties such as rheological behavior or homogeneity. The rheological properties, in turn, depend strongly on the temperature and shear stress, which makes the control of the processes not always easy. Mechanical systems provide more spatial control whereas the piston driven system often show leakage at the end of extrusion [49]. For screw driven systems more components need to be sterilized and a cell friendly design of the screw is desirable. After extrusion, crosslinking the bioink can be induced in various ways such as photopolymerization or ionic crosslinking. In EBB relatively low resolutions from 100 to 1000 μm can be achieved and high viscous material up to 6×10^7 mPa/s can be processed. The method is convincing with a high fabrication speed, high possible cell densities and the possibility to include spheroids or cell aggregates. In contrast to the others methods, cell viability is relatively low in a range of 40 to 80% [9]. However, there is also the strategy to seed the cells subsequently after printing [50]. The result and success is also dependent on the used hardware. For example, the nozzle geometry generates shear forces on cells and needs to be considered. There are already many extrusion based bioprinters with different degrees of

automation and equipment [50]. A constant extrusion rate, automated coordinate calibration and reliable temperature control of the cartridge and nozzle for temperature-sensitive materials are desirable. By using multiple print heads, different materials with different cell types can be printed. There are also already printers that have several print heads with the different methods. Constructs have also been made from a combination of several methods [51].

1.2.1 Hydrogels and bioinks

Hydrogels consist of a water-insoluble polymer network that can bind high amounts of water [52]. These polymeric network can be synthesized from one monomer as homopolymers, from multiple species of monomers as copolymers or from at least two independent networks as multipolymer [53]. Hydrogels can either be of natural, e.g. based on alginate or collagen, or of synthetic origin, e.g. based on polyethyleneglycol (PEG) or polylactid acid (PLA). Chemical or physical bonds crosslink the monomers and the gelation process is introduced by ionic interactions, photopolymerization, hydrophobic interactions, and changes in pH-values or temperature. The choice of the polymer with respective crosslinking method, the molecular weight of polymer, and the initial polymer concentration define the physiochemical properties such as porosity, swelling behavior, stiffness, diffusivity characteristics and degradation [54]. The high water content in combination with the porous structure provide an environment comparable to the ECM which makes hydrogels attractive for biomedical applications. Hydrogels are already commercially used in drug delivery, tissue engineering, wound dressing, contact lenses and hygiene products [11, 55–57]. The compatibility with biological systems advanced the development of hydrogels with regard to an application in tissue engineering and as biosensors [58]. Especially for the production in bioprinting, hydrogels are a promising scaffold material which offers mild conditions for cells or biological material [3]. Hydrogels with incorporated cells are referred to as bioinks [59]. The main requirement of the hydrogel is the biocompatibility to allow cells later to grow and proliferate. This can also be enhanced by, e.g. modifying the polymers with arginine-glycine-aspartic acid (RGD) tags or incorporation of growth factors [11, 54]. During the printing process, the rheological properties of the hydrogel are of great importance. For extrusion based bioprinting, a shear-thinning behavior is desirable, as a lower pressure during extrusion reduces shear stress on the cells [14]. Thickening agents such as methylcellulose can be added to increase the viscosity and thus the dimensional stability after printing [60, 61]. After printing, this should also be reinforced by crosslinking the network. The main challenge is the development of bioinks for each specific kind of tissue which all have individual requirements.

1.2.1.1 Alginate

Alginate is an anionic polysaccharide extracted from brown algae or bacteria [62]. The chemical building blocks of this polymer are α -L-guluronate (G) and β -D-mannuronate (M) which are linear (1,4)-linked. The blocks can be consecutive (GGGG or MMMM) or alternating (GMGM). The M and G contents depend on the sources. Only the G-blocks participate in the crosslinking process with divalent cations in which an egg-box-like structure is formed [63]. Alginate is 'Generally Recognized As Safe (GRAS)' by the Food and Drug Administration (FDA) [64]. Due to the high biocompatibility, it is already used as wound dressing, forming material in dental medicine and in the food industry [65–68]. The mild gelation conditions at room temperature make alginate a perfect candidate as scaffold material for bioink development. The desired viscosity can be adjusted

by polymer concentration. The degradation is induced by ionic replacement and not enzymatically. A disadvantage for cell proliferation is the lack of natural RGD-tags, but interaction with cells can be enabled by material modification [69]. The diffusion-based crosslinking is not easy to control and as for all natural raw materials, batch-to-batch variances can occur. Nonetheless, alginate has proven and, particularly in combination with hydrogels which possess natural cell binding sequences, to be a suitable material for bioprinting. Alginate based bioinks are investigated in tissue engineering for several tissues such as bone or cartilage [70–73].

1.2.1.2 Gelatine-methacrylat

Gelatine-methacrylate (GelMA) consists of gelatin, which in turn is a partially-hydrolyzed form of collagen. Collagen is the main component of the ECM resulting in a high biocompatibility. Since collagen supports nutrient permeability, it is valued as a scaffold material in bioink development. Another advantage of GelMA is its biodegradability and the presence of RGD tags, which promote cell adhesion [74, 75]. Gelatin is in a triple helix form as gel at low temperatures and as random coil structure above the sol-gel transition temperature. The thermal crosslinking process is reversible and as under physiological conditions the network structure dissolves, gelatin is often functionalized with regard to design the crosslinking process more controllable [76]. For this purpose, gelatin is modified with methacrylic anhydride (MA) which attaches to the free amino groups of the gelatin with elimination of methacrylic acid. The product is referred to as GelMA. The bioactive RGD motifs remain unchanged and the transparency of the gel is beneficial with regard to microscopic examination. Different degrees of functionalization (DoF) are possible and it represents what percentage of the amines of the gelatin has been functionalized. Higher pH values during the reaction result in higher degrees of substitutions. During this reaction, photosensitive groups are introduced which allow for photopolymerization of the network. A photoinitiator is needed to start the reaction and it is important to select for biomedical applications a photoinitiator which is not cytotoxic. Frequently used is lithium-phenyl-2,4,6-trimethylbenzoylphosphine (LAP) which is water soluble, decomposes into radicals under light irradiation and starts the chain reaction [74]. With a higher DoF, there are more crosslinking points and the more stable is the resulting network. The DoF, polymer concentration, photoinitiator concentration, wave length, intensity of the light source can be used to adapt the network to the respective application [77]. GelMA based bioinks were used, e.g. for the bioprinting of liver construct which are supposed to serve a liver test models or for the production of artificial skin [78, 79].

1.2.1.3 Kolliphor

A hydrogel based on poloxamer 407 copolymer belongs to the synthetic hydrogels and is also referred to as Kolliphor[®], Lutrol[®] or Pluronic[®]. The thermoreversible properties of the amphiphilic triblock copolymer structure are of great interest for biomedical applications. It consists of two hydrophilic poly(ethylene oxide) (PEO) segments and one hydrophobic poly(propylene oxide) (PPO) segment in PEO-PPO-PEO triblocks [80, 81]. In general, it is readily soluble in water and forms a clear gel from a concentration of 20 % (w/v). Poloxamer solutions undergo a sol-gel transition with increasing temperature in which at first the copolymers arrange into spherical micelles with a dehydrated PPO core and a hydrated PEO shell. If the temperature rises further, the micelles form a cubic pack network. The sol-gel transition temperature decreases with increasing poloxamer concentration [81]. This process is reversible which makes poloxamer interesting for drug delivery applications and the

amphiphilic properties allow for incorporation of hydrophilic and hydrophobic drugs. Poloxamer is suitable as bioink due to its biocompatibility and good printing performance. One disadvantage is that cell proliferation and long-term cell viability is not promoted. However, it can be applied as sacrificial material, which is removed after printing. For example, poloxamer has already been used to embed vascularization systems [82–84]. In another study, it was already modified and osteogenic differentiation could be reached [51].

1.2.2 Analytics

The following chapter provides an overview of analysis methodologies which are essential for the evaluation of bioprinting processes. This includes rheological tests of bioinks, geometric form evaluation of printed objects and cell viability determination.

1.2.2.1 Rheology and rheometry

In general, rheology is the study of the flow and deformation of materials, and the term itself originates from the Greek words *rhei* 'to flow' and *logos* 'words, speech' [85]. One fundamental equation is the Hooke's law which describes the deformation of ideal elastic solids when their deformation is proportional to an applied force (see Equation 1.1). This behaviour is typical for metals under light loads.

$$\sigma = E\epsilon \tag{1.1}$$

σ in Pa is the stress, E in Pa is the modulus of elasticity and ϵ the strain in direction of the load [86]. An additional fundamental equation for the description of the viscoelastic materials is the Newton's law which describes the behavior of ideal viscous fluids. According to Equation 1.2, stress is linear proportional to the shear rate.

$$\tau = \eta\dot{\gamma} \tag{1.2}$$

Here, τ in Pa is the shear stress, η in Pas represents the dynamic viscosity and $\dot{\gamma}$ is the shear rate in s^{-1} . The viscosity is a parameter of resistance of fluids to shearing. For Newtonian fluids, the viscosity is unaffected by shear rate [86]. Furthermore, viscosity is besides shear rate dependent on multiple parameter such as temperature, polymer concentration, ionic strength, and pH [85]. However, this is not applicable to all liquids, as through relative intermolecular movements friction forces and resistances occur [87]. Viscoelastic materials combine the properties of solids and liquids. There are different models to describe their flow curves, to describe their rheological properties (see Figure 1.2).

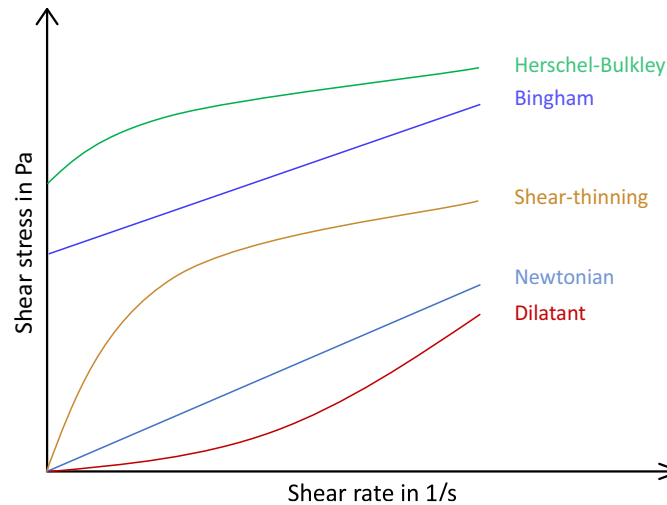


Figure 1.2 Typical flow curves of fluids showing shear stress as a function of shear rate. Newtonian fluids show a linear relationship (light blue). The same applies for Bingham fluids, but a certain shear stress is necessary to overcome a yield point (dark blue). If the shear stress is rising with higher shear rates, this is defined as dilatant behavior (red). If the opposite occurs and shear stress is decreasing, this is defined as shear-thinning behavior (ocher). A Herschel-Bulkley fluid shows a yield stress and a non-linear behavior (green).

Just as Newtonian fluids, Bingham fluids also show a linear stress dependence on shear rate, but a certain shear rate must be exceeded. This point is defined as the yield stress that represents the limit of elastic behavior and from this point on, the material will not reversibly deform with increasing stress. If the course of the stress does not increase linearly with increasing shear rate, one speaks of dilatant behavior. For shear-thinning material, viscosity decreases under shear strain and consequently the slope of the shear stress decreases with increasing shear rate. Another model for fluids with yield stress and a non-linear behavior is the Herschel-Bulkley model [88, 89]. With regard to the compositions of bioinks, a polymer with a yield point should be preferred to prevent leakage out of the cartridge and to prevent destruction of objects when a growing mass of layers is built up. Furthermore, a polymer is favourable which shows shear-thinning behavior to enable an extrusion at relative low pressures so that the biological components are not exposed to high shear stress.

Rheometry is defined as the measuring technology to quantify rheological characteristics of materials and includes different devices and methodologies. A basic distinction is made between two measurement methods, namely between rotational and oscillatory tests [85].

Rotational tests

Rotational testing provides information on the rheological behavior of fluids under steady flow conditions. In rotational testings, a fluid is placed between two rotationally symmetrical components arranged around an axis. The measurement can be operated in two different modes. The first mode is the controlled shear rate test (CSR-test) in which the angular velocity ω and consequently the shear rate is fixed. The shear rate $\dot{\gamma}$ is increased or decreased gradually over time and the shear stress τ is measured for each shear rate. Used in Equation 1.2, this test provides information about the viscosity at a certain shear rate. The second method is called controlled shear stress (CSS-test)

in which the torque and as a result the shear stress is fixed. The shear stress is increased gradually over time and for each point the deformation is measured. When the deformation is plotted over shear stress, the tangential-crossover-method can be used for yield point determination. A first tangent is drawn through the reversible area in which the deformation is linearly dependent on the shear stress and a second is drawn in the irreversible area and the intersection point represents the critical shear stress which identifies the yield point.

Oscillatory tests

For the characterization of viscoelastic materials which exhibit viscous and elastic behavior simultaneously oscillatory tests are performed. This method is also known as dynamic mechanical analysis (DMA). During the measurement the bottom plate is stationary and the upper plate is moved with sinusoidal oscillations back and forth by the shear force. Input parameters are the stress amplitude and frequency and output parameters are the deformation amplitude and frequency. Viscoelastic material have a linear-viscoelastic region (LVE) in which the deformation is proportional to the shear stress. For the identification of the LVE, amplitude sweeps are performed. Here, the amplitude is varied at a steady frequency and the shear modulus is determined. G' represents the storage modulus which is the elastic component. It can be regarded as the resistance against deformation. After deformation, the energy stored can be used for reformation of the sample. G'' is the loss modulus and can be understood as the proportion of deformation energy which is lost due to material changes or to friction. The ratio of loss modulus to storage modulus is defined as loss tangent (see Equation 1.3).

$$\tan(\delta) = \frac{G''}{G'} \quad (1.3)$$

Ideal elastic behavior is represented by $\tan(\delta) = 0$ when G' dominates over G'' . For ideal viscous behavior G'' dominates over G' and $\tan(\delta) = \infty$. Within the LVE both functions stay constant, but by exceeding the yield point when the structure is changed irreversibly, both functions change [85, 86, 89].

With regard to the structure analysis, frequency sweeps are examined. Here, the amplitude stays constant and the frequency is varied. It is important to choose a τ within the LVE and the LVE can be determined in a previous amplitude sweep. If G' dominates over G'' a gel-like behavior is indicated [88].

Oscillatory tests are performed for bioprinting applications as typical bioink materials are viscoelastic. In amplitude sweeps, the LVE can be determined and from which shear stress on the material is irreversibly deformed. The LVE is also important to be known to choose a shear stress within the LVE for frequency sweeps. The frequency sweeps analyze the structure of the materials and at least after extrusion a gel-like behavior is desirable.

1.2.2.2 Image processing

Image processing is generally understood as the processing of digital images with mathematical algorithms using a computer. The whole process consists of several steps, namely image acquisition, image enhancement and image extraction [90, 91]. The sensor data obtained during image acquisition, which is determined differently depending on the imaging system, is stored in pixels. A pixel is a discrete picture element and a digital image is displayed by a large number of pixels on a monitor. Each pixels contains information on color and the gradients to neighboring pixels allow conclusions

to be drawn about texture and shape. For the definition of color, for example, the RGB code is often used, where each color can be represented from a proportion of red, yellow and blue. For the texture determination there are several methods, most of them based on statistical methods. Methods are developed which calculate the degree of contrast or regularity. Shapes can be found, for example, by regions of uniform color [92]. In a first step, a preprocessing is conducted with the intention to improve the images' quality. Possible steps are such as processing color and contrast, resolution or cropping of the region of interest (ROI). In the following step the image is segmented and objects are detected from which application-specific characteristics can be extracted [92, 93]. In order to minimize computationally intensive and time-consuming post-processing of the images, the available technology should be exploited during acquisition. This includes the choice of suitable optics with appropriate lighting. Especially an optimal illumination is crucial for the quality and should be chosen problem specific. Decision factors are colour or monochrome application, speed, operating time, characteristics that are to be investigated and object properties, such as dimension, color, structure or reflectance [94]. The illumination angle distinguishes between incident illumination, when the light is on the side of the camera, and background illumination, when the light is behind the object. For both illumination angles, a bright field or a dark field illumination can be used. In a bright field illumination the light is reflected by the object and directed into the camera. This setup is most often used for coarse surfaces which are not reflective. In a dark field illumination the light reflected by object is deflected past the detector and only refractions on the surface direct rays to the detector. This setup is therefore suitable for detecting scratches on surfaces [95, 96]. The choice of whether to use diffuse or collimated light also affects the result. In a bright field, diffuse light is preferred for uneven surfaces, and collimated light is preferred for flat surfaces to detect elevations. In a dark field illumination, collimated light is used to show the silhouette of the object [94].

In general, image processing offers multiple advantages since it is non-invasive, fast, the results can be long-time documented and automation is possible. These lead to vision systems and image processing being used in many fields such as agriculture, robotic vision, industrial manufacturing, and medical field [17, 91, 93, 97, 98]. In combination with artificial intelligence (AI) this technology will experience a strong upswing in the course of the next years [99].

For bioprinting applications, machine vision is a promising tool for assessing the printability of bioinks or the influence of printing parameters. There are already methods developed for evaluating the uniformity of extruded filaments, filament width, angle sharpness, filament collapse tests and filament fusion tests, to name but a few. At the present time, however, many evaluations are still carried out manually and thus subjective evaluations of individuals are still possible [100–103].

1.2.2.3 Flow cytometry in cell analysis

Flow cytometry is a highly versatile cell analytical tool allowing for the determination of multiple parameters. Large number of cells can be analyzed in combination with fluorescent dyes. Dyes with affinities to specific cellular components are used and ideally the signal strength is proportional to the cell number. The staining methods can be deoxyribonucleic acid (DNA), protein or metabolite targeted. One example is the live/dead staining with calcein-acetoxymethyl ester (CAM) for living cells and with propidium iodide (PI) for dead cells. CAM can be transported by living cells through the membrane into the interior and there the enzyme esterase splits off the acetomethyl and acetate groups. Calcein remains, which is able to form a complex with calcium ions, producing green fluorescent light. Propidium iodide is used as a dead cell marker because it can pass the perforated

membrane of dead cells and intercalate into DNA, but not of intact cells. This produces red fluorescent light [104–106]. A laser beam of a certain wavelength is directed onto the sample at right angles. The cells are individually sent through the laser beam in suspension in a laminar flow. Depending on the required wavelength, appropriate filters are used and it is possible to use several wavelengths simultaneously. The scattered light is detected and if it is in a narrow angle to the excitation light, it is referred to as forward scatter (FSC) which represents a relative measure of cell count. The scattering at a 90° angle is called side scatter (SSC) and provides information about the granularity or complexity of the cell. The light signals are converted into digital ones by a photomultiplier (PMT). When selecting the dyes, however, it is important to ensure that the dye spectra do not overlap and falsify the result [107, 108]. For the correct evaluation of the results, a calibration is necessary beforehand [108]. As already mentioned, this method allows an evaluation of cell numbers in a statistically relevant range. In microscopic evaluation, a large number of images must be acquired for this purpose. In view of the application of 3D printed constructs, images have to be taken on several levels. In general, for all fluorescence staining techniques, it must be ensured that suitable dyes are selected. The substances must be able to diffuse through the scaffold and also have sufficient time to reach the interior. Here, adulterations due to interactions with the matrix must be excluded. Flow cytometry is a destructive method and the cells must be in suspension. This requires detachment from the matrix and can be stressful for the cells [64, 109]. An alternative is examination in microtiter plates and fluorescent dyes. Here, many differing samples can be examined in a few minutes [105]. Here, polymer influences of the polymeric solutions have to be considered. The polymer can scatter and diffract the light which again impacts the results. Furthermore, the dyes and possible products should not be diffusion limited by the polymer. These problems do not occur by flow cytometry and all cells in total can be analyzed in contrast to only one focal plane. Besides, it is possible to analyze multiple cell types at once and to sort the cells.

Chapter references

- [1] Y. Yu, Q. Wang, C. Wang, and L. Shang, „Living Materials for Regenerative Medicine“, *Engineered Regeneration*, vol. 2, no. August, pp. 96–104, 2021.
- [2] F. Berthiaume, T. J. Maguire, and M. L. Yarmush, „Tissue engineering and regenerative medicine: History, progress, and challenges“, *Annual Review of Chemical and Biomolecular Engineering*, vol. 2, pp. 403–430, 2011.
- [3] J. Malda *et al.*, „25th anniversary article: Engineering hydrogels for biofabrication“, *Advanced Materials*, vol. 25, no. 36, pp. 5011–5028, 2013.
- [4] H. G. Yi, H. Kim, J. Kwon, Y. J. Choi, J. Jang, and D. W. Cho, „Application of 3D bioprinting in the prevention and the therapy for human diseases“, *Signal Transduction and Targeted Therapy*, vol. 6, no. 1, 2021.
- [5] W. Wu, Q. Zheng, X. Guo, J. Sun, and Y. Liu, „A programmed release multi-drug implant fabricated by three-dimensional printing technology for bone tuberculosis therapy“, *Biomedical Materials*, vol. 4, no. 6, 2009.
- [6] D. G. Hwang *et al.*, „A 3D bioprinted hybrid encapsulation system for delivery of human pluripotent stem cell-derived pancreatic islet-like aggregates“, *Biofabrication*, vol. 14, no. 1, 2022.
- [7] S. Panda *et al.*, „A focused review on three-dimensional bioprinting technology for artificial organ fabrication“, *Biomaterials Science*, vol. 10, no. 18, pp. 5054–5080, 2022.
- [8] C. Mota, S. Camarero-Espinosa, M. B. Baker, P. Wieringa, and L. Moroni, „Bioprinting: From Tissue and Organ Development to in Vitro Models“, *Chemical Reviews*, vol. 120, no. 19, pp. 10547–10607, 2020.
- [9] S. V. Murphy and A. Atala, „3D bioprinting of tissues and organs“, *Nature Biotechnology*, vol. 32, no. 8, pp. 773–785, 2014.
- [10] S. M. Hull, L. G. Brunel, and S. C. Heilshorn, *3D Bioprinting of Cell-Laden Hydrogels for Improved Biological Functionality*, 2022.
- [11] B. V. Slaughter, S. S. Khurshid, O. Z. Fisher, A. Khademhosseini, and N. A. Peppas, „Hydrogels in regenerative medicine“, *Advanced Materials*, vol. 21, no. 32-33, pp. 3307–3329, 2009.
- [12] M. P. Sekar *et al.*, „Current standards and ethical landscape of engineered tissues—3D bioprinting perspective“, *Journal of Tissue Engineering*, vol. 12, 2021.
- [13] M. Kesti, P. Fisch, M. Pensalfini, E. Mazza, and M. Zenobi-Wong, „Guidelines for standardization of bioprinting: A systematic study of process parameters and their effect on bioprinted structures“, *BioNanoMaterials*, vol. 17, no. 3-4, pp. 193–204, 2016.
- [14] N. Paxton, W. Smolan, T. Böck, F. Melchels, J. Groll, and T. Jungst, „Proposal to assess printability of bioinks for extrusion-based bioprinting and evaluation of rheological properties governing bioprintability“, *Biofabrication*, vol. 9, no. 4, p. 44107, 2017.
- [15] K. F. Freed and S. F. Edwards, „Polymer viscosity in concentrated solutions“, *The Journal of Chemical Physics*, vol. 61, no. 9, pp. 3626–3633, 1974.
- [16] S. S and R. G, „Robot assisted sensing, control and manufacture in automobile industry“, *Journal of ISMAC*, vol. 01, no. 03, pp. 180–187, 2019.
- [17] Y. Tang *et al.*, „Recognition and Localization Methods for Vision-Based Fruit Picking Robots: A Review“, *Frontiers in Plant Science*, vol. 11, no. May, pp. 1–17, 2020.
- [18] S. Mellor, L. Hao, and D. Zhang, „Additive manufacturing: A framework for implementation“, *International Journal of Production Economics*, vol. 149, pp. 194–201, 2014.
- [19] D. Bourell *et al.*, „Materials for additive manufacturing“, *CIRP Annals - Manufacturing Technology*, vol. 66, no. 2, pp. 659–681, 2017.
- [20] M. A., R. K. Y., and K. L., „Improve the accuracy, surface smoothing and material adaption in STL file for RP medical models“, *Journal of Manufacturing Processes*, vol. 21, pp. 46–55, 2016.
- [21] I. Gibson, D. Rosen, B. Stucker, and M. Khorasani, *Additive Manufacturing Technologies*. Cham: Springer International Publishing, 2021, vol. 89, pp. 82–86.
- [22] C. Kohtala, „Addressing sustainability in research on distributed production: An integrated literature review“, *Journal of Cleaner Production*, vol. 106, pp. 654–668, 2015.
- [23] S. Ford and M. Despeisse, „Additive manufacturing and sustainability: an exploratory study of the advantages and challenges“, *Journal of Cleaner Production*, vol. 137, pp. 1573–1587, 2016.
- [24] J. Plocher and A. Panesar, „Review on design and structural optimisation in additive manufacturing: Towards next-generation lightweight structures“, *Materials and Design*, vol. 183, 2019.
- [25] B. Blakey-Milner *et al.*, „Metal additive manufacturing in aerospace: A review“, *Materials and Design*, vol. 209, p. 110008, 2021.

- [26] R. Leal *et al.*, „Additive manufacturing tooling for the automotive industry“, *International Journal of Advanced Manufacturing Technology*, vol. 92, no. 5-8, pp. 1671–1676, 2017.
- [27] A. A. Zadpoor and J. Malda, „Additive Manufacturing of Biomaterials, Tissues, and Organs“, *Annals of Biomedical Engineering*, vol. 45, no. 1, pp. 1–11, 2017.
- [28] S. C. Ligon, R. Liska, J. Stampfl, M. Gurr, and R. Mülhaupt, „Polymers for 3D Printing and Customized Additive Manufacturing“, *Chemical Reviews*, vol. 117, no. 15, pp. 10 212–10 290, 2017.
- [29] E. Pei *et al.*, Eds., *Springer Handbook of Additive Manufacturing* (Springer Handbooks). Springer International Publishing, 2023.
- [30] *DIN EN ISO/ASTM 52900:2022-03, Additive Fertigung – Grundlagen – Terminologie (ISO/ASTM 52900:2021)*. Berlin: Beuth Verlag, 2022.
- [31] L. J. Tan, W. Zhu, and K. Zhou, „Recent Progress on Polymer Materials for Additive Manufacturing“, *Advanced Functional Materials*, vol. 30, no. 43, 2020.
- [32] K. V. Wong and A. Hernandez, „A Review of Additive Manufacturing“, *ISRN Mechanical Engineering*, vol. 2012, pp. 1–10, 2012.
- [33] J. Kruth, „Material Incess Manufacturing by Rapid Prototyping Techniques“, *CIRP Annals*, vol. 40, no. 2, pp. 603–614, 1991.
- [34] J. P. Kruth, X. Wang, T. Laoui, and L. Froyen, „Lasers and materials in selective laser sintering“, *Assembly Automation*, vol. 23, no. 4, pp. 357–371, 2003.
- [35] P. Nandwana, A. M. Elliott, D. Siddel, A. Merriman, W. H. Peter, and S. S. Babu, „Powder bed binder jet 3D printing of Inconel 718: Densification, microstructural evolution and challenges“, *Current Opinion in Solid State and Materials Science*, vol. 21, no. 4, pp. 207–218, 2017.
- [36] S. J. Yoo, T. Spray, E. H. Austin, T. J. Yun, and G. S. van Arsdell, „Hands-on surgical training of congenital heart surgery using 3-dimensional print models“, *Journal of Thoracic and Cardiovascular Surgery*, vol. 153, no. 6, pp. 1530–1540, 2017.
- [37] S. Amrhein, M. L. Schwab, M. Hoffmann, and J. Hubbuch, „Characterization of aqueous two phase systems by combining lab-on-a-chip technology with robotic liquid handling stations“, *Journal of Chromatography A*, vol. 1367, pp. 68–77, 2014.
- [38] L. Wenger, C. P. Radtke, J. Göpper, M. Wörner, and J. Hubbuch, „3D-Printable and Enzymatically Active Composite Materials Based on Hydrogel-Filled High Internal Phase Emulsions“, *Frontiers in Bioengineering and Biotechnology*, vol. 8, pp. 1–17, 2020.
- [39] C. Fee, „3D-printed porous bed structures“, *Current Opinion in Chemical Engineering*, vol. 18, pp. 10–15, 2017.
- [40] S. Nawada, S. Dimartino, and C. Fee, „Dispersion behavior of 3D-printed columns with homogeneous microstructures comprising differing element shapes“, *Chemical Engineering Science*, vol. 164, pp. 90–98, 2017.
- [41] B. Schmieg, A. Schimek, and M. Franzreb, „Development and performance of a 3D-printable poly(ethylene glycol) diacrylate hydrogel suitable for enzyme entrapment and long-term biocatalytic applications“, *Engineering in Life Sciences*, vol. 18, no. 9, pp. 659–667, 2018.
- [42] J. Groll *et al.*, „Biofabrication: reappraising the definition of an evolving field“, *Biofabrication*, vol. 8, no. 1, p. 013001, 2016.
- [43] V. Mironov, T. Boland, T. Trusk, G. Forgacs, and R. R. Markwald, „Organ printing: Computer-aided jet-based 3D tissue engineering“, *Trends in Biotechnology*, vol. 21, no. 4, pp. 157–161, 2003.
- [44] F. Guillemot, V. Mironov, and M. Nakamura, „Bioprinting is coming of age: Report from the International Conference on Bioprinting and Biofabrication in Bordeaux (3B'09)“, *Biofabrication*, vol. 2, no. 1, 2010.
- [45] J. P. Vacanti and R. Langer, „Tissue engineering: the design and fabrication of living replacement devices for surgical reconstruction and transplantation“, *The Lancet*, vol. 354, no. SUPPL.1, S32–S34, 1999.
- [46] W. Sun *et al.*, „The bioprinting roadmap“, *Biofabrication*, vol. 12, no. 2, 2020.
- [47] A. B. Dababneh and I. T. Ozbolat, „Bioprinting Technology: A Current State-of-the-Art Review“, *Journal of Manufacturing Science and Engineering*, vol. 136, no. 6, p. 061016, 2014.
- [48] L. Ning *et al.*, „Process-induced cell damage: pneumatic versus screw-driven bioprinting“, *Biofabrication*, vol. 12, no. 2, 2020.
- [49] L. R. Darwish, M. T. El-Wakad, and M. M. Farag, „Towards an Ultra-Affordable Three-Dimensional Bioprinter: A Heated Inductive-Enabled Syringe Pump Extrusion Multifunction Module for Open-Source Fused Deposition Modeling Three-Dimensional Printers“, *Journal of Manufacturing Science and Engineering*, vol. 143, no. 12, 2021.
- [50] I. T. Ozbolat and M. Hospodiuk, „Current advances and future perspectives in extrusion-based bioprinting“, *Biomaterials*, vol. 76, pp. 321–343, 2016.

- [51] P. Diloksumpan *et al.*, „Combining multi-scale 3D printing technologies to engineer reinforced hydrogel-ceramic interfaces“, *Biofabrication*, vol. 12, no. 2, 2020.
- [52] A. S. Hoffman, „Hydrogels for biomedical applications“, *Advanced Drug Delivery Reviews*, vol. 64, no. SUPPL. Pp. 18–23, 2012.
- [53] E. M. Ahmed, „Hydrogel: Preparation, characterization, and applications: A review“, *Journal of Advanced Research*, vol. 6, no. 2, pp. 105–121, 2015.
- [54] K. Y. Lee and D. J. Mooney, „Hydrogels for tissue engineering“, *Chemical Reviews*, vol. 101, no. 7, pp. 1869–1879, 2001.
- [55] Y. Liang, J. He, and B. Guo, „Functional Hydrogels as Wound Dressing to Enhance Wound Healing“, *ACS Nano*, vol. 15, no. 8, pp. 12 687–12 722, 2021.
- [56] E. Caló and V. V. Khutoryanskiy, „Biomedical applications of hydrogels: A review of patents and commercial products“, *European Polymer Journal*, vol. 65, pp. 252–267, 2015.
- [57] P. Franco and I. De Marco, „Contact Lenses as Ophthalmic Drug Delivery Systems: A Review“, *Polymers*, vol. 13, no. 7, p. 1102, 2021.
- [58] N. A. Peppas and D. S. Van Blarcom, „Hydrogel-based biosensors and sensing devices for drug delivery“, *Journal of Controlled Release*, vol. 240, pp. 142–150, 2016.
- [59] J. Groll *et al.*, „A definition of bioinks and their distinction from biomaterial inks“, *Biofabrication*, vol. 11, no. 1, 2019.
- [60] T. Ahlfeld *et al.*, „Development of a clay based bioink for 3D cell printing for skeletal application“, *Biofabrication*, vol. 9, no. 3, p. 034 103, 2017.
- [61] S. Dani *et al.*, „Homogeneous and reproducible mixing of highly viscous biomaterial inks and cell suspensions to create bioinks“, *Gels*, vol. 7, no. 4, pp. 1–17, 2021.
- [62] O. Smidsrød, G. Skja, *et al.*, „Alginate as immobilization matrix for cells“, *Trends Biotech*, vol. 8, no. March, pp. 71–78, 1990.
- [63] K. Y. Lee and D. J. Mooney, „Alginate: Properties and biomedical applications“, *Progress in Polymer Science (Oxford)*, vol. 37, no. 1, pp. 106–126, 2012.
- [64] S. V. Murphy, A. Skardal, and A. Atala, „Evaluation of hydrogels for bio-printing applications“, *Journal of Biomedical Materials Research - Part A*, vol. 101 A, no. 1, pp. 272–284, 2013.
- [65] G. Kloeck *et al.*, „Biocompatibility of mannuronic acid-rich alginates“, *Biomaterials*, vol. 18, no. 10, pp. 707–713, 1997.
- [66] Y. Cao, H. Cong, B. Yu, and Y. Shen, „A review on the synthesis and development of alginate hydrogels for wound therapy“, *Journal of Materials Chemistry B*, no. 1, pp. 2801–2829, 2023.
- [67] W. Cook, „Alginate dental impression materials: Chemistry, structure, and properties“, *Journal of Biomedical Materials Research*, vol. 20, no. 1, pp. 1–24, 1986.
- [68] D. Li, Z. Wei, and C. Xue, „Alginate-based delivery systems for food bioactive ingredients: An overview of recent advances and future trends“, *Comprehensive Reviews in Food Science and Food Safety*, vol. 20, no. 6, pp. 5345–5369, 2021.
- [69] J. a. Rowley, G. Madlambayan, and D. J. Mooney, „Alginate hydrogels as synthetic extracellular matrix materials“, *Biomaterials*, vol. 20, no. 1, pp. 45–53, 1999.
- [70] A. Iglesias-Mejuto and C. A. García-González, „3D-printed alginate-hydroxyapatite aerogel scaffolds for bone tissue engineering“, *Materials Science and Engineering C*, vol. 131, no. October, 2021.
- [71] E. Y. Heo *et al.*, „Novel 3D printed alginate–BFP1 hybrid scaffolds for enhanced bone regeneration“, *Journal of Industrial and Engineering Chemistry*, vol. 45, pp. 61–67, 2017.
- [72] D. Nguyen *et al.*, „Cartilage Tissue Engineering by the 3D Bioprinting of iPS Cells in a Nanocellulose/Alginate Bioink“, *Scientific Reports*, vol. 7, no. 1, pp. 1–10, 2017.
- [73] R. Ahmad Raus, W. M. F. Wan Nawawi, and R. R. Nasaruddin, „Alginate and alginate composites for biomedical applications“, *Asian Journal of Pharmaceutical Sciences*, vol. 16, no. 3, pp. 280–306, 2021.
- [74] K. Yue, G. Trujillo-de Santiago, M. M. Alvarez, A. Tamayol, N. Annabi, and A. Khademhosseini, „Synthesis, properties, and biomedical applications of gelatin methacryloyl (GelMA) hydrogels“, *Biomaterials*, vol. 73, pp. 254–271, 2015.
- [75] S. Naahidi *et al.*, „Biocompatibility of hydrogel-based scaffolds for tissue engineering applications“, *Biotechnology Advances*, vol. 35, no. 5, pp. 530–544, 2017.
- [76] S. Chen, Y. Wang, J. Lai, S. Tan, and M. Wang, „Structure and Properties of Gelatin Methacryloyl (GelMA) Synthesized in Different Reaction Systems“, *Biomacromolecules*, vol. 24, no. 6, pp. 2928–2941, 2023.
- [77] A. G. Kurian, R. K. Singh, K. D. Patel, J. H. Lee, and H. W. Kim, „Multifunctional GelMA platforms with nanomaterials for advanced tissue therapeutics“, *Bioactive Materials*, vol. 8, no. June 2021, pp. 267–295, 2022.

- [78] M. C. Bouwmeester *et al.*, „Bioprinting of Human Liver-Derived Epithelial Organoids for Toxicity Studies“, *Macromolecular Bioscience*, vol. 21, no. 12, p. 2100327, 2021.
- [79] N. R. Barros *et al.*, „Biofabrication of endothelial cell, dermal fibroblast, and multilayered keratinocyte layers for skin tissue engineering“, *Biofabrication*, vol. 13, no. 3, p. 035030, 2021.
- [80] E. Russo and C. Villa, „Poloxamer hydrogels for biomedical applications“, *Pharmaceutics*, vol. 11, no. 12, 2019.
- [81] G. Dumortier, J. L. Grossiord, F. Agnely, and J. C. Chaumeil, „A review of poloxamer 407 pharmaceutical and pharmacological characteristics“, *Pharmaceutical Research*, vol. 23, no. 12, pp. 2709–2728, 2006.
- [82] D. B. Kolesky, R. L. Truby, A. S. Gladman, T. A. Busbee, K. A. Homan, and J. A. Lewis, „3D bioprinting of vascularized, heterogeneous cell-laden tissue constructs“, *Advanced Materials*, vol. 26, no. 19, pp. 3124–3130, 2014.
- [83] P. S. Gungor-Ozkerim, I. Inci, Y. S. Zhang, A. Khademhosseini, and M. R. Dokmeci, „Bioinks for 3D bioprinting: An overview“, *Biomaterials Science*, vol. 6, no. 5, pp. 915–946, 2018.
- [84] N. E. Fedorovich, J. R. De Wijn, A. J. Verbout, J. Alblas, and W. J. Dhert, „Three-dimensional fiber deposition of cell-laden, viable, patterned constructs for bone tissue printing“, *Tissue Engineering - Part A*, vol. 14, no. 1, pp. 127–133, 2008.
- [85] T. G. Mezger, *The Rheology Handbook*, 4th ed. Hanover: Vincentz Network GmbH & Co. KG, 2014.
- [86] T. Osswald and N. Rudolph, *Carl Hanser Verlag*. 2006, pp. 1–8.
- [87] M. Rubinstein and R. H. Colby, *Polymer Physics*. Oxford University Press, 2003.
- [88] C. Verdier, „Rheological Properties of Living Materials . From Cells to Tissues“, vol. 5, no. June 2003, pp. 67–91, 2004.
- [89] P. A. Janmey, P. C. Georges, and S. Hvidt, „Basic Rheology for Biologists“, *Methods in Cell Biology*, vol. 83, 2007.
- [90] N. R. Pal and S. K. Pal, „A review on image segmentation techniques“, *Pattern Recognition*, vol. 26, no. 9, pp. 1277–1294, 1993.
- [91] F. Perez-Sanz, P. J. Navarro, and M. Egea-Cortines, „Plant phenomics: an overview of image acquisition technologies and image data analysis algorithms“, *GigaScience*, vol. 6, no. 11, pp. 1–18, 2017.
- [92] Y.-S. Chen, *Image Processing*, Y.-S. Chen, Ed. InTech, 2009.
- [93] M. L. Giger, H.-P. Chan, and J. Boone, „Anniversary Paper: History and status of CAD and quantitative image analysis: The role of Medical Physics and AAPM“, *Medical Physics*, vol. 35, no. 12, pp. 5799–5820, 2008.
- [94] J. Beyerer, F. P. León, and C. Frese, *Automatische Sichtprüfung: Grundlagen, Methoden und Praxis der Bildgewinnung und Bildauswertung*. Springer-Verlag, 2016.
- [95] F. Pernkopf and P. O’Leary, „Image acquisition techniques for automatic visual inspection of metallic surfaces“, *NDT and E International*, vol. 36, no. 8, pp. 609–617, 2003.
- [96] B. Jähne and H. Haußecker, *Computer vision and applications*. Academic Press, 2000.
- [97] D. Casasent and X. W. Chen, „New training strategies for RBF neural networks for X-ray agricultural product inspection“, *Pattern Recognition*, vol. 36, no. 2, pp. 535–547, 2003.
- [98] O. Semeniuta, S. Dransfeld, K. Martinsen, and P. Falkman, „Towards increased intelligence and automatic improvement in industrial vision systems“, *Procedia CIRP*, vol. 67, pp. 256–261, 2018.
- [99] J. F. Arinez, Q. Chang, R. X. Gao, C. Xu, and J. Zhang, „Artificial Intelligence in Advanced Manufacturing: Current Status and Future Outlook“, *Journal of Manufacturing Science and Engineering*, vol. 142, no. 11, pp. 1–16, 2020.
- [100] T. Gao *et al.*, „Optimization of gelatin-alginate composite bioink printability using rheological parameters: A systematic approach“, *Biofabrication*, vol. 10, no. 3, 2018.
- [101] A. Ribeiro *et al.*, „Assessing bioink shape fidelity to aid material development in 3D bioprinting“, *Biofabrication*, vol. 10, no. 1, 2018.
- [102] Y. He, F. Yang, H. Zhao, Q. Gao, B. Xia, and J. Fu, „Research on the printability of hydrogels in 3D bioprinting“, *Scientific Reports*, vol. 6, pp. 1–13, 2016.
- [103] M. Uzun-Per *et al.*, „Automated Image Analysis Methodologies to Compute Bioink Printability“, *Advanced Engineering Materials*, vol. 2000900, pp. 1–12, 2020.
- [104] C. Riccardi and I. Nicoletti, „Analysis of apoptosis by propidium iodide staining and flow cytometry“, *Nature Protocols*, vol. 1, no. 3, pp. 1458–1461, 2006.
- [105] N. Grigoryeva, *Fluorescence Methods for Investigation of Living Cells and Microorganisms*. BoD–Books on Demand, 2020.
- [106] N. G. Papadopoulos, G. V. Dedoussis, G. Spanakos, A. D. Gritzapis, C. N. Baxevanis, and M. Papamichail, „An improved fluorescence assay for the determination of lymphocyte-mediated cytotoxicity using flow cytometry“, *Journal of Immunological Methods*, vol. 177, no. 1-2, pp. 101–111, 1994.

- [107] A. Adan, G. Alizada, Y. Kiraz, Y. Baran, and A. Nalbant, *Flow cytometry: basic principles and applications*. 2017, vol. 37, pp. 163–176.
- [108] C. Ortolani, *Flow Cytometry Today*. Springer Nature, 2022.
- [109] S. Gretzinger, N. Beckert, A. Gleadall, C. Lee-Thedieck, and J. Hubbuch, „3D bioprinting – Flow cytometry as analytical strategy for 3D cell structures“, *Bioprinting*, vol. 11, no. March, e00023, 2018.

Thesis outline

2.1 Research proposal

The overarching aim of bioprinting is the manufacturing of cell-loaded structures analogous to natural tissues or organs. The goal is a safe, effective and large-scale employment of this artificial tissues for customized medical applications. This requires an understanding of the interplay between materials science, biologically active components and process engineering steps. For production of artificial tissues, hydrogels are often used to mimic the physical structure of the extracellular matrix into which cells are deposited with spatial control. These three-dimensional complexes can be employed, for example, as transplants or for lab-on-the-chip devices. Remarkable results have already been achieved in individual research projects. At the moment, bioprinting technology in the main is still at development stage. However, in order to manage the transfer to clinical applications, standardization of preparation methods, processing strategies and analytical methodologies will become relevant. The still missing standardization is the reason that results are not generally comparable. Eventually, acquiring the approval for medical applications relies on robust processes and, hence, the accomplishment of quality-by-design. Strictly speaking, the manufacturing process is ultimately required to guarantee the targeted quality of the finished product without extensive additional quality control activities. Therefore, the integration of process analytical technology (PAT) is widely acknowledged. Two challenges have been identified which can be directly associated with the currently observed lack of standardization for processing and analytical methodologies. First, the development of bioinks needs to be performed specifically for each application. This leads to a wide range of bioinks with differing physical and biological properties. Second, the technical maturity of commercially available bioprinter systems is not at a level for clinical applications. In combination with the chosen bioink, the available control parameters for extrusion-based bioprinters (e.g. the pressure applied to the cartridge during extrusion) are neither suitable to control nor to reproduce the geometry of the printed layer at a high accuracy.

The objective of this research is to increase the understanding of these challenges and to enable

their technical manageability. For this purpose, five studies are carried out within the framework of this doctoral thesis.

In the first study (Chapter 3), the feasibility of image processing as means to evaluate printing accuracy is investigated. This approach is assumed to be applicable to a wide range of bioinks and allows for an objective and time-efficient comparison of printed objects. Thus, a line analysis tool is developed and raw data images are provided by the cell confluence method of a plate reader. The limitation due to material transparency is tested by five materials of varying transparencies and also the effect of food coloring on the recognition is evaluated. Afterwards, the tool is applied in a case study to monitor the shrinkage behavior of printed lines. Hence, lines are printed with two commercially available bioinks and the shrinkage behavior is characterized for a period of 10 min.

In the second study (Chapter 4), the flow rate is examined as process control parameter and is supposed to increase process reproducibility. The currently available pneumatic printer designs are controlled over pneumatic pressure which is not adaptive to bioink changes, e.g. due to inhomogeneities or batch-to-batch variances when working with natural materials, and other disturbances. By keeping the conventional printing parameters constant, object geometries can be reproduced globally, however, significant deviations can be observed locally. The flow rates measured at the nozzle is considered to enable a more robust geometrical reproduction of objects, as influences on the flow between cartridge and nozzle can be better corrected. The study consists of two parts. Initially a flow meter is incorporated into the bioprinter system and a proof of concept is performed. Secondly, the flow rate is measured during the complete emptying of a cartridge on two different printing devices to evaluate both the influence of cartridge filling level and transferability of printing processes between devices. For both experimental parts, model polymeric solutions were employed consisting either of alginate or Kolliphor in varying concentrations.

At first, the sensor accuracy is to be determined for respective formulations by comparing cylinder volumes calculated based on sensor data with cylinder volumes calculated based on gravimetric measurements. Calibration lines are determined and used in the following reproducibility investigation. In the course of the reproducibility investigation, two approaches or process strategies are compared. During the first approach, cylinders are repeatedly printed by using the same extrusion pressure and in the second approach, the flow meter is used as calibration tool to adapt the pressure to generate a target flow rate before the experiments are carried out. Respective volumes of the cylinders are calculated and statistically evaluated.

The second part serves to examine the impact of the cartridge filling level and the impact of different bioprinting systems on the flow rate. Thus, the flow rate is recorded during the complete emptying of cartridges. The experiments are conducted on two bioprinter models to evaluate the transferability between different bioprinter designs. The experiments are repeated three times as triplicate.

Based on the outcomes of the second study, the flow meter is used to automatically regulate the flow rate in a third study (Chapter 5). The intention of this study is to tackle the challenge of a missing process monitoring and control. However, a feedback loop has to be established to monitor the sensor data and to automatically adapt the extrusion pressure based on real-time data. As evidence of the functionality, the setup performance is examined in three use cases: a) the complete emptying of one cartridge, b) the adaption to inhomogeneities is investigated by filling a cartridge with layers of varying viscosities, c) transferability is simulated by testing three different nozzles.

In a forth study (Chapter 6), standardized methods are developed to compare bioink performance and the process effect on cell viability is investigated. The knowledge gained so far on image evaluation and process control strategy is combined, expanded and also applied to working with cells. An additional approach for flow rate control is tested which has no need for the installation of additional sensors. The volume flow is calculated in accordance with bioink specific flow behavior. The approach is tested for two in-house developed bioink formulations consisting of alginate and gelatin methacryloyl (GelMA), with the alginate content differing by 1% (w/v). The applied pressure was set with a barometer beforehand as the pressure indication in the printer software differs from the actual pressure. Printing accuracy is evaluated by extending the image processing tool box from the first study. Therefore, the automated image processing toolbox is optimized in the hardware with a monochrome camera and a proper illumination to enable a fast image acquisition for low-contrast materials. New evaluation methods are developed to additionally analyze circle and angle structures. A printing performance evaluation is carried out for both formulations once without cells and once with cells. The success of an intact artificial tissue does not only depend on the accurate fabrication of the structures, but also on a high cell viability. Thus, bioprinting processes should be evaluated more in its entirety. Cell viability is investigated during bioink material preparation as well as during printing process and analyzed in statistical relevant numbers. Therefore, cell staining is conducted after each processing step and afterwards analyzed by a flow cytometer.

Since all results were obtained in one laboratory, in the fifth and last study (Chapter 7), a round robin test is performed to see how comparable printing results in different laboratories can be reached under current conditions. This study is intended to see how far standardization has progressed, where deviations occur during experiment conduction and show potential for optimization. Furthermore, three image analysis groups from different backgrounds develop their own image processing strategy and analyse all images. It will become apparent to what extent the results differ and whether IA is a suitable method for bioink printing accuracy evaluation. Therefore, data are collected in 12 academic independent laboratories, and the results, explicitly raw images of printed objects, are analyzed by three independent image analysis groups. In a visual inspection of the images, occurring deviations are to be identified and which sources for disturbance factors exist. The identification of them will show potential for optimization and standardization. The automated image analysis results provide information on the extent to which the objects differ in terms of their dimensions and also whether three independent analysis strategies lead to same results.

In summary, the aim of this thesis is to gain an overview of how far standardization currently is progressed and at which points in the workflow there is still potential for optimization. Simultaneously to increase standardization, one proposal is introduced to implement image processing methods for a robust bioink printing accuracy evaluation. This method is applicable for the wide range of bioinks needed and accelerates the bioink development by making them comparable. Therefore, a proper image acquisition and an image processing tool box should be developed during the thesis for line, circle and angle structures. In the last study, three groups being specialized in image processing, also develop three independent analysis strategies. Furthermore, the flow rate is investigated as a feasible control parameter for increasing process robustness. This can be realized by incorporating a sensor or by calculating the needed pressure based on the flow behavior of the bioink.

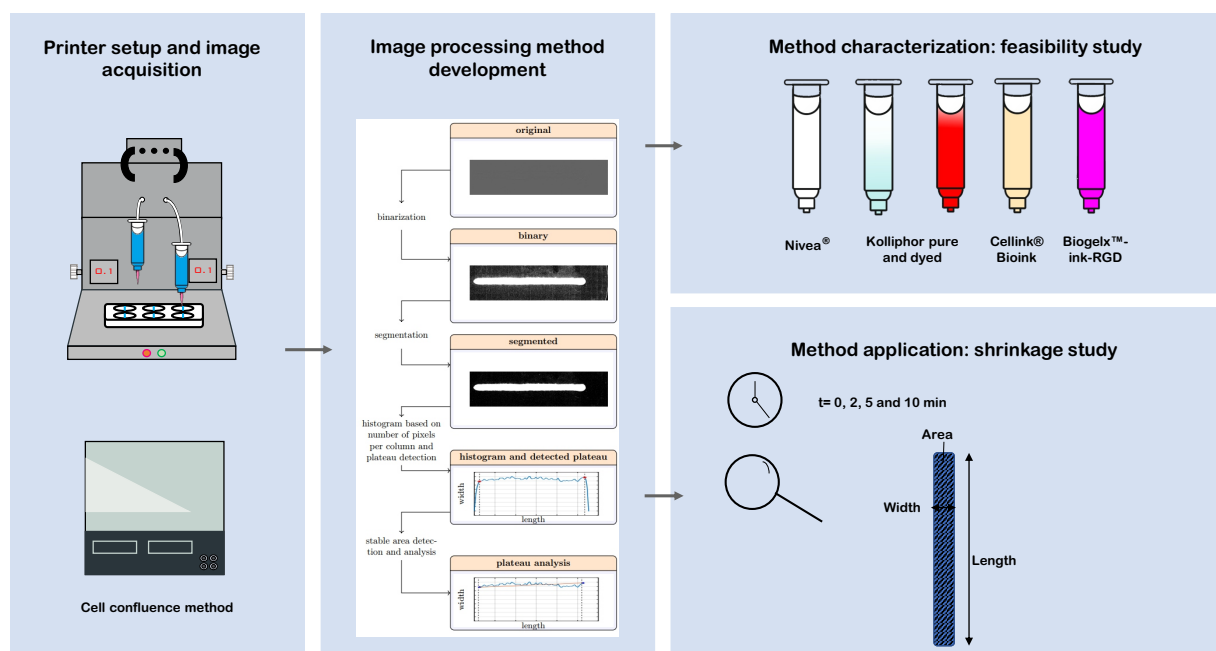
2.2 Manuscript overview

This subsection presents a brief summary of all manuscripts which have been published in the framework of this research thesis. Each manuscript is presented with an overview illustration, a short summary and the number of pages for the chapter containing the respective manuscript. In several of the following manuscripts, first authorship was shared (contributed equally) among colleagues and me. This was undertaken to increase the quality of our common publication. A detailed listing of author contributions signed by the respective authors is added as a separate supplement to the examination copy. The manuscript presented in Chapter 5 is also published in the thesis of the co-author Lukas Wenger. The two manuscripts reproduced in Chapter 6 and Chapter 7 can also be found in the thesis of the co-author David Grijalva Garces. The publications have been slightly modified. Furthermore, some diagrams and pictures have been changed in size and to fit the format of this dissertation.

Chapter 3

Image Analysis as PAT-Tool for Use in Extrusion-Based Bioprinting 33

Svenja Strauß, Rafaela Meutelet, Luka Radosevic, Sarah Gretzinger and Jürgen Hubbuch

published in Bioprinting, Volume 21, 2021, e00112<https://doi.org/10.1016/j.bprint.2020.e00112>

In this study with regard to introducing PAT, image processing is tested as a potential analytical technique. Thus, an automated image processing method is developed allowing for bioprinted line analysis with regard to length, width, and area. The raw data images are captured by a plate reader using a cell confluence method and the images are automated analyzed. In a screening using materials with different optical properties, lines are analyzed to find potential limitations. A subsequent case study using two commercially available bioinks demonstrates a shrinkage of printed lines for a period of 10 min. Image processing proved to be a suitable methodology for the analysis of high-water content materials in the bioprinting field.

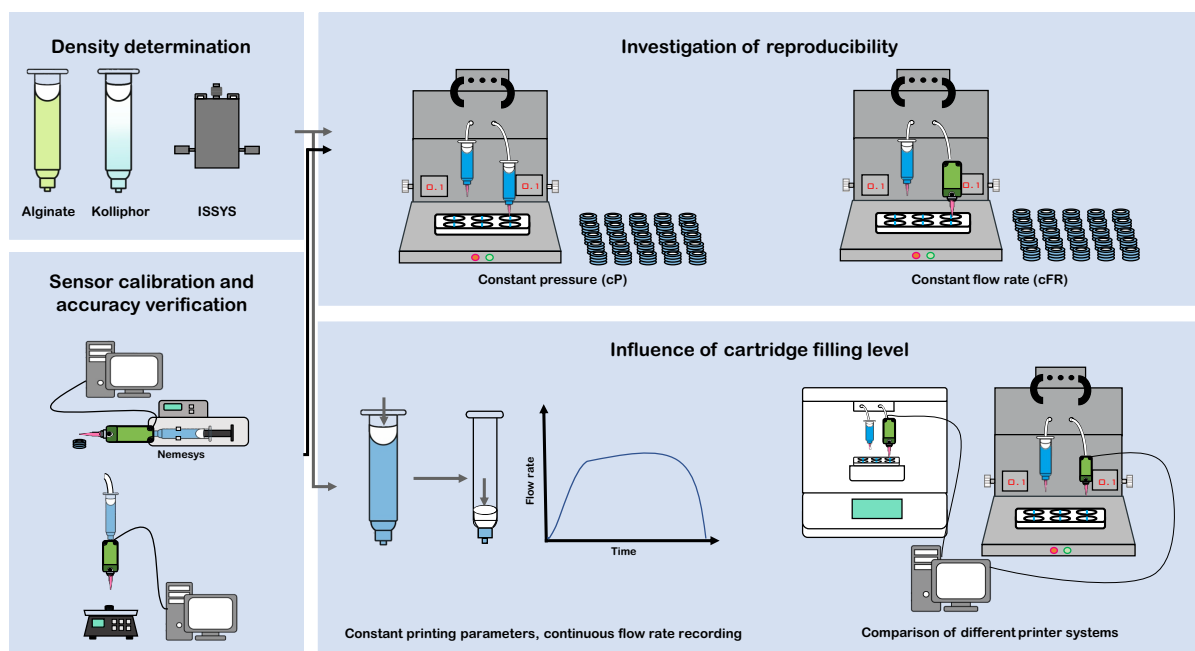
Chapter 4

Evaluation of the Reproducibility and Robustness of Extrusion-Based Bioprinting Processes Applying a Flow Sensor.....51

Svenja Strauß, Bianca Schroth and Jürgen Hubbuch

published in Frontiers in Bioengineering and Biotechnology, Volume 10, 2022, Article 831350

<https://doi.org/10.3389/fbioe.2022.831350>



This study investigates the reproducibility for one bioprinter system using a liquid flow meter and simultaneously inspects flow rate as a suitable printing parameter to increase bioprinting process robustness. This approach is expected to be able to compensate for system and environmental deviations and allow for more comparability. At first, alginate and Kolliphor densities are determined which are required for volume calculation of printed cylinders based on the sensor data. In a following assessment, the sensor accuracy is verified by comparing cylinder volumes calculated based on flow sensor data with data determined via gravimetric methods. The reproducibility is tested in two different setups in which three cylindrical samples are printed in six runs each. In the first approach, the extrusion pressure is kept constant (cP) as pressure printing parameter, and in the second approach, the extrusion pressure is previously adjusted until a constant flow rate (cFR) is reached by using the flow meter as a calibration tool. The results are compared and statistically evaluated. In a further examination, it is tested whether the filling level within a cartridge has an impact on the consequential flow rate. For this purpose, a cartridge is completely emptied and the flow rate is recorded with the sensor. This is done for alginate and Kolliphor in varying concentrations

and also on two different printer systems to see if the printer systems are comparable with regard to intersystem transferability. This study demonstrated that there is a multitude of influencing parameters in bioprinting that affect the flow rate and therefore by controlling the flow rate rather than the extrusion pressure the robustness can be increased. Furthermore, it is indicated that the filling level within the cartridge has an influence on the flow rate when the extrusion pressure is kept constant for pneumatic systems.

Chapter 5

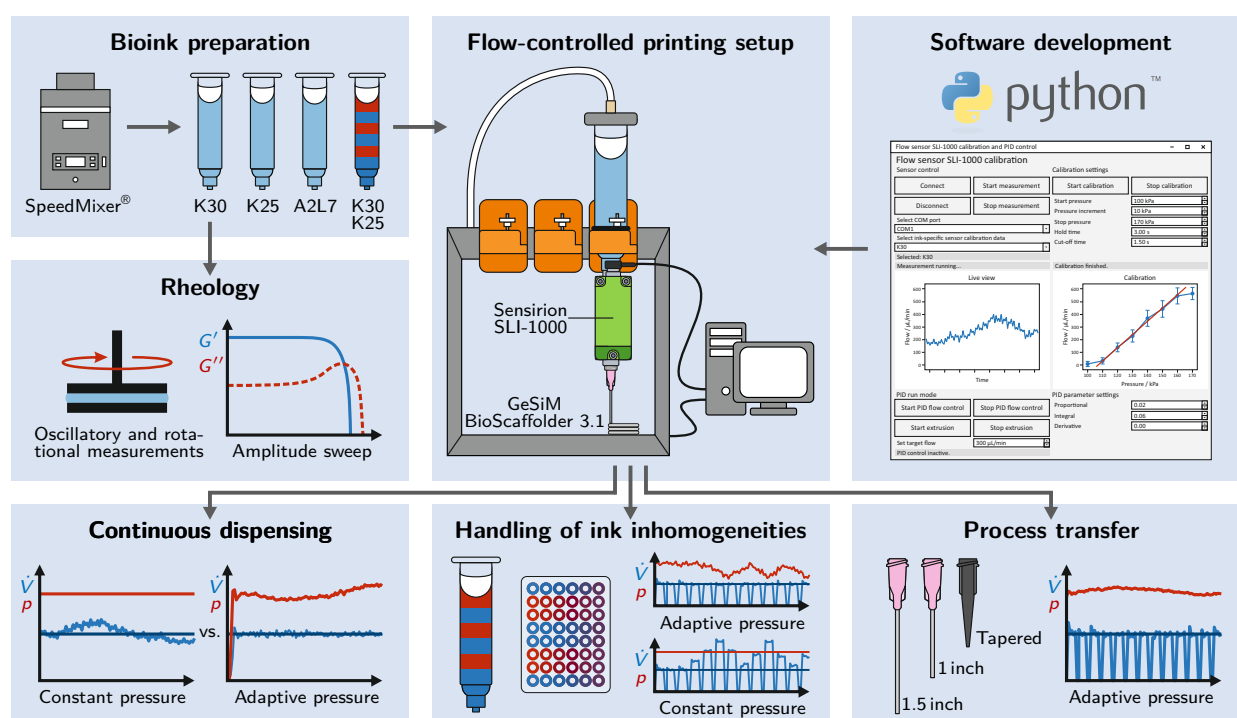
Automated and Dynamic Extrusion Pressure Adjustment Based on Real-Time Flow Rate Measurements for Precise Ink Dispensing in 3D Bioprinting.....75

Lukas Wenger*, Svenja Strauß* and Jürgen Hubbuch

* contributed equally

published in *Bioprinting*, Volume 28, 2022, e00229

<https://doi.org/10.1016/j.bprint.2022.e00229>



The previous study has shown the feasibility of a flow rate-based process control to improve the reproducibility, so the next logical step is to automate the process control. This offers the advantage to save lengthy and subjective parameter screenings and to be suitable for a wide range of materials. In this study, a python-based software control is established which processes real-time data and reacts dynamically to changes. This is realized by adjusting the extrusion pressure in a PID feedback loop so that the flow rate is kept constant. The setup is tested using three different materials and in three case studies. The general performance is evaluated by dispensing continuously from one cartridge. The reaction to ink inhomogeneities is simulated by extruding from a cartridge which is intentionally filled with layers that have different viscosities. Process transferability is tested by using different nozzles with different geometries. This study points out one possible way to implement the currently missing process monitoring for bioprinting.

This study was carried out mutually with Lukas Wenger and all experimental planning was mutually agreed. Lukas Wenger focused on the programming of the PID control, while I performed the

rheological investigations. The experiments for the case studies were carried out and analyzed in cooperation. Graphical illustration, drafting the manuscript and revising the manuscript critically was done in collaboration. All authors read and approved the final script.

Chapter 6

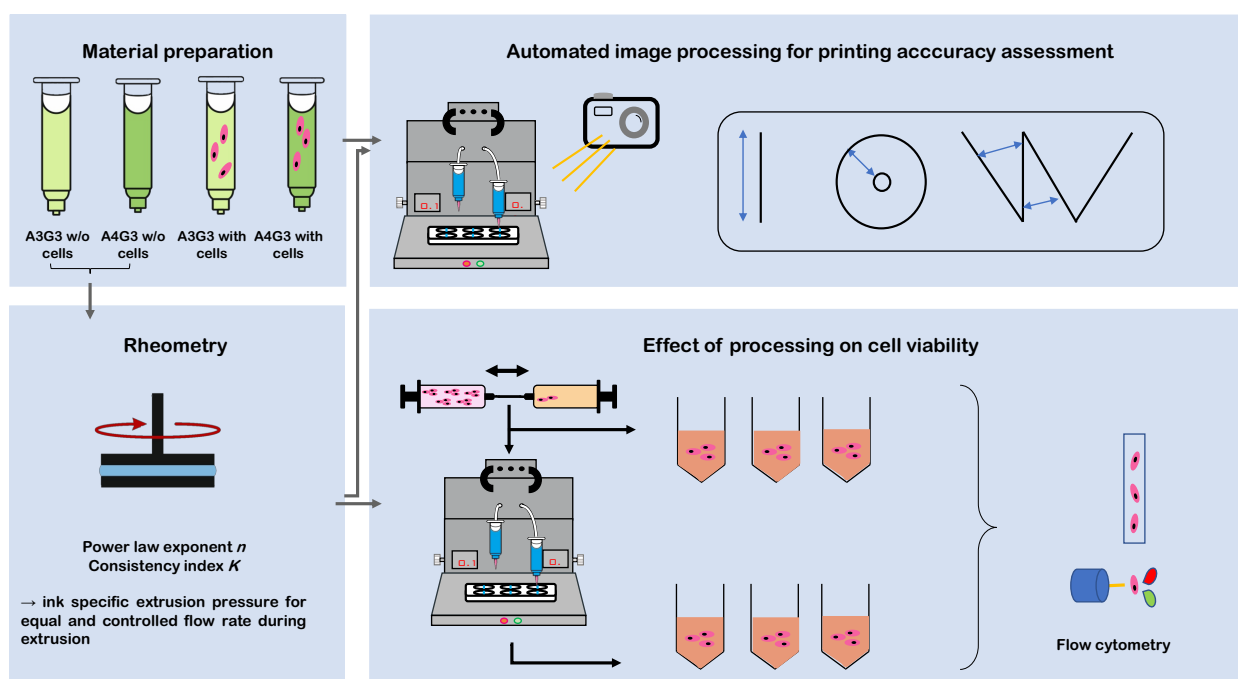
Analytics in Extrusion-based Bioprinting: Standardized Methods improving Quantification and Comparability of the Performance of Bioinks 103

Svenja Strauß*, David Grijalva Garces* and Jürgen Hubbuch

* contributed equally

published in Polymers, Volume 15(8), 2023, 1829

<https://doi.org/10.3390/polym15081829>



This study describes the standardization of flow rate control based on the specific flow behavior of bioinks. With the knowledge of the nozzle geometry and without installation of additional equipment the parameter screenings can be omitted while increasing reproducibility and objectivity. Viscosities for two polymeric solutions based on mixture of alginate and GelMA, which differ in 1% (w/v) alginate content, are investigated as a function of shear rate. After fitting according to Ostwald-de Waele relationship, the power law exponent n and the consistency index K were determined. The Hagen-Poiseuille equation for cylindrical capillaries is used to calculate the necessary pneumatic pressure for both formulations. Subsequent, a printing performance assessment is performed for both formulations, with and without cells. Lines, circles, and angle structures are printed, photographed and analyzed via image processing. The production of functional tissue structures requires not only printable materials, but also a manufacturing process in which cell viability remains high and the cells are not affected by shear stress. To gain process knowledge, cell viability is determined after

the mixing step when cells are introduced into the polymeric solutions and after extrusion through the bioprinter. Therefore, the cells are stained and analyzed with flow cytometry which allows the analysis of a high number of cells. This study demonstrated that the increase of 1% (w/v) alginate content had little impact on printing accuracy, however, had a significant impact on cell viability after both, the mixing and extrusion step.

In order to enhance the quality of this research and to carry out printing performance evaluations with cell containing bioinks, a cooperation with David Grijalva Garces was carried out. The experimental procedure was planned together. David Grijalva Garces worked on the cell culture and the cell analytics. My focus was the expansion of the image processing toolbox as workflows developed in Matlab[®]. Data evaluation, visualization and writing the main draft was done jointly. All authors read and approved the final script.

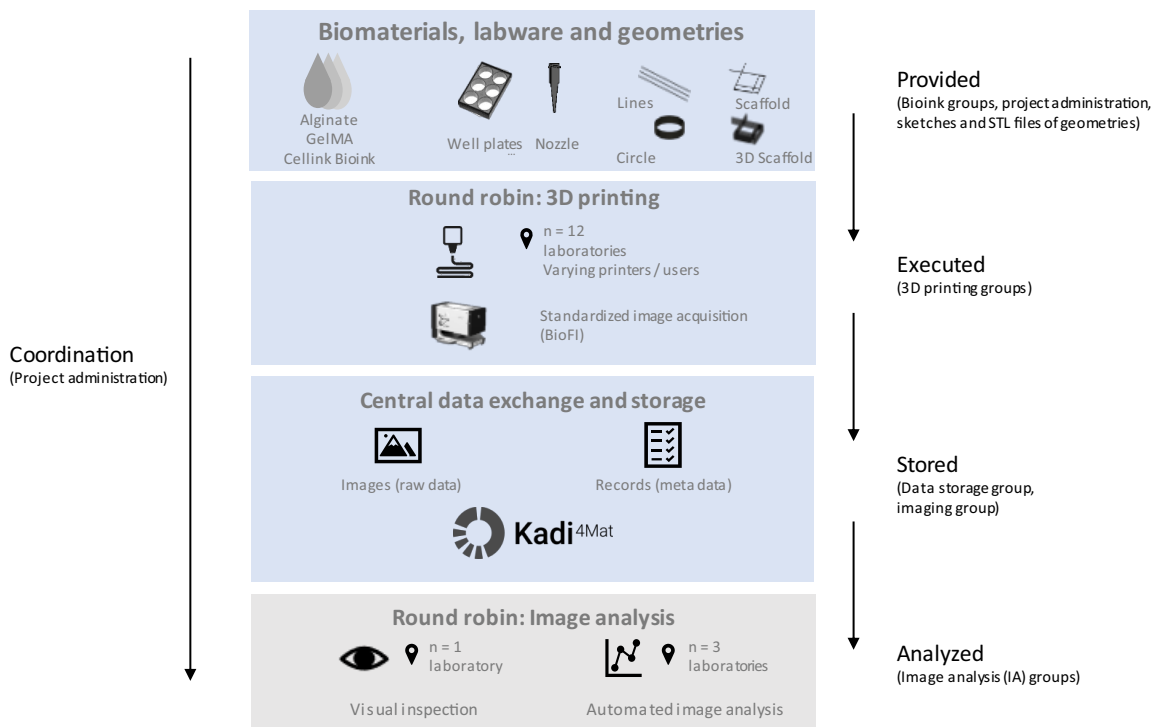
Chapter 7

On the Reproducibility of extrusion-based Bioprinting: Round Robin Study on Standardization in the Field 125

David Grijalva Garces*, Svenja Strauß*, Sarah Gretzinger, Barbara Schmiege, Tomasz Jüngst, Jürgen Groll, Lorenz Meinel, Isabelle Schmidt, Hanna Hartmann, Katja Schenke-Layland, Nico Brandt, Michael Selzer, Stefan Zimmermann, Peter Koltay, Alexander Southan, Günter Tovar, Sarah Schmidt, Achim Weber, Tilman Ahlfeld, Michael Gelinsky, Thomas Scheibel, Rainer Detsch, Aldo R. Boccaccini, Toufik Naolou, Cornelia Lee-Thedieck, Christian Willems, Thomas Groth, Stephan Allgeier, Bernd Köhler, Tiaan Friedrich, Heiko Briesen, Janine Buchholz, Dietrich Paulus, Anselm von Gladiss and Jürgen Hubbuch

* contributed equally

published in *Biofabrication*, Volume 16(10), 2023, 015002
<https://doi.org/10.1088/1758-5090/acfe3b>



As there are no empirical data available on the reproducibility of bioprinting processes, this nationwide round robin study serves to depict how comparable identical structures can be printed independently of laboratory and operator. While preparing this study, all materials and process

steps have been standardized as far as possible. This includes in explicit the writing of SOPs for bioink preparation and setting printing parameters. An infrastructure is established for the upload of experiment records and the image storage. The images are taken standardized using a specially developed imaging device. Four structures are printed in 12 academic laboratories for three materials in three replicates. All images are analyzed qualitatively to identify which deviation occur and to what extent. In a subsequent quantitative analysis, the evaluable structures are analyzed via image processing by three independent groups. This study led to the conclusion that it was not yet possible to receive similar results. However, the identification of weaknesses and the establishment of an infrastructure for distribution of material and methods, for data transfer and storage paves the way to accelerate standardization in the bioprinting field. Automated image processing turned out to be a suitable methodology for quality assurance.

The project presented here was a collaborative project between KIT and 10 further research institutions. The data was generated by laboratories in subcontracts as well as in our laboratory. The KIT team consisted of Sarah Gretzinger, Barbara Schmiege, David Grijalva Garces, Svenja Strauß and Jürgen Hubbuch. Sarah Gretzinger, Barbara Schmiege and Jürgen Hubbuch focused on the administrative and organizational work. The publication of the manuscript was performed as a collaboration between David Grijalva Garces and me. Data evaluation, visualization and writing of the manuscript were done by David Grijalva Garces and me. Additionally, the communication for the review of the manuscript by all authors as well as the coordination of the submission process were conducted by David Grijalva Garces and me. All authors read and approved the published version of the manuscript.

3

Image Analysis as PAT-Tool for Use in Extrusion-Based Bioprinting

Svenja Strauß¹, Rafaela Meutelet¹, Luka Radosevic¹, Sarah Gretzinger^{1,2} and Jürgen Hubbuch^{1,2}

¹ Institute of Functional Interfaces, Karlsruhe Institute of Technology (KIT), Eggenstein-Leopoldshafen, Germany

² Institute of Process Engineering in Life Sciences, Section IV: Biomolecular Separation Engineering, Karlsruhe Institute of Technology (KIT), Karlsruhe, Germany

3.1 Abstract

The technology of bioprinting is arousing a growing interest in biopharmaceutical research and industry. In order to accelerate process development in the field of bioprinting, image-based analysis methods are non-invasive, time- and cost-saving tools which are usable for printer characterization, bioink printability evaluation, and process optimization. Image processing can also be used for the study of reproducibility, since reliable production is important in the transition from research to industrial application, and more precisely to clinical studies. This study revolves around the establishment of an automated and image-based line analysis method for bioprinting applications which enables an easy comparison of 3D-printed lines. Diverse rheological properties of bioinks and the printing process affect the geometry of the resulting object. The line represents a simple geometry, where the influence of the rheological properties and printing parameters is directly apparent. Therefore, a method for line analysis was developed on the basis of image recognition. At first, the method is tested for several substances such as Nivea[®], pure and colored Kolliphor solutions, and two commercially available hydrogel formulations which can be used as bioinks. These are Biogelx[™]-ink-RGD by Biogelx and Cellink[®] Bioink by Cellink. The examination of limitations showed that transparent materials such as Kolliphor-based solutions cannot be analyzed with the developed method whereas opaque materials such as Nivea[®] and both bioinks can be analyzed. In the course of process characterization, the method was used to investigate the shrinkage behavior for both bioinks. With the help of the line analysis tool, a shrinkage behavior of both bioinks was demonstrated and thus, process time could be identified as a critical process parameter.

3.2 Introduction

In recent developments, bioprinting is arising in the field of regenerative medicine (RM) and tissue engineering (TE) [110, 111]. The use of 3D-printing technology allows additive manufacturing (AM) of artificial tissues in a layer-by-layer deposition of materials containing cells [112]. These artificial tissues are promising for patient-specific implants which can be employed as tissue replacement or as drug delivery systems [113]. Furthermore, tissue models can be used for clinical and pharmaceutical studies as they are mimicking natural living conditions [114, 115].

The lack of tissue-specific bioinks with suitable properties represents a major issue in development [116]. On the one hand, bioinks have to be optimized in terms of printability and shape accuracy. On the other hand, mild conditions must be guaranteed, as the bioink contains cells and biological material [117]. Due to their high water content, bioinks mainly consist of hydrogels which are water-containing but water-insoluble polymers whose molecules are crosslinked to form a three-dimensional network. The network can be designed for immobilization of cells and biologic macromolecules, while enabling diffusion of substrates and products [118, 119]. Therefore it is important to know and control the width of a printed element to avoid mass transfer limitations in printed systems containing cells [120]. The used polymers can be either synthetic, such as polyethylene glycol (PEG), or of natural origin [121, 122]. Natural polymers can be divided into polymers of polysaccharides (like alginate, chitosan, dextran, and hyaluronic acid) and protein-based polymers (like gelatine and collagen) [123–129]. It is assumed that natural polymers have a good biocompatibility and do not trigger an inflammatory reaction of the immune system [130]. Depending on the application, hydrogels are modified, e.g. by incorporation of ligands and copolymers. This allows a better control of the number and size of meshes, biodegradation, and cell adhesion [131–134]. The different origins

and modifications result in diverse optical properties of the hydrogels from completely transparent like gelatine to opaque and white [135].

In addition, each specific tissue has different requirements, e.g., mechanical integrity and stability, and a universal bioink is most likely not to be found [112].

A general problem is the absence of standardized analytical methods to simplify the comparability and selection of bioinks. For bioink characterization, rheological measurements have been established to determine the printability and behavior during extrusion [14, 136–138]. However, the exact printing parameters cannot yet be derived from the rheological properties. Bioprintability is classified by checking the bioprinted object in comparison to the given computer-aided design (CAD) model [139, 140]. Another rather qualitative approach is to use overhanging structures to test filament collapse and to compare the degree of strand fusion of parallel printed filaments [141]. These examinations are carried out offline and sometimes take a long time, so that no high-throughput analysis is possible. Image-based methods offer other options as they evaluate large data sets automatically. Online monitoring with a camera system is also conceivable. The analysis of images cannot only be used for classifying the printability of bioinks, but also for printer characterization and printing process optimization in a standardized way.

Image processing is widely used for quality inspection in production processes in several industries such as the printing and packaging industry and the automotive industry, and also, medical image processing is used for diagnostic purposes [142, 143].

In the field of 3D-printing, image analysis is already being investigated for characterization of the strands generated by melt electro writing [144]. The printability and shape accuracy of bioinks is often evaluated by analyzing the shape of an extruded strand and measuring the widths and angles of extruded objects after bioprinting [139, 145–147]. The measurement takes place individually and manually by marking the widths in a software [148]. Consequently, these methods are susceptible to differences when used by different users. Even simple line width determination is prone to errors as the width can be influenced by the local measurement point at which it is measured because not all lines must have constant widths at every position. In the light of the above and even though we are standing on a new aera of bioprinting as a production and formulation tool in the fields of regenerative medicine (RM) and tissue engineering (TE) [110, 111] process analytics are not present or ready for it.

The aim of this study is to establish an automated image-based line analysis tool which measures line width, length, and area based on images of extruded bioink strands in a standardized way, where line width measurements are only possible within a defined stable area. The intention is to establish a method which can be used to recognize the impact of changes in bioink formulation, in printer systems, and on the outcome of printing processes. This PAT-tool was then used to measure the shrinkage behavior of bioinks to evaluate if the process time is a critical process parameter as bioinks might dehydrate over time.

3.3 Materials and Methods

3.3.1 Bioprint substances and bioink preparation

Syringes including pistons were ordered from Nordson Corporation (Westlake, USA) and six-well glass bottom plates were purchased from IBL Baustoff + Labor GmbH (Gerasdorf, Austria). Conical 25 G nozzles were obtained from Cellink (Gothenburg, Sweden). As printed substances, Nivea® Creme by

Beiersdorf AG (Hamburg, Germany) and a solution of 30 % (w/w) Kolliphor P 407 (Sigma-Aldrich, USA) dissolved in ultrapure water (arium[®] pro VF, Satorius AG, Göttingen, Germany) were used. Two commercially available bioinks, namely Cellink[®] Bioink (Cellink, Gothenburg, Sweden) and Biogelx[™]-ink-RGD (Biogelx Ltd, Newhouse, United Kingdom) were also printed. According to manufacturer specification, 149 mg bioink powder were dissolved in 2.25 ml of the kit’s solution B and were kept in the refrigerator over night at 4 °C. Then, the solution was mixed with 1.25 ml of Dulbecco’s Modified Eagle’s Medium (DMEM) (ThermoFisher Scientific, Waltham, USA) and incubated for 2 h at 37 °C.

30 % (w/w) Kolliphor solution as base and manufactured as described in the upper section was colored with different dyes to increase contrast. Therefore, a solution of 2.5 % (w/w) red powder food coloring (Brauns Heitmann GmbH & Co. KG, Warburg, Germany), a solution of 2.5 % (w/w) red paste-like food coloring (Dr. August Oetker Nahrungsmittel KG, Bielefeld, Germany), and a solution with a spike by Sicopharm Cochineal Red (BASF, Ludwigshafen, Germany) were produced.

3.3.2 Bioprinting process

All 3D-printing experiments were carried out with a pneumatic extrusion-based bioprinter 3D Discovery[™] provided by regenHU company (Villaz-St-Pierre, Switzerland). With the BioCAD software (regenHU, Villaz-St-Pierre, Switzerland), 3 cm long lines were designed and printed in each well of a six-well plate. The respective printing parameters of materials are listed in table 3.1.

Table 3.1 Printing parameters of the respective materials. Pure and all colored Kolliphor-based solutions were printed with similar parameters.

Parameter	Nivea	Kolliphor hydrogels	Cellink Bioink	Biogelx-ink-RGD
Pressure [MPa]	0.33	0.13	0.03	0.025
Speed [mm/s]	30	10	10	10
Layer height [mm]	0.1	0.1	0.1	0.1
Offset [mm]	0.05	0.05	0.05	0.05

3.3.3 Image processing

Images of the printed lines were taken using the microplate reader Spark[®] provided by Tecan Group AG (Männedorf, Switzerland), and each well was measured using the cell confluence method in the SparkControl Software[™] (Tecan Group AG, Männedorf, Switzerland). Two image files were generated as output files. One has already been analyzed by the software and one is comparable to a stitched microscope image in grayscale which was imported into Matlab[®] R2019a (TheMathWorks, Natick, USA) for further study. The image processing sequence is shown schematically in Figure 3.1 a).

Before processing the images, the file directory is chosen, the reference width which is equal to the nozzle diameter and the conversion factor from pixel to millimeter are imported. The image processing is shown by an example image in Figure 3.1 b). Initially, the original image is read in and converted into a binary image. Then, the image is segmented by deleting small objects, clearing the borders and detecting the object. As the limitations of the method were also investigated and this is a critical step, a user query was here introduced. After the user’s confirmation of correct line

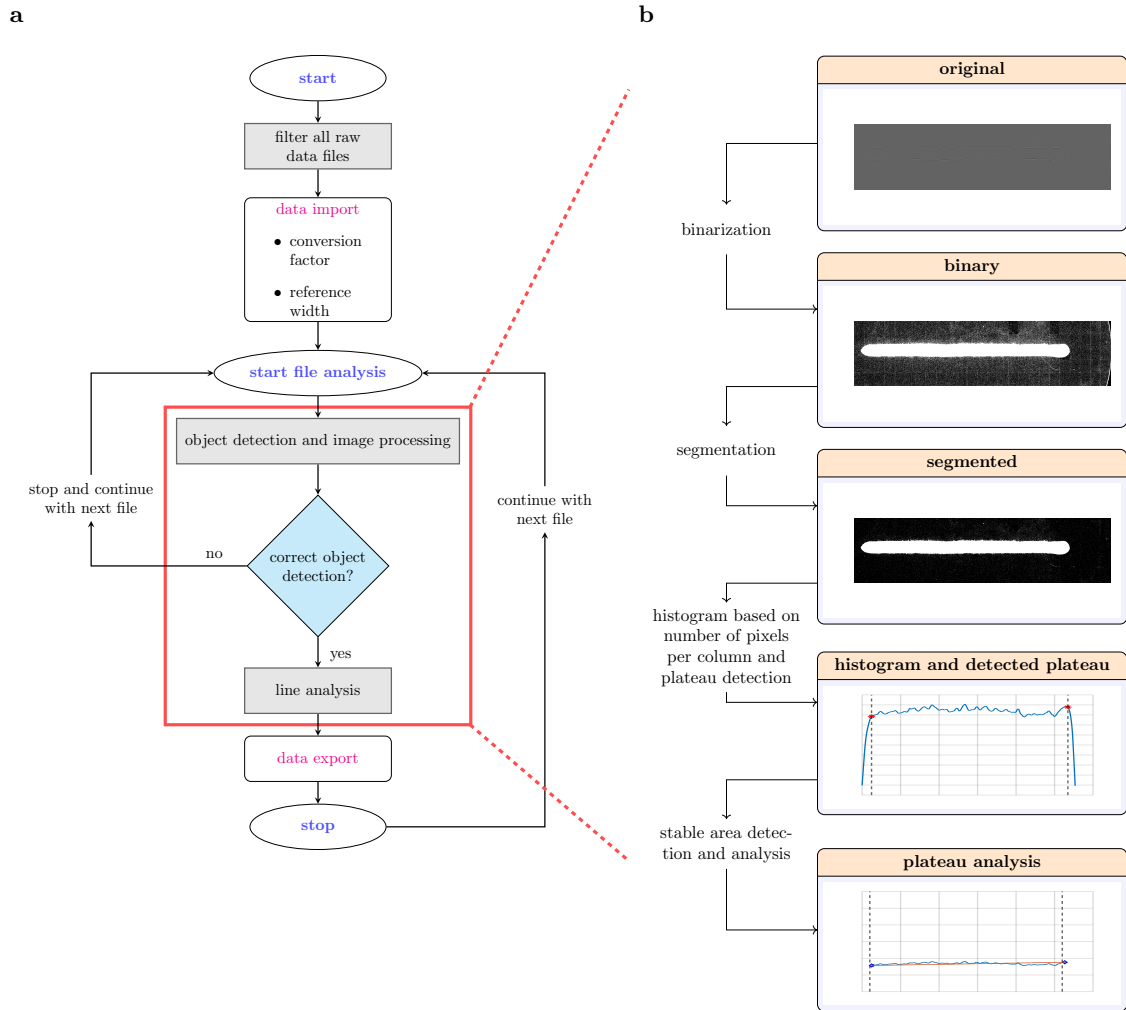


Figure 3.1 Overview of the data and image processing: a) represents a schematic flow chart of data processing. At first, raw image files are filtered and application-specific parameters are imported. Each file is analyzed individually in a loop in which the user has to confirm or deny correct object detection. In the case of correct object detection the actual line analysis starts. At the end, all results are saved and exported for each file.

b) shows exemplarily the image processing: The original image is converted to binary, the image is segmented, and small objects are deleted. Then, a histogram is created by counting and converting pixels per column. Area and length can be determined. Line width is only determined if a plateau containing a stable area is found.

detection, the actual line analysis starts. At first, a histogram is created by counting white pixels for each column and by converting them in millimeters. The length is calculated as the number of white pixel columns and the area is determined as the conversion of the sum of all white pixels in all columns as described in Equations 3.1 and 3.2.

$$length = number\ of\ columns\ containing\ white\ pixels \cdot conversion\ factor \quad (3.1)$$

$$area = \sum white\ pixels \cdot conversion\ factor^2 \quad (3.2)$$

In order to measure the width, the corner points in the first and last third of the histogram are recognized and the distance between the corner points is isolated as a plateau. This plateau will be further examined if there is a stable area which is useful for a line width determination. The plateau is divided into 10 parts and for each section, the slope, which is ideally 0, is calculated individually. A tolerance criterion was introduced; it is shown in Equation 3.3.

$$tol = \frac{\frac{deviation}{l}}{reference\ width} \quad (3.3)$$

The tolerance (tol) is defined as the permitted percentage deviation of the reference width per the length of one millimeter strand (l). Consequently, the tolerance is dependent on the nozzle diameter and is higher with a bigger diameter. A deviation of 3% was used, and the reference width corresponds to the nozzle diameter of 0.26 mm. As long as the slope of the section was within this tolerance, the section extended constantly to both sides and the slope was calculated for each extension until the criterion was no longer met or the edge was reached. If the length was greater than 5 mm, it was determined as a stable area and the line width was calculated by averaging the values of the section. Otherwise, the line was not considered constant and a line width determination was not possible.

3.3.4 Shrinkage study

Three cartridges by Cellink® Bioink and Biogelx™-ink-RGD (n=3) were prepared on three different days for investigating the drying and shrinkage behavior of bioinks. Each cartridge was used for printing in each well of one six-well plate (n=6) so that in total 18 lines were printed for each bioink. A schematic representation is shown in figure 3.2.

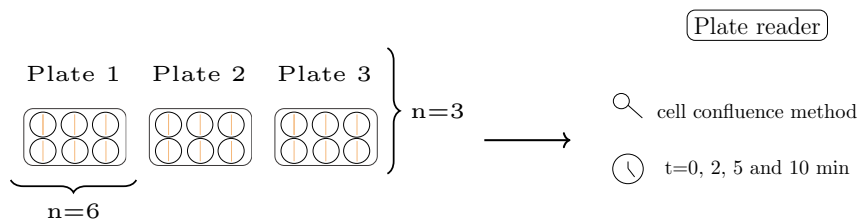


Figure 3.2 Schematic process of the shrinkage study: 3 cartridges were prepared as biological replicate (n=3) and with each cartridge one plate was printed containing 6 lines as technical replicate (n=6) so that in total 18 lines were printed for Cellink® Bioink and Biogelx™-ink-RGD. The plates were analyzed by the cell confluence method in the multimode plate reader after 0, 2, 5, and 10 min.

The plates were analyzed after 0, 2, 5, and 10 min as described in Section 3.3.3.

3.3.5 Data analysis and statistical analysis

Data evaluation, image processing, statistical data analysis, and visualization were done with Matlab® R2019a (TheMathWorks, Natick, USA). In the case of failed object detection, data were examined for outliers and these were removed if they deviated from the median by more than three scaled mean absolute deviations. All results for one property obtained from one plate were checked for normal distribution using the Anderson-Darling test, and one-way analysis of variance (ANOVA) was performed. An additional repeated-measures ANOVA was carried out during the examination of shrinkage behavior. Here, ANOVA was between the values for each point of time with time zero for each property of each plate. For all ANOVA investigations, α was set to 0.05 and a p-value below 0.05 was classified as statistically significant.

3.4 Results

3.4.1 Line analysis tool

In order to simplify the systematic process development in the field of 3D-bioprinting, the line analysis tool was established which enables a reproducible and automated analysis. At first, the applicability for bioinks with different optical properties was examined. It was started using Nivea® as a model ink with good optical properties, followed by experiments with Cellink Bioink due to its opaque appearance and due to the fact that it is a real bioink. Then, Biogelx™-ink-RGD was tested as it is more transparent and finally completely transparent Kolliphor solution was assessed. The results of Nivea® lines are shown in Figure 3.3.

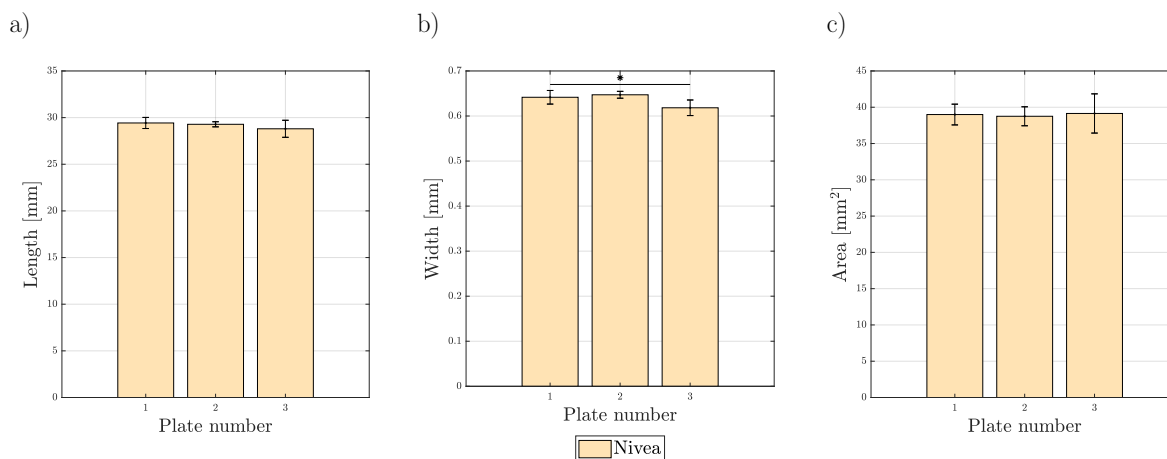


Figure 3.3 Results of the analysis of 3 cm long printed lines with Nivea®. Length (a)), width (b)), and area (c)) were determined via image processing. Three plates were printed with six lines each ($n=6$) resulting in 18 lines in total and compared as biological triplicates. Statistical significance (one-way ANOVA) was found for the width of the lines ($p=0.007$).

In each well of a six-well plate, a line was printed ($n=6$) and was examined for length, width, and area. This was done for three plates so that in total, 18 lines were analyzed. Shown is the mean of

length, width, and the area for each plate with standard deviation. The mean length is 29.1 mm (+/- 0.2 mm), and the mean area is 38.9 mm² (+/- 0.3 mm). Both properties are comparable for all three plates and not statistically significant. A statistical significance was found with a p-value of 0.007 for the width. The mean width of 0.64 mm by plate three differs from the mean value of 0.61 mm of plate one and plate two.

Experiments using the more opaque Cellink[®] Bioink and the more transparent Biogelx[™]-ink-RGD also showed a successful line detection and analysis. These two bioinks have been examined in more detail; the results are shown in Section 3.4.2. Kolliphor is a polymer which forms a completely transparent hydrogel after being dissolved and this hydrogel was also tested. Here, the object detection failed. In a subsequent approach, the contrast of Kolliphor solution was increased in three approaches with food coloring powder, paste, and Cochineal Red. The lines of these three approaches were also wrongly identified during image processing. The results are summarized in Table 3.2. A table showing exemplary pictures of typical detection and misdetection for the different materials can be found in the supplementary data.

Table 3.2 Results of the line detection feasibility study with four bioinks.

Material	Correct line detection
Nivea [®]	✓
Pure Kolliphor solution	×
Kolliphor with food coloring powder	×
Kolliphor with food coloring paste	×
Kolliphor with Cochineal Red	×
Cellink Bioink	✓
Biogelx-ink-RGD	✓

3.4.2 Shrinkage study

Hydrogels have a high water content and over time, the water evaporates. The evaporation becomes visible by the shrinking of the bioprinted structures. The larger an object, the longer the printing time. Hence, it may start to shrink while it is still in production. A shrinkage study was conducted using the line analysis tool with Cellink[®] Bioink and Biogelx[™]-ink-RGD to assess whether the process time is a critical process parameter. The bioinks were chosen as both are already commercially available and are based on different materials. In addition, the results at time t=0 min were compared to investigate the reproducibility of the printing process. For each bioink, lines were printed in each well of a six-well plate (n=6) and this was done as triplicate (n=3) on three different days. In total, 18 lines per ink were printed and analyzed for t=0, 2, 5, and 10 min. For each point of time, the mean values for length, width, and area for each plate were calculated. The analysis of the lines directly after printing is shown in Figure 3.4 a)-c) and the results for Biogelx[™]-ink-RGD are displayed in d)-f). Based on the results, the reproducibility of the printing process was statistically examined.

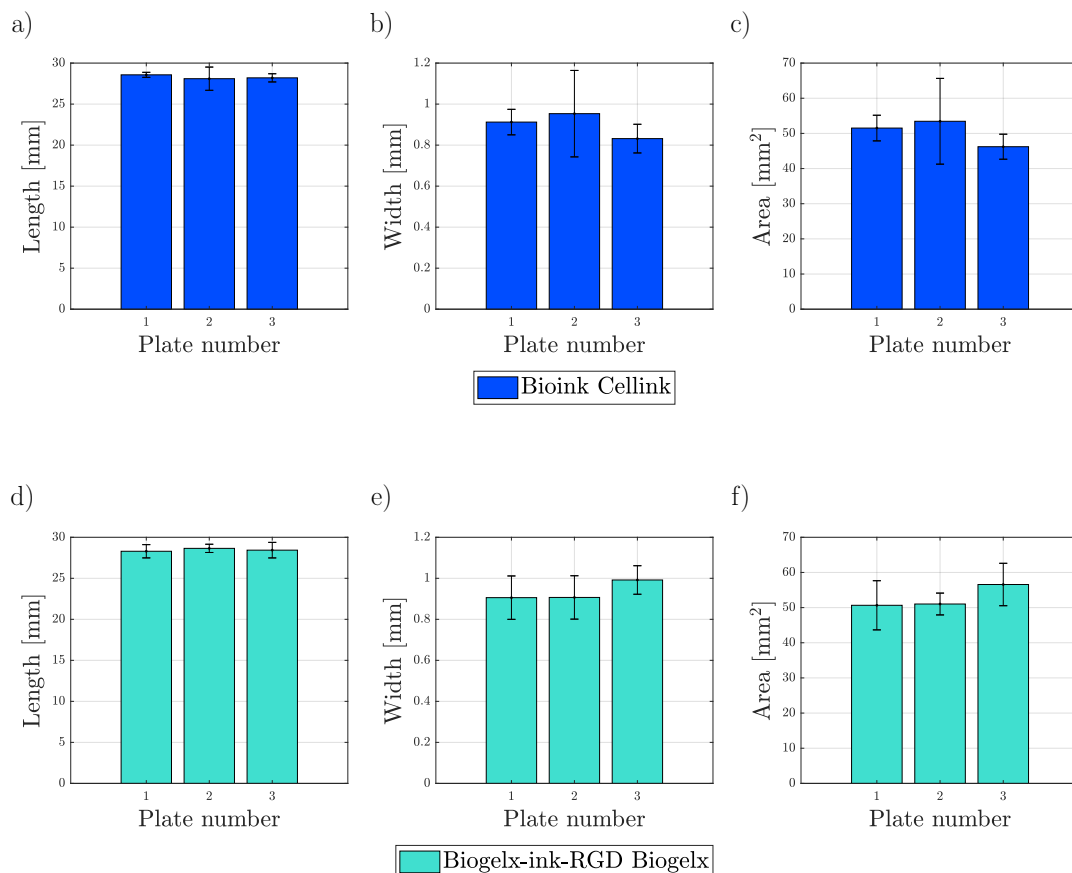


Figure 3.4 Results of the analysis of 3 cm printed long lines in a)-c) with Cellink[®] Bioink and in d)-f) with Biogelx[™]-ink-RGD. Length, width, and area were determined via image processing directly after printing ($t=0$ min). The experiment was run as triplicate on three different days ($n=3$) where one plate was printed. Six lines ($n=6$) were printed on each plate, resulting in 18 lines in total, and no statistical significance (one-way ANOVA) was found for any property.

The means of length, width, and area with standard deviation are plotted in a separate bar chart. The values were calculated based on the six lines of each plate at $t=0$ min and the results of the three plates are shown side by side for the respective properties. The results are visualized in a)-c) for Cellink[®] Bioink and in d)-f) for Biogelx[™]-ink-RGD.

The mean length for Cellink[®] Bioink is plotted in a). The maximum length is 28.56 mm and the minimum length is 28.56 mm. The mean width for Cellink[®] Bioink is from maximum 0.95 mm to minimum 0.83 mm. The maximum mean area is 53.44 mm² and the minimum is 46.21 mm². The values are comparable and during one-way ANOVA, no statistical significance was found.

For Biogelx[™]-ink-RGD, the averages of plates one and two were calculated based on five lines, because object detection failed for one line. In d), the length of Biogelx[™]-ink-RGD is in the range of

minimum 28.29 mm to maximum 28.65 mm. The mean width is maximum 0.99 mm and minimum 0.9 mm. The maximum mean area is 6.57 mm² and the minimum mean area is 50.66 mm²). Both, width and area, are higher in plate three than in plates one and two. For all three properties, the p-value was higher than 0.05 and no statistical significance (one-way ANOVA) was observed.

To observe the shrinkage behavior of the bioinks, the same lines were again analyzed for all three properties using the identical method after two, five, and ten minutes. The results are presented in Figure 3.5 for Bioink and in Figure 3.6 for BiogelxTM-ink-RGD. For each plate length, width, and area are plotted as mean values of the six lines with associated standard deviation for the respective points in time. Here, each plate is shown in a separate row.

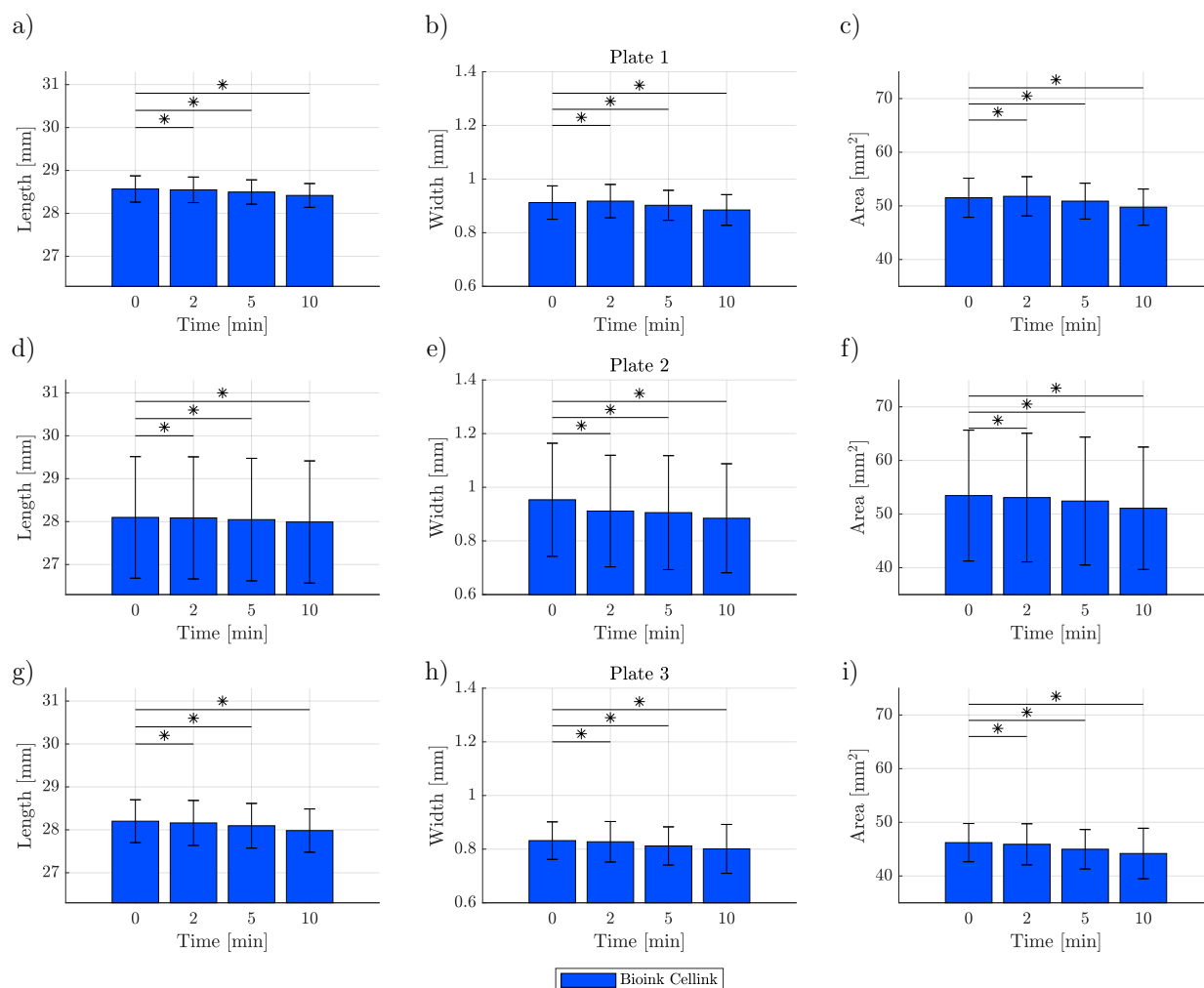


Figure 3.5 Results of the analysis of 3 cm printed long lines with Cellink® Bioink. Six lines were printed per plate (n=6) and the experiment was run as triplicate with three plates (n=3) printed on three different days resulting in 18 lines in total. Length, width, and area were determined via image processing for different points in time (t=0, 2, 5, and 10 min). The results for plate one are shown in a)-c), for plate two in d)-f), and for plate three in g)-i). For length, width, and area, a repeated measures ANOVA analysis of all three plates showed statistical significance with p-values below 0.005.

In general, the results shown in Figure 3.5 reveal in all properties a declining trend which means that the size is shrinking with time. The standard deviation on plate two is a factor of three times higher in comparison to the other two plates. A repeated-measures ANOVA was performed for every property for all plates where mean values of the points of time were compared to time zero. For all data sets a statistical significance was found with p-values below 0.005. The statistical significance between the data sets is marked with an asterisk in the figure.

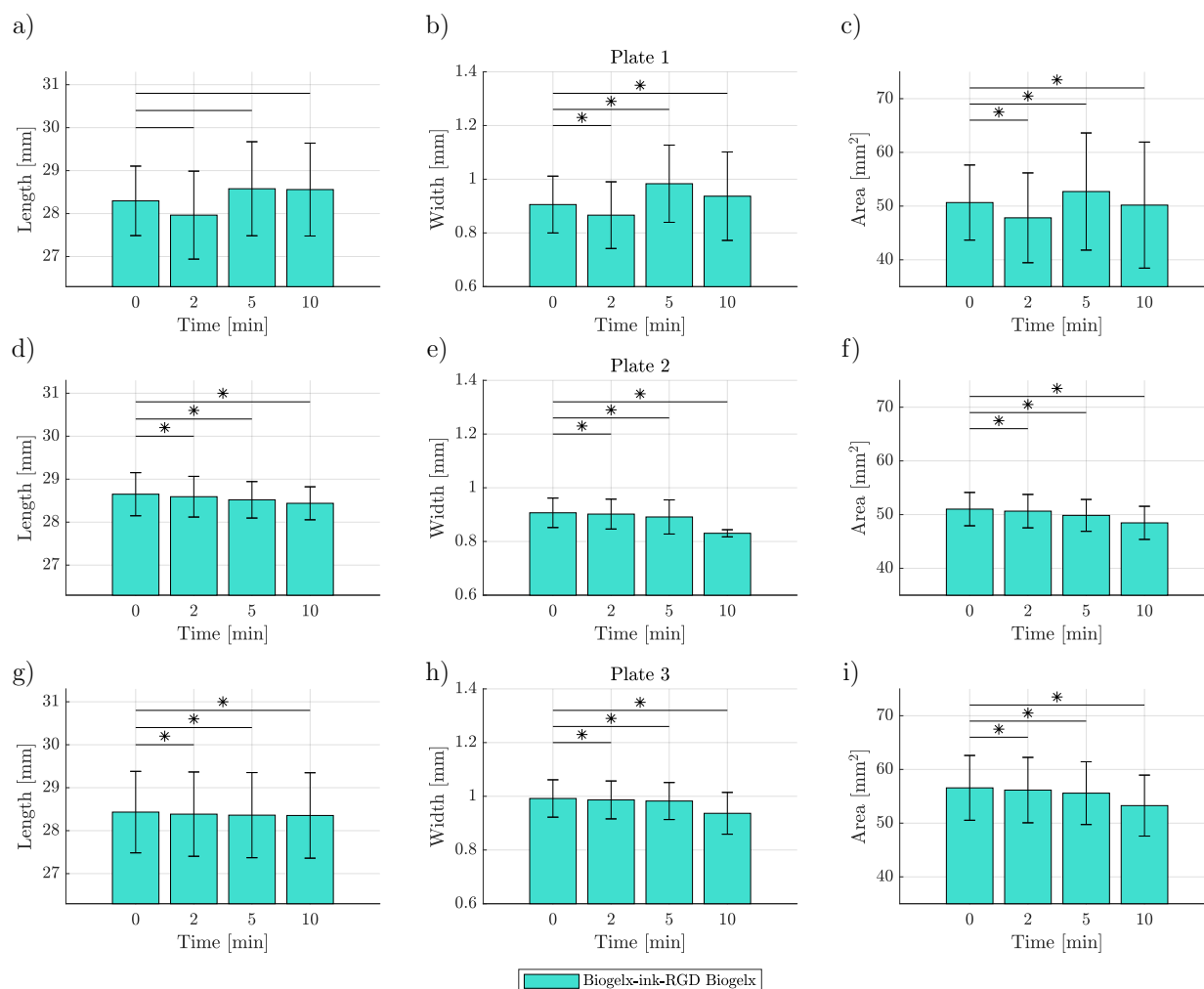


Figure 3.6 Results of the analysis of 3 cm long printed lines with Biogelx™-ink-RGD (n=6). Six lines were printed per plate (n=6) and the experiment was run as triplicate with three plates (n=3) printed on three different days resulting in 18 lines in total. Length, width, and area were determined via image processing for different points in time (t=0, 2, 5, and 10 min). The results for plate one are shown in a)-c), for plate two in d)-f), and for plate three in g)-i). Repeated-measures ANOVA analysis of all three plates showed statistical significance with p-values below 0.005. Only the length of the first plate shows no statistical significance with a p-value of 0.437.

In Figure 3.6, the length decreases constantly from 28.64 mm (+/- 0.8 mm) to 28.44 mm (+/- 0.3 mm) for plate two and from 28.43 mm (+/- 0.9 mm) to 28.35 mm (+/- 0.9 mm) for plate three. On the first plate, the length of 28.58 mm (+/- 1 mm) measured after five minutes is higher than that of 27.96 mm (+/- 1 mm) which was measured after two minutes. The same applies to the width. The width of plate two decreases from 0.9 mm (+/- 0.05 mm) to 0.83 mm (+/- 0.01 mm). The highest

mean width was measured for plate three with a width of 0.99 mm (+/- 0.07 mm) which drops to 0.94 mm (+/- 0.08 mm). On plate one, the value of the width measured after two minutes is 0.86 mm (+/- 0.12 mm) and increases to 0.98 mm (+/- 0.14 mm) after five minutes. Also, the highest mean area was measured on plate three which decreased from 56.57 mm² (+/- 6 mm²) to 53.27 mm² (+/- 5.68 mm²) within ten minutes. The mean area of plate two decreases from 51.02 mm² (+/- 3.1 mm²) to 48.47 mm² (+/- 3.08 mm²). On plate one, there is again an increase in the mean area after two minutes from 47.81 mm² (+/- 8.36 mm²) to 52.71 mm² (+/- 10.91 mm²). Except for the length of plate one with a p-value of 0.437, repeated-measures ANOVA analysis of all three plates showed a statistical significance between the data sets with p-values below 0.005. The statistical significance between the data sets is again marked with an asterisk in the figure.

3.5 Discussion

In order to simplify the process development for bioprinting, especially cell based applications where material thickness plays a major role, the image-based line analysis tool was developed to characterize the length, width, and area reproducibly. This tool is intended to make the printing process safer for clinical applications and facilitates the evaluation of printed lines. As automated imaging of 3d-printed objects is not yet possible with the in house tested commercially available cameras incorporated into 3d-printers, images were generated offline. For example one camera is oriented at a certain angle so that an imaging of objects within a well is not possible. Also, the camera's focus is fixed to the needle and it is not possible to take a photo automated after having finished the bioprint. Additionally the quality is not high enough for further image processing. Thus, imaging was done using a multiwell-plate reader as it easily enables an automated imaging for each well with the same method under an identical illumination set up. The developed method is important because it allows the analysis of a simple structure. Each complex geometry can be traced back to a few simple geometries and if already the first layer of an 3d-printed object is defective then this affects the entire 3D structure as the layers no longer adhere properly to one another. Of course, the line analysis is a first step but other structures such as circles and angle accuracy should be analyzed as well. Another possibility is to use the method for the comparison and characterization of bioprinting systems which again is important to increase reproducibility.

At first, the method was tested with model ink Nivea[®] as used as standard or control for pretests in 3d-printing processes [149]. Nivea[®] can be used for pretests without bioactive molecules as it is lacking biocompatibility but as Paxton [14] already argued it "is cheap, has a constant quality and composition, and is an example of a soft colloidal ink. Amongst other products, Nivea Crème, which has been established by bioprinter manufacturing company RegenHU (Switzerland) as demonstration ink, shows very good print fidelity."

On three days, one cartridge was prepared and one plate printed so that the experiment was run as a biological triplicate. An image was taken from each of the six lines of each plate and was imported into Matlab[®] and evaluated using the image processing method. During image processing, all Nivea[®] lines were detected correctly as objects. The line widths showed a statistical significance between the data sets for each plate, which means that they differ from each other, although all lines were printed under the same conditions using identical printing parameters. All line widths are bigger than the nozzle diameter of 0.26 mm due to expansion. The deviations are due to changes within the printer system. The printer system does not work reproducibly and differences in applied

pressure, speed, and offset can occur. Line width is a sensitive parameter in which slight variations are directly visible.

Due to the different compositions of bioinks, they also have different optical properties. Therefore, the limitations of the method were investigated. In the following attempts to analyze lines printed with pure and colored Kolliphor solutions, object detection failed. The reason is the transparency of material which is caused by the high water content of the hydrogel. Light is reflected on the object surface and creates bright areas. During the binarization step, these areas are transferred to white pixels so that the object contour is interrupted and the algorithm recognizes the object only partially. On the other hand, both bioinks, Bioink and Biogelx™-ink-RGD, are more opaque and can again be recognized by the algorithm. They have ingredients that lead to light scattering which prevents light reflections.

As the bioinks have a high water content and the water evaporates over time, the line analysis tool was then applied to investigate whether the process time is a critical process parameter. A shrinkage study was conducted where all lines were analyzed directly after printing and again after 2, 5, and 10 min. In addition, all lines were compared at time $t=0$ min to investigate whether they differ significantly statistically and to evaluate the reproducibility of the printing process. On two plates, one Biogelx™-ink-RGD line was detected incorrectly. Biogelx™-ink-RGD is more transparent than Cellink® Bioink. Thus, again, high transparency leads to fail detection. By comparing the lines right after printing, there was no statistical significance found between the mean data sets of each plate. Especially the lengths of the lines are comparable, as a maximum mean length for Cellink® Bioink was measured to be 28.56 mm (+/- 0.31 mm) and a minimum length to be 28.09 mm (+/- 1.4 mm). The mean length of Biogelx™-ink-RGD was from maximum 28.65 mm (+/- 0.5 mm) to minimum 28.3 mm (+/- 0.81 mm). The width measured with Cellink® Bioink ranges from maximum 0.95 mm (+/- 0.96 mm) to a minimum width of 0.83 mm (+/- 0.99 mm). With Biogelx™-ink-RGD the width varies from maximum 0.99 mm (+/- 0.06 mm) to minimum 0.91 mm (+/- 0.11 mm). Also, the area varies in a range from maximum 56.67 mm² (+/- 6.99 mm) for plate three with Biogelx™-ink-RGD to a minimum area of 46.22 mm² (+/- 3.55 mm²) on plate three for Cellink® Bioink. The widths and areas are more sensitive to fluctuations within the printer system. When considering the high water content of hydrogels and the change in properties over time, the shrinkage of the lines becomes obvious. The water evaporates and hence the size of the lines changing decreases. For building up a 3D model, the printing time and the change of the object height should be considered and can be limiting [150]. If an object is built with many layers, the height is calculated for each layer. The larger the object, the longer the printing process. If this takes too long, the object will start to shrink and the layer height will not be correct after a certain time. This will cause the object to become faulty. As a result, the process time is a critical process parameter which poses two problems. Firstly, the printing time or the CAD model must be optimized or shrinkage can be prevented by a regulated humidity chamber. Secondly, the analysis of printed objects must be carried out immediately after printing and as quickly as possible because the properties already change after a few minutes. A general disadvantage of the used method is the long imaging process when using the plate reader because it takes 2 min to generate one picture for one well. It can be assumed that the high water content of bioinks decreases especially at the beginning. On the other hand, the constant conditions are advantageous, as the illumination and recording settings are always the same. For future applications, a set-up has to be found which enables a fast imaging process with a proper illumination which allows the analysis of transparent bioinks. The shrinkage behavior should be evaluated again with a more suitable set-up. The change in size is also confirmed by the significance in the repeated-measures ANOVA. Here, the data sets of all points in time were

examined for statistical significance with time zero. The data at different points in time are differing and are not comparable. One exception is plate one of BiogelxTM-ink-RGD. Here, the lines seem to grow in time, but this can be a detection problem due to the bioink's transparency.

3.6 Conclusion

Imaging-based analysis methods are promising PAT-tools for evaluating 3D-printed objects. These can be applied for printer characterization, for evaluating the printability of bioinks, and for optimization of printing processes in a non-invasive way in order to facilitate the application of bioprinting in the fields of regenerative medicine (RM) and tissue engineering (TE) [110, 111].

The established method was applied successfully for printed-line characterization. A first layer characterization is important as the printing accuracy for simple structures can be analyzed and a correct first layer is important to build up a whole object in layers. Object heights can also be analyzed by image processing. The length, area, and width can be determined. A new criterion and strategy were introduced to calculate the width within a stable area, otherwise a wide variation for width determination is possible. Nevertheless, the method showed some limitation during pre-tests. At current state, light reflections cause a discontinuous object contour for transparent materials and therefore the objects are detected incorrectly. For future application, the lighting has to be optimized to achieve an appropriate illumination. The second limitation is the speed of the imaging process as the image generation takes 2 min in the cell confluence method. Nevertheless, a shrinkage behavior of bioinks has been demonstrated and should be considered for planing bioprinting processes.

In general, the image processing method can be adapted to arbitrary image files and is a progress because multiple images can be analyzed in a completely automated way. This is a progress for systematic process development and a prerequisite for the transfer from research to clinical applications and industry. Advantageous is the high reproducibility and the minimization of variation as it is independent of the user. At the same time, it is a robust and time-saving method as the user can analyze all images at once.

Declaration of interests

The authors declare that they have no known competing financial interests or personal relationships that could have appeared to influence the work reported in this paper.

CRedit authorship contribution statement

S. Strauß: Conceptualization, Methodology, Software, Writing - Original Draft. **R. Meutelet:** Investigation. **L. Radosevic:** Experimental work. **S. Gretzinger:** Conceptualization, Writing - Review & Editing. **J. Hubbuch:** Conceptualization, Writing - Review & Editing.

Acknowledgments

This work was funded by the German Federal Ministry of Education and Research (BMBF) as project SOP-Bioprint under contract number 13XP5071B.

Chapter references

- [14] N. Paxton, W. Smolan, T. Böck, F. Melchels, J. Groll, and T. Jungst, „Proposal to assess printability of bioinks for extrusion-based bioprinting and evaluation of rheological properties governing bioprintability“, *Biofabrication*, vol. 9, no. 4, p. 44107, 2017.
- [110] J. Groll *et al.*, „Biofabrication: Reappraising the definition of an evolving field“, *Biofabrication*, vol. 8, no. 1, p. 013001, 2016.
- [111] S. Duin *et al.*, „3d bioprinting of functional islets of langerhans in an alginate/methylcellulose hydrogel blend“, *Advanced Healthcare Materials*, vol. 8, no. 7, p. 1801631, 2019.
- [112] J. Malda *et al.*, „25th anniversary article: Engineering hydrogels for biofabrication“, *Advanced Materials*, vol. 25, no. 36, pp. 5011–5028, 2013.
- [113] A. Atala, „Engineering organs“, *Current Opinion in Biotechnology*, vol. 20, no. 5, pp. 575–592, 2009.
- [114] S. Murphy and A. Atala, „3d bioprinting of tissues and organs“, *Nature biotechnology*, vol. 32, 2014.
- [115] F. Groeber, M. Holeiter, M. Hampel, S. Hinderer, and K. Schenke-Layland, „Skin tissue engineering — in vivo and in vitro applications“, *Advanced Drug Delivery Reviews*, vol. 63, no. 4, pp. 352–366, 2011.
- [116] T. Jungst, W. Smolan, K. Schacht, T. Scheibel, and J. Groll, „Strategies and molecular design criteria for 3d printable hydrogels“, *Chemical Reviews*, vol. 116, no. 3, pp. 1496–1539, 2016.
- [117] A. S. Hoffman, „Hydrogels for biomedical applications“, *Advanced Drug Delivery Reviews*, vol. 64, pp. 18–23, 2012.
- [118] S. Krishnamoorthi, A. Banerjee, and A. Roychoudhury, „Immobilized enzyme technology: Potentiality and prospects“, *J Enzymol Metabol*, vol. 1, no. 1, pp. 010–104, 2015.
- [119] B. Schmiege, A. Schimek, and M. Franzreb, „Development and performance of a 3d-printable poly(ethylene glycol) diacrylate hydrogel suitable for enzyme entrapment and long-term biocatalytic applications“, *Engineering in Life Sciences*, vol. 18, no. 9, pp. 659–667, 2018.
- [120] B. Schmiege, M. Nguyen, and M. Franzreb, „Simulative minimization of mass transfer limitations within hydrogel-based 3d-printed enzyme carriers“, *Frontiers in Bioengineering and Biotechnology*, vol. 8, p. 365, 2020.
- [121] K. Y. Lee and D. J. Mooney, „Hydrogels for tissue engineering“, *Chemical Reviews*, vol. 101, no. 7, pp. 1869–1879, 2001.
- [122] J. Zhu, „Bioactive modification of poly(ethylene glycol) hydrogels for tissue engineering“, *Biomaterials*, vol. 31, no. 17, pp. 4639–4656, 2010.
- [123] T. Vermonden, R. Censi, and W. E. Hennink, „Hydrogels for protein delivery“, *Chemical Reviews*, vol. 112, pp. 2853–2888, 2012.
- [124] A. G. Tabriz, M. A. Hermida, N. R. Leslie, and W. Shu, „Three-dimensional bioprinting of complex cell laden alginate hydrogel structures“, *Biofabrication*, vol. 7, no. 4, p. 045012, 2015.
- [125] T. T. Demirtaş, G. Irmak, and M. Gümüşderelioglu, „A bioprintable form of chitosan hydrogel for bone tissue engineering“, *Biofabrication*, vol. 9, no. 3, p. 035003, 2017.
- [126] J. Y. Park *et al.*, „A comparative study on collagen type i and hyaluronic acid dependent cell behavior for osteochondral tissue bioprinting“, *Biofabrication*, vol. 6, no. 3, p. 035004, 2014.
- [127] J. D. Kosmala, D. B. Henthorn, and L. Brannon-Peppas, „Preparation of interpenetrating networks of gelatin and dextran as degradable biomaterials“, *Biomaterials*, vol. 21, no. 20, pp. 2019–2023, 2000.
- [128] B. V. Slaughter, S. S. Khurshid, O. Z. Fisher, A. Khademhosseini, and N. A. Peppas, „Hydrogels in regenerative medicine“, *Advanced Materials*, vol. 21, no. 32-33, pp. 3307–3329, 2009.
- [129] M. Du *et al.*, „3d bioprinting of BMSC-laden methacrylamide gelatin scaffolds with CBD-BMP2-collagen microfibers“, *Biofabrication*, vol. 7, no. 4, p. 044104, 2015.
- [130] S. Naahidi *et al.*, „Biocompatibility of hydrogel-based scaffolds for tissue engineering applications“, *Biotechnology Advances*, vol. 35, no. 5, pp. 530–544, 2017.
- [131] R. A. Scott and N. A. Peppas, „Highly crosslinked, peg-containing copolymers for sustained solute delivery“, *Biomaterials*, vol. 20, no. 15, pp. 1371–1380, 1999.
- [132] S. Bertlein *et al.*, „Thiol–ene clickable gelatin: A platform bioink for multiple 3d biofabrication technologies“, *Advanced Materials*, vol. 29, no. 44, p. 1703404, 2017.
- [133] A. C. Jen, M. C. Wake, and A. G. Mikos, „Review: Hydrogels for cell immobilization“, *Biotechnology and Bioengineering*, vol. 50, no. 4, pp. 357–364, 1996.
- [134] K. Yue, G. [-d. Santiago], M. M. Alvarez, A. Tamayol, N. Annabi, and A. Khademhosseini, „Synthesis, properties, and biomedical applications of gelatin methacryloyl (gelma) hydrogels“, *Biomaterials*, vol. 73, pp. 254–271, 2015.

- [135] L. Wenger, C. Radtke, J. Göpper, M. Wörner, and J. Hubbuch, „3d-printable and enzymatically active composite materials based on hydrogel-filled high internal phase emulsions“, *Frontiers in Bioengineering and Biotechnology*, vol. 8, p. 713, 2020.
- [136] T. Gao *et al.*, „Optimization of gelatin–alginate composite bioink printability using rheological parameters: A systematic approach“, *Biofabrication*, vol. 10, no. 3, p. 034106, 2018.
- [137] K. Markstedt, A. Mantas, I. Tournier, H. Martínez Ávila, D. Hägg, and P. Gatenholm, „3D bioprinting human chondrocytes with nanocellulose–alginate bioink for cartilage tissue engineering applications“, *Biomacromolecules*, vol. 16, no. 5, pp. 1489–1496, 2015.
- [138] T. Lorson *et al.*, „A Thermogelling Supramolecular Hydrogel with Sponge-Like Morphology as a Cytocompatible Bioink“, *Biomacromolecules*, vol. 18, no. 7, pp. 2161–2171, 2017.
- [139] N. Soltan, L. Ning, F. Mohabatpour, P. Papagerakis, and X. Chen, „Printability and Cell Viability in Bioprinting Alginate Dialdehyde–Gelatin Scaffolds“, *ACS Biomaterials Science and Engineering*, vol. 5, no. 6, pp. 2976–2987, 2019.
- [140] B. Webb and B. J. Doyle, „Parameter optimization for 3d bioprinting of hydrogels“, *Bioprinting*, vol. 8, pp. 8–12, 2017.
- [141] A. Ribeiro *et al.*, „Assessing bioink shape fidelity to aid material development in 3d bioprinting“, *Biofabrication*, vol. 10, no. 1, p. 014102, 2017.
- [142] E. N. Malamas, E. G. Petrakis, M. Zervakis, L. Petit, and J.-D. Legat, „A survey on industrial vision systems, applications and tools“, *Image and Vision Computing*, vol. 21, no. 2, pp. 171–188, 2003.
- [143] L. S. Chow and R. Paramesran, „Review of medical image quality assessment“, *Biomedical Signal Processing and Control*, vol. 27, pp. 145–154, 2016.
- [144] F. M. Wunner *et al.*, „Printomics: The high-throughput analysis of printing parameters applied to melt electrowriting“, *Biofabrication*, vol. 11, 2019.
- [145] F. Yang, H. Zhao, Q. Gao, B. Xia, and F. Jianzhong, „Research on the printability of hydrogels in 3d bioprinting“, *Scientific Reports*, vol. 6, p. 29977, 2016.
- [146] Q. Gao *et al.*, „3d printing of complex GelMA-based scaffolds with nanoclay“, *Biofabrication*, vol. 11, no. 3, p. 035006, 2019.
- [147] M. Alonzo *et al.*, „A comparative study in the printability of a bioink and 3d models across two bioprinting platforms“, *Materials Letters*, vol. 264, p. 127382, 2020.
- [148] M. K. Włodarczyk-Biegun, J. I. Paez, M. Villiou, J. Feng, and A. del Campo, „Printability study of metal ion crosslinked peg–catechol based inks“, *bioRxiv*, 2019.
- [149] C. P. Radtke, N. Hillebrandt, and J. Hubbuch, „The biomaker: An entry-level bioprinting device for biotechnological applications“, *Journal of Chemical Technology & Biotechnology*, vol. 93, no. 3, pp. 792–799, 2018.
- [150] T. Billiet, M. Vandenhaute, J. Schelfhout, S. [Vlierberghe], and P. Dubruel, „A review of trends and limitations in hydrogel-rapid prototyping for tissue engineering“, *Biomaterials*, vol. 33, no. 26, pp. 6020–6041, 2012.

4

Evaluation of the Reproducibility and Robustness of Extrusion-based Bioprinting Processes applying a Flow Sensor

Svenja Strauß¹, Bianca Schroth¹, and Jürgen Hubbuch^{1,2}

¹ Institute of Functional Interfaces, Karlsruhe Institute of Technology (KIT), Eggenstein-Leopoldshafen, Germany

² Institute of Process Engineering in Life Sciences, Section IV: Biomolecular Separation Engineering, Karlsruhe Institute of Technology (KIT), Karlsruhe, Germany

Abstract

Bioprinting is increasingly regarded as a suitable additive manufacturing method in biopharmaceutical process development and formulation. In order to manage the leap from research to industrial application, higher levels of reproducibility and a standardized bioprinting process are prerequisites. This said, the concept of process analytical technologies, standard in the biopharmaceutical industry, is still at its very early steps. To date most extrusion-based printing processes are controlled over pneumatic pressure and thus not adaptive to environmental or system related changes over several experimental runs. A constant set pressure applied over a number of runs, might lead to variations in flow rate and thus to unreliable printed constructs. With this in mind, the simple question arises whether a printing process based on a set flow rate could improve reproducibility and transfer to different printing systems. The control and monitoring of flow rate aim to introduce the concept of PAT in the field of bioprinting.

This study investigates the effect of different processing modes (set pressure vs. set flow rate) on printing reproducibility occurring during an extrusion-based printing process consisting of 6 experimental runs consisting of 3 printed samples each. Additionally, the influence of different filling levels of the ink containing cartridge during a printing process was determined. Different solutions based on a varying amount of alginate polymer and Kolliphor hydrogels in varying concentrations showed the need for individual setting of printing parameter. To investigate parameter transferability among different devices two different printers were used and the flow was monitored using a flow sensor attached to the printing unit.

It could be demonstrated that a set flow rate controlled printing process improved accuracy and the filling level also affects the accuracy of printing, the magnitude of this effects varies as the cartridge level declined. The transferability between printed devices was eased by setting the printing parameters according to a set flow rate of each bioink disregarding the value of the set pressure. Finally, by a bioprinting process control based on a set flow rate, the coefficient of variance for printed objects could be reduced from 0.2 to 0.02 for 10 % (w/v) alginate polymer solutions.

4.1 Introduction

In the fields of regenerative medicine (RM) and tissue engineering (TE), the precise manufacturing of unique and artificial tissues is the key element enabling the development towards personalized medicine [110, 113, 114, 151]. These systems can be used for the replacement of damaged tissues or as drug delivery systems. Moreover, they can facilitate and standardize clinical or pharmaceutical studies [152–154]. 3D bioprinting as an advanced additive manufacturing method opens up the possibility to build complex tissue constructs by applying a bioink, which usually consists of a hydrogel cell mixture, in layers with spatial control [59, 112]. Hydrogels are suitable for engineering bioinks as they closely resemble natural tissues, offer mild conditions for cells or biological materials, and are biocompatible [117, 130]. Depending on the specific chemical and mechanical requirements for each artificial tissue, different hydrogels with varying modifications are employed [155, 156]. Much research has been done on the engineering of bioinks and companies already offer prepackaged bioinks commercially. However, bioinks are currently sold only for research purposes and not for clinical applications. In this study Kolliphor or also called poloxamer is used as it is a synthetic model hydrogel which is partly employed to establish new methods and as sacrificial material in the bioprinting field [141, 157, 158]. Natural alginate solutions were also used, as alginate,

with the advantages of a natural polymer and its viscous properties, is often the basis for bioink formulations [159, 160]. In terms of process engineering or process development within the field of 3D bioprinting, hydrogels and their characteristics are the dominant factor being the carrier of biological material. As hydrogels are viscoelastic materials which combine the characteristics of elastic solids and Newtonian fluids, the success of an extrusion process is strongly influenced by the rheological properties of the bioink [141, 157, 161]. The viscosity is highly temperature-sensitive, and is further influenced by process parameters such as polymer concentration, pH, ionic strength, environmental pressure and UV radiation for UV-responsive polymers [162–164]. The yield point is also dependent on the material and represents the stress level at which the material starts to flow, meaning that the elastic behaviour turns into a plastic one [165]. A perfectly controlled environment would actually be needed to take all of this into account, but in reality fluctuating temperatures and humidity levels are usual. Additional problems arise through often observed inhomogeneities in the polymer solution occurring as a function of time and temperature, leading in some cases to nozzle clogging [166, 167]. When working with materials from natural sources, the batch-to-batch variance must be taken into account and also the filling level within the cartridge might require an extrusion pressure adaptation. In order to counteract these challenges, bioprinters are developed within an atmospheric enclosure system for controlling the environmental conditions such as temperature, humidity, and carbon dioxide concentration [168]. Such systems are certainly expensive and cannot react to material changes. Therefore, cheaper and more general solutions are needed that can react to environmental and material changes.

Currently, printing parameters are determined during a printing process setup and thus kept constant during several runs (Figure 4.1, level 1). However, as described above, it is important to react to environmental and material changes. Instead of tackling each of these issues individually, a more general and effective approach may be to define an optimal flow rate which is adjusted during the printing process. A bioprinting system developed by Philipp Fisch et al. using a progressive cavity pump which controls the volume flow by displacement already showed an improved printing accuracy, when compared to a constant pressure approach [166]. In order to set a desired flow rate for a conventional pneumatic system, the pressure could be adjusted based on the feedback of a flow sensor. Handling changes in temperature or cartridge fill level during the print would require a dynamic pressure adaptation in real-time [166]. To do so, a necessary requirement would be to equip each bioprinter with a mass flow sensor which regulates the mass flow e.g. via pressure in real time. Mass or flow rates can be determined with sensors based on mechanical, ultrasonic, electrical, or thermal methods [169]. Flow sensors are widespread in the automotive industry, but are becoming more prevalent in the medical field where they are used for the controlled administration of infusions to patients [170, 171]. Here, sensors with thermal measuring principle are established which are only in indirect contact with the medium and work under sterile conditions [172]. However, it is to be evaluated if such a process control during each sample is needed or if the adjustment before each run is enough (see Figure 4.1). To date, flow rates are realized by syringe pumps or using mechanical extrusion systems and flow rates are determined by weighing extruded material. A poster was published for a project in which a flow sensor was used to measure the flow rate. The results are not completely congruent with the weighed flow rates and, in general, there is currently a lack of flow sensors that are suitable for visco-elastic materials [173–175].

Following this line of argumentation, this study revolves around the hypothesis that the reproducibility of bioprinting processes based on pneumatic extrusion can be improved by choosing a flow rate controlled process mode over a pressure controlled process mode. In order to evaluate the effect of this change, a flow sensor is incorporated in an extrusion-based bioprinter and similar samples

are printed and compared in two different process modes. In the first case, the samples are printed with the same extrusion pressure (set pressure, cP) determined in the experimental setup (Figure 4.1, level 1), and in the second case, a constant flow rate (set flow rate, cFR) is set by adapting the pressure of the printer system prior to each run (Figure 4.1, level 2). For this purpose, the flow sensor was used for initial calibration of the pressure required for the desired flow rate. In order to analyze the effect of filling level in the cartridges used (and thus need for a more dynamic control), the flow sensor is used to measure the flow rate for constant printing parameters during the complete emptying of one printer cartridge to examine the influence of the cartridge filling level. The investigation was carried out using two different extrusion printing systems and two inks with varying concentrations of Kolliphor and alginate.

4.2 Materials and methods

In general, when analyzing 3D bioprints, the experimental design is important and influences the conclusions drawn. A clear distinction should be made between hierarchical levels but also between the types of replicates performed. An overview graphic of the hierarchical order is shown in Figure 4.1.

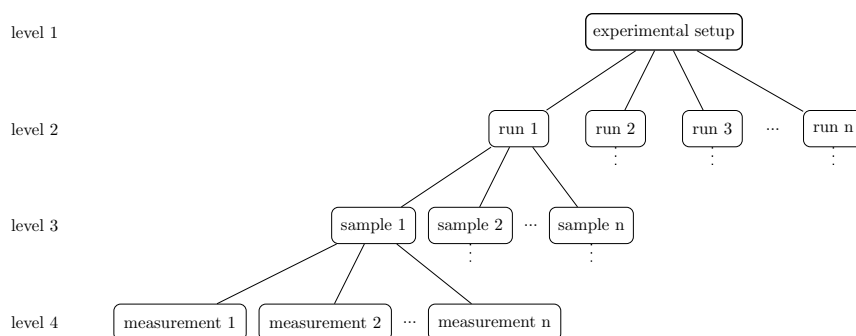


Figure 4.1 A hierarchical overview of the experiment design. Level 1 includes the experimental setup, which for 3D bioprinting is represented, for example, by the bioprinter used, the printing parameters, and the bioink. Level 2 consists of biological replicates, the runs. Several objects can be printed in one run which are the samples (level 3). These samples are technical replicates of the printing process and can be analyzed in a further step. The result is a measurement and in the case of a multiple determination, these measurements are also technical replicates of the analysis method.

Right at the top (level 1) is the experimental setup, which for 3D bioprinting is represented, for example, by the printer used, the printing parameters, and the bioink. For the course of this paper we define the term 'bioink' as an ink containing cellular material, while we use the term 'ink' for a hydrogel or polymer solution without any additional biological material. The level below or level 2 consists of biological replicates, the runs. Biological replicates 'are parallel measurements of biologically distinct samples, which may be random biological variation that is itself the subject of the study or a source of noise source' [176]. Transferred to bioprinting this means the independent production of bioink batches according to the same method. This said, this paper also speaks of biological replicates when the ink is produced without cells. Level 3 consists of samples when several objects are printed from the same bioink production. Thus, one sample is a technical replicate and

if the samples are measured several times, the results are measurements, which are also technical replicates.

4.2.1 Ink preparation and printing systems

For both printer systems, cartridges including pistons were obtained from Nordson Corporation (Westlake, USA), and plastic, conical 25 G nozzles with an inner diameter of 250 μm were ordered from Cellink (Gothenburg, Sweden) which were used for all experiments. Sodium alginate and Kolliphor P 407 were both obtained from Sigma Aldrich (St. Louis, USA) and were used for ink manufacturing in respective concentrations. The appropriate amount of powder for each ink was dissolved in ultrapure water (arium[®] pro VF, Satorius AG, Göttingen, Germany). During filling the cartridges, attention was closely paid to a uniform distribution. Since the inks are not pipettable, 3 ml of water was first poured into the cartridges as a reference and the level was marked. Then, the cartridges were filled up to the optical mark while ensuring a uniform distribution without air bubbles. The inks were made no more than 12 h prior to filling and were stored in the refrigerator at 4 °C. The samples were taken out of the refrigerator 15 min prior to each experiment. Each trial was carried out at room temperature.

The comparison of both process modes, namely cP and cFR, were performed with a pneumatic extrusion-based bioprinter 3D Discovery[™] provided by regenHU company (Villaz-St-Pierre, Switzerland). The BioCAD software (regenHU, Villaz-St-Pierre, Switzerland) was used to create the CAD model and G-Code for printed objects. Additionally, filling level experiments were done with a BIO X bioprinter and the BIO X software v.1.8.1 was used (Cellink, Gothenburg, Sweden).

4.2.2 Density calibration

With regard to a gravimetric verification of the flow sensor data, the densities for sodium alginate (0.25, 0.5, 0.75, 1, 1.5, 2, 2.5, 3 % (w/v) concentration) and Kolliphor (1, 2, 3, 5, 10, 15 % (w/v) concentration) were measured for 10 s using a micro liquid density sensor (ISSYS, Ypsilanti, USA). All measurements were performed in triplicates ($n = 3$), and the densities for higher concentrations were calculated with the straight line equation, since higher densities are no longer within the measurement range of the ISSYS.

4.2.3 SLI liquid flow meter

In this study, a flow sensor SLI-1000 FMK obtained from Sensirion (Staefa, Switzerland) was attached which is suitable for measurements of up to 10 mL/min. Figure 4.2 shows how the sensor was incorporated for the investigation of cartridge filling level influence into BIO X (A) and into 3D Discovery[™] (B). The reproducibility experiments were only performed with the 3D Discovery[™] and a different attachment of the sensor depicted in (C).

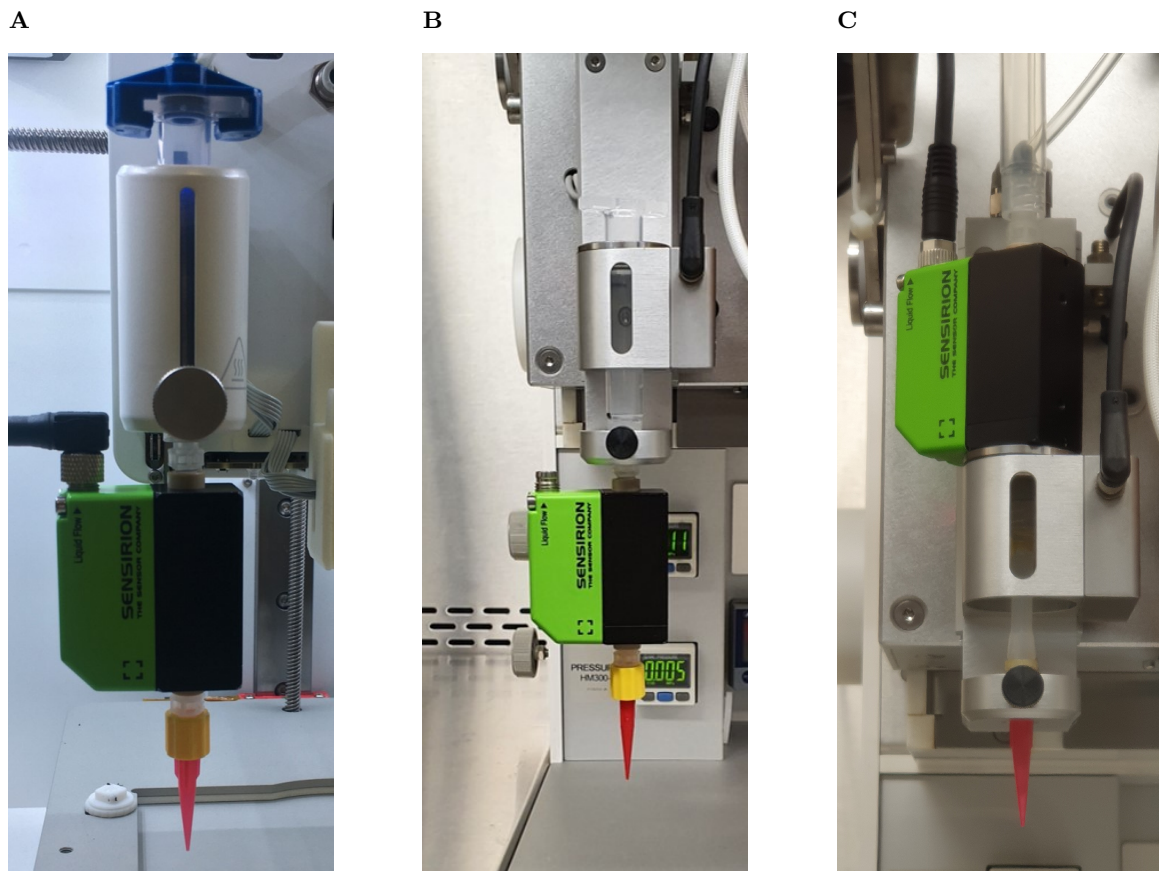


Figure 4.2 Different incorporation setups for the flow sensor into the bioprinters. For the investigation of cartridge filling level influence it was attached to BIO X as shown in (A) and to 3D DiscoveryTM as shown in (B).The reproducibility experiments were only performed with the 3D DiscoveryTM and a different attachment of the sensor depicted in (C).

Inside there is a borosilicate glass capillary with an internal diameter of 1 mm and a wall thickness of 100 μm . The total internal capillary volume is 25 μL and the capillary was prefilled before each experiment. The flow rate is determined using a thermally based measuring principle, which is shown in Figure 4.3. It consists of a heating element between two temperature sensors on the outside of the capillary and the flow rate is calculated in the software using the temperature difference between the temperature sensors. The liquid is never in direct contact with the measuring chip and the detection delay is 40 ms.

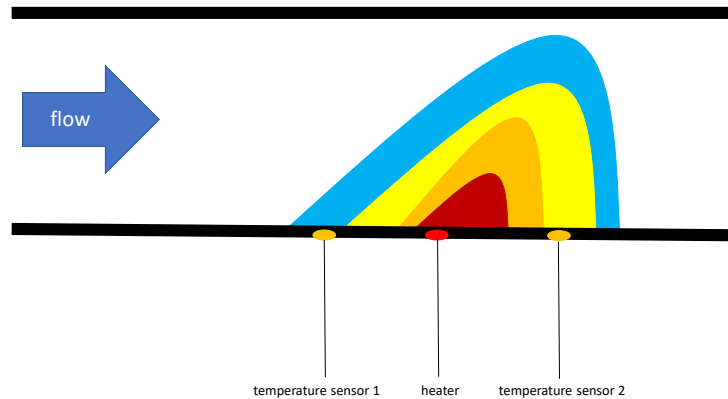


Figure 4.3 Illustration of the thermal based measuring principle of the flow sensor adapted from Kuo [177].

4.2.3.1 Flow sensor calibration

Since the sensor was originally developed for liquids, the applicability for the selected inks first had to be verified and calibrated for the respective inks. This was done for ink containing alginate with the concentrations of 8, 10, 12, and 15 % (w/v) and for ink containing Kolliphor with 15, 20, 25, 28, and 30 % (w/v). The sensor was connected via Luer lock to a syringe pump neMESYS (Cetoni GmbH, Korbußen, Germany). For each concentration of alginate and Kolliphor, a rough screening was carried out beforehand to ensure that the maximum adjustable speed of the pump was still in the measuring range of the sensor. Thereafter, at least seven flow rates for every concentration were measured in triplicates ($n = 3$).

4.2.3.2 Flow sensor accuracy

After calibration, measurement accuracy was analyzed and defined as the deviation between cylinder volumes calculated based on sensor data and cylinder volumes based on weighed values:

$$\text{Deviation} = \frac{V_Q}{V_m} \quad (4.1)$$

V_Q is here the cylinder volume in μL calculated with the sensor data using the following Equation 4.2 where \dot{Q} is the flow rate in $\mu\text{L}/\text{min}$ measured by the sensor:

$$V_Q = \int \dot{Q} dt \quad (4.2)$$

V_m is the volume in μL for each cylinder based on the weighed mass m in g divided by the density ρ in g/cm^3 . Using the density determined as described in Section 4.2.2, the volume for each cylinder could be calculated according to Equation 4.3:

$$V_m = \frac{m}{\rho} \quad (4.3)$$

To determine the accuracy, five hollow cylinders ($n_{sample} = 5$) each with a diameter of 10 mm and 15 layers with a 0.33 mm layer height were printed and weighed immediately after printing using an analytical balance AB204-S obtained from Mettler-Toledo GmbH (Gießen, Germany). This was done for alginate concentrations of 8, 10, 12, and 15 % (w/v) and for Kolliphor concentrations of 15, 20, 25, 28, and 30 % (w/v). The printing parameters are listed in Table 4.1 and were defined in a print optimization with the aim of printing intact hollow cylinders.

Table 4.1 Printing parameters for testing the sensor accuracy with inks of different alginate and Kolliphor concentrations. Z offset is the distance between nozzle and substrate when the first layer is printed.

Concentration [% (w/v)]	Ink _{Kolliphor}					Ink _{Alginate}			
	15	20	25	28	30	8	10	12	15
Pressure [MPa]	0.01	0.105	0.195	0.22	0.36	0.06	0.08	0.12	0.27
Speed [mm/s]	10	10	10	10	20	20	20	20	20
Height [mm]	0.33	0.33	0.33	0.33	0.33	0.33	0.33	0.33	0.33
Z offset [mm]	0.05	0.05	0.05	0.05	0.05	0.05	0.05	0.05	0.05

4.2.4 Investigation of cartridge filling level influence

Table 4.2 Summary of all setups for the investigation of cartridge filling level influence. Ink_{Alginate} is an abbreviation for all tested alginate concentrations of 8, 10, 12, and 15 % (w/v) and Ink_{Kolliphor} for all tested Kolliphor concentrations of 15, 20, 25, 28, and 30 % (w/v). Process mode means either constant pressure (cP) or constant flow rate (cFR).

Bioprinter	Setup		No. of runs	No. of samples
	Ink	Process Mode		
BIO X	Ink _{Alginate}	cP	3	1
3D Discovery TM	Ink _{Alginate}	cP	3	1
BIO X	Ink _{Kolliphor}	cP	3	1
3D Discovery TM	Ink _{Kolliphor}	cP	3	1

To obtain an overview of whether the filling level within a cartridge influences the bioprinting process, cartridges were filled with maximal filling level of 3 ml of ink containing Kolliphor concentrations of 15, 20, and 25 % (w/v) and with alginate concentrations of 10, 12, and 15 % (w/v) were dispensed at a constant pressure (see Table 4.3) until only air was extruded. This was repeated for three runs ($n_{run} = 3$) on both bioprinters, BIO X and 3D DiscoveryTM. A summary of all setups is shown in Table 4.2. The flow rate was monitored over the entire period using the flow sensor which was incorporated into the bioprinters as presented in Figure 4.2 (A) and (B).

4.2.5 Reproducibility experiments

In order to investigate the reproducibility of the bioprinter, again a hollow cylinder with a diameter of 10 mm and 15 layers with 0.33 mm layer height was printed. In the experimental setup, the 3D DiscoveryTM was used (Figure 4.1, level 1) and the flow sensor was attached as presented in Figure 4.2 (C). A summary of all setups is shown in Table 4.4. In total 6 runs printing ink

Table 4.3 Set pressures applied during filling level investigations for the ink with the respective alginate and Kolliphor concentration.

Concentration [% (w/v)]	Ink _{Kolliphor}			Ink _{Alginate}			
	15	20	25	8	10	12	15
Pressure [MPa]	0.015	0.105	0.195	0.05	0.1	0.15	0.195

Table 4.4 Summary of all setups for the reproducibility experiments. Ink_{Alginate} is an abbreviation for all tested alginate concentrations of 10, 12, and 15 % (w/v) and Ink_{Kolliphor} for all tested Kolliphor concentrations of 25, 28, and 30 % (w/v). Process mode means either constant pressure (cP) or constant flow rate (cFR).

Bioprinter	Setup		No. of runs	No. of samples
	Ink	Process Mode		
3D Discovery TM	Ink _{Alginate}	cP	6	3
3D Discovery TM	Ink _{Alginate}	cFR	6	3
3D Discovery TM	Ink _{Kolliphor}	cP	6	3
3D Discovery TM	Ink _{Kolliphor}	cFR	6	3

containing Kolliphor with a concentration of 25, 28, and 30 % (w/v) and ink containing alginate with a concentration of 10, 12 and 15 % (w/v) were performed (Figure 4.1, level 2). For each run, 3 cartridges were filled with 3 ml of one batch and one sample printed from one cartridge (Figure 4.1, level 3). We thus carried out 6 biological replicates ($n_{run} = 6$, level 2) and for each of those 3 technical replicates ($n_{sample} = 3$, level 3). Thus in total 18 cylinders were printed for each ink composition.

In the experimental setup (level 1) it was decided to compare two modes of processing. In the first case, a constant pressure (cP) for all runs was applied and in the second case, the pressure was adjusted to set a constant flow rate (cFR) for all runs. The latter was achieved by manually adjusting the pressure prior to each run until the desired flow rate was set. The respective printing parameters and flow rate target settings of all inks are listed in Table 4.5. In general, several printing parameter combinations can be selected for a printing process in order to achieve the same result. If the speed is increased, the pressure must also be increased. Because different speeds were set for the combinations in a screening before the study, the pressure does not increase with increasing concentration. The aim of the screening was to be able to print intact cylinders.

Table 4.5 Printing parameters for the investigation of reproducibility. The set flow rate values for the cFR case (last line) correspond to the sensor data and not to the actual flow rates. The Z offset means the distance between nozzle and substrate when the first layer is printed.

Concentration [% (w/v)]	Ink _{Kolliphor}			Ink _{Alginate}		
	15	20	25	10	12	15
Pressure [MPa]	0.3	0.22	0.36	0.08	0.12	0.27
Speed [mm/s]	15	10	20	20	20	20
Layer height [mm]	0.33	0.33	0.33	0.33	0.33	0.33
Z offset [mm]	0.05	0.05	0.05	0.05	0.05	0.05
Flow rate [μ l/min]	7636.2	6323.4	6617	1500.4	1645.2	1941.7

4.2.6 Data analysis

Data evaluation, statistical data analysis, and visualization were done with Matlab[®] R2019a (TheMathWorks, Natick, USA). Statistical analysis was performed with the calculated cylinder volumes of the reproducibility experiments. Since the normal distribution check using the Anderson-Darling test did not result in a normal distribution for all data sets, Mann Whitney U test as non-parabolic test was chosen. It was used to compare the two data sets of the two different process strategies cP and cFR. This was done for each of the six evaluated inks containing different concentrations of Kolliphor and alginate. For these investigations, α was set to 0.1 and a p-value below 0.05 was classified as statistically significant. Statistical significance is marked by an asterix in the figure.

4.3 Results

4.3.1 Sensor calibration

In preparation to use the sensor for ink measurements, a calibration for all inks containing different concentrations of Kolliphor and alginate was performed. This was done for each concentration with at least five flow rates in triplicates ($n = 3$) using a syringe pump. All data sets can be found in the supplementary data.

4.3.2 Printing accuracy

Accuracy is a measure of a deviation between an obtained object or measurement performed and its theoretical model / value. The volumetric deviation obtained by determining the applied volume gravimetrically and the calculated volume by using Equation 4.1. The density for the specific concentrations was also measured in triplicates ($n = 3$) in order to convert the volumetric flow rates into mass flows and data are shown in the supplementary data.

The same hollow model cylinder was printed five times ($n_{sample} = 5$) with identical model and printing parameters in a single run. The respective deviation of the sensor data from the gravimetrically determined data is shown for the Ink_{Kolliphor}, applying different concentrations in Figure 4.4 (A) and for Ink_{Alginate}, applying different concentrations in Figure 4.4 (B).

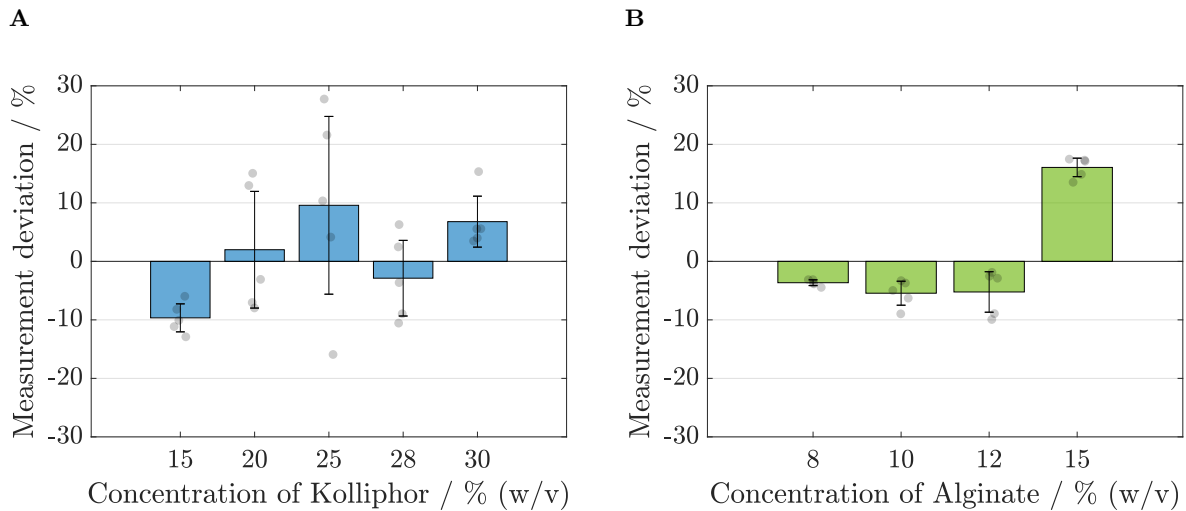


Figure 4.4 Analysis of the calibration and measurement accuracy of the flow sensor for the respective Kolliphor (A) and alginate (B) concentrations. Each time, five identical cylinders ($n_{sample} = 5$) were printed, and the calculated volumes based on the sensor data were compared with the data from the gravimetric determination. The deviation of the sensor measurement is given in percent.

For none of the Kolliphor concentrations, the mean deviation obtained for the five samples is higher than 10 %, and the maximum deviation was found to be $-9.66 \% \pm 2.39 \%$ for a 15 % (w/v) concentration. The smallest deviation is $1.99 \% \pm 9.97 \%$ for a 20 % (w/v) Kolliphor solution. The standard deviation is highest for ink containing 25 % (w/v) Kolliphor at 15.19 % and lowest at 2.39 % for ink containing 15 % (w/v) Kolliphor. For alginate containing inks, the maximum deviation is $16.06 \% \pm 1.58 \%$ for a 15 % (w/v) alginate solution and the smallest is at $-3.65 \% \pm 0.49 \%$ for a concentration of 8 % (w/v) alginate solution. In comparison to Kolliphor containing inks, the standard deviation obtained with the alginate containing inks is lower by a factor of about 5 with a maximum of 3.46 % for ink containing 12 % (w/v) alginate and a minimum of 0.49 % for 8 % (w/v) alginate solution. For alginate containing inks, it can be stated that the sensor’s measurement accuracy decreases with rising alginate concentration and the associated increase in viscosity. For Kolliphor containing inks a random distribution was obtained.

4.3.3 Influence of cartridge filling level

From a process engineering point of view it is of utmost importance to assess whether dynamic changes within the system i.e. the bioink filling level within a cartridge has an impact on the extrusion flow and thus on the whole bioprinting process. Therefore, cartridges were filled up to the same level with 3 ml of ink containing different concentrations of Kolliphor or alginate. Then, a constant pressure was applied to the cartridge and the flow rate was monitored by the flow sensor. The set pressure was different depending on the ink, but identical in each case for the two printing systems used (see Table 4.3). This was done for all concentrations in triplicates ($n_{run} = 3$). The results are depicted in Figures 4.5 and 4.6. The flow rate is shown over time during which the cartridge was emptied. On the left side are the flow rates that were measured for the BIO X and on the right side data from the 3D DiscoveryTM for comparison. The course of each experiment can be divided qualitatively into three phases: P1 - start-up, P2 - constant flowrate, P3 - flow rate drop.

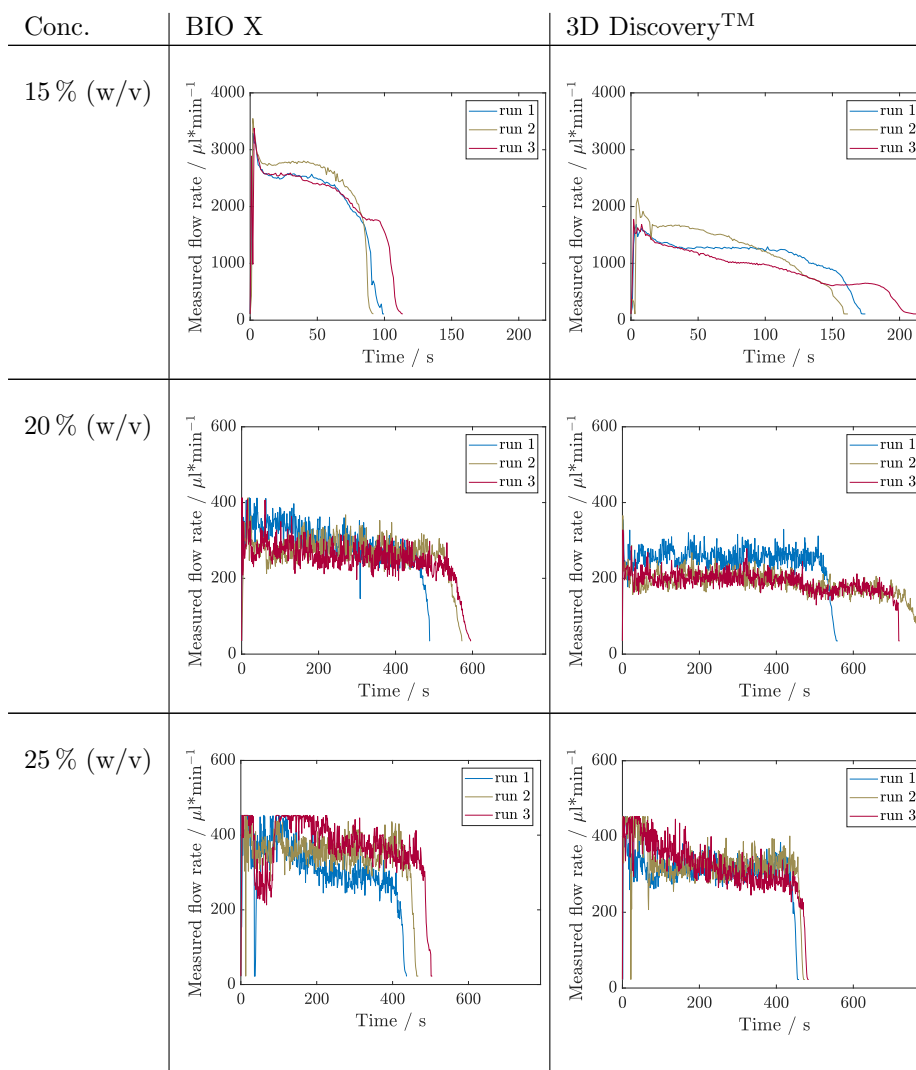


Figure 4.5 Results of filling level influence investigation for inks containing Kolliphor concentrations of 15, 20, and 25 % (w/v) by measuring the flow rate during the complete emptying of a cartridge. This experiment was carried out in triplicates ($n_{run} = 3$) for each concentration and on two bioprinter systems, namely BIO X and 3D DiscoveryTM. The respective set pressures are listed in Table 4.3

From a first glance at the Kolliphor ink runs, it is noticeable that for both printing systems data of 20 % (w/v) and 25 % (w/v) are noisier compared to data of solutions with 15 % (w/v) Kolliphor. All runs with 15 % (w/v) Kolliphor solution show using the BIO X printer an initial peak (P1), which then falls to a relatively constant flow rate between 2500 and 2800 $\mu\text{L}/\text{min}$ (P2) and then drops for each run differently (P3). P3 sets in latest at run 3. In comparison, the 3D DiscoveryTM shows less distinct initial peaks during P1 and run 1 reaches a constant flowrate during P2. The flow rate of the other two runs falls permanently and inconsistently. In P3, the drops are inconsistent and thus exhibit different extrusion rates. A comparison of the two systems shows that the BIO X achieves higher flow rates with maximum values in P2 between 2500 and 2800 $\mu\text{L}/\text{min}$ compared to the flow

rates at 3D DiscoveryTM, which are between 1300 and 1700 $\mu\text{L}/\text{min}$ at the most. Accordingly, the cartridges for the BIO X are empty after 90-120 s and for 3D DiscoveryTM later after 155-210 s. For 20 % (w/v) Kolliphor solution the earlier observed characteristic peak in P1 could not be observed and the extrusion process started directly in P2. Both, BIO X with a decreasing flow rate from approximately 330 $\mu\text{L}/\text{min}$ to 270 $\mu\text{L}/\text{min}$ and the 3D DiscoveryTM with flow rates in range of 200-260 $\mu\text{L}/\text{min}$, show no stable flow rate in P2 and the runs are not comparable. During P1 and the beginning of P2 of the 25 % (w/v) Kolliphor solution, the maximum measurable flow rate was exceeded for both bioprinters and therefore the values are partially truncated at the top. Thus a clear statement on the development of P1 can not be made. The BIO X runs in fluctuate strongly in P1. No clear trend is discernible, and the flow rates only stabilize after approximately 250 s in P2. The level of the flow rate of the individual runs in P2 differs and is in a range of 250-350 $\mu\text{L}/\text{min}$. In P2 of the 3D DiscoveryTM runs, all three runs have a flow rate of 300-350 $\mu\text{L}/\text{min}$ after 150 s, whereby run 3 continuously drops from 400 to 260 $\mu\text{L}/\text{min}$ and does not reach a stable phase.

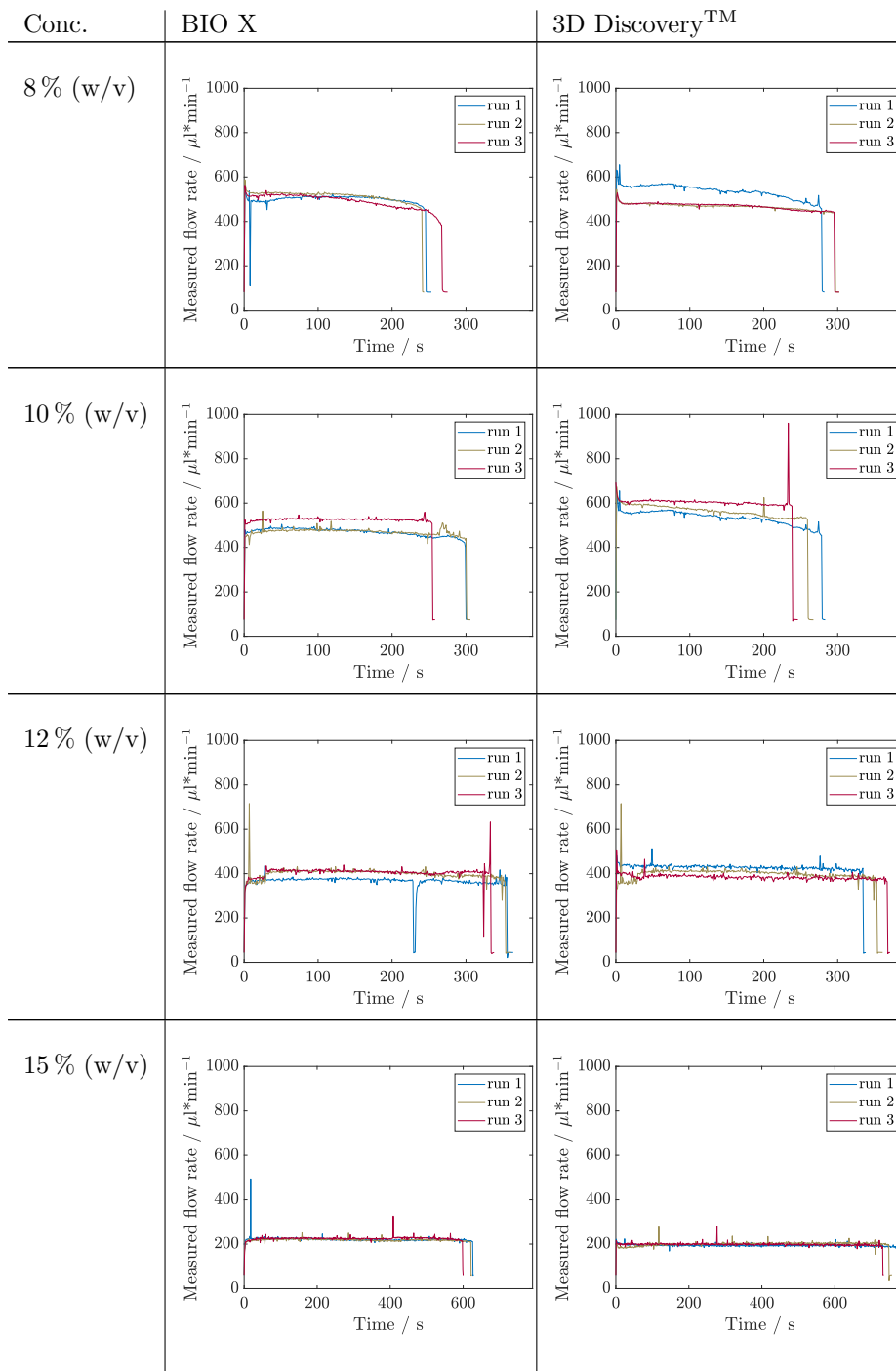


Figure 4.6 Results of filling level influence investigation for inks containing alginate concentrations of 8, 10, 12, and 15 % (w/v) by measuring the flow rate during the complete emptying of a cartridge. This experiment was carried out in triplicates ($n_{run} = 3$) for each concentration and on two bioprinter systems, namely BIO X and 3D DiscoveryTM. The respective set pressures are listed in Table 4.3

The data obtained for the alginate inks is not as noisy as that of Kolliphor inks, however, the noise again increases with increasing alginate concentration. No initial peak in P1 could be detected in any run. In P2 of the 8 % (w/v) alginate solution, the three runs show a stable flow rate above 500 $\mu\text{L}/\text{min}$ with temporary differences up to 20 $\mu\text{L}/\text{min}$. Run 3 decreases constantly. Except for ink containing 15 % (w/v) alginate, the same pressure on the 3D DiscoveryTM resulted in higher flow rates up to a factor of 1.4 during P2 for 10 % (w/v) alginate ink. The flow rate curves at 15 % (w/v) alginate ink are on the BIO X constant in P2 for 600 s at 220 $\mu\text{L}/\text{min}$ and again slightly higher compared to the P2 on 3D DiscoveryTM where the flow rates are around 200 $\mu\text{L}/\text{min}$. Here, run 1 decreases constantly and run 2 increases during emptying. So, again, no trend is visible.

4.3.4 Reproducibility experiments

Reproducibility is a measure describing the potential of producing an object or measurement repeatedly with the same accuracy. To deliver a brief and general overview of the reproducibility for the two different process modes cP and cFR, 6 runs ($n_{run} = 6$) were carried out in which 3 identical cylinder samples per alginate and per Kolliphor concentration were printed ($n_{sample} = 3$). In the first cP approach, the same predefined pressure was used for each run (see Table 4.5). In the second cFR approach, the pressure was adjusted by using the flow sensor as calibration tool prior to each run to meet a predefined flow rate. The results obtained are depicted in Figure 4.7, where the mean volumes of the 3 samples of 1 run with standard deviation are plotted against the respective concentration.

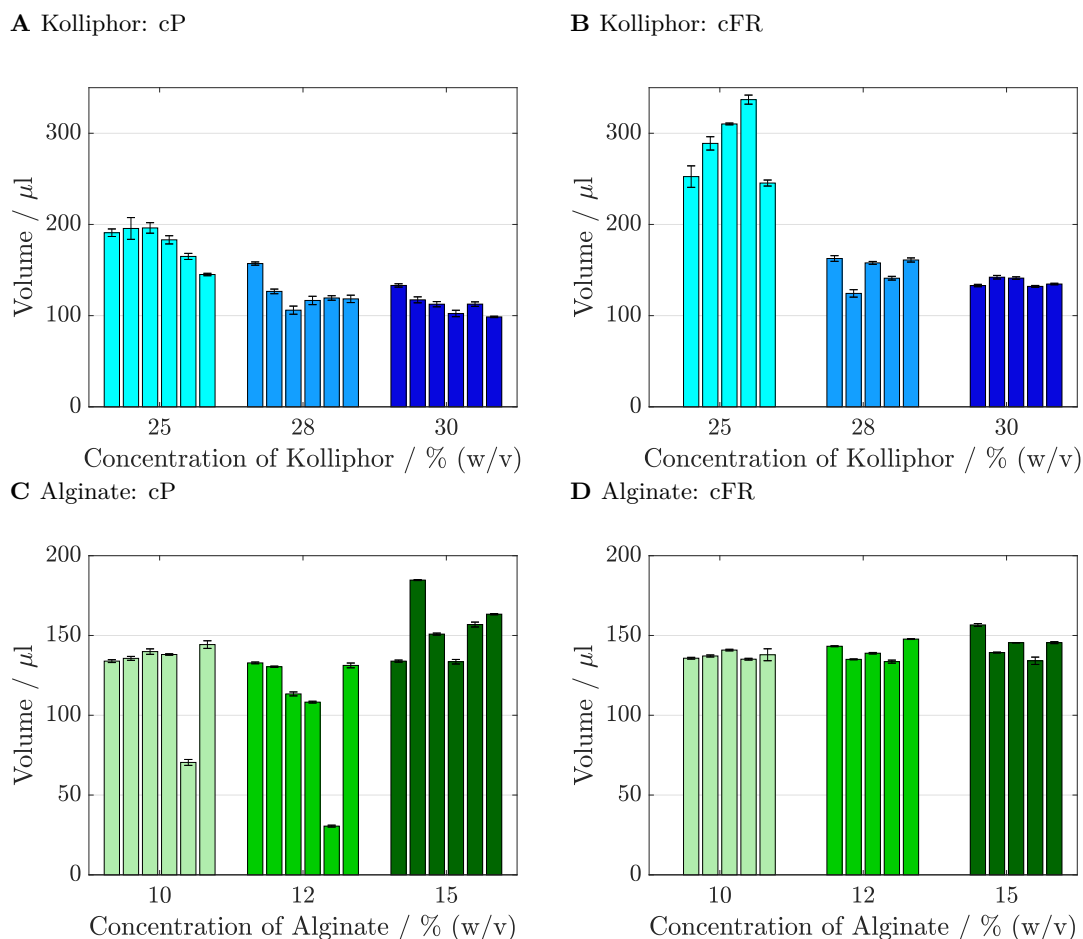


Figure 4.7 Results of the reproducibility tests for Kolliphor containing inks ((A)-(B)) and Alginate containing inks ((C)-(D)). Six runs ($n_{run} = 6$) were carried out in which 3 samples ($n_{sample} = 3$) were printed each for the cP and the cFR approach. Consequently, 18 cylinders for the cP approach and 18 cylinders for the cFR approach were printed in total. The obtained mean values and deviations of the 3 samples belonging to one run are shown in one bar. The cP results where the pressure was kept constant for all six runs are presented in (A) and (C), and the cFR results where the pressure was adapted to set a constant flow rate are shown in (B) and (D). As the 3 samples from run 1 with cFR were used as calibration set for the flow rate determination, there is one bar less.

For 25 % (w/v) Kolliphor containing ink, the minimum volume at cP was 145 μL and the maximum volume was 196.18 μL . The deviation was in the range of $1.3 \mu\text{L} \pm 11.95 \mu\text{L}$ during the 6 runs. In comparison, the cFR values are higher, i.e. in the range of 245.42-336.89 μL with a standard deviation of maximum $\pm 11.79 \mu\text{L}$ during the 6 runs. The cP values with 28 % (w/v) Kolliphor containing ink are lower with volumes in the range from 118.37-157.11 μL with a maximum standard deviation of 4.58 μL during the 6 runs. The cFR results are varying from 124.37-162.66 μL during the 6 runs with a maximum standard deviation of 4.09 μL . For 30 % (w/v) Kolliphor containing ink with cP process strategy, volumes in the range of 98.6-133.1 μL with a deviation between 0.76-3.52 μL were measured during the 6 runs in comparison to the cFR strategy with volumes between 132.08-142.15 μL and a standard deviation of up to $\pm 1.96 \mu\text{L}$ during the 6 runs. The

cylinders printed with alginate containing ink are smaller than the cylinders printed with Kolliphor containing ink. For 10% (w/v) alginate containing ink, the cFF cylinder volumes are in the range of 70-144.4 μL with a maximum deviation of $\pm 1.52 \mu\text{L}$ during the 6 runs, but run 5 falls out with only about half the weight compared to the others. There is no outlier for the cFR results, which are in the range of 135.15-140.86 μL with a maximum standard deviation of $\pm 3.74 \mu\text{L}$ during the 6 runs. For the 12% (w/v) alginate containing ink cP results, the cylinders of run 5 are smaller with 30.53 $\mu\text{L} \pm 0.58 \mu\text{L}$ for that run in comparison to the other 5 runs which is between 113.38-132.82 μL with a maximum deviation of 1.23 μL . The cFR volumes using the same ink concentration are slightly higher with volumes between 133.61-147.74 $\mu\text{L} \pm$ maximum 1.5 μL during 6 runs. For 15% (w/v) alginate solutions, the range of volumes is from 133.56-163.35 $\mu\text{L} \pm$ maximum 1.42 μL during the 6 runs. In general, there are higher deviations between the individual runs for cP than for cFR, in which the volumes are between 134.15-156.61 μL with a maximum standard deviation of $\pm 2.3 \mu\text{L}$.

As the Anderson-Darling test did not result in a normal distribution for all data sets, a Mann Whitney U test was performed. For a better comparison and statistical evaluation of the distribution of the data sets of cP and cFR, Figure 4.8 visualizes the box plots of the two strategies for each ink concentration. The cylinders of every ink from all runs were summarized in one box plot and cP was compared with cFR.

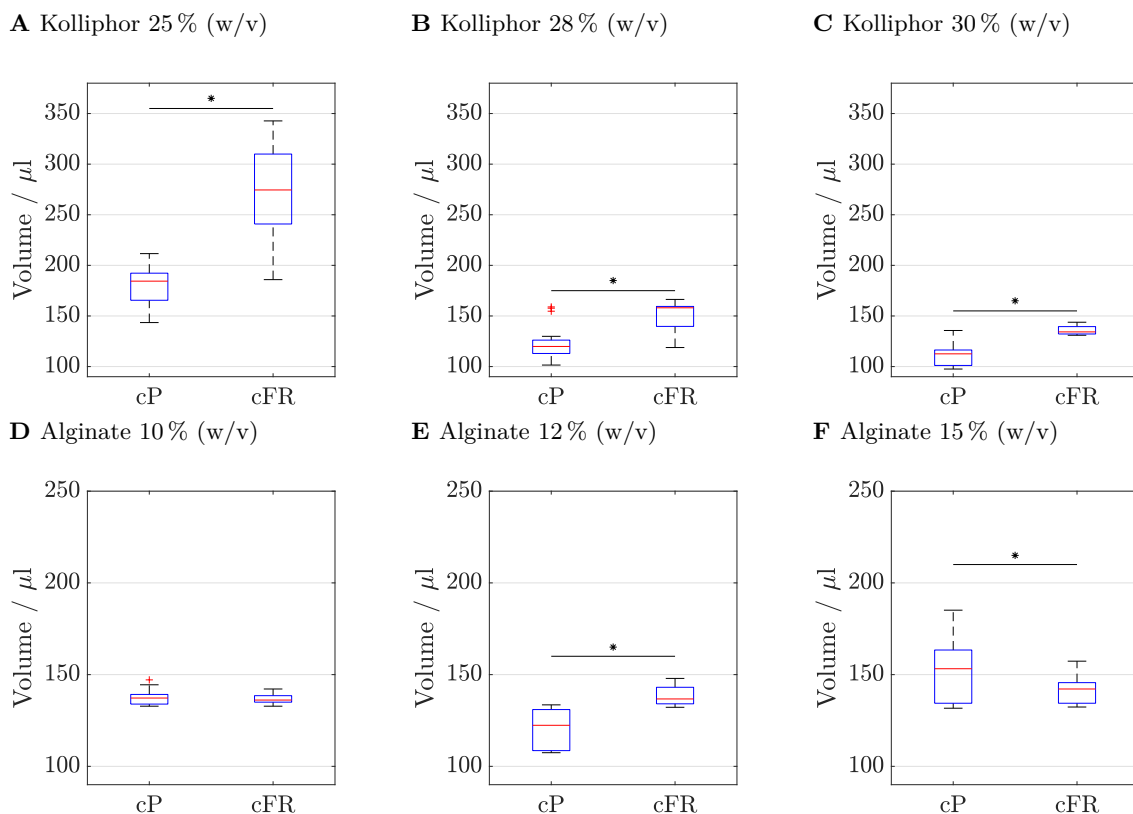


Figure 4.8 Cylinder volumes ($n_{run} = 6$ with $n_{sample} = 3$ resulting in 18 cylinders) of the reproducibility test comparing the two process strategies: on the left side using constant pressure (cP) and on the right side applying a constant flow rate (cFR). Values are considered outliers if they are more than 1.5 times the interquartile range from the bottom or top of the box. The results obtained with inks containing different Kolliphor concentrations are shown in (A)-(C) and with inks containing different alginate concentrations in (D)-(F). Statistically significant differences between cFR and cP were found between all data sets except for ink containing 10% (w/v) alginate. The specific p-values are: (A) 4×10^{-6} , (B) 1×10^{-6} , (C) 5×10^{-6} , (D) 2×10^{-6} , and (F) 0.047.

Statistically significant differences between the two process strategies were found for all data sets, except for ink containing 10% (w/v) alginate. To make the comparison easier, key figures for the box plots are listed for Kolliphor containing inks in Table 4.6 and for alginate containing inks in Table 4.7.

Table 4.6 Boxplot key figures of Kolliphor containing inks boxplots shown in Figure 4.8 (A)-(C).

Ink _{Kolliphor} [% (w/v)]	Constant pressure (cP)			Constant flow rate (cFR)		
	25	28	30	25	28	30
Min. volume [μl]	143.48	101.5	97.57	185.9	118.82	130.96
Max. volume [μl]	211.6	158.94	135.66	342.72	166.35	143.81
Range [μl]	68.12	57.44	38.1	156.81	47.53	12.86
Median	184.4	119.9	112.59	274.51	158.08	134.27
Lower quartile	165.51	112.95	101.12	240.88	139.7	132.21
Upper quartile	192.28	126.13	116.38	309.97	159.42	139.5
Variance	406.41	283.72	138.47	2×10^3	206.45	19.71
Standard deviation	20.16	16.84	11.77	49.45	14.37	4.44
Coefficient of variance	0.11	0.14	0.1	0.18	0.1	0.03
Interquartile distance	26.76	13.18	15.25	69.1	19.72	7.29

In the following, only the coefficient of variance is discussed for the sake of clarity. The advantage is that outliers do not have such a strong influence, as with the range and the data distribution is considered more than if only the mean values were considered. The advantage is that the standard deviation is considered in relation to the mean value. The coefficient of variance increased by 63% for 25% (w/v) Kolliphor ink. For 28% and 30% (w/v) Kolliphor ink, the coefficient of variance decreased by 29 and 70%, respectively.

Table 4.7 Boxplot key figures of alginate containing boxplots shown in Figure 4.8 (D)-(F).

Ink _{Alginate} [% (w/v)]	Constant pressure (cP)			Constant flow rate (cFR)		
	10	12	15	10	12	15
Min. volume [μl]	67.83	29.87	131.68	132.79	132.19	132.34
Max. volume [μl]	147.14	133.52	185.13	142.16	147.93	157.33
Range [μl]	79.31	103.65	53.44	9.38	15.74	24.99
Median	137.24	122.37	153.21	136.14	136.74	142.17
Lower quartile	133.94	108.58	134.4	134.99	134.09	134.4
Upper quartile	139.2	130.96	163.41	138.53	143.1	145.63
Variance	692.59	1×10^3	330.92	8.1	31.4	66.6
Standard deviation	26.32	36.85	18.2	2.85	5.6	8.16
Coefficient of variance	0.2	0.34	0.11	0.02	0.04	0.06
Interquartile distance	5.26	22.38	29.01	3.54	9.01	11.23

For alginate containing inks, the results are even clearer and the coefficient of variance drops at least 46% for 15% (w/v) alginate ink when printed by a constant flow rate. For a 10% (w/v) alginate ink, the coefficient of variance was reduced by 90%.

4.4 Discussion

Progress in the field of bioprinting has been made, but the shift from research to market is still far from being complete. This study served to evaluate whether the reproducibility of bioprinting processes is improved using a set flow rate as a process parameter, since robust and reliable processes are a basic requirement for medical applications. Already in another study it is concluded that extrusion based bioprinting process is affected by bioink and process-related influences which again can result in a low reproducibility [178]. To investigate how reproducibility can be increased in pneumatic systems a flow sensor was incorporated into the printing systems and calibrated for appropriate ink compositions. The deviation of the sensor data from the weighed data is acceptable for Kolliphor inks being below 10 % for all concentrations. The standard deviations at inks containing 20 % (w/v) and 25 % (w/v) Kolliphor are relatively high when compared to the other systems analyzed. A possible explanation is the sol-gel transition temperature which is closer to room temperature at 20-25 % (w/v) Kolliphor than for the other examined concentrations [81]. Here, the applied sensor may have problems to measure gels as it was developed and optimized for liquids. Likewise, no deviation greater than 10 % was measured for alginate inks, except for ink containing 15 % (w/v) alginate with a deviation of 16 %. The obtained standard deviations for alginate inks are much smaller than those containing Kolliphor. This said, both inks show a correlation between deviations obtained and ink concentration applied. A reason might be that the viscosity increase decreases the accuracy of the sensor. The sensor used in this study, employs a thermal principle which means that temperature changes impact the sensor output and network inhomogeneities can result in different heat conduction coefficients, which impair the measuring accuracy. Local inhomogeneities also have an influence on the material flow [166, 167, 179]. Taken together, inhomogeneities might lead to both, fluctuating measurements and to unsteady flow. On the basis of the data, no discrimination is possible to what extent the two effects lead to noisy data. However, in conclusion, sensor performance was considered sufficient and was used for further experiments. What is also becoming apparent is that each ink composition needs different pressures and behaves differently. An automated setting of the pressure at a fixed flow rate would be of great advantage here (see behaviour of different inks in Section 4.3.2).

In a following step, the influence of the filling level inside the cartridge on the flow rate was examined with the aid of the sensor using a constant pressure setup (cP) for all concentrations at two bioprinters, namely BIO X and 3D DiscoveryTM. The flow rate during a complete emptying - until no ink was extruded anymore - of a cartridge was recorded in triplicates for different alginate and Kolliphor concentrations. Here, again, it is generally noticeable that higher viscosity inks lead to noisy data. The data, however, could not be averaged because the runs were not comparable. The Kolliphor time courses of the flow rate in particular differ greatly and hardly any stable areas could be specified. Alginate as a polymer solution has shown more reproducible processes, but again exceptions with a steady drop of the flow rate were experienced. It is particularly noticeable that the same pressure setup resulted in different flow rates in different bioprinter systems. The same parameters on the 3D DiscoveryTM resulted in lower flow rates for Kolliphor and higher flow rates for alginate. Thus, there is no trend, and a simple inter-system transferability is not given. These results confirm that the flow rates can vary depending on the materials used during a printing process and that constant control of the flow rate may improve printing results by ensuring a steady flow rate (see data on filling level in Section 4.3.3).

In order to investigate whether an extrusion process based on flow rates leads to an increase in reproducibility, three cylinder samples were printed during 6 runs with two different process controls.

In the constant pressure approach (cP) in every run the same pressure was applied. This is in accordance with the common procedure given by system manufacturers. In the other cFR approach, the pressure was adapted to obtain a set flow rate which was verified with the flow sensor as calibration tool. The results indicate that the run-to-run deviations were inconsistent and rather high for the cP process mode, while the standard deviation within one run is quite low. One reason for this might be that environmental conditions fluctuate strongly between days and printing sessions, but only marginally during the relatively short duration of the printing session itself. This requires that the pressure or process parameters need to be adjusted prior to each run or printing session (see behaviour over 6 runs in Section 4.3.4). This said, considering the high deviations in flow rate as a function of cartridge filling level, continuous pressure adjustment would be necessary for longer printing processes. Except for ink containing 25 % (w/v) Kolliphor, the standard deviation and coefficient of variance could be improved by a calibration before each run. The review of the sensor performance already showed the measurement problems of the sensor for ink containing 25 % (w/v) Kolliphor which can be explained by the sol-gel-transition temperature of Kolliphor close to room temperature [81]. As can be seen from the fluctuations of flow during the runs examining the influence of the cartridge filling level, the noisiness of the data increases with higher polymer concentration and it becomes increasingly difficult to set the flow rate precisely. However, to put it all in a nutshell, it could be shown that a flow rate-based cFR principle leads to more comparable and more reproducible results. Of course, research work is necessary to implement the principle on bioprinters and to construct bioprinters with flow sensors which have been developed and appropriated for inks or rather bioinks. It is beneficial to control the pneumatic extrusion as changes in the bioink viscosity results in flow inhomogeneities which do not allow a reproducible extrusion of filament [178]. Other mechanical extrusion systems which are screw or piston driven promise a higher spatial control and constant flow rates as no gas volume is compressed before. Compared to the pneumatic systems, they are more complex with more components and are not as widespread [180]. They are able to extrude higher viscosity materials, but large driving forces can cause damage to cell walls [181, 182]. During the construction, problems with the pneumatic transport regime must be taken into account because the concentration and velocity of bioinks is sometimes network inhomogeneous [183]. In the future, a distinction must then also be made between two process controls. Calibration directly before the printing process allows a reaction to daily environmental fluctuations, changes of printer systems, and changes of bioinks. On the other hand, a continuous pressure control would allow an adjustment of the pressure, which may be necessary due to temperature changes already during the printing process, changes of the cartridge filling level, larger inhomogeneities, and nozzle clogging.

4.5 Conclusion

Reproducible and robust processes are necessary to make the leap from research to medical application. We demonstrated that employing a flow rate-based extrusion process can reduce the variations between printed objects and increase the reproducibility of bioprinting applications.

In preliminary tests, the sensor used was found to be suitable for the measurement of bioinks. Furthermore, it has been demonstrated that the filling level in the cartridge and the printer type have an influence on the flow rate. It was shown that the cFR approach led to a higher reproducibility than the cP approach as it was possible to respond well to variations in environmental conditions between different runs and printing sessions. An automated calibration for automatic pressure

determination for a defined flow rate would be desirable. Even better would be automated pressure readjustment in a feed back loop to keep a flow rate constant. This would turn the static monitoring of the flow rate in a dynamic, adaptable proces and variations such as cartridge filling level and inhomogeneities can be responded to directly. In addition, the sensor must be adapted to the respective viscosity ranges of the bioinks and the sensor should also be compatible for the respective temperature range. Bioinks are sometimes printed at different temperatures and the temperature has an influence both on the rheological properties of the bioink and on the thermally based measuring principle of the sensor. But another measuring principle would also be conceivable. In summary, the experiments provided a proof of concept for the flow rate-based process management to increase reproducibility and this must now be integrated into the bioprinters.

Declaration of interests

The authors declare that they have no known competing financial interests or personal relationships that could have appeared to influence the work reported in this paper.

CRedit authorship contribution statement

S. Strauß: Conceptualization, Methodology, Software, Writing - Original Draft. **B. Schroth:** Experimental work, Investigation. **J. Hubbuch:** Conceptualization, Writing - Review & Editing.

Acknowledgments

This work was funded by the German Federal Ministry of Education and Research (BMBF) as project SOP-Bioprint under contract number 13XP5071B. Special thanks go to Lukas Wenger for the valuable contribution during the project.

Chapter references

- [59] J. Groll *et al.*, „A definition of bioinks and their distinction from biomaterial inks“, *Biofabrication*, vol. 11, no. 1, 2019.
- [81] G. Dumortier, J. L. Grossiord, F. Agnely, and J. C. Chaumeil, „A review of poloxamer 407 pharmaceutical and pharmacological characteristics“, *Pharmaceutical Research*, vol. 23, no. 12, pp. 2709–2728, 2006.
- [110] J. Groll *et al.*, „Biofabrication: Reappraising the definition of an evolving field“, *Biofabrication*, vol. 8, no. 1, p. 013001, 2016.
- [112] J. Malda *et al.*, „25th anniversary article: Engineering hydrogels for biofabrication“, *Advanced Materials*, vol. 25, no. 36, pp. 5011–5028, 2013.
- [113] A. Atala, „Engineering organs“, *Current Opinion in Biotechnology*, vol. 20, no. 5, pp. 575–592, 2009.
- [114] S. Murphy and A. Atala, „3d bioprinting of tissues and organs“, *Nature biotechnology*, vol. 32, 2014.
- [117] A. S. Hoffman, „Hydrogels for biomedical applications“, *Advanced Drug Delivery Reviews*, vol. 64, pp. 18–23, 2012.
- [130] S. Naahidi *et al.*, „Biocompatibility of hydrogel-based scaffolds for tissue engineering applications“, *Biotechnology Advances*, vol. 35, no. 5, pp. 530–544, 2017.
- [141] A. Ribeiro *et al.*, „Assessing bioink shape fidelity to aid material development in 3d bioprinting“, *Biofabrication*, vol. 10, no. 1, p. 014102, 2017.
- [151] A. S. Mao and D. J. Mooney, „Regenerative medicine: Current therapies and future directions“, *Proceedings of the National Academy of Sciences of the United States of America*, vol. 112, no. 47, pp. 14452–14459, 2015.
- [152] H. R. Culver, J. R. Clegg, and N. A. Peppas, „Analyte-Responsive Hydrogels: Intelligent Materials for Biosensing and Drug Delivery“, *Accounts of Chemical Research*, vol. 50, no. 2, pp. 170–178, 2017.
- [153] S. Caddeo, M. Boffito, and S. Sartori, „Tissue engineering approaches in the design of healthy and pathological in vitro tissue models“, *Frontiers in Bioengineering and Biotechnology*, vol. 5, no. AUG, pp. 1–22, 2017.
- [154] Y. Chen *et al.*, „Noninvasive in vivo 3d bioprinting“, *Science Advances*, vol. 6, no. 23, 2020.
- [155] K. A. Smeds and M. W. Grinstaff, „Photocrosslinkable polysaccharides for in situ hydrogel formation“, *Journal of Biomedical Materials Research*, vol. 54, no. 1, pp. 115–121, 2001.
- [156] K. Yue, G. Trujillo-de Santiago, M. M. Alvarez, A. Tamayol, N. Annabi, and A. Khademhosseini, „Synthesis, properties, and biomedical applications of gelatin methacryloyl (GelMA) hydrogels“, *Biomaterials*, vol. 73, pp. 254–271, 2015.
- [157] N. Paxton, W. Smolan, T. Böck, F. Melchels, J. Groll, and T. Jungst, „Proposal to assess printability of bioinks for extrusion-based bioprinting and evaluation of rheological properties governing bioprintability“, *Biofabrication*, vol. 9, no. 4, p. 044107, 2017.
- [158] C. P. Radtke, N. Hillebrandt, and J. Hubbuch, „The biomaker: An entry-level bioprinting device for biotechnological applications“, *Journal of Chemical Technology & Biotechnology*, vol. 93, no. 3, pp. 792–799, 2018.
- [159] J. A. Rowley, G. Madlambayan, and D. J. Mooney, „Alginate hydrogels as synthetic extracellular matrix materials“, *Biomaterials*, vol. 20, no. 1, pp. 45–53, 1999.
- [160] E. Axpe and M. L. Oyen, „Applications of alginate-based bioinks in 3d bioprinting“, *International journal of molecular sciences*, vol. 17, no. 12, p. 1976, 2016.
- [161] A. F. Bonatti, I. Chiesa, G. Vozzi, and C. De Maria, „Open-source cad-cam simulator of the extrusion-based bioprinting process“, *Bioprinting*, vol. 24, e00172, 2021.
- [162] T. G. Mezger, *Das Rheologie Handbuch*, 5th ed. Vincentz Network, 2016.
- [163] T. Jungst, W. Smolan, K. Schacht, T. Scheibel, and J. Groll, „Strategies and Molecular Design Criteria for 3D Printable Hydrogels“, *Chemical Reviews*, vol. 116, no. 3, pp. 1496–1539, 2016.
- [164] Y. Zhao, Y. Li, S. Mao, W. Sun, and R. Yao, „The influence of printing parameters on cell survival rate and printability in microextrusion-based 3d cell printing technology“, *Biofabrication*, vol. 7, no. 4, p. 045002, 2015.
- [165] T. Osswald and N. Rudolph, *Polymer rheology : fundamentals and applications* (Hanser eLibrary). München: Hanser, 2014.
- [166] P. Fisch, M. Holub, and M. Zenobi-Wong, „Improved accuracy and precision of bioprinting through progressive cavity pump-controlled extrusion“, *bioRxiv*, 2020.
- [167] S. Seiffert and J. Sprakel, „Physical chemistry of supramolecular polymer networks“, *Chemical Society Reviews*, vol. 41, no. 2, pp. 909–930, 2012.
- [168] M. Matamoros *et al.*, „Temperature and humidity pid controller for a bioprinter atmospheric enclosure system“, *Micromachines*, vol. 11, no. 11, 2020.

- [169] A. Rasmussen and M. Zaghoul, „The design and fabrication of microfluidic flow sensors“, in *1999 IEEE International Symposium on Circuits and Systems (ISCAS)*, vol. 5, 1999, 136–139 vol.5.
- [170] W. J. Fleming, „Overview of automotive sensors“, *IEEE Sensors Journal*, vol. 1, no. 4, pp. 296–308, 2001.
- [171] N. Nguyen, „Micromachined flow sensors—a review“, *Flow Measurement and Instrumentation*, vol. 8, no. 1, pp. 7–16, 1997.
- [172] G. Schnell and R. Schäfer, „Ein thermischer Durchflußsensor.für die Infusionstechnik“, *Biomedizinische Technik*, vol. 40, no. 3, pp. 50–53, 1995.
- [173] L. Banović and B. Vihar, „Development of an extruder for open source 3d bioprinting“, *Journal of Open Hardware*, vol. 2, no. 1, 2018.
- [174] C. Yan, M. E. Mackay, K. Czymbek, R. P. Nagarkar, J. P. Schneider, and D. J. Pochan, „Injectable solid peptide hydrogel as a cell carrier: Effects of shear flow on hydrogels and cell payload“, *Langmuir*, vol. 28, no. 14, pp. 6076–6087, 2012.
- [175] R. V. Opel, W. Hynes, M. Moya, *et al.*, „Flow sensor integration for precision dispensing of visco-elastic biomaterials“, 2017.
- [176] P. Blainey, M. Krzywinski, and N. Altman, „Replication: Quality is often more important than quantity“, *Nature Methods*, vol. 11, no. 9, pp. 879–881, 2014.
- [177] J. T. Kuo, L. Yu, and E. Meng, „Micromachined thermal flow sensors—a review“, *Micromachines*, vol. 3, no. 3, pp. 550–573, 2012.
- [178] M. Kesti, P. Fisch, M. Pensalfini, E. Mazza, and M. Zenobi-Wong, „Guidelines for standardization of bioprinting: A systematic study of process parameters and their effect on bioprinted structures“, *BioNanoMaterials*, vol. 17, no. 3-4, pp. 193–204, 2016.
- [179] Z.-Y. .-. Wang, Q.-Z. .-. Zhang, M. Konno, and S. Saito, „Sol–Gel transition of alginate solution by the addition of various divalent cations: A rheological study“, *Biopolymers*, vol. 34, no. 6, pp. 737–746, 1994.
- [180] S. V. Murphy and A. Atala, „3d bioprinting of tissues and organs“, *Nature biotechnology*, vol. 32, no. 8, pp. 773–785, 2014.
- [181] L. Ning *et al.*, „Process-induced cell damage: Pneumatic versus screw-driven bioprinting“, *Biofabrication*, vol. 12, no. 2, p. 025011, 2020.
- [182] L. Ning and X. Chen, „A brief review of extrusion-based tissue scaffold bio-printing“, *Biotechnology journal*, vol. 12, no. 8, p. 1600671, 2017.
- [183] I. Barratt, Y. Yan, B. Byrne, and M. Bradley, „Mass flow measurement of pneumatically conveyed solids using radiometric sensors“, *Flow Measurement and Instrumentation*, vol. 11, no. 3, pp. 223–235, 2000.

5

Automated and Dynamic Extrusion Pressure Adjustment Based on Real-Time Flow Rate Measurements for Precise Ink Dispensing in 3D Bioprinting

Lukas Wenger^{1*}, Svenja Strauß^{2*} and Jürgen Hubbuch^{1,2}

¹ Institute of Process Engineering in Life Sciences, Section IV: Biomolecular Separation Engineering, Karlsruhe Institute of Technology (KIT), Karlsruhe, Germany

² Institute of Functional Interfaces, Karlsruhe Institute of Technology (KIT), Eggenstein-Leopoldshafen, Germany

* Contributed equally

Abstract

Extrusion-based printing relying on pneumatic dispensing systems is the most widely employed tool in bioprinting. However, standardized and reliable methods for process development, monitoring and control are still not established. Suitable printing parameters are often determined in a trial-and-error approach and neither process monitoring nor real-time adjustments of extrusion pressure to environmental and process-related changes are commonly employed.

The present study evaluates an approach to introduce flow rate as a main process parameter to monitor and control extrusion-based bioprinting. An experimental setup was established by integrating a liquid flow meter between the cartridge and nozzle of a pneumatically driven bioprinter to measure the actual flow of dispensed ink in real-time. The measured flow rate was fed to a Python-based software tool implementing a proportional-integral-derivative (PID) feedback loop that automatically and dynamically adapted the extrusion pressure of the bioprinter to meet a specified target flow rate.

The performance of the employed experimental setup was evaluated with three different model inks in three application examples. a) Continuous dispensing: Several runs of continuous dispensing showed that the PID-based pressure control was able to generate a steady flow rate more consistently and precisely than constant pressure settings. b) Adaptation to ink inhomogeneities: Deliberately created ink inhomogeneities were successfully compensated for by real-time pressure adjustments which profoundly enhanced the printing quality compared to printing without adaptive pressure. c) Process transfer to other nozzle types: Experiments with different nozzle types demonstrated the potential of the established setup to facilitate and accelerate process transfer and development.

The present study provides an alternative approach for process design, monitoring and control by introducing flow rate as a main process parameter. We propose bioprinting processes to be based on flow rate specifications instead of constant pressure settings. This approach has the potential to save time by avoiding tedious parameter screenings and to introduce an active, real-time control over the printing process. Subjective influences by individual users during process development can be reduced and the process transfer between different devices and experimental setups can be facilitated and accelerated.

5.1 Introduction

Additive manufacturing, or 3D printing, is a collective term for a variety of fabrication techniques to produce three-dimensional objects by gradually adding material in a layer-by-layer buildup process [184]. 3D printing is already established in areas like mechanical engineering and the aerospace industry and is increasingly spreading into other fields like biotechnology [25, 185–187]. Novel applications in disciplines such as tissue engineering [188], smart materials [189] or bioprocess engineering [38, 190] already show the potential of this technique. Tissue engineering aims at designing artificially made and functional substitutes to restore, maintain or support the function of natural tissues [191]. The fabrication of such substitutes requires the embedding of living cells within a supporting matrix material mimicking the natural environment of living tissue [52]. Hydrogels are typically chosen for that purpose due to their aqueous nature and high biocompatibility [52]. Another common application for hydrogels is the immobilization of enzymes by physical entrapment [192]. Hydrogels or hydrogel precursor solutions are often employed in bioprinting, an interdisciplinary

field combining 3D printing and biofabrication with the objective to print biologically functional constructs like living tissues [50]. In this context, the hydrogel precursor solutions are typically referred to as *bioinks* when containing living cells, or as *biomaterial inks* if they are cell-free [59]. Depending on the field of application and the printing method, bioinks need to meet certain criteria like cytocompatibility, specific rheological properties and the ability for crosslinking [50]. To meet these requirements, bioinks are often hybrid materials containing several components like polymers, rheological additives and crosslinkable components. The polymers can be synthetic, e. g. based on polyethylene glycol (PEG) or poloxamer, or naturally derived, e. g. based on agarose, alginate, chitosan, hyaluronic acid, fibrin, or collagen. Depending on the intended use, the polymers can be chemically modified and, for example, ligands for cell adhesion can be incorporated. The polymers can be crosslinked physically, chemically, thermally, enzymatically or by photopolymerization [3, 193]. Certain hydrogels, e. g. based on poloxamer, are also used as a sacrificial support material that is removed after printing [194].

In bioprinting, a variety of methods like inkjet-, laser- or stereolithography-based bioprinting is available. The most common method, especially in cell-based printing, is extrusion-based bioprinting (EBB) [50] which relies on a steady flow of material being dispensed from a cartridge. EBB methods can be classified by the employed dispensing system which can be based on pneumatic or mechanical extrusion, with each method having different advantages and disadvantages [50, 188]. Pneumatic systems use pressurized air to extrude material, while mechanical systems are driven by a piston or a screw [50]. Piston-based systems theoretically allow a more precise control of the extruded volume as the flow rate is directly correlated to the movement of the piston and the cartridge dimensions. The flow rate can be set independently of the material by defining the piston speed, but there is a tendency of lagging leakage at the end of an extrusion process which can be counteracted by retracting the piston or adding a valve [49, 195]. Screw-based systems allow excellent control of the extruded volume, but cleaning the system is tedious and often accompanied by a high loss of material due to dead volume [166]. This may be problematic when working with costly bioinks and slowly growing cells. The screw-driven mechanism induces higher shear forces which can result in increased cell damage, depending on the design of the screw and the printing conditions [196].

Pneumatic dispensing is widely employed due to its simplicity [188], but it is prone to delays due to the compression of gas volume within the cartridge which can reduce the printing precision [3, 197]. In pneumatic dispensing systems, the resulting flow rate cannot be controlled directly, as it is not only dependent on the applied pressure, but also on the rheological properties of the bioink and the components of the experimental setup like the nozzle. This makes the method susceptible to unintended variations of the experimental conditions. Therefore, environment-related parameters like temperature or humidity, system-related parameters like cartridge fill level, or material-related parameters, such as inhomogeneities or batch-to-batch variations of the bioinks, can have a relevant effect on the generated flow rate and hence the outcome of the printing process [14, 85, 167, 198, 199]. Compensating for such variations may require a change in extrusion pressure to achieve the desired flow rate. However, the most common approach to bioprinting process development is to define constant printing parameters or working windows either systematically or by trial and error [14, 139, 199]. These approaches are usually based on indirect parameters like rheological properties of inks [14] or qualitative aspects like filament formation [200]. Other methods include the analysis of strand widths [201] or filament fusion [199] by structural image analysis. In order to handle variations of bioink properties or environmental conditions, all these approaches may require parameter screenings before performing a printing run, depending on the robustness of

the process. An alternative approach is to reduce the environmental variations to a minimum by placing the bioprinter in a temperature- and humidity-controlled environment [168]. However, both strategies cannot equally handle both batch-to-batch variations of the bioink and time-dependent environmental changes.

Direct real-time monitoring of bioprinting processes is relatively uncommon, but previous studies have shown that liquid flow sensors can be employed to monitor the flow rate during bioprinting and to observe batch- and time-related changes in the relation of pressure and flow [202, 203]. Flow sensors are currently used for industrial applications in the automotive, oil and gas industry, but also in the food and beverage and pharmaceutical industry [204–210]. A range of different flow sensors are available which can be classified based on the employed measurement principle. Thermal flow sensors derive the flow rate from the travel time of heat pulses or the temperature profile around a heater [211]. Non-thermal sensors are based on other physical principles [211]. Today, very small flow meters can be produced with many advantages such as a lack of moving parts, better dynamic characteristics, low power consumption, low cost and easier integration into other systems [212]. Progress in the production of microelectromechanical systems allowed the development of micromachined thermal flow sensors which can be applied in the medical field to monitor blood and respiratory flow or drug delivery [208, 213, 214].

While it has been shown that flow sensors can be employed in bioprinting for process monitoring [203], there is still no demonstration of how to use the flow data obtained during extrusion in order to dynamically adapt the pressure and create a steady flow, independent of interference factors like temperature, cartridge fill level and other parameters. The present work introduces an experimental setup including a liquid flow sensor as a part of a feedback-loop controlling the pressure of a pneumatically driven bioprinter. A Python-based software tool is developed to read and record the sensor data and to generate a steady flow rate by continuously adapting the pressure based on a proportional-integral-derivative (PID)-controlled feedback loop. The developed setup is tested with three different model inks, two of which are based on the synthetic polymer poloxamer 407 (also known as Pluronic[®]F-127 or Kolliphor[®]P407) in different concentrations. Poloxamer 407 inks are suitable model inks due to their excellent printability and simple preparation [14, 81, 194]. Additionally, an ink based on the natural polymer alginate and the additive Laponite[®] RD is investigated. Alginate is a very common component of bioinks due to its gelling properties [69, 215–217] and Laponite[®] RD is typically employed as an inorganic filler to increase viscosity and enhance printability [190, 218, 219]. The performance of the employed adaptive pressure control setup was investigated in three application examples. a) Continuous dispensing: The general behavior of the flow sensor and the ability of the PID control to generate a constant flow were tested using continuous dispensing runs. b) Adaptation to ink inhomogeneities: The suitability for realistic printing applications was tested by printing from a cartridge with an intentionally inhomogeneous ink created by alternating layers of poloxamer 407 inks of different concentrations. c) Process transfer to other nozzle types: As an example for process transfer, the ability of the setup to adapt to different nozzle types was tested. An overview of the employed workflow is depicted in Figure 5.1.

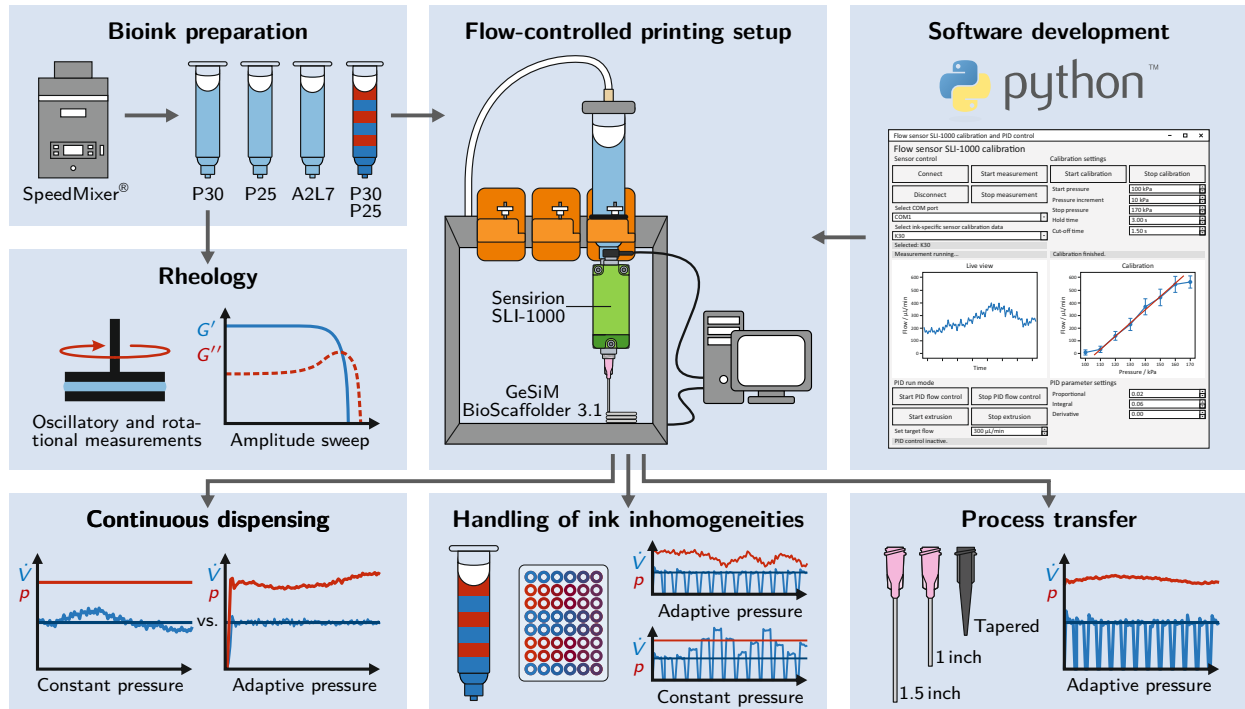


Figure 5.1 Schematic of the workflow applied in the present study. Three different inks are prepared and analyzed with rheological methods. A Python-based software tool is developed that implements a PID control loop to continuously adapt the extrusion pressure of a pneumatic bioprinter based on real-time data from a liquid flow meter. The integrated PID control setup is evaluated in three separate application examples.

5.2 Materials and methods

5.2.1 Ink preparation

Sodium alginate and poloxamer 407 were both obtained from Sigma Aldrich (St. Louis, USA) and Laponite[®] RD from BYK-Chemie GmbH (Wesel, Germany). Three different inks were prepared by dissolving the appropriate amounts of the respective components in ultrapure water (arium[®] pro VF, Satorius AG, Göttingen, Germany) and mixing at 3500 rpm in a SpeedMixer[®] (Hauschild GmbH & Co. KG, Hamm, Germany), until a homogenous mixture was obtained. Poloxamer-based inks were cooled in an ice bath between mixing steps to increase solubility. Three different ink compositions were prepared, the first one containing 30 % (w/w) poloxamer 407 (P30), the second one 25 % (w/w) poloxamer 407 (P25) and the third one 2 % (w/w) sodium alginate with 7 % (w/w) Laponite[®] RD (A2L7). An overview of the employed inks and their components is given in Table 5.1. The prepared inks were filled into 10 mL cartridges (Nordson Corporation Westlake, USA) and centrifuged at 600 g for 10 min to minimize the amount of entrapped air bubbles. The cartridges were sealed with pneumatic pistons (Nordson Corporation Westlake, USA) for printing.

Abbreviation	Poloxamer 407 (% (w/w))	Alginate (% (w/w))	Laponite [®] RD (% (w/w))	Extrusion pressure (kPa)
P30	30	—	—	436
P25	25	—	—	256
A2L7	—	2	7	329

Table 5.1 Ink compositions with the corresponding extrusion pressure, as employed for printing runs with a constant pressure setting. The pressure was determined from the first adaptive dispensing run with a 1 inch nozzle and a target flow rate of 300 $\mu\text{L}/\text{min}$ by averaging the applied pressure over a period of 10 min.

5.2.2 Rheology

The rheological behavior of P30, P25, and A2L7 was investigated using the rheometer Physica MCR301 (Anton Paar GmbH, Graz, Austria). A setup with parallel stainless steel plates with a diameter of 25 mm was employed for all rheological experiments. The gap width was 150 μm and all measurements were performed at 20 $^{\circ}\text{C}$ as technical triplicates ($n = 3$).

Yield stress values were determined from shear stress-controlled rotational tests. The deformation was plotted against shear stress on a logarithmic scale. The yield stress was determined by fitting the two linear regions of the plot with tangents and calculating the shear stress at their point of intersection.

Oscillatory measurements were performed with controlled shear stress τ in a range of 1 to 1000 Pa at an angular frequency of $\omega = 10 \text{ s}^{-1}$. For each measurement, the loss factor $\tan \delta = G''/G'$ was determined by averaging G' and G'' in the region from $\tau = 10 \text{ Pa}$ to $\tau = 100 \text{ Pa}$ which was within the linear viscoelastic (LVE) region and low in noise for each measurement.

5.2.3 Adaptive PID pressure control: hardware and software setup

The main objective of the present study was to establish a tool that enables flow-based process control for pneumatic extrusion-based bioprinting. The approach was to employ a software-based proportional-integral-derivative (PID) control that uses input data from a liquid flow meter to adapt the extrusion pressure of a pneumatic bioprinter in real-time. The components of the established setup and their interactions are described in the following sections.

5.2.3.1 Hardware configuration

All conducted dispensing and printing experiments were performed on a BioScaffolder 3.1 bioprinter (GeSiM mbH, Radeberg, Germany) with three pneumatic extrusion heads. An SLI-1000 liquid flow meter (Sensirion, Stäfa, Switzerland) was employed to measure the flow rate of inks during printing. The SLI-1000 contains a straight glass capillary with an inner diameter of 1 mm and is specified for flow rates up to 1000 $\mu\text{L}/\text{min}$ with water. The sensor relies on calorimetric sensing, a measurement principle that derives flow rates from thermal profiles forming around a heating element depending on the current fluid flow [212]. In the case of the Sensirion SLI-1000, two thermal sensors are placed up- and downstream of the heating element to detect the thermal profile, as indicated in Figure 5.2A. The flow sensor was attached below one of the extrusion heads of the

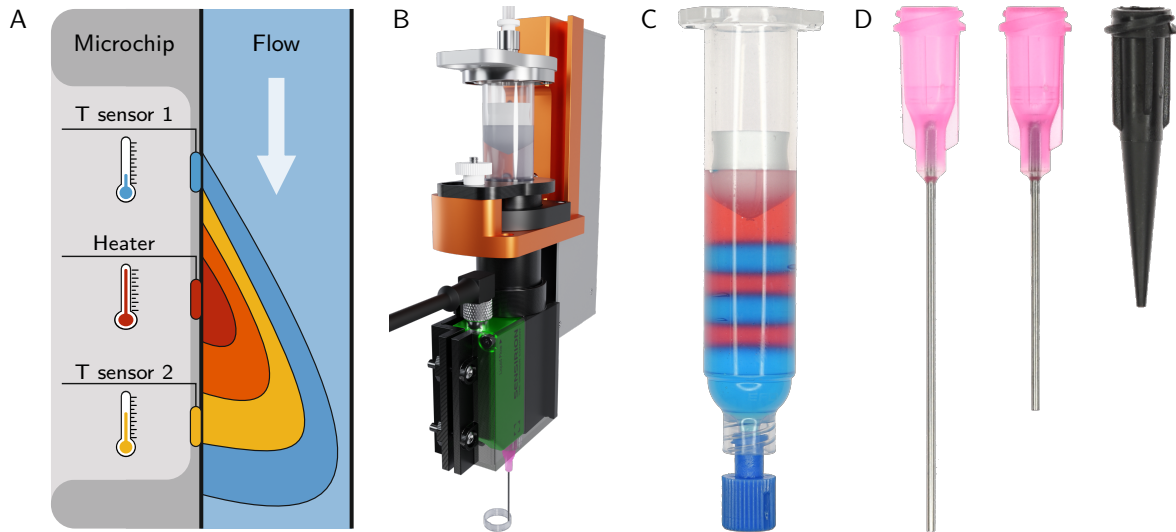


Figure 5.2 (A) Schematic representation of the thermal measuring principle of the liquid flow meter. Adapted from Schnell *et al.* [172] and Kuo *et al.* [212]. (B) 3D visualization of the arrangement of the hardware components of the PID control setup. The sensor is attached below the extrusion head of the bioprinter using a 3D-printed mount. The right part of the mount is shown as transparent to reveal the flow sensor. A cartridge is connected to the sensor inlet on the top, a nozzle to the outlet at the bottom. The CAD file of the sensor was obtained from Sensirion [220]. (C) Printer cartridge filled with alternating layers of P30 (blue) and P25 (red). The layered material served as a performance test for the PID-controlled printing setup. (D) Dispensing tips used in this study, from left to right: 1.5 inch straight nozzle, 1 inch straight nozzle, tapered nozzle. All nozzles had an orifice diameter of 0.58 mm. Depending on length and geometry, even dispensing tips with identical orifice diameter can generate massively different back pressures.

BioScaffolder using a customized, 3D-printed mount. A USB cable enabled the communication between flow sensor and computer via RS485 interface.

The arrangement of the components allowed a cartridge to be directly attached to the inlet on the upper side of the liquid flow meter and a nozzle to the outlet at the bottom side. The setup reduced the amount of available space in the z-direction, but otherwise enabled unrestricted printing. Figure 5.2B shows the employed setup while printing a hollow cylinder.

5.2.3.2 Software development

A software tool based on Python 3.8.5 (Python Software Foundation, Delaware, USA) was developed to integrate the liquid flow meter and the pneumatic extrusion bioprinter into a PID-controlled feedback loop that constantly adapts the extrusion pressure to keep the resulting ink flow at a constant target value. A scheme representing all the components involved in the PID control and their interactions is shown in Figure 5.3. In short, the user sets the target flow rate and PID parameters using a graphical user interface (GUI). The Python-based software receives real-time data from the liquid flow meter which is converted to flow rate values using imported calibration curves. To generate the desired target flow rate, the software-based PID control constantly adapts

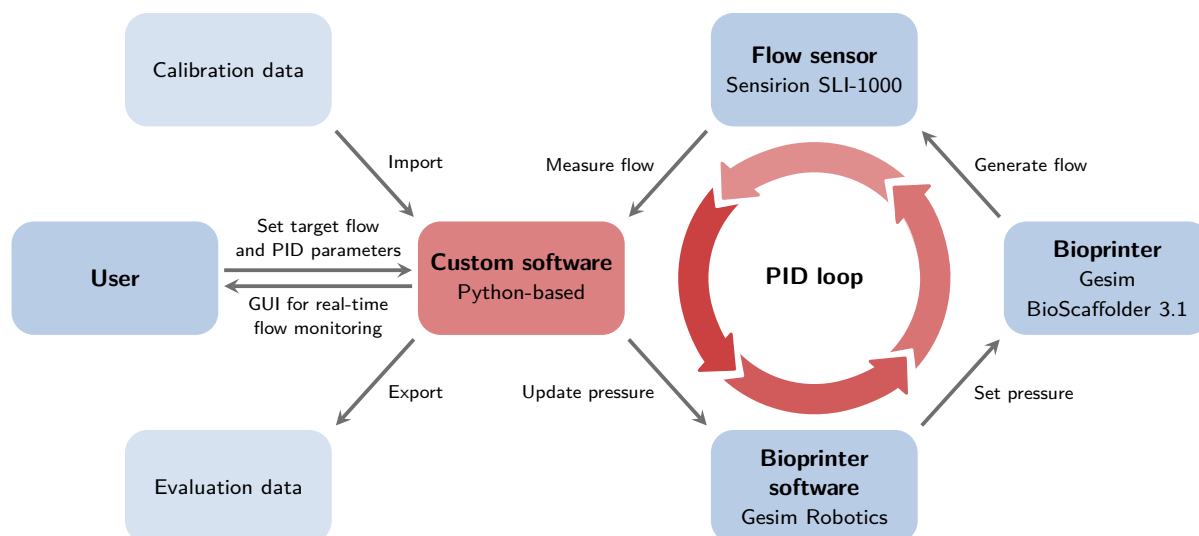


Figure 5.3 Schematic of the interactions between the relevant components of the PID control setup.

the pressure by sending commands to the GeSiM Robotics software which controls the GeSiM BioScaffolder. The flow rate and pressure settings are stored and exported for later evaluation.

Graphic user interface For easy interaction with the user, a graphical user interface (GUI) was developed that allowed controlling the flow sensor, performing calibrations and adjusting the PID control. Figure 5.4 shows the GUI of the developed Python tool with the GUI of the GeSiM Robotics software in the background. The GUI was split in several sections. The top left section provided the flow sensor control panel including buttons to connect and disconnect and to start and stop measurements. The COM port of the flow sensor and the appropriate ink calibration could be selected from drop-down menus. Depending on the selection, the ink-specific calibration data necessary to convert the sensor output to flow values were loaded from an external Excel file. Section 5.2.4.1 describes how the calibration data were generated using a syringe pump and an adapted version of the Python tool. Below the sensor control panel, the GUI showed a graph with a live view of the current flow measurement.

Another control panel to perform pressure-flow calibrations was located in the top right part of the GUI, accompanied by an additional graph showing the determined calibration points with the respective calibration curve. This feature allows determining the correlation between applied pressure and resulting flow rate for a specific ink and experimental setup. Within the scope of this paper, this feature was not applied but it may be used to characterize the flow behavior of inks under certain conditions. The bottom part of the GUI accommodated the PID control panel including buttons to start and stop the PID control and the extrusion process. Input fields allowed setting the target flow rate and the PID parameters.

Device communication Communication between the Sensirion SLI-1000 liquid flow meter and Python could be established by customizing code provided by Sensirion. The code was based on the *pySerial* package (version 3.5) which enables communication over the serial port. While running, the software constantly read out the current flow from the liquid flow meter at a rate of roughly

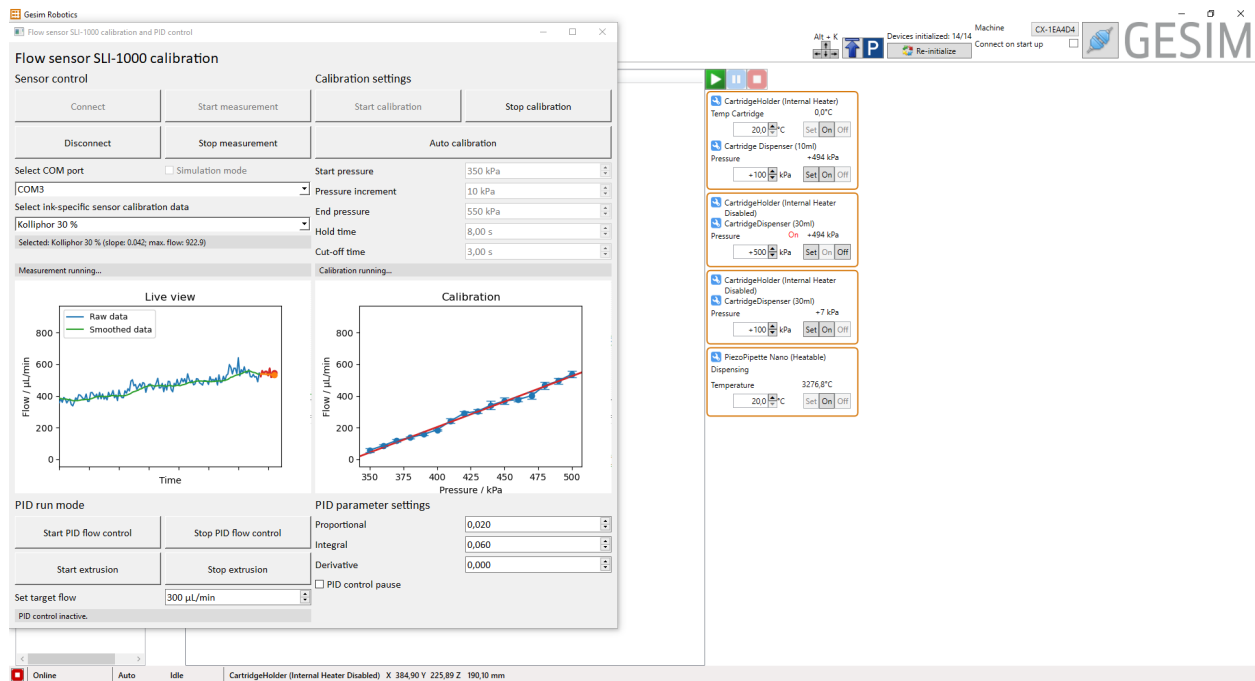


Figure 5.4 Screenshot of the graphical user interface of the Python-based PID control tool. The example shows the calibration of the ink P30. The left graph represents a live view of the flow measurement data, the right graph shows data points obtained during the calibration. The GeSiM Robotics software being automatically operated by the Python tool is visible in the background.

five readings per second. During printing processes, the pressure is frequently turned on and off when switching from one strand or layer to the next. These switching operations are accompanied by a drop in flow rate that is irrelevant to the PID control. To ignore these irrelevant data points, only flow rate values larger than 3% of the sensor output limit were regarded as valid. To ignore spikes in flow rate that sometimes occurred with the switching operations, all data points deviating from the previous data point by more than 20% relative to the sensor output limit were regarded as invalid. Besides the raw flow rate data, an additional curve with smoothed data was plotted in the live view of the GUI. The smoothed data was obtained by determining a rolling average over the last 15 valid data points.

Direct communication between Python and the BioScaffolder 3.1 allowing real-time changes in pressure could not be established. As a workaround, the GeSiM Robotics software controlling the BioScaffolder was automatically operated by Python to trigger pressure changes. For this purpose, the *PyAutoGUI* package (version 0.9.52) was employed that allows performing automated operations on third-party GUIs like clicking buttons or entering text into input fields. This workaround allowed controlling the extrusion pressure of the BioScaffolder indirectly via Python, even during an active printing process.

PID-based pressure control The software-based PID control loop was implemented in Python using the package *simple-pid* (version 0.2.4). In the active state, the PID loop was fed every 0.25 s with the last valid data point and the pressure in the GeSiM Robotics software was updated

Table 5.2 Proportional, integral and derivative gain, as applied for all experiments involving the PID control for automatic pressure adjustment.

Gain parameter	Value
K_p (proportional)	0.02
K_i (integral)	0.06
K_d (derivative)	0.00

every 0.5s based on the output of the PID loop. Suitable PID control parameters (proportional, integral and derivative gain) were determined iteratively by trial-and-error and kept constant for all performed experiments, as shown in Table 5.2.

The applied PID algorithm of the *simple-pid* package is based on the controller output function

$$u(t) = K_p e(t) + K_i \int_0^t e(t) dt + K_d \frac{de(t)}{dt} \quad (5.1)$$

with the gain parameters K_p (proportional), K_i (integral) and K_d (derivative) and the error term

$$e(t) = r(t) - y(t) \quad (5.2)$$

where $r(t)$ is the reference input and $y(t)$ is the process variable [221, 222]. In the given case, $u(t)$ is used as an input variable for the printer to set the current extrusion pressure, $r(t)$ is the set point of the flow rate for the PID control and $y(t)$ is the flow rate measured by the flow sensor. The integration of the PID controller within the experimental setup and the interaction between the components and their respective input and output variables is schematically shown in Figure 5.5.

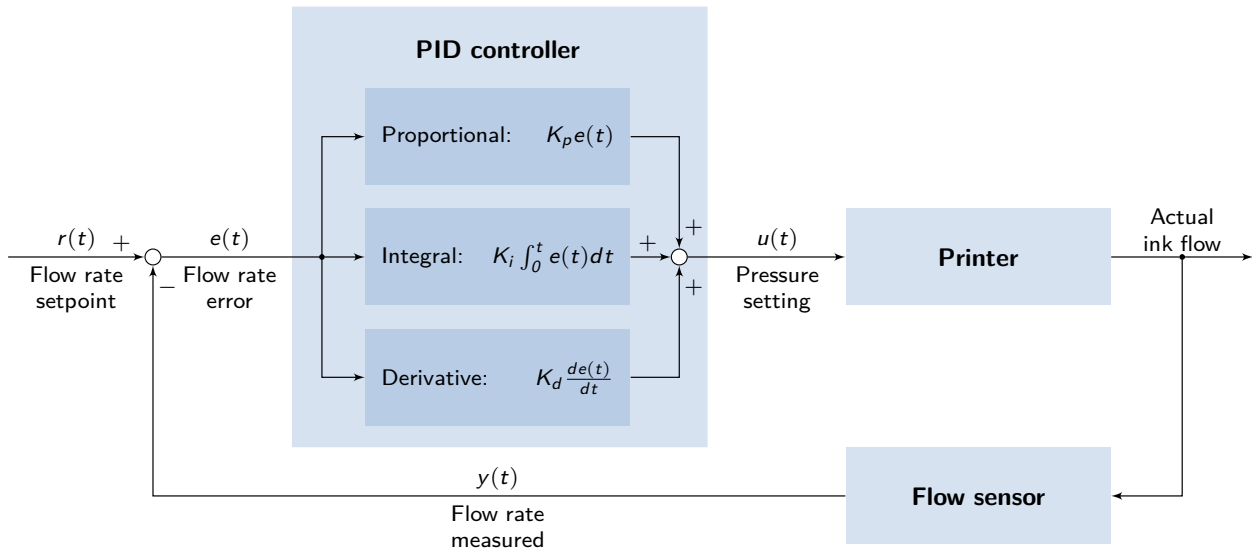


Figure 5.5 Schematic block diagram of the employed PID feedback loop showing the interaction between printer, flow sensor and PID controller in combination with the respective input and output variables. Scheme adapted from [221, 222].

5.2.4 Application of the adaptive pressure control

5.2.4.1 Flow sensor calibration

The employed liquid flow meter SLI-1000 determines flow rates indirectly from heat distribution profiles within the fluid [223]. As such, it is substantially influenced by the specific thermal conductivity properties of the specific fluid [212] and requires individual calibrations when working with a variety of inks. Accordingly, calibration curves were determined for P30, P25 and A2L7 that allowed converting the sensor output data to flow rate values. To generate a defined volumetric flow rate through the SLI-1000 liquid flow meter, a Nemesys 290N syringe pump with a 10 mL syringe (both Cetoni GmbH, Korbußen, Germany) was employed. A slightly adapted version of the described Python software tool was applied to record the output data of the sensor and to adjust the syringe pump to different flow rates by operating the control software of the syringe pump (QmixElements, version 20140605). A screenshot of the software tool and the QmixElements software is shown in the supplementary material. Data points for the calibration curves were determined by setting a fixed flow rate for 30 s and determining the mean value of the sensor output of the last 20 s of this period. The flow rate was increased step-wise, until the sensor output limit was reached. The obtained data points were fitted with a linear equation. The resulting calibration curves are shown in the supplementary material and the equation parameters were stored in an Excel file that served as an input for the Python-based PID software tool.

5.2.4.2 Continuous dispensing

Continuous dispensing runs were performed as an initial performance test of the adaptive pressure control. For each ink, three runs were carried out with active PID control and three runs with a constant pressure setting ($n = 3$). Ink was dispensed from a 10 mL cartridge continuously for 30 min through a 1 inch straight nozzle with an inner orifice diameter of 0.58 mm (Vieweg GmbH, Kranzberg, Germany, see Figure 5.2D). During the runs with adaptive pressure, a target flow rate of 300 $\mu\text{L}/\text{min}$ was specified and the pressure was continuously adapted by the Python-based PID control tool described in Section 5.2.3.2. The applied pressure of the first run with adaptive pressure control was averaged over a period of 10 min and used as the pressure setting of the runs with constant pressure. The obtained constant pressure settings are presented in Table 5.1.

5.2.4.3 Adaptation to ink inhomogeneities

To verify the capability of the PID control to generate a constant flow independent of changing rheological properties of the ink, two cartridges were filled with alternating layers of P30 and P25. In order to highlight the different layers optically, P30 was spiked with blue and P25 with red food coloring. Before the cartridge was filled, the inks were liquefied by cooling to allow the handling with pipettes. After addition to the cartridge, each layer was allowed to solidify at room temperature, before the next layer was added. At the bottom of the cartridge was a layer of 2 mL P30, followed by 4 alternating 1 mL layers of P25 and P30, and at the top was a 2 mL layer of P25. A photograph of one of the cartridges is shown in Figure 5.2C.

Hollow cylinders with a diameter of 10 mm and a height of 3 mm were printed as simple test objects onto a glass plate heated to 35 °C to avoid ink spreading. The layer height of the cylinders was 300 μm and the printing speed 10 mm/s. All prints were carried out with a straight 1 inch nozzle with an inner orifice diameter of 0.58 mm. One cartridge was used for each printing run. To evaluate

the performance of the adaptive pressure control, the first run was performed with active adaptive pressure control and a target flow rate of 300 $\mu\text{L}/\text{min}$. Before starting the printing process, the adaptive pressure control was run for 30 to 60 s, until a constant flow was reached. The second printing was carried out with a constant pressure of 436 kPa which was determined to be suitable for P30 during the continuous dispensing runs (see Table 5.1).

5.2.4.4 Process transfer to other nozzle types

To investigate whether a flow rate-based process control facilitates the process transfer between different nozzle types, additional prints of hollow cylinders were carried out with the already employed 1 inch straight nozzle, a 1.5 inch straight nozzle and a tapered nozzle, all with an inner orifice diameter of 0.58 mm and obtained from Vieweg GmbH. The three nozzle types are depicted in Figure 5.2D. Again, runs with adaptive pressure control were compared to runs with fixed extrusion pressure. With every run, two 3 mm high cylinders with a diameter of 10 mm and a layer height of 300 μm were printed at a speed of 10 mm/s on a plate heated to 35 $^{\circ}\text{C}$. Before the runs with adaptive pressure control, the target flow rate was set to 300 $\mu\text{L}/\text{min}$ and the adaptive pressure control was run for 30 to 60 s, until a constant flow was reached. The runs with constant pressure setting were carried out with the pressure that was determined to be suitable for the respective ink in combination with the 1 inch straight nozzle during the continuous dispensing runs (see Table 5.1).

5.3 Results and discussion

5.3.1 Implementation of the experimental setup

As the application of flow sensors is not an established practice in 3D bioprinting, a customized setup was designed to implement a Sensirion SLI-1000 liquid flow meter on a GeSiM BioScaffolder 3.1 bioprinter. As shown in Figure 5.2B, the flow sensor was attached between the cartridge and the nozzle using a 3D-printed mount which allowed fast and easy assembly. However, the arrangement added a certain amount of complexity and some disadvantages to the experimental setup. The height of the sensor of 53 mm caused a reduction of available space in the z-direction despite the cartridge being mounted above its default location. The capillary of the sensor and the required Luer lock adapters added some dead volume which may be problematic when working with costly bioinks and sterile operation of the setup was made more difficult. These disadvantages can largely be attributed to the lack of optimization of the established setup. The employed flow sensor was neither optimized for the use with hydrogels, nor for the interoperability with a bioprinter. A more wide-spread application of flow sensors in bioprinting would require targeted adaptations like a reduction in size and cost. Smaller sensors with Luer locks would reduce both space requirements and dead volumes. Lower cost could enable the use of flow sensors as disposable products to simplify sterile operation.

The calibration of the flow sensor with different inks revealed a strong influence of the material on the measurements. The calibration curves for P30 and P25 could be fitted well ($R^2 = 0.9989$ and 0.9987) with an equation of the form $y = mx$, while A2L7 required an additional y-intercept ($y = mx + c$) which led to invalid measurement values at low flow rates and has to be considered when assessing the validity of measurements.

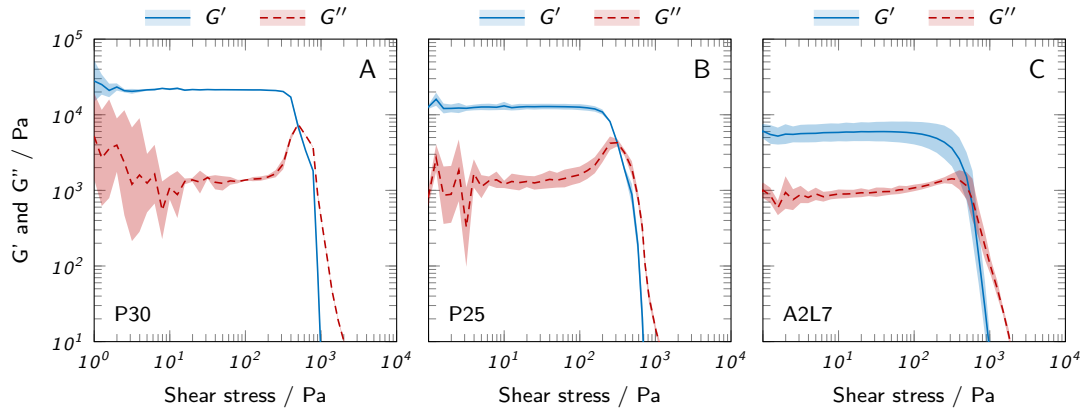


Figure 5.6 Shear stress-controlled oscillatory measurements showing the storage modulus G' and loss modulus G'' for all prepared inks at an angular frequency of $\omega = 10 \text{ s}^{-1}$. The results are depicted as mean values, the shaded areas represent the standard deviation ($n = 3$).

5.3.2 Rheology

The rheological behavior of inks is one of the most relevant factors determining printability in extrusion-based bioprinting. The characteristics of the inks employed in this study were analyzed with oscillatory and rotational measurements. The storage and loss moduli (G' and G'') and the loss factor $\tan \delta$ were determined in oscillatory measurements. Figure 5.6 shows the performed amplitude sweeps in a range of 1 to 10 000 Pa. For all samples, the storage modulus G' was higher than the loss modulus G'' within the linear viscoelastic region, indicating a gel-like behavior for all investigated inks. The exact ratio of G' and G'' is expressed in the loss factor $\tan \delta = G''/G'$ and was derived from the same measurements. The resulting values of $\tan \delta$ are shown in Figure 5.7, alongside the yield stress values determined in rotational measurements. Gel-like behavior is implied by $\tan \delta < 1$ and lower values indicate a stronger dominance of elastic properties over viscous properties [85]. The lowest $\tan \delta$ was found for P30 with 0.060 ± 0.006 and the highest for A2L7, but all samples were below $\tan \delta = 0.17$ showing a strong dominance of elastic properties. The same trends are represented in the yield stress which was highest for P30 at $(861 \pm 32) \text{ Pa}$ and lowest for A2L7 at $(474 \pm 5) \text{ Pa}$. A yield point could be detected for all inks. The results demonstrate the general suitability of the employed inks for bioprinting applications, as they all showed gel-like behavior ($\tan \delta < 1$) and the presence of a yield point. High yield stress is an important factor determining printability [200], as it represents the ability of the ink to maintain its shape after extrusion.

5.3.3 Application of the adaptive pressure control

The performance of the presented setup for an adaptive PID pressure control was investigated employing three separate approaches. a) Continuous dispensing: To generally compare the resulting ink flow with and without adaptive pressure control, ink was continuously dispensed from a cartridge without printing any defined objects. The actual applicability of the setup in realistic scenarios was evaluated in two additional studies involving the printing of hollow cylinders as test objects. b) Adaptation to ink inhomogeneities: The ability to compensate for ink inhomogeneities by pressure adjustments was tested by printing from a cartridge with an intentionally inhomogeneous ink created

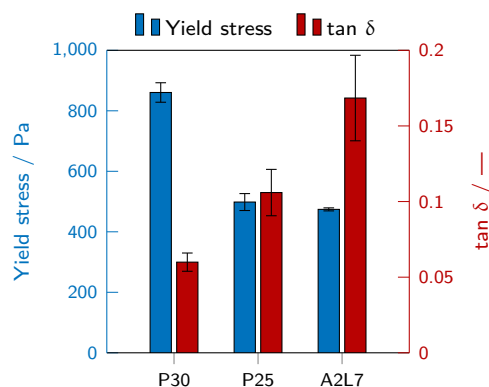


Figure 5.7 Yield stress, as determined from rotational measurements, and loss factor $\tan \delta$, as determined from oscillatory measurements, for all evaluated inks. The results show mean values \pm standard deviation ($n = 3$).

by alternating layers of poloxamer 407 inks of different concentrations. c) Process transfer to other nozzle types: As an example for process transfer, the ability of the setup to adapt to nozzles with different lengths and geometries was investigated.

5.3.3.1 Continuous dispensing

The general capability of the real-time, adaptive pressure control to ensure a constant and reproducible ink flow was initially evaluated by simple, continuous dispensing runs. This approach allowed avoiding interference factors like pressure switching operations between printed layers. A separate ink-filled cartridge was used for each run and the ink was continuously dispensed for 30 min without printing any defined objects. Six runs were performed per ink, three with a constant pressure setting and three with the adaptive pressure control being active. Every run aimed at meeting a target flow of 300 $\mu\text{L}/\text{min}$. For the runs with adaptive pressure control, this could be achieved automatically without any preparatory work apart from the ink-specific flow sensor calibration to convert the sensor output to flow rate values. The continuous dispensing runs were then started with a pressure setting of 0 kPa and the pressure was automatically adapted by the PID control to an appropriate value within roughly 30 s. For the runs with constant pressure setting, a suitable pressure had to be determined first which was derived from the first adaptive run by averaging the applied pressure within a constant region over a period of 10 min. Flow measurements and pressure settings were recorded for the entire duration of each run.

Figure 5.8 shows the recorded flow rate and pressure for P30 over time. A slightly smoothed flow rate is depicted in light blue and represents a rolling average over 15 data points, only including the valid data points as defined in section 5.2.3.2 (absolute value $> 3\%$ of the sensor output limit and $< 20\%$ change compared to the previous data point, also relative to the sensor output limit). The target flow rate is indicated in dark blue. The graphs A-C show the results of dispensing ink with a constant pressure setting, the graphs D-F represent the runs with adaptive pressure control.

A certain level of relatively uniform noise (roughly $\pm 50 \mu\text{L}/\text{min}$) was observed for the flow data of all runs, apparently a phenomenon that is inherent to the measurement method in combination with the investigated inks. It should be noted that the flow sensor is not designed for hydrogels or complex material compositions and showed considerably less noise in combination with water

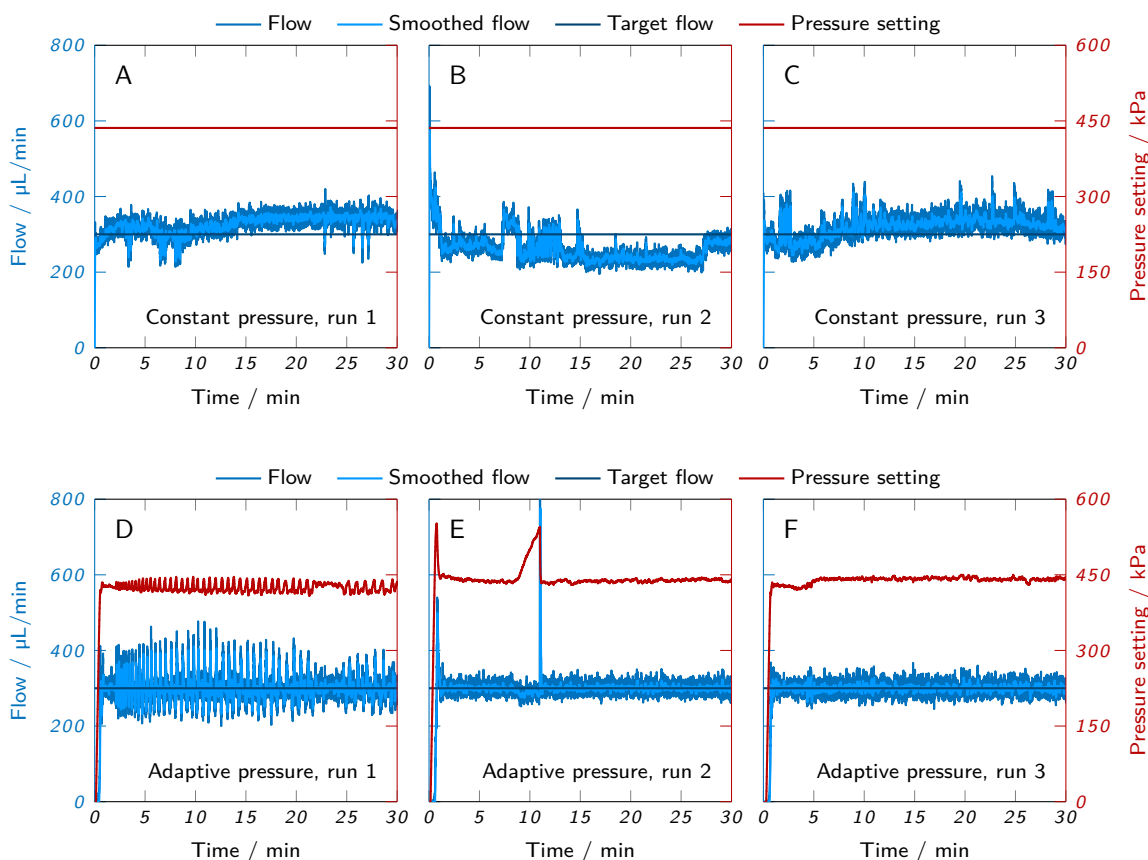


Figure 5.8 Continuous dispensing runs of P30. The measured flow and the pressure setting are plotted over time. (A-C) Runs with constant pressure setting are compared to (D-F) runs with adaptive PID pressure control and a target flow rate of 300 $\mu\text{L}/\text{min}$.

(data not shown). This implies that a large proportion of the observed noise can be attributed to the non-homogeneous nature of the inks containing micelles (P30 and P25) [224] or nanoclay and polymers (A2L7). A noticeably different noise pattern was observed for the first adaptive run with P30 (Figure 5.8D), as the sensor noise was overlaid by additional fluctuations with higher amplitude and longer cycle length. These fluctuations also appeared in the recorded pressure settings indicating that they were not caused by measurement noise but by actual fluctuations of the applied pressure. The regularity of the fluctuations implies that the PID controller entered an oscillatory state, caused by repeatedly overshooting the desired set point and overcorrecting for it. This behavior can be counteracted by retuning the PID control loop, e.g. based on oscillatory characteristics or perturbation signals [225, 226]. The mostly stable amplitude of the oscillations after 5 min implies a marginally stable system. For the second and third run of P30 with adaptive pressure control (Figure 5.8E and F) and all runs with other inks, no oscillations occurred and the amount of noise corresponded to the runs with constant pressure setting, despite the same PID parameters being applied. As the oscillatory behavior was only observed in one of nine runs, it was not interpreted as an inherent issue of the employed setup. However, it revealed a potential pitfall when working with PID-controlled systems and a more systematic tuning of the PID parameters could increase the stability of the system [226].

Besides noise, additional irregularities on a larger timescale could be observed in the flow signal of the P30 runs with constant pressure setting (Figure 5.8A-C). These irregularities did not follow a certain pattern, but seemed entirely erratic. A relatively similar behavior was observed for the first and third run. During the initial phase, the flow rate of both runs showed considerable variations that stabilized after 10 to 15 min at a flow rate of roughly 350 $\mu\text{L}/\text{min}$. Overall, the flow rate showed a slightly increasing trend and was mostly above the target flow. The second run showed erratic and sudden flow variations during the entire measurement, only with one relatively constant period between 15 min and 25 min where the flow was around 250 $\mu\text{L}/\text{min}$. Overall, the flow rate decreased during the run and was mostly below the target value. These results demonstrate that with regards to flow rate, both the consistency within a single run and the reproducibility between separate runs are limited when applying a constant pressure. Due to their erratic nature, no clear causes could be identified for the observed signal fluctuations and drifts. Potential influencing factors are ink inhomogeneities, temporary and partial nozzle clogging or manufacturing variations of cartridges and plugs [166, 167]. The trends of increasing or decreasing flow rate suggest possible time-dependent parameters like temperature drifts or the cartridge fill level.

A very different behavior was observed for the runs with adaptive pressure control (Figure 5.8D-F). Each run was started with a pressure setting of 0 kPa. The PID control was activated and performed the pressure adaptation automatically. The pressure was increased steadily, until the appropriate flow was achieved. This initial adaptation phase took roughly 30 to 60 s, before the pressure was stabilized at an appropriate level to generate a flow of 300 $\mu\text{L}/\text{min}$ on average, corresponding to the desired target flow. For all three runs, the average flow was reliably kept constant for the whole duration of the measurement. However, as mentioned before, the first run showed considerable oscillations around the target value due to a suboptimal pressure regulation. In contrast, the second and third run achieved a similar amount of noise as the runs with constant pressure. During the second run (Figure 5.8E), a continuous pressure increase from roughly 440 kPa to 540 kPa occurred between 9 min and 11 min, accompanied by a minor drop in flow rate. After 11 min, the flow rate suddenly jumped to the output limit of the sensor causing the pressure to drop quickly back to the base level. As a result, the flow rate also returned to the target value. Apparently, a partial clogging of the nozzle occurred here that was appropriately counteracted by the PID control by increasing the pressure, resulting in only a minor and short-term drop of flow rate. This demonstrates the suitability of the adaptive pressure control to compensate for unpredictable and erratic influencing factors like ink inhomogeneities or nozzle clogging and keep the flow at a constant rate.

For a more compact overview and simple comparison of different inks, all runs performed are depicted as swarm plots in Figure 5.9. For P25 and A2L7, the corresponding plots of flow and pressure over time are shown in the supplementary material. Figure 5.9 shows every performed run as a separate swarm of data points. The width of the swarm indicates the kernel density estimation, i. e. the number of data points at the corresponding flow rate. Additionally, all data points are plotted on a color map indicating the time point of the measurement. Thus, trends like a changing flow rate over the course of the measurement can be recognized in the form of color gradients.

The already discussed runs of P30 are shown in Figure 5.9A. The first three swarms represent the runs with constant pressure, two of which are located largely above the target flow, while one is located below. The color gradients of the swarms indicate that each of these runs was accompanied by a steady change in flow rate implying a time-dependent influencing factor, as discussed before. The inconsistent positioning above and below the target flow demonstrates the lack of reproducibility

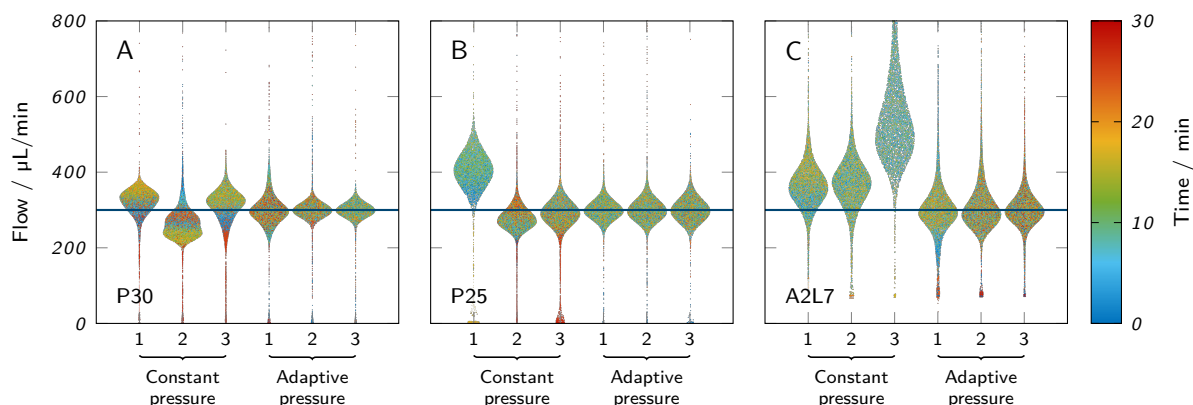


Figure 5.9 Overview of all performed continuous dispensing runs depicted as swarm plots. Each swarm represents the first 30 min of a run performed with (A) P30, (B) P25 or (C) A2L7. The blue horizontal line indicates the target flow rate.

and the limited capability to constantly meet the desired flow rate. By contrast, the swarms of the runs with an adaptive pressure setting are almost ideally centered around the target flow rate. The high fluctuations of the first run are reflected in the extended spread of the swarm along the y-axis.

Very similar observations could be made for the runs with P25 (Figure 5.9B). While all runs with an adaptive pressure control met the target flow rate very accurately, this was only the case for the third run with constant pressure. The other runs were largely off the target flow, again indicating a lack of reproducibility. The noise of the measurements, represented by the extent of the swarms along the y-axis, was similar for all runs with adaptive pressure control and not larger than for the runs with constant pressure. No pressure oscillations due to inadequate PID tuning occurred.

Figure 5.9C represents the measurements with A2L7. The comparison between runs with constant and adaptive pressure confirmed the previously made observations that the adaptive pressure control leads to an improved agreement between measured flow rate and target flow rate. The most noticeable difference of the A2L7 runs compared to P30 and P25 was the massively increased amount of noise across all runs. This behavior was also observed during the recording of calibration curves and seems to be inherent to the ink composition of A2L7. A systematic evaluation of noise behavior was not within the scope of this study. However, the stark contrast between the noise levels of the different inks implies that certain components typical for bioinks have a strong influence on the behavior and measurement quality of the flow sensor. While P30 and P25 only contain water and polymers, A2L7 has a more complex composition including solid nanoparticles. A systematic evaluation of the impact of different ink components and concentrations on the quality of the flow measurement should be the subject of future investigations. This investigation should also consider alternative types of flow sensors that might be better suited to provide accurate flow data for complex media like bioinks.

The continuous dispensing runs prove the suitability of the adaptive pressure control to rapidly generate a constant and defined ink flow, independent of the material and without the need for extensive parameter screenings. Adopting the flow rate as a relevant parameter in process development could simplify the transfer between different inks by aiming at a common target flow

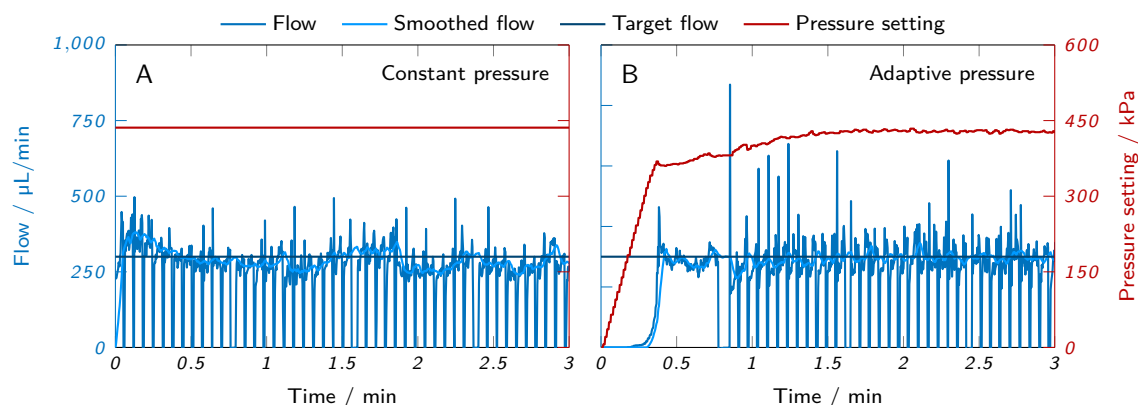


Figure 5.10 Initial phase of hollow cylinder printing with an inhomogeneous ink. The graphs show flow rate and pressure setting over time for (A) a run with constant pressure and (B) a run with adaptive pressure control. With constant pressure, the printing process was started immediately. Adaptive runs were started with an initial adaptation phase of 30 to 60 s during which the pressure was adapted, until a constant ink flow was achieved

rate. Larger flow rate fluctuations could be shown to be reduced by the adaptive PID pressure control.

5.3.3.2 Adaptation to ink inhomogeneities

While continuous dispensing tests can provide valuable insights about the general behavior of the adaptive pressure control, they do not represent the intended application in 3D bioprinting. To investigate the capabilities of the adaptive pressure control more thoroughly in a realistic use case, simple 3D objects were printed from a cartridge with an intentionally inhomogeneous ink. The inhomogeneity was created by filling the cartridge with alternating layers of P30 and P25 to create a situation where the extrusion conditions change repeatedly over time due to the different rheological properties of both inks. For better visualization, the inks were dyed with food coloring, as depicted in Figure 5.2B. To reduce the complexity of the printing process to a minimum, simple hollow cylinders were printed (10 mm diameter, 3 mm in height, 300 µm layers, 10 mm/s printing speed). For both runs, the sensor output was converted to flow rates based on the calibration curve of P30. A new cartridge containing three layers of P30 and three layers of P25 was used for each run.

Figure 5.10 shows the initial phase of the two runs performed with constant and adaptive pressure side-by-side. Before starting a print with the adaptive pressure control, the pressure was set to zero and a continuous dispensing process was started to allow the PID control to gradually adapt the pressure, until a stable ink flow of 300 µL/min was achieved. This adaptation phase is represented in the first 45 s of Figure 5.10B. The transitions from one printed layer to the next are clearly visible in the form of sudden drops in flow rate, as the pressure is released from the cartridge during the transition and no ink is extruded. Particularly in the run with adaptive pressure, short spikes in flow rate occurred when the pressure was reapplied for the next layer. The PID control and the smoothed flow rate, depicted in the graphs light blue, were not affected by the flow rate drops and spikes, as they ignored invalid data points. All data points that were higher than 3% of the sensor output limit and changed less than 20% relative to the output limit compared to the previous data point were regarded as valid.

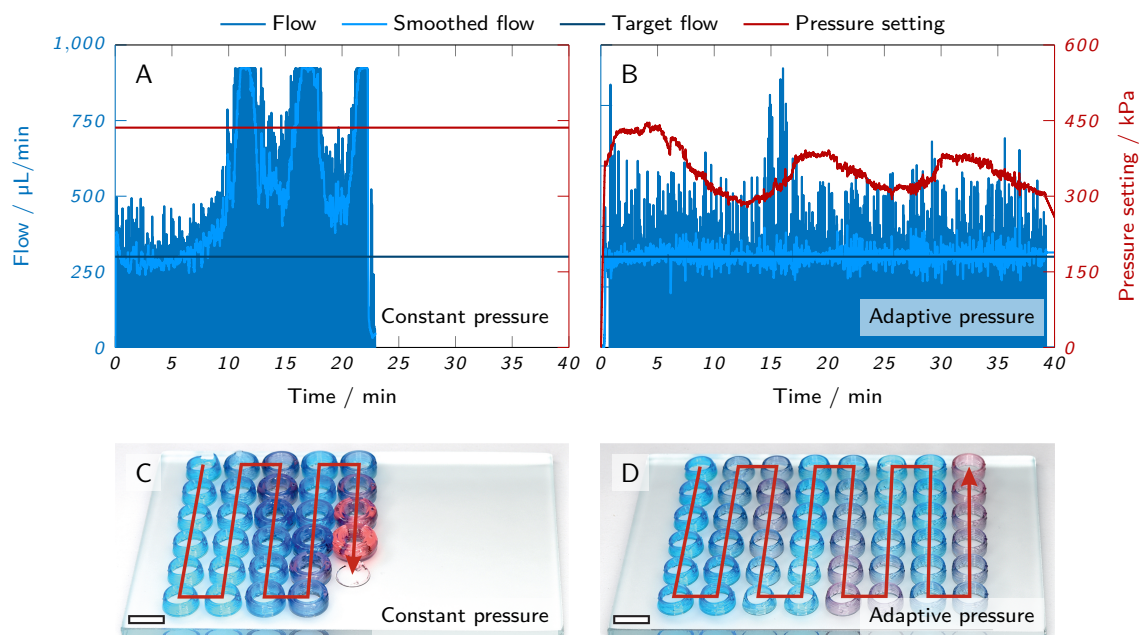


Figure 5.11 Printing of hollow cylinders with an inhomogeneous ink. The graphs show flow rate and pressure setting over time, the photographs the printed cylinders of (A and C) a run with constant pressure and (B and D) a run with adaptive pressure control. The scale bars in (C) and (D) represent 10 mm.

Figure 5.11 presents the entire results of the two performed printing runs. Figure 5.11A clearly visualizes the fluctuating flow rate when printing with a constant pressure setting optimized for P30. The measured flow rate was close to the target value of $300 \mu\text{L}/\text{min}$ at the beginning of the run when only P30 was extruded. The beginning extrusion of P25 after approximately 7 to 8 min was accompanied by a massive increase in flow rate. Thus, the three layers of P25 are reflected in the graph as three peaks of flow rate exceeding the output limit of the flow sensor. Between the layers, the flow rate did not return to the target value, but constantly exceeded it due to the mixing of the layers. As a result of the increased ink flow, the cartridge was already emptied after less than 23 min.

The PID control proved to be effective in compensating the rheologically different ink layers by continuously adapting the extrusion pressure. The three pressure peaks in Figure 5.11B reflect the three layers of P30 which require a higher extrusion pressure than P25. The pressure minima of the same graph correspond to the layers of P25. The change in pressure was not sudden, but relatively gradual, indicating a certain degree of blending between the two inks. This effect is also manifested in the absolute values of the pressure maxima and minima that did not reach the same values as in the dispensing tests of the unblended inks. The frequent and relatively regular spikes in flow rate, especially observed in the run with adaptive pressure, were mainly caused by the sudden application of pressure to the cartridge at the start of a layer. They were accompanied by spikes of negative flow rate when the pressure was suddenly released again (not shown in the graph due to the cut-off at $y = 0$). In general, these spikes were randomly observed in several printing runs and were not related to the PID control, but probably the presence of air bubbles in the cartridge. The available

data are not sufficient to assess whether these spikes are negligible measurement artifacts or a real and significant effect with potential negative impacts on the printed objects.

The printed cylinders are shown in Figure 5.11C and D. It is obvious that the cylinders printed with constant pressure exhibited a large range of different wall thicknesses due to the non-constant flow rate. Also, the cartridge was empty after only 28 cylinders, while 48 cylinders could be printed with the adaptive pressure control without emptying the cartridge entirely. Here, the wall thicknesses of the cylinders were relatively constant, independent of the extruded ink, but slight deviations in the wall thicknesses could still be observed. This can partially be attributed to drying effects, as the whole printing process lasted for nearly 40 min, but another important contributor is the suboptimal calibration applied in this experiment. For every ink, a specific calibration curve was determined that allowed converting the sensor output data to flow rate values. In this case, the calibration curve of P30 was applied whose slope was about 12 % higher than for P25 (see supplementary material). This resulted in a deviation between measured and real flow rate and caused a reduced ink flow when P25 was extruded.

The test prints with an inhomogeneous ink demonstrate the capability of the adaptive pressure control to perform real-time corrections of the extrusion pressure. The ink flow can be kept at a relatively constant value, even when conditions like ink viscosity vary over time due to inhomogeneities or environmental changes. Unlike the continuous dispensing, these experiments also demonstrate the applicability of the setup for printing and its potential profound impact on the resulting prints.

5.3.3.3 Process transfer to other nozzle types

Changing certain parameters in the experimental setup like nozzles, cartridges or printers usually requires adapting the extrusion pressure in order to achieve satisfactory printing results. Determining the appropriate pressure requires extensive parameter screenings and is often not done systematically based on objective criteria. Consequently, the process is susceptible to subjective, user-specific influences. To evaluate whether the adaptive pressure control based on flow measurements can facilitate the process transfers from one experimental setup to another, printing runs were performed with different nozzles. Besides the rheological properties of the ink, the employed nozzle has the most substantial effect on the required pressure for printing. Due to different lengths, diameters and geometries (straight vs. tapered), the pressure drop along the nozzle can vary drastically. Here, the straight 1 inch nozzle employed in all other experiments was compared to another straight nozzle with a length of 1.5 inch and a tapered nozzle, as shown in Figure 5.2C. All nozzles had the same orifice diameter of 0.58 mm. The underlying assumption of this experiment was that satisfactory printing results should be achievable with every nozzle, as long as the same flow rate of 300 $\mu\text{L}/\text{min}$ is maintained. To examine the capability of the PID control to adapt to a new nozzle, four hollow cylinders were printed with each nozzle, two with a constant pressure setting, as determined for the 1 inch nozzle, and two with the adaptive pressure control being active. As before, the PID control was run for 30 to 60 s, until a relatively constant pressure was reached and the printing process could be started.

Figure 5.12 shows an overview of all printed cylinders. With the 1 inch nozzle, there was hardly any difference between cylinders printed with constant pressure compared to the adaptive pressure control. For the 1.5 inch nozzle, there was an entirely different outcome. All cylinders printed with the adaptive pressure control looked virtually identical to the ones printed with the 1 inch nozzle. When applying the constant pressure setting optimized for the 1 inch nozzle, hardly any ink could

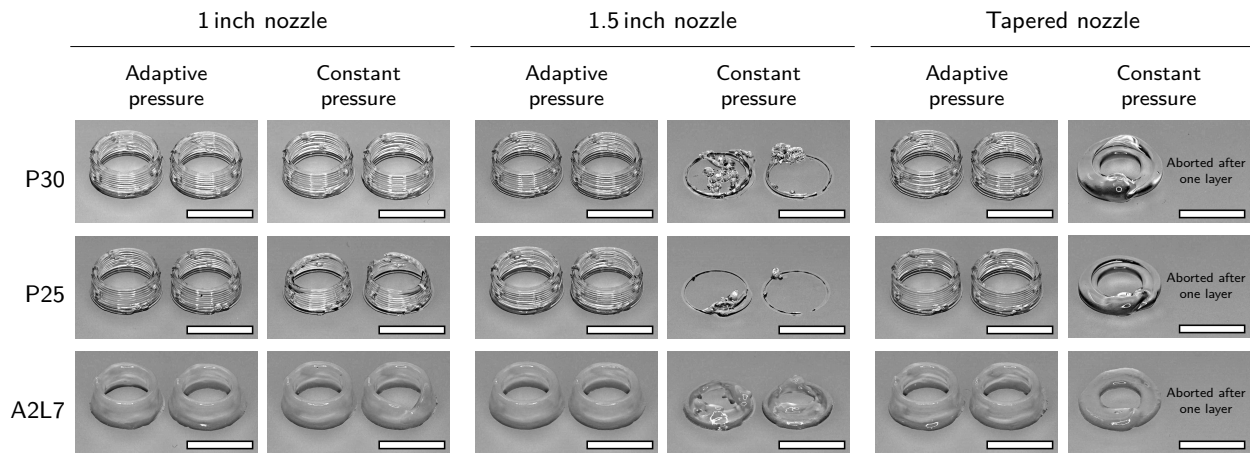


Figure 5.12 Hollow cylinders printed with different inks and nozzles. The prints were performed with either a constant pressure optimized for a 1 inch straight nozzle or with adaptive pressure control after an adjustment phase of 30 to 60 s. The scale bars represent 10 mm.

be extruded, resulting in failed prints. The opposite effect was observed for the tapered nozzle. Here, the constant extrusion pressure caused an excessive amount of ink to be extruded which is why all prints were aborted after a single layer. In combination with the adaptive pressure control, intact cylinders could be printed with the tapered nozzle.

These results demonstrate the need to adjust the pressure for every nozzle separately. Typically, such adjustments are done manually and iteratively. The PID pressure control established here was shown to achieve this adjustment within a short time frame of 30 to 60 s and with a minimal loss of sample volume. Further improvements of time and material need are possible by systematically tuning the employed PID parameters. Regarding the change of nozzle types as a *pars pro toto*, it can be assumed that the adaptive pressure control also allows transfers to other experimental systems like different bioprinters. However, this would require basic process variables like printing speed, layer height and nozzle orifice diameter to remain unchanged.

5.3.4 Potential challenges of working with complex cell-laden bioinks

When working with cells or biological material, maintaining sterile conditions is an important aspect which can be accounted for by employing low-cost disposable sensors or autoclavable models. Wireless sensors may facilitate the handling in a biosafety cabinet. Considering the high sensitivity of cells, the sensor and connector design should be chosen carefully to minimize shear stress by avoiding sharp edges and using high-diameter capillaries.

Due to the commonly high cost of bioinks and cells, the potential loss of material should be considered in the design of sensors and connectors to minimize dead volumes. Optimizing the PID settings may contribute to minimizing the loss of material during the initial flow adaptation phase.

It should be considered that the addition of cells and the optimization of the biological functionality of inks may impair other ink properties like flow behavior, homogeneity, printability and the interaction with the flow sensor. As a result, limitations of the calibration range and differences in noise behavior and reproducibility have to be investigated in a material-specific approach. Within the scope of this paper, we already observed the influence of different additives at several concentrations

on sensor noise and calibration range (see calibration curves in the supplementary material). To assess the applicability of the presented flow control method for a wider range of complex bioinks, a systematic investigation about the influence of additives (e.g. nanoclay and polymers) and cells or special ink types (e.g. emulsions) on sensor performance is necessary. Incompatibilities with commercially available flow sensors may occur with certain types of bioinks that require more specialized equipment to guarantee printability. This includes thermo-sensitive bioinks, e.g. based on gelatin or agarose, that need to be extruded at a controlled temperature. Employing these inks in combination with the presented flow control would require either a controlled environment with constant temperature or a specialized flow sensor with an integrated temperature control.

5.3.5 Implications for process development, monitoring and control

Currently, process development for bioprinting applications often involves testing different settings for a range of parameters like pressure or printing speed. The results are assessed and suitable parameters chosen by the user in an iterative process. There is a range of approaches to find and provide objective and quantifiable criteria to determine suitable printing parameters. This includes mostly off-line analytics like evaluations of the fibre formation and rheological properties of inks [14] or filament collapse and fusion tests by image analysis [199]. Printability windows are often expressed as functions of extrusion pressure [14]. The presented application examples of the adaptive pressure control show an alternative approach based on flow rate as the leading parameter. When keeping certain parameters like nozzle orifice diameter, printing speed and layer height constant, processes can simply be transferred between different experimental systems, e.g. nozzle types or printers, by aiming at the same target flow rate. Transfers between different inks could be achieved with the same strategy, providing a material-independent approach. Adopting the flow rate as a material-independent, system-independent and user-independent parameter could lead to a paradigm shift in process development by allowing the definition of printability windows as a function of flow rate instead of pressure.

Flow rate measurements can also provide process monitoring data which are mostly not available in bioprinting. Often, there is no process monitoring at all or only qualitative monitoring, e.g. in the form of video recordings. Collecting data of the flow rate as an objective and quantifiable measurement parameter could support process validation and troubleshooting.

The main goal of the present study was to demonstrate the feasibility of an automatic adaptation of the extrusion pressure in real-time. Changes of extrusion conditions can occur when the viscosity of the extruded ink varies, e.g. due to inhomogeneities, time-dependent effects or shifting environmental conditions like temperature. Other factors like cartridge fill levels can alter extrusion conditions, as well. The performed case studies demonstrate the significant impact of actively and dynamically adapting the extrusion pressure to control the resulting ink flow. Thus, the PID-controlled setup provides a material-independent, system-independent and user-independent method to actively control and improve the printing process.

5.4 Conclusion

A PID-regulated pressure control for pneumatic extrusion-based bioprinting was established to monitor and control the flow rate of the dispensed ink. A Python-based software tool was implemented to process real-time data from a liquid flow meter and to continuously adapt the pressure in the

bioprinter software to meet the specified target flow rate. The performance of the setup was evaluated with three different inks. A distinction was made between experiments with an active adaptive pressure control and experiments with a constant pressure setting. As use case we investigated the following three scenarios: a) continuous dispensing, b) adaptation to ink inhomogeneities, c) process transfer to other nozzle types.

a) Continuous dispensing: Several runs of continuous dispensing demonstrated the successful automatic adjustment of pressure to consistently meet a specified target flow rate independently of the user. Compared to the constant pressure setting, the adaptive pressure control proved effective in compensating for environmental or system-related influences like nozzle clogging.

b) Adaptation to ink inhomogeneities: A more realistic use case was investigated by printing hollow cylinders from a cartridge filled with layers of two differently concentrated poloxamer 407 inks to simulate ink inhomogeneities. The adaptive pressure control proved effective in keeping a constant flow rate by adapting the pressure appropriately during the printing process. As a result, relatively consistent cylinders could be printed, whereas the constant pressure setting resulted in cylinders with strongly deviating wall thicknesses.

c) Process transfer to other nozzle types: To demonstrate the simple process transferability between different experimental setups, test prints were carried out with three different nozzle types with the same orifice diameter. The adaptive pressure control was able to generate the same constant flow rate with all three nozzle types within 30 to 60 s. The resulting cylinders were of consistent quality, independent of the nozzle. Prints with constant pressure setting suffered from a lack or abundance of extruded ink, if not performed with a pressure specifically determined for the corresponding nozzle type.

The presented PID-regulated adaptive pressure control proved effective in generating a specified target flow, compensating in real-time for varying extrusion conditions and adapting to changes of the experimental setup. The method provides a user-independent, material-independent and system-independent approach for process development, monitoring and control. A remaining challenge is the observed high noise level in the flow rate signal of the employed sensor depending on ink type. The employment or development of more suitable sensors for complex fluids like bioinks should be considered.

Conflict of interest

The authors declare that the research was conducted in the absence of any commercial or financial relationships that could be construed as a potential conflict of interest.

Author contributions

Lukas Wenger: Conceptualization, data curation, investigation, methodology, software, validation, visualization, writing – original draft. Svenja Strauß: Conceptualization, data curation, investigation, methodology, validation, writing – original draft. Jürgen Hubbuch: Conceptualization, writing – review & editing.

Acknowledgments

Funding: This work was supported by the German Federal Ministry of Education and Research (BMBF) as project SOP-Bioprint under contract number 13XP5071B. Furthermore, special thanks go to Bianca Schroth for her support.

Chapter references

- [3] J. Malda *et al.*, „25th anniversary article: Engineering hydrogels for biofabrication“, *Advanced Materials*, vol. 25, no. 36, pp. 5011–5028, 2013.
- [14] N. Paxton, W. Smolan, T. Böck, F. Melchels, J. Groll, and T. Jungst, „Proposal to assess printability of bioinks for extrusion-based bioprinting and evaluation of rheological properties governing bioprintability“, *Biofabrication*, vol. 9, no. 4, p. 44107, 2017.
- [25] B. Blakey-Milner *et al.*, „Metal additive manufacturing in aerospace: A review“, *Materials and Design*, vol. 209, p. 110008, 2021.
- [38] L. Wenger, C. P. Radtke, J. Göpper, M. Wörner, and J. Hubbuch, „3D-Printable and Enzymatically Active Composite Materials Based on Hydrogel-Filled High Internal Phase Emulsions“, *Frontiers in Bioengineering and Biotechnology*, vol. 8, pp. 1–17, 2020.
- [49] L. R. Darwish, M. T. El-Wakad, and M. M. Farag, „Towards an Ultra-Affordable Three-Dimensional Bioprinter: A Heated Inductive-Enabled Syringe Pump Extrusion Multifunction Module for Open-Source Fused Deposition Modeling Three-Dimensional Printers“, *Journal of Manufacturing Science and Engineering*, vol. 143, no. 12, 2021.
- [50] I. T. Ozbolat and M. Hospodiuk, „Current advances and future perspectives in extrusion-based bioprinting“, *Biomaterials*, vol. 76, pp. 321–343, 2016.
- [52] A. S. Hoffman, „Hydrogels for biomedical applications“, *Advanced Drug Delivery Reviews*, vol. 64, no. SUPPL. Pp. 18–23, 2012.
- [59] J. Groll *et al.*, „A definition of bioinks and their distinction from biomaterial inks“, *Biofabrication*, vol. 11, no. 1, 2019.
- [69] J. a. Rowley, G. Madlambayan, and D. J. Mooney, „Alginate hydrogels as synthetic extracellular matrix materials“, *Biomaterials*, vol. 20, no. 1, pp. 45–53, 1999.
- [81] G. Dumortier, J. L. Grossiord, F. Agnely, and J. C. Chaumeil, „A review of poloxamer 407 pharmaceutical and pharmacological characteristics“, *Pharmaceutical Research*, vol. 23, no. 12, pp. 2709–2728, 2006.
- [85] T. G. Mezger, *The Rheology Handbook*, 4th ed. Hanover: Vincentz Network GmbH & Co. KG, 2014.
- [139] N. Soltan, L. Ning, F. Mohabatpour, P. Papagerakis, and X. Chen, „Printability and Cell Viability in Bioprinting Alginate Dialdehyde-Gelatin Scaffolds“, *ACS Biomaterials Science and Engineering*, vol. 5, no. 6, pp. 2976–2987, 2019.
- [166] P. Fisch, M. Holub, and M. Zenobi-Wong, „Improved accuracy and precision of bioprinting through progressive cavity pump-controlled extrusion“, *bioRxiv*, 2020.
- [167] S. Seiffert and J. Sprakel, „Physical chemistry of supramolecular polymer networks“, *Chemical Society Reviews*, vol. 41, no. 2, pp. 909–930, 2012.
- [168] M. Matamoros *et al.*, „Temperature and humidity pid controller for a bioprinter atmospheric enclosure system“, *Micromachines*, vol. 11, no. 11, 2020.
- [172] G. Schnell and R. Schäfer, „Ein thermischer Durchflusssensor.für die Infusionstechnik“, *Biomedizinische Technik*, vol. 40, no. 3, pp. 50–53, 1995.
- [184] I. Gibson, D. Rosen, B. Stucker, and M. Khorasani, *Additive Manufacturing Technologies*, 3rd ed. Springer, 2021.
- [185] E. Kroll and D. Artzi, „Enhancing aerospace engineering students’ learning with 3D printing wind-tunnel models“, *Rapid Prototyping Journal*, vol. 17, no. 5, pp. 393–402, 2011.
- [186] C. Parra-Cabrera, C. Achille, S. Kuhn, and R. Ameloot, „3D printing in chemical engineering and catalytic technology: structured catalysts, mixers and reactors“, *Chemical Society Reviews*, vol. 47, no. 1, pp. 209–230, 2018.
- [187] K. V. Wong and A. Hernandez, „A Review of Additive Manufacturing“, *ISRN Mechanical Engineering*, vol. 2012, pp. 1–10, 2012.
- [188] S. V. Murphy and A. Atala, „3D bioprinting of tissues and organs“, *Nature biotechnology*, vol. 32, no. 8, pp. 773–785, 2014.
- [189] N. J. Castro, C. Meinert, P. Levett, and D. W. Huttmacher, „Current developments in multifunctional smart materials for 3D/4D bioprinting“, *Current Opinion in Biomedical Engineering*, vol. 2, pp. 67–75, 2017.
- [190] B. Schmiege, J. Döbber, F. Kirschhöfer, M. Pohl, and M. Franzreb, „Advantages of Hydrogel-Based 3D-Printed Enzyme Reactors and Their Limitations for Biocatalysis“, *Frontiers in Bioengineering and Biotechnology*, vol. 6, no. JAN, pp. 1–12, 2019.
- [191] R. Langer and J. P. Vacanti, „Tissue Engineering“, *Science*, vol. 260, no. 5110, pp. 920–926, 1993.
- [192] S. Krishnamoorthi, A. Banerjee, and A. Roychoudhury, „Immobilized Enzyme Technology: Potentiality and Prospects“, *Journal of Enzymology and Metabolism*, vol. 1, no. 1, pp. 1–11, 2015.

- [193] M. Hospodiuk, M. Dey, D. Sosnoski, and I. T. Ozbolat, „The bioink: A comprehensive review on bioprintable materials“, *Biotechnology Advances*, vol. 35, no. 2, pp. 217–239, 2017.
- [194] C. P. Radtke, N. Hillebrandt, and J. Hubbuch, „The Biomaker: an entry-level bioprinting device for biotechnological applications“, *Journal of Chemical Technology and Biotechnology*, vol. 93, no. 3, pp. 792–799, 2018.
- [195] D. Bociaga, M. Bartniak, K. Sobczak, and K. Rosinska, „An Integration of a Peristaltic Pump-Based Extruder Into a 3D Bioprinter Dedicated to Hydrogels“, *Materials*, vol. 13, no. 19, 2020.
- [196] L. Ning *et al.*, „Process-induced cell damage: pneumatic versus screw-driven bioprinting“, *Biofabrication*, vol. 12, no. 2, 2020.
- [197] K. Hölzl, S. Lin, L. Tytgat, S. Van Vlierberghe, L. Gu, and A. Ovsianikov, „Bioink properties before, during and after 3D bioprinting“, *Biofabrication*, vol. 8, no. 3, pp. 1–19, 2016.
- [198] Y. Zhao, Y. Li, S. Mao, W. Sun, and R. Yao, „The influence of printing parameters on cell survival rate and printability in microextrusion-based 3D cell printing technology“, *Biofabrication*, vol. 7, no. 4, 2015.
- [199] A. Ribeiro *et al.*, „Assessing bioink shape fidelity to aid material development in 3D bioprinting“, *Biofabrication*, vol. 10, no. 1, 2018.
- [200] V. H. M. Mouser, F. P. W. Melchels, J. Visser, W. J. A. Dhert, D. Gawlitta, and J. Malda, „Yield stress determines bioprintability of hydrogels based on gelatin-methacryloyl and gellan gum for cartilage bioprinting“, *Biofabrication*, vol. 8, no. 3, p. 035003, 2016.
- [201] B. Webb and B. J. Doyle, „Parameter optimization for 3D bioprinting of hydrogels“, *Bioprinting*, vol. 8, no. July, pp. 8–12, 2017.
- [202] R. Opel, W. Hynes, and M. Moya, *Flow Sensor Integration for Precision Dispensing of Visco-Elastic Biomaterials*, 2017.
- [203] S. Strauß, B. Schroth, and J. Hubbuch, „Evaluation of the Reproducibility and Robustness of Extrusion-Based Bioprinting Processes Applying a Flow Sensor“, *Frontiers in Bioengineering and Biotechnology*, vol. 10, pp. 1–14, 2022.
- [204] W. J. Fleming, „Overview of Automotive Sensors“, *IEEE Sensors Journal*, vol. 1, no. 4, pp. 296–308, 2001.
- [205] U. Schmid, G. Krötz, and D. Schmitt-Landsiedel, „A volumetric flow sensor for automotive injection systems“, *Journal of Micromechanics and Microengineering*, vol. 18, no. 4, 2008.
- [206] Y. Li *et al.*, „Gas/oil/water flow measurement by electrical capacitance tomography“, *Measurement Science and Technology*, vol. 24, no. 7, 2013.
- [207] R. Thorn, G. A. Johansen, and B. T. Hjertaker, „Three-phase flow measurement in the petroleum industry“, *Measurement Science and Technology*, vol. 24, no. 1, 2013.
- [208] D. L. Polla *et al.*, „Microdevices in Medicine“, *Annual Review of Biomedical Engineering*, vol. 2, no. 1, pp. 551–576, 2000.
- [209] C. J. Okereke, O. A. Lasode, and I. O. Ohijeagbon, „Exergoeconomic analysis of an industrial beverage mixer system: Process data“, *Data in Brief*, vol. 32, p. 106125, 2020.
- [210] L. D. Pedersen, „Assessment of sensors used in the food industry“, *Food Control*, vol. 2, no. 2, pp. 87–98, 1991.
- [211] N. T. Nguyen, „Micromachined flow sensors - A review“, *Flow Measurement and Instrumentation*, vol. 8, no. 1, pp. 7–16, 1997.
- [212] J. T. Kuo, L. Yu, and E. Meng, „Micromachined Thermal Flow Sensors - A Review“, *Micromachines*, vol. 3, no. 3, pp. 550–573, 2012.
- [213] S. Silvestri and E. Schena, „Micromachined Flow Sensors in Biomedical Applications“, *Micromachines*, vol. 3, no. 2, pp. 225–243, 2012.
- [214] C. Li *et al.*, „Smart catheter flow sensor for real-time continuous regional cerebral blood flow monitoring“, *Applied Physics Letters*, vol. 99, no. 23, pp. 10–14, 2011.
- [215] A. D. Augst, H. J. Kong, and D. J. Mooney, „Alginate hydrogels as biomaterials“, *Macromolecular Bioscience*, vol. 6, no. 8, pp. 623–633, 2006.
- [216] F. Pahlevanzadeh *et al.*, „Recent Trends in Three-Dimensional Bioinks Based on Alginate for Biomedical Applications“, *Materials*, vol. 13, no. 18, p. 3980, 2020.
- [217] S. Duin *et al.*, „3D Bioprinting of Functional Islets of Langerhans in an Alginate/Methylcellulose Hydrogel Blend“, *Advanced Healthcare Materials*, vol. 8, no. 7, pp. 1–14, 2019.
- [218] F. F. Cai, S. Heid, and A. R. Boccaccini, *Potential of Laponite® incorporated oxidized alginate-gelatin (ADA-GEL) composite hydrogels for extrusion-based 3D printing*, 2021.
- [219] M. Shen, Y. Sun, J. Xu, X. Guo, and R. K. Prud'Homme, „Rheology and Adhesion of Poly(acrylic acid)/Laponite Nanocomposite Hydrogels as Biocompatible Adhesives“, *Langmuir*, vol. 30, no. 6, pp. 1636–1642, 2014.

- [220] Sensirion, *STEP file Sensirion SLI*, <https://sensirion.com/resource/cad/sli>, Accessed: 2022-01-26, 2021.
- [221] V. Dubey, H. Goud, and P. C. Sharma, „Role of PID Control Techniques in Process Control System: A Review“, in *Data Engineering for Smart Systems*, P. Nanda, V. K. Verma, S. Srivastava, R. K. Gupta, and A. P. Mazumdar, Eds., Singapore: Springer, 2022, pp. 659–670.
- [222] R. A. Paz, „The Design of the PID Controller“, Ph.D. dissertation, Klipsch School of Electrical and Computer Engineering, 2001.
- [223] G. Wolterink, A. Umrani, M. Schouten, R. Sanders, and G. Krijnen, „3D-Printed Calorimetric Flow Sensor“, *2020 IEEE Sensors*, pp. 1–4, 2020.
- [224] I. R. Schmolka, „Physical Basis for Poloxamer Interactions“, *Annals of the New York Academy of Sciences*, vol. 720, no. 1, pp. 92–97, 1994.
- [225] H. Seki and T. Shigemasa, „Retuning oscillatory PID control loops based on plant operation data“, *Journal of Process Control*, vol. 20, no. 2, pp. 217–227, 2010.
- [226] H. O. Bansal, R. Sharma, and P. R. Shreeraman, „PID Controller Tuning Techniques: A Review“, *Journal of Control Engineering and Technology*, vol. 2, no. 4, pp. 168–176, 2012.

6

Analytics in Extrusion-Based Bioprinting: Standardized Methods improving Quantification and Comparability of the Performance of Bioinks

Svenja Strauß^{1,2*}, David Grijalva Garces^{1,2*} and Jürgen Hubbuch^{1,2}

¹ Institute of Functional Interfaces, Karlsruhe Institute of Technology (KIT), Eggenstein-Leopoldshafen, Germany

² Institute of Process Engineering in Life Sciences, Section IV: Biomolecular Separation Engineering, Karlsruhe Institute of Technology (KIT), Karlsruhe, Germany

* Contributed equally

Abstract

Three-dimensional bioprinting and especially extrusion-based printing as a most frequently employed method in this field is constantly evolving as a discipline in regenerative medicine and tissue engineering. However, the lack of relevant standardized analytics does not yet allow an easy comparison and transfer of knowledge between laboratories regarding newly developed bioinks and printing processes. This work revolves around the establishment of a standardized method, which enables the comparability of printed structures by controlling for the extrusion rate based on the specific flow behavior of each bioink. Furthermore, printing performance was evaluated by image-processing tools to verify the printing accuracy for lines, circles, and angles. In addition, and complementary to the accuracy metrics, a dead/live staining of embedded cells was performed to investigate the effect of the process on cell viability. Two bioinks, based on alginate and gelatin methacryloyl, which differed in 1% (*w/v*) alginate content, were tested for printing performance. The automated image processing tool reduced the analytical time while increasing reproducibility and objectivity during the identification of printed objects. During evaluation of the processing effect of the mixing of cell viability, NIH 3T3 fibroblasts were stained and analyzed after the mixing procedure and after the extrusion process using a flow cytometer, which evaluated a high number of cells. It could be observed that the small increase in alginate content made little difference in the printing accuracy but had a considerable strong effect on cell viability after both processing steps.

6.1 Introduction

Artificially generated scaffolds loaded with cellular material in the field of tissue engineering find their application as implants to replace damaged tissue and as models to study diseases or the effect of active compounds [50, 188]. In this context, hydrogels are commonly employed, as these biomaterials form a highly swollen network in the aqueous phase resembling the physical structure of the extracellular matrix [227]. The biochemical composition of such tissue analog can be formulated according to the specific application. Therefore, naturally derived polymers, such as polysaccharides, e.g., alginate and hyaluronic acid, as well as proteins, e.g., collagen and gelatin, are suitable components [228]. Biofabrication methods, such as three-dimensional (3D) bioprinting, have gained attention in this field, as a wide range of material compositions can be used, and the method is relatively easy to scale-up [3]. So-called bioinks are produced for this purpose, which comprise polymer solutions with embedded cells [59]. Extrusion-based bioprinting (EBB) processes have to fulfill several requirements for the layer-by-layer generation of 3D structures intended for the application as tissue analogs. From the structural point of view, predefined geometries, which can be traced back to a series of simple structures that are stacked on top of each other, have to be produced accurately. In the final stages, the bioinks should retain the fabricated shape. During and after the printing process, high cell viability has to be maintained as the cells undergo mechanical stress during the process. The created network must support both vascularization and metabolic activities during cell culture. Meeting the structural and biological requirements has been accepted as a compromise. This is because parameters that increase the stability of printed scaffolds have a negative impact on cell viability, as those increase shear stress [50, 198, 229]. Although the rheological characterization of bioinks is a standard in bioprinting, the gained information is rarely exploited in the settings of printing parameters [230–232]. The common systematics of printability studies relies on a constant pneumatic pressure and/or printing speed while using different bioink

compositions [230, 233, 234], and no relationship between those parameters is presented. Other studies simply set the printing parameters for each tested bioink in a rather arbitrary manner [232, 235]. Furthermore, the aforementioned approaches may result in unequal amounts of extruded material since the rheological properties of the bioinks depend on the polymer content and the type of polymer. Therefore, such methodologies do not allow an adequate comparison of the structural characteristics from the printed scaffolds based solely on the material properties. This issue was addressed in the review by Gillispie et al. [236]. Furthermore, methodologies for the evaluation of printed structures are lacking standards as well. Methods in that field consist of the manual extraction of the metrics of the produced structures [237–241]. Such methods are prone to observer-dependent errors and are not reproducible. One possible post-printing analysis method circumventing this drawback is automated image analysis. This method shows the advantages of automation, leading to higher reproducibility as well as objectivity. In addition, images and extracted data undergo long-time storage. These methods are well established for quality control in production processes [242, 243]. There have been advances in the image analysis field, but workflows still include several manual observer-dependent steps [239]. The determination of cellular viability mostly consists of evaluation of images acquired by microscopy. On the one hand, specific characteristics, such as the morphology and size of the cells can be extracted from the images, but on the other hand, the images represent only a small portion of the printed structure. Studies in the field are limited to a low number of cells in the range of hundreds of cells [244, 245]. The reproducibility as well as the significance of the results regarding cell viability can be increased by the implementation of automated image processing workflows, as well [246, 247]. A further option to quantify several thousand cells is flow cytometry as already tested in a few studies in the field [109, 248]. The lack of standardized printing methodologies as well as techniques for the evaluation of the printing performance of bioinks presents a limitation in the development of formulations as a comparison within and between laboratories.

In this work, we aim to establish robust and objective methods for the evaluation of the printing performance of biomaterial inks and bioinks. The rheological properties of two biomaterial inks were characterized in order to determine the relationship between the printing speed and pneumatic pressure of each biomaterial ink and, therefore, control the flow rate within experiments. The assessment of the printing performance considered the accuracy of printing single-layer structures, i.e., lines, circles, and angles. For this purpose, automated image processing workflows were developed to extract geometrical features from the produced structures. The developed tools were used in order to characterize the effect of the bioink composition as well as the presence of cells on the resulting geometry. As a second part of the investigation of the printing performance, the viability of cells embedded in the bioink was determined directly after the mixing step and after bioprinting via staining and data acquisition by means of flow cytometry.

6.2 Materials and methods

6.2.1 Cell culture

NIH 3T3 mouse fibroblasts (CLS Cell Lines Service GmbH, Eppelheim, Germany) were incubated in Dulbecco’s Modified Eagle Medium (DMEM, high glucose, GlutaMAX™) supplemented with 10% (*w/v*) fetal bovine serum (FBS), 50 U/mL penicillin, and 50 µg/mL streptomycin. Cell culture media and supplements were acquired from Gibco™(Thermo Fisher Scientific, Waltham, MA,

USA). Fibroblasts were cultured in tissue culture (TC) flasks at 37 °C in a humidified atmosphere containing 5 % CO₂. Cells were passaged upon reaching 70 to 80 % confluency.

6.2.2 Biomaterial ink and bioink preparation

Gelatin methacryloyl (GelMA) was produced from Type A Gelatin (300 bloom strength, Sigma-Aldrich, St. Louis, MO, USA) according to the method published by Grijalva Garces et al. [249]. The degree of functionalization of used GelMA was 65 % determined by the method by Habeeb [250]. Alginate sodium salt was obtained from Sigma-Aldrich (A2033, from brown algae). The adequate quantities of biomaterial were dissolved in Dulbecco's Phosphate Buffered Saline (DPBS, without calcium and magnesium, Thermo Fisher Scientific) and mixed at 3500 rpm for 5 min in a SpeedMixer® (Hauschild GmbH & Co. KG, Hamm, Germany). The biomaterial ink was filled directly to a final volume of 3 mL into 10 mL cartridges (Nordson Corporation, Westlake, OH, USA) for cell-free printing. Not all formulations employed in this study contained cells, which is why they are referred to as 'biomaterial inks' instead of 'bioink' for the sake of clarity. Alginate and GelMA solutions for the cell-containing experiments were prepared as mentioned above. However, the initial concentration was higher, taking into account the dilution of the biomaterial ink after the mixing of the cell suspension with the cell-free biomaterial ink. The concentrated biomaterial ink was transferred to 5 mL syringes (B. Braun SE, Melsungen, Germany). Cells were harvested from the TC flasks with trypsin/ethylenediaminetetraacetic acid (Gibco™), centrifuged at 300 rcf for 5 min, and resuspended in 150 µL fresh DPBS. Subsequently, the cell suspension was transferred into 3 mL syringes (B. Braun). The syringe filled with biomaterial ink and the cell containing syringe were connected via a Luer-Lock adapter and mixed by pushing five times back and forth between both syringes. The cell-laden bioink was then loaded into the 10 mL cartridges for printing and sealed with pneumatic pistons (Nordson Corp.). The first formulation was prepared with 3 % (*w/v*) alginate and with 3 % (*w/v*) GelMA (A3G3), the second 4 % (*w/v*) alginate and 3 % (*w/v*) GelMA (A4G3). The final cell count was set to 2×10^6 cells/mL for the bioinks. A summary of the formulations with the respective components is shown in Table 6.1.

Table 6.1 Biomaterial ink compositions as employed in this study and abbreviations used throughout this work. Power law exponent and consistency index according to the Ostwald–de Waele relationship were determined as mentioned in Section 6.2.3 and used for the calculation of the specific pneumatic pressure for printing performance experiments.

Abbr.	Alginate (% (<i>w/v</i>))	GelMA (% (<i>w/v</i>))	Power Law Exponent n	Consistency Index K (Pa s ^{n})	Pneum. Pressure (kPa)
A3G3	3	3	0.35	146.39	80.5
A4G3	4	3	0.32	284.09	129.1

6.2.3 Rheological characterization

The rheological behavior of the polymer solutions was characterized based on the shear rate-dependent viscosity. For this purpose, a rotational rheometer Physica MCR301 (Anton Paar GmbH, Graz, Austria) with a cone-plate geometry (diameter 25 mm, cone angle 1°) was used. Additionally, a solvent trap was used to prevent the sample drying during measurements. The viscosity of both cell-free formulations, i.e., A3G3 and A4G3, was determined as a function of the shear rate in the

range of 1×10^{-1} to 1×10^3 1/s. The data of the viscous behavior were fitted according to the Ostwald–de Waele relationship, and the values of the power law exponent n and the consistency index K were determined for this model using Origin 2021 (OriginLab Corporation, Northampton, MA, USA). The rheological characterization was carried out as three biological replicates ($n = 3$) with a set of three technical triplicates ($n = 3$) each, resulting in data sets of nine replicates. For each biological replicate, an independently prepared solution was used.

In order to control the extrusion rate, i.e., the deposited material amount, the Ostwald–de Waele relationship was coupled with the Hagen–Poiseuille equation for the volumetric flow rate Q through a cylindrical capillary, see Equation (6.1), where R and l represent the capillary radius and length, respectively. The geometric variables of the capillary were taken according to the nozzle (inner diameter 0.61 mm, length 12.7 mm, Nordson Corp.) intended for the printing process. For evaluation of the printing accuracy in Section 6.2.4.1, the printing speed was set equal to the mean velocity \bar{v} during extrusion at 10 mm/s, and the required pneumatic pressure p was calculated. The pneumatic pressures used for printing of both formulations are given in Table 6.1 .

$$Q = \bar{v} \pi R^2 = \frac{n\pi}{3n+1} \left(\frac{R^{3n+1} p}{2 K l} \right)^{1/n} \quad (6.1)$$

6.2.4 Printing performance evaluation

A key aspect of bioprinting is the reproducibility and accurate fabrication of scaffolds while maintaining a high viability of the cells within the bioink. Therefore, the characterization of the printing performance consists of two parts, namely, the assessment of the printing accuracy, where the printed structures were compared to the predefined computer-aided design (CAD) model, and the determination of the living and dead cell counts after the extrusion process via fluorescent staining.

All printing and extrusion experiments were performed with a BioScaffolder 3.1 bioprinter (GeSiM mbH, Radeberg, Germany). The cartridge with the attached stainless-steel nozzle (inner diameter 0.61 mm, length 12.7 mm, Nordson Corp.) was placed on the holder and connected to the air supply. The structures were printed on glass microscopy slides with a distance of 0.5 mm to the nozzle tip. The applied pneumatic pressures were calculated as mentioned in Section 6.2.3. The specific values are listed in Table 6.1. The applied pressure was verified beforehand with a barometer Go Direct® (Vernier Software & Technology, Beaverton, OR, USA), and adjusted, if required.


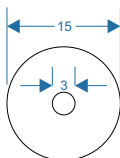
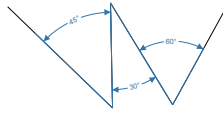
6.2.4.1 Printing accuracy assessment

The aim of the printing accuracy assessment was to find out how accurately the printed structure matches the CAD model. Three single-layer structures, namely a line, a circle, and an object consisting of multiple angles, were printed, imaged, and analyzed. An overview of the objects with corresponding dimensions is given in Table 6.2.

Each structure was printed as a set of 3 biological replicates ($n = 3$) and 8 technical replicates ($n = 8$) resulting in total in 24 objects per bioink and biomaterial ink. The biological replicates of the cell-free experiments consisted of independently prepared biomaterial inks. For the bioinks, cells were additionally harvested directly prior to the mixing step from independent TC flasks. Each object was printed on glass microscope slides. Immediately after printing, each object was

individually photographed. For image acquisition, a monochrome camera (DALSA GENIE NANO-M2420, Stemmer Imaging AG, Puchheim, Germany) with 52 pixel/mm was used. The object was placed on a slide on a black background and illuminated with a white light-emitting diode (LED) ring light (CCS HPR2-150 SW, Stemmer Imaging AG). In order to obtain an objective quantification of the printed geometries, an image processing workflow was developed using Matlab[®] R2022a (TheMathWorks Inc., Natick, MA, USA). In a first step, all images were binarized using local thresholding algorithms. Therefore, each pixel was replaced by the median value of the 3-by-3 surrounding pixels. The image processing workflow is shown schematically in Figure 6.1. Subsequently, the binary images were cropped to the region of interest depending on the structure. From then on, the objects were segmented, and images were evaluated for the specific structure characteristics.

Table 6.2 Graphic models of the printing path. Images of the printed objects are taken and analyzed as a part of the printing accuracy assessment. The dimensions in the line and circle sketches are given in millimeter (mm), the dimensions in the angle sketch in degrees (°). Each structure was examined for characteristic parameters, which are shown with the respective formulae for calculation.

Structure	Evaluation Parameter	Formula/Equation
Line 	normalized width	$w_n = \frac{w}{d_{nozzle}}$ (2)
	normalized length	$l_n = \frac{l}{l_{model}}$ (3)
Circle 	normalized width	see Equation (2)
	normalized radii to midline	$r_n = \frac{r_i + r_o}{2r_{model}}$ (4)
Angle 	normalized width	see Equation (2)
	normalized angle to midline	$\alpha_n = \frac{\alpha_i + \alpha_o}{2\alpha_{model}}$ (5)

The parameters extracted based on the image files are also listed in Table 6.2. The accuracy of printing all three geometries was evaluated by the normalized width w_n , i.e., the filament width w divided by the diameter of the nozzle. In the case of the line geometry, the filament width was

calculated as the mean pixel count along the line. The filament width of the printed circles was measured at 180° from the starting point and 2% of the circle was evaluated. The line width of the angle composite structure was determined at five different points along the printed structure. The analysis of the line also included the normalized length l_n . Therefore, the length of the line l was divided by the length of the CAD model of 30 mm. The assessment of the accuracy of the printed circles and angle composite structures was performed by including a midline as a reference and by combining the inner and outer boundaries of the structure into a single parameter. The midline represents the center of the nozzle, i.e., the axis of movement of the printer equipment. In the case of the circles, the normalized radii to midline r_n were calculated as the sum of inner radius r_i and outer radius r_a detected on the binary image divided by two times the circle radius, i.e., 15 mm as designed in CAD. The 3 mm diameter circle was needed solely as a starting point for the image processing workflow. The angle composite structure was evaluated by the normalized angle α_n . This parameter was calculated as the sum of each inner angle α_i and outer angle α_o of the boundaries on the binary image divided by two times the corresponding angle on the CAD file.

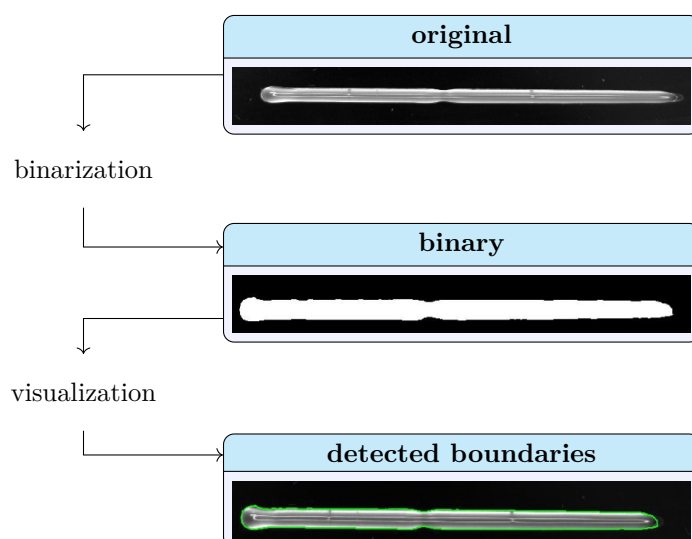


Figure 6.1 Exemplary representation of the object recognition. The original image (**top**) is binarized using local thresholding algorithms (**middle**), and an overlay with the detected boundaries of the identified structure on the original image was created as a visual control (**bottom**).

6.2.4.2 Effect of processing on cell viability

A high cell viability is essential throughout the manufacturing process of cell-loaded scaffolds. The effect of processing on the cell viability was determined after a mixing step and after extrusion. The analytical methodology for the determination of the cell viability is schematically shown in Figure 6.2.

The bioink was prepared as mentioned in Section 6.2.2. Three fractions were collected after mixing, weighed, and subsequently diluted 20-fold by weight with DPBS. Similarly, the bioink was extruded as three fractions, which were diluted with DPBS, as well. Fluorescent stains were added to the diluted bioink to a final concentration of $0.1 \mu\text{M}$ calcein-AM and $1.5 \mu\text{M}$ propidium iodide (PI); both

stains were purchased from Invitrogen (Thermo Fisher Scientific). The samples were analyzed after an incubation of 15 min at room temperature. Data acquisition was performed with a MACSQuant[®] Analyzer 10 flow cytometer (Miltenyi Biotec B.V. & Co. KG, Bergisch Gladbach, Germany) at 100 mL/min. The acquired data were gated using FlowJo (Becton, Dickinson & Company, Ashland, OR, USA). This step was used to exclude debris and agglomerates. The distinction between live and dead cells was based on the green and red signals, respectively. Dead cells were gated using a control sample with fixated and permeabilized cells before staining with PI. For fixation, the cells were resuspended in a 3.7% (*v/v*) paraformaldehyde (AppliChem GmbH, Darmstadt, Germany) in DPBS solution and incubated for 10 min. After a wash step with DPBS, the cells were permeabilized with a 0.1% (*v/v*) Triton-X (Sigma-Aldrich) in DPBS solution for 15 min. Then, a further wash step was proceeded. Fixation and permeabilization were performed at room temperature. The experiment to monitor the effect of the extrusion process on the cells consisted of three biological replicates ($n = 3$); therefore, independently prepared polymer solutions were used. Additionally, cells were harvested directly prior to the mixing step from a separate TC flask. Each fraction of diluted bioink containing stained cells ($n = 3$) was analyzed as technical triplicates ($n = 3$) resulting in data sets of 27 values. The processing steps and the subsequent determination of cell viability were completed before starting a new biological replicate. The cell viability was calculated as the number of viable cells divided by the total number of cells, i.e., both viable and dead cells present in a single technical replicate. The analytical methodology for the determination of the cell viability is schematically shown in Figure 6.2.

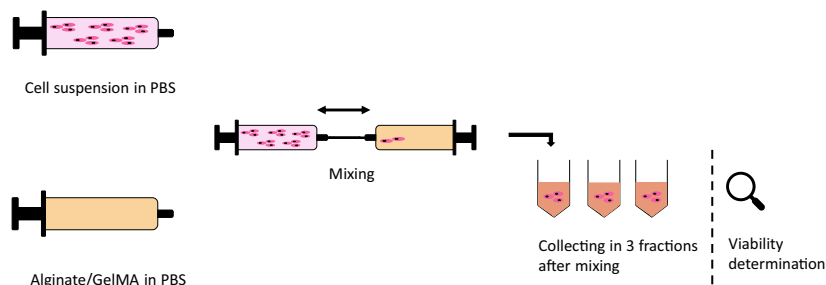
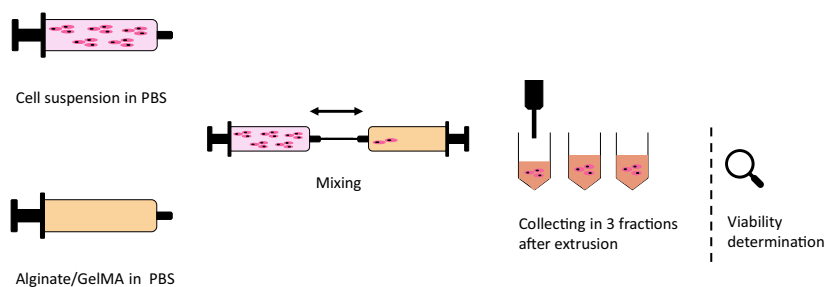
A Effect of processing on cell viability after mixing**B** Effect of processing on cell viability after extrusion

Figure 6.2 Schematic of the workflow applied for the determination of the processing effects on cell viability. A biological replicate consisted of cells harvested independently and mixed with the biomaterial ink. In **(A)**, the processing ended after mixing the cellular material into the biomaterial ink, which was collected in three fractions. In **(B)**, the processing of the bioink consisted of mixing it with the cell suspension and extrusion with the printer. The extruded bioink was collected in three fractions. Each collected fractions was diluted separately before cellular staining and data acquisition with a flow cytometer. Three biological replicates of each process were performed; therefore, each biological replicate was completed before starting the next replicate.

6.2.5 Data handling and statistical analysis

Data evaluation, image processing, data visualization, and statistical analysis were performed with Matlab[®] R2022a (TheMathWorks Inc., Natick, MA, USA). Errors related to the calculated parameters were determined after the first-order Taylor series method for uncertainty propagation. The normal distribution of data sets was verified using the Jarque–Bera test with an α -value set to 0.05. A one-way analysis of variance (ANOVA) was carried out in order to find significant differences, and a p -value below 0.05 was classified as statistically significant.

6.3 Results and discussion

6.3.1 Rheological characterization

The rheological behavior of the bioink has a great influence on the process as the biomaterial flows through a nozzle and induces stress on the embedded cells. Hence, the viscosity was determined for the cell-free biomaterial inks A3G3 and A4G3 as a function of the shear rate in the range of 1×10^{-1} to 1×10^3 $1/s$. Figure 6.3 provides the associated results.

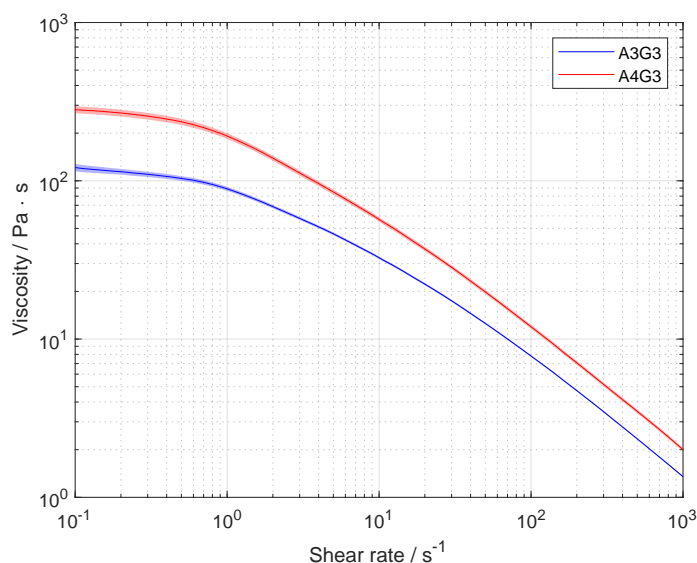


Figure 6.3 Rheological characterization of biomaterial inks A3G3 and A4G3. Viscosity is shown as a function of the shear rate. The results are presented as mean values, the shaded areas, the standard deviation. Each formulation was prepared separately for three times ($n = 3$), and three technical replicates were tested ($n = 3$) from each batch, resulting in data sets of nine values.

Both biomaterial inks showed a similar non-Newtonian behavior at different magnitudes. The course of the viscosity functions showed a plateau at the low range of the shear rate and a shear thinning regime with an increasing shear rate. The viscosity plateaus had values of about 150 Pa·s, and 300 Pa·s for biomaterial inks A3G3 and A4G3, respectively. The shear thinning regime was fitted using the Ostwald–de Waele relationship to better describe the behavior of the biomaterial inks during extrusion. The power law exponent n and the consistency index K are listed in Table 6.1. The increase in viscosity of A4G3 by a factor of up to 1.9 in comparison to the viscosity of A3G3 can be explained by the higher content of alginate in solution, as a higher amount of water is bound and the entanglement of polymers increases with concentration [251]. In order to set an equal flow rate for both formulations during extrusion, the determined fitting parameters were used to calculate the required pneumatic pressure according to the Hagen–Poiseuille equation shown in Equation (6.1). The results are listed in Table 6.1. The pressure for the extrusion experiments of the A3G3 biomaterial ink was 80.5 kPa. A higher pressure with a value of 129.1 kPa was required for the extrusion of A4G3 due to the higher viscosity of the biomaterial ink.

6.3.2 Printing performance

6.3.2.1 Printing accuracy assessment

As part of the printing performance studies, printing accuracy was evaluated as the deviation from the set printing path, taking into account the 0.61 mm nozzle diameter as well. Line, circle, and angle structures were printed and characterized by the respective geometrical features. The printed structures and evaluation parameters are presented in Table 6.2. For all results in this section, every structure was printed as a set of 3 biological replicates ($n = 3$) and 8 technical replicates ($n = 8$), resulting in a total of 24 objects per biomaterial ink and bioink. The differences between evaluation parameters were examined for statistical significance. Each bar represents the mean value with the respective standard deviation for one of the four formulations.

In Figure 6.4A, the normalized width in relation to the nozzle diameter for each formulation is shown. The highest normalized width was found for A4G3 without cells with a value of 1.58 ± 0.11 , the lowest for A3G3 without cells with a value of 1.48 ± 0.17 . Higher standard deviations are shown by the bioinks with values of 0.24 and 0.28 for the A3G3 and A4G3 formulations, respectively. The normalized width of biomaterial inks did not differ significantly. Similarly, the difference between cell-containing bioinks was not significant either. A statistical significance was observed between A3G3 without cells and A4G3 with cells. All determined values are higher than 1, as the filament thickness increases after exiting the nozzle, due to the elastic properties of polymer solutions [251]. The distances between the nozzle tip and printing surface also influence the filament width, as was shown by Habib et al. [233]. In this study, the distance was set to 0.5 mm in order for the filament to adhere to the glass surface, thus leading to thicker filaments than nozzle. In general, it is expected that the increasing viscosity of the bioink leads to thinner filaments as shown by other studies [233, 238, 240, 252]. The increasing printing pressure is also known to increase the filament width [201, 233]. In the presented study, the printing pressure was calculated according to the individual viscosity of each formulation in order to control the flow rate. The comparable normalized widths of both formulations can be attributed to the similar amount of material deposition. This approach increases the comparability of results, as printing parameters are objectively set on the basis of rheological data and not determined according to user-dependent impressions. Further methods to control the flow rate as performed by Wenger et al. [253] showed increasing reproducibility during extrusion-based bioprinting. The higher standard deviations shown by the cell-containing bioinks can be explained by air entrapment when the cells are mixed into the polymer solution between two syringes. This process is not reproducible, and air bubbles lead to inhomogeneity within the cartridge, resulting in fluctuations of the filament width. Air bubbles entrapped after the mixing steps have been addressed in the literature [14, 236, 241, 247]. The mentioned studies implement strategies by either mixing, using a spatula or centrifuge, the cartridges or syringes to remove the entrapped air. The first imposes a non-reproducible step, while the latter can lead to redistribution or even to complete sedimentation of the cells in the bioink. For future medical applications, it is a basic requirement to develop reproducible mixing processes [241, 254].

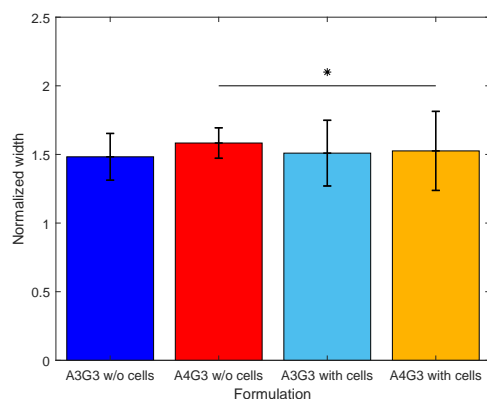
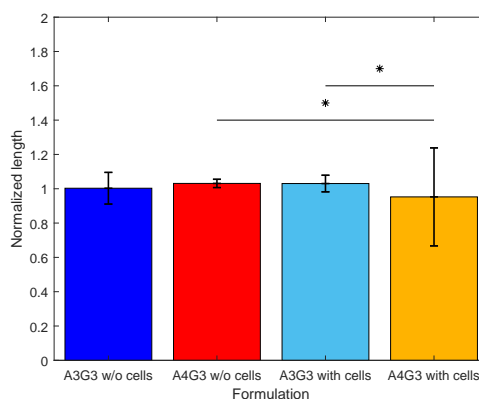
A Normalized line width**B** Normalized line length

Figure 6.4 Printing accuracy study line structure. In (A), the normalized line width is shown, and in (B), the normalized line length. For all four formulations, three biological replicates ($n = 3$) were produced, and eight technical replicates ($n = 8$) printed for each structure, resulting in a total of 24 objects, of which the mean is shown in a bar with the associated standard deviation. Significant differences are denoted with an asterisk ($p < 0.05$).

In Figure 6.4B, the length of the printed lines normalized to the full length of the planned structure, i.e., 3 mm, is presented for all four formulations. The highest deviation from 1 and the highest standard deviation with a value of 0.95 ± 0.29 are shown by the bioink A4G3 containing cells. The length of the line of this bioink is significantly different than that of A3G3 without cells and A3G3 with cells. The sample set of printed lines of the A4G3 bioink containing cells includes four interrupted lines, and the cell-laden A3G3 bioink includes one interrupted structure, while both cell-free formulations could be printed to the full length. Values higher than 1 can be attributed to post-flow of the formulation after releasing the air pressure. The printing of non-continuous filaments can be attributed to heterogeneities in the printing cartridge that arise during the mixing of cells by the two-syringe method as air is introduced into and entrapped in the mixture. Exemplary images of a continuous as well as an interrupted line are depicted in Figure 6.5.

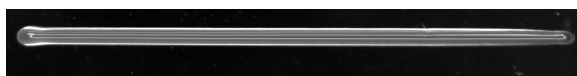
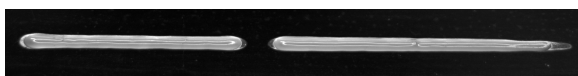
A Continuous line**B** Interrupted line

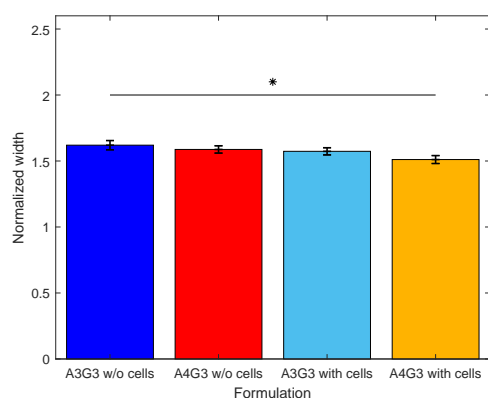
Figure 6.5 Exemplary raw images of printed lines with bioink A4G3 containing cells. In (A), a continuous and, in (B), an interrupted line is shown.

The width of the filament in the printed circle was also determined, and was normalized to the nozzle diameter. The results are shown in Figure 6.6A. The greatest deviation from 1 was measured for A3G3 without cells with a value of 1.62 ± 0.03 . A4G3 containing cells showed the lowest deviation with a value of 1.51 ± 0.03 . A statistically significance difference was found between both values. Comparing the normalized width of the bioinks containing cells, the values did not differ significantly. Similarly, no statistically significant differences were observed between the cell-free biomaterial inks. Figure 6.6B presents the normalized radii to the midline. This parameter offers the advantage of combining two parameters, namely the inner and outer radii. The midline corresponds

to the printing path, i.e., the radius of the model. In the ideal case, the inner and outer radii of the filament overlap the path line \pm half nozzle diameter. Here, the comparability of the deviation is easier with one output. Similar to the normalized width of the printed circle, the largest deviation from 1 was measured for A3G3 without cells with a value of 1.02 ± 0.0008 , and the lowest, for A4G3 containing cells with a value of 1.01 ± 0.0007 . The radii normalized to the midline of both compositions differed significantly, as well.

The lack of differences between the normalized widths of formulations that differ in alginate content is explained by the selection of the printing pressure to set an equal flow rate for both biomaterial inks, as previously described. The standard deviations of the normalized width are smaller compared to the standard deviations of the width of the line structure. This is due to the fact that the width of the circle is measured at only a small portion of the filament, namely 2% of the circle at 180° from the starting point and, thus, measures fewer data points than the line structure, where the width is determined in the middle third. The higher values of the A3G3 can be explained by the lower viscosity of the A3G3 biomaterial ink, as bioinks tend to keep flowing after printing, especially as no crosslinking was performed after printing. All values are higher than 1 due to the elasticity of the polymer solution [251].

A Normalized circle width



B Circle radii normalized to midline

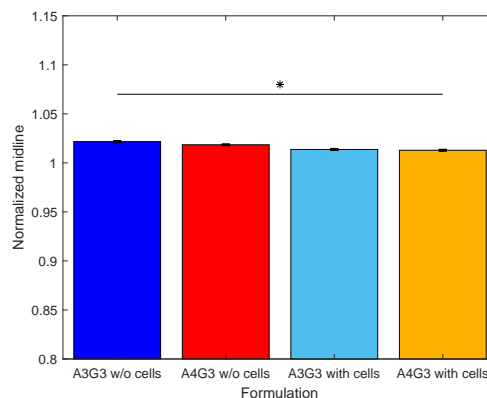


Figure 6.6 Printing accuracy study for the circle structure. In **(A)**, the normalized line width is shown and, in **(B)**, the normalized radius to the midline. For all four formulations, three biological replicates ($n = 3$) were produced and eight technical replicates ($n = 8$) printed for each structure resulting in total in 24 objects, of which the mean is shown in a bar with the associated standard deviation. Significant differences are denoted with an asterisk ($p < 0.05$).

As a final part of this study, the accuracy of printed angles was characterized by means of the normalized filament width and the normalized angle to the midline. The corresponding data are shown in Figure 6.7A, B, respectively. The printed structure consisted of a continuous structure with angles of 30° , 45° , and 60° . Considering the normalized filament width, the highest deviation from 1 was observed for the A3G3 without cells with a value of 1.74 ± 0.02 . The lowest normalized width was produced with A4G3 containing cells with a value of 1.62 ± 0.01 . No statistically significant differences between the normalized filament widths were proven between any of the tested formulations. As previously explained, there are no differences in printing accuracy due to the normalization of the volumetric flow rate.

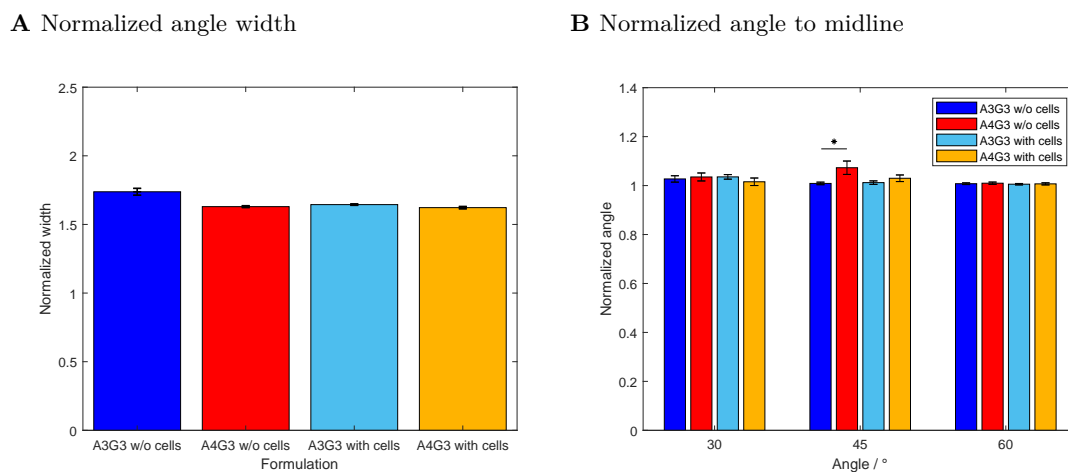


Figure 6.7 Printing accuracy study for the angle structure. In (A), the normalized line width is shown and, in (B), the normalized angle to the midline. For all four formulations, three biological replicates ($n = 3$) were produced, and eight technical replicates ($n = 8$) printed for each structure, resulting in a total of 24 objects, of which the mean is shown in a bar with the associated standard deviation. Significant differences are denoted with an asterisk ($p < 0.05$).

Comparing the normalized width of the filament determined in the angle structure to the normalized width of the simple line structure, it is noteworthy that the standard deviation of the first is lower than that of the latter. The reason lies in the analytical method itself since the width of the filament of the angle structure was measured at five points along the whole structure. This data set is smaller compared to the data set used to determine the filament width along the line structure at every pixel of the evaluated section of the image. The quantification along the angle structure is less accurate, but the output serves as a rough estimate to compare whether the more complex movement of the print head has an effect on the produced structure. During the angle analysis shown in (B), the inner and outer angles were again combined together to one parameter; hence, the angles were normalized to the angle of the trajectory of the print head. The cell-free A4G3 showed the highest deviation from 1 with a value of 1.07 ± 0.03 overall. There were no significant differences between the normalized angles of all four formulations printed as a 30° angle. Similarly, no effect of the formulation on the normalized angle was observed while printing 60° angles. By comparing the 45° angle, the values of the biomaterial inks A3G3 and A4G3, both without cells, differed significantly. The differences can be explained by the different alginate concentrations, as the bioinks tend to keep flowing after printing. The analysis of the printed angles was performed with an automated image processing workflow. There have been similar studies regarding printing and characterizing angular structures by He et al. [255] and Naghieh et al. [256]. Both studies state the importance of characterizing such angular patterns, as these simple patterns build up the bases of printed structures of higher complexity. However, the studies fail to give precise information on the estimation of the angles, which is a basic requirement for the standardization of processes.

It must be noted that the air pressure acting on the cartridge and the set pressure of the printing software did not match. The air pressure was, therefore, controlled with a pneumatic sensor before printing processes were started. Especially when it comes to medical applications, it is a basic requirement for the construction of 3D bioprinters that they work reliably and that the air supply is stable and not affected by the position of the printhead. There is still great potential on the side of

the bioprinter manufacturers that needs to be improved. The single-layer structures characterized in this study represent the starting point since later complex geometries can be broken down into them. Characterizing the first layer is important, as defects in the base layer can prevent all subsequent layers from adhering to it. Similarly, defects on the layer can lead to the collapsing of the structure, especially with an increasing amount on layers piling on top of the basis. Future studies should include the characterization of the effect of the amount of extruded material in top of the base layer. Additionally, the strategies should be developed for the evaluation of 3D structures using automated image processing. At the moment, image acquisition takes place externally and not within the bioprinting system online. It would be desirable in the future to integrate the camera into the bioprinter with a suitable and adaptable illumination setup, as the transparency of bioinks is an issue during image acquisition that is particularly important in the choice of lighting and background to reach enough contrast. Regarding image processing, local thresholding should be preferred so that as little information as possible is lost. Such an image processing step is of particular interest if even illumination cannot be performed. Even though there were slight limitations on the imaging methods, the field of bioprinting can benefit from the application of automated image processing and analysis. The presented method proved to be robust for printed object evaluation, as it saves analytical time and reduces observer-dependent errors.

The aim of bioprinting is the production of scaffolds with high accuracy. Simultaneously, the printing of bioinks should meet the requirement of maintaining high cell viability after this process, as shear stress can induce irreversible cell damage.

6.3.2.2 Effect of processing on cell viability

Besides the printing accuracy, the effect of processing on cell viability after the mixing process and after the extrusion process was further studied. Here, three biological replicates for A3G3 with cells and A4G3 with cells were produced and analyzed. Each cartridge containing bioink was collected in three fractions. Each fraction was diluted with DPBS, and cells were stained in the resulting suspension. For the detection of fluorescent signals and, thus, the determination of cell viability, flow cytometry was used. Each diluted fraction was analyzed in technical triplicate. The respective results are presented in Figure 6.8. The bar chart shows the cell viability for both tested bioinks directly after the mixing step and after the extrusion. process.

The increasing alginate content of the bioinks led to a decreasing cell viability. This effect was observed after the mixing step as well as after mixing and subsequent extrusion. The viability of cells mixed into the A3G3 formulation and into the A4G3 formulation showed a value of $96.3 \pm 4.9\%$, and $77.9 \pm 16.4\%$, respectively. Both values differed significantly. The viability of cells extruded within the A3G3 bioink was slightly reduced to $95.3 \pm 3.0\%$. However, the difference was not statistically significant. Considering cells in the A4G3 formulation, viability decreased in a significant manner to $66.4 \pm 12.7\%$. After mixing and extrusion, the viability of cells contained in the A3G3 formulation differed significantly from that of cells present in the A4G3 bioink. As cells were harvested directly prior to both processes and the proceeding analysis, the contact between cells and biomaterial was the same for each sample, i.e., effects on cell viability arose from the processing steps. The decreasing amount of viable cells can be explained by the shear stress during mixing and extrusion that leads to cell disruption. The shear stress increases with the viscosity of the polymer solution as well as with increasing pneumatic pressure. The effect of the alginate concentration and thus the increasing viscosity on decreasing cell viability is in accordance with similar studies [234, 245,

257]. Increasing printing pressure leading to lower cell viability was also demonstrated in further studies [234, 245, 258, 259]. Moreover, the use of flow cytometry for data acquisition increased the precision of the determined cell viability as this value was calculated with larger amounts of counted cells. Other studies in the field of bioprinting and tissue engineering analyze a low number of microscopy images containing a low number of cells [240, 244, 245]. Commercially available assays, such as live/dead staining kits, lactate dehydrogenase assay, and alamar blue staining, are commonly applied in order to evaluate cell viability [260]. The assays are developed for culture methods where cells adhere to planar surfaces, i.e., two-dimensional cell culture, or cells are suspended in cell culture media. The assay components are added to the fluid phase and the molecules diffuse easily to the cells, and the absorbance or fluorescence are measured in plate readers. In tissue engineering and biofabrication, cells are embedded within a polymeric network, and the diffusion of solutes within the structures is limited. This is an issue to be considered in the application of commercially available kits. The protocols can be adapted to 3D cell culture substrates by adjusting incubation times or implementing the permeabilization of the hydrogels. By dilution of the bioink to a low viscosity cell suspension, the fast diffusion of the used stains is enabled as well as the use of the flow cytometer. Each technical replicate of this study part of the study regarding the assessment of the processing effects on viability consists of cell numbers in the range of 450 up to about 10.000. Considering the 20-fold dilution required for analysis with flow cytometry, the cell count in the bioink is calculated to be in the range between 9×10^3 cells/mL and 0.2×10^6 cells/mL, considerably lower than the cell count of 2×10^6 cells/mL to be set in the bioink. The amount of cells in each fraction differed due to the inhomogeneous mixing of the used method, where a syringe containing the cell suspension is connected to a second syringe containing the polymer solution, and a mixing effect is produced by transferring the solution back and forth between both syringes. Even though this method requires significant improvement, it was applied in the presented study, as it is commonly used in studies [261, 262], and it shows the benefits of low biomaterial loss compared to static mixer components. Additionally, mixing of cells in this manner can be compliant to good manufacturing practice (GMP) conditions compared to the mixing of cells in open containers. The reduction in waste of biomaterial by improvement of the static mixing units was studied by Dani et al. [241] and should be implemented in further studies. The quantified number of cells did differ in each technical sample due to inhomogeneous mixing; however, the viability was in a similar range, as it is the ratio between viable and dead cells. As mentioned in Section 6.3.2.1, bioprinting can benefit from standardization of the mixing method as air bubbles are introduced in the bioink [236, 241]. A further benefit is the comparability of data regarding cell viability, as the mixing method proved to be a critical step. The use of flow cytometry can also reduce observer-dependent errors while increasing reproducibility, as image acquisition mostly relies on the manual focusing of the samples during image acquisition. It is noteworthy that the use of flow cytometry is a destructive method, as the bioink has to be diluted in order to be analyzed. Microscopy is still required as a supplementary cell analytical method regarding cell adhesion, morphology, and migration during longer periods of cultivation.

Gillespie et al. [236] mentioned the limitation of the lack of control of the extruded amount of biomaterial. Measured characteristics of printed structures could differ either due to the mechanical properties of the used bioinks, or due to different amounts of bioinks deposited during printing. This presented method overcomes the mentioned difficulty by controlling the volumetric flow rate according to the specific flow behavior of each bioink. Additionally, the printing speed was set equal to the mean velocity of the biomaterial ink based on the rheological properties; thus, this parameter

is directly related to the pneumatic pressure. Furthermore, the alginate content of both bioinks differed by 1% (w/v) and, thus, showed different values of viscosity. By controlling the flow rate, no differences were observed regarding the printing accuracy between both bioinks. In contrast, the increasing viscosity led to a significant decrease in cell viability directly after mixing and after extrusion. Bioinks should enable the accurate production of scaffolds while maintaining high viability and supporting biological needs. Meeting both requirements is accepted as a limitation, as increasing the concentration and thus viscosity leads to higher structural stability but increases the resulting cell disruption [50, 198, 252]. In this study, the bioink with the lower alginate content showed better printing performance overall, as the method compared the samples printed with a controlled flow rate. The presented methods show further advantages. The setting of printing parameters did not include the screening of printability by an observer, which is still commonly used in the bioprinting field. There are many printing parameters that can be set during a study on printing performance, and each affects the accuracy of the product in a different magnitude. Therefore, the setting of printing speed in relation to the pneumatic pressure increases the objectivity of the study, as only one was chosen arbitrarily and not both of them. The use of automated image processing to characterize printed structures reduces observer-dependent errors while saving the time required for image analysis. The presented methods increase the comparability of data between bioinks and can allow the transfer of gained knowledge between laboratories.

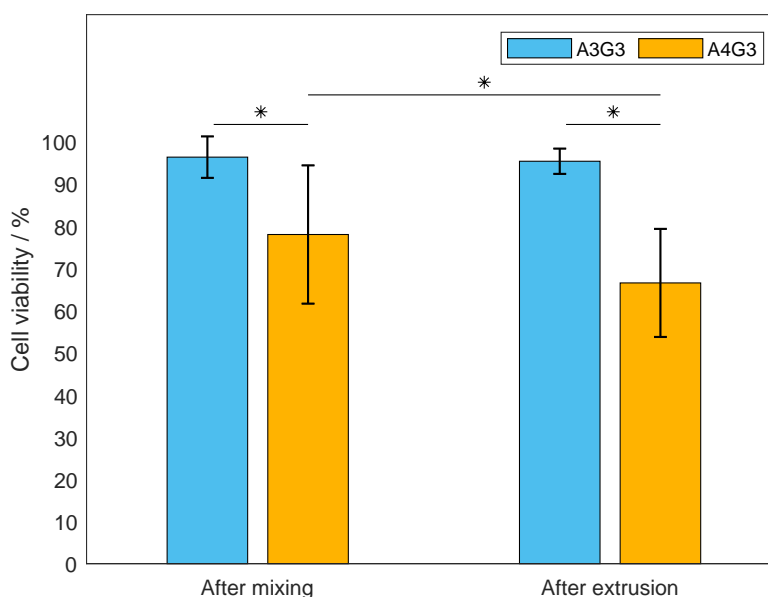


Figure 6.8 Characterization of the effect of processing on cells. The viability was determined after the mixing step and after the extrusion process. For both bioinks, the mean viability is shown as a bar with the associated standard deviation. The experiments were performed as biological triplicates ($n = 3$). For both bioinks, each biological replicate was divided into three fractions, diluted separately ($n = 3$), and analyzed as technical triplicates ($n = 3$), resulting in data sets consisting of 27 values. Significant differences are denoted with an asterisk ($p < 0.05$).

6.4 Conclusion

Universal methodologies should be developed and applied starting from the bioink preparation, including process analytical technology (PAT) strategies as well as standardized analytical methodologies. In this study, the focus lies on the development of analytical methods that enable the comparability of bioprinting processes regarding the metrics of printed structures as well as the effect on cell viability. First, the used bioinks and biomaterial inks were printed with the same flow rate, thus enabling the comparison of structures with the same amount of extruded material. The required pneumatic pressure was determined and set according to the specific flow behavior of each biomaterial ink that differed in alginate concentration by 1% (*w/v*) with a constant GelMA concentration. Additionally, the printing speed was directly related the pneumatic pressure applied during printing. This setting of printing parameters enabled the adequate comparison of printed structures produced with an equal amount of material. Second, image-processing tools were developed in order to accurately characterize the printed structures in an automated manner. The application of automated image analysis allowed the time-saving assessment of printed geometries, while reducing observer-dependent variations, and therefore, the robustness of the analytical method was enhanced. The study focused on the analysis of the first layer, as this is the base of any multi-layered structure. In the future, the developed image processing should be expanded and implemented into the characterization of 3D structures. Using the developed tools, no effect of the increasing viscosity on the structural features was shown. However, the cell mixing process did have an effect on the geometrical characteristics of the printed structures, as air was entrapped while mixing the biomaterial ink with the cellular material. Future research should include testing the control of flow rate in 3D objects, as, here, only single-layer structures were investigated. Third, cell viability was determined by flow cytometry, thereby increasing the amount of quantified cells and enhancing the precision of the acquired data compared to the conventionally used microscopy. Moreover, the increasing alginate content showed a significantly negative impact on viability during both processing steps, mixing as well as extrusion. Some issues still have to be studied, e.g., the lack of standardized and effective cell mixing processes. The used mixing strategy was the transfer of biomaterial ink and cells back and forth between two syringes, which is commonly used in the field of bioprinting. This method proved to produce an inhomogeneous cell distribution and air bubbles entrapment in the cartridge. The proposed methods show great potential for saving time and costs by eliminating the need for user-dependent print parameter screenings and enables an easy transfer between devices and laboratories. The lack of standardized methods will constitute an issue in bioprinting by the stage prior to clinical applications when meeting with regulatory agencies. The requirements include robust production processes that lead to quality attributes, independent of the location and operator.

Conflict of interest

The authors declare that the research was conducted in the absence of any commercial or financial relationships that could be construed as a potential conflict of interest.

Author contributions

Conceptualization: S.S., D.G.G. and J.H.; Data curation: S.S. and D.G.G.; Formal analysis: S.S. and D.G.G.; Funding acquisition: J.H.; Investigation: S.S. and D.G.G.; Methodology: S.S. and D.G.G.; Project administration: J.H.; Resources: J.H.; Software: S.S. and D.G.G.; Supervision: J.H.; Validation: S.S. and D.G.G.; Writing—original draft: S.S. and D.G.G.; Writing—review and editing: J.H. All authors have read and agreed to the published version of the manuscript.

Funding

This project received funding from the German Federal Ministry of Education and Research (BMBF) as project SOP–Bioprint under contract number 13XP5071B.

Data availability statement

The raw data supporting the conclusions of this article will be made available by the authors without undue reservation.

Acknowledgments

We would like to thank Lea Bensinger, Jasmin Egner, and Christian Lachmuth for their valuable contribution in form of experimental work for this project. We acknowledge support by the KIT-Publication Fund of the Karlsruhe Institute of Technology

Chapter references

- [3] J. Malda *et al.*, „25th anniversary article: Engineering hydrogels for biofabrication“, *Advanced Materials*, vol. 25, no. 36, pp. 5011–5028, 2013.
- [14] N. Paxton, W. Smolan, T. Böck, F. Melchels, J. Groll, and T. Jungst, „Proposal to assess printability of bioinks for extrusion-based bioprinting and evaluation of rheological properties governing bioprintability“, *Biofabrication*, vol. 9, no. 4, p. 44107, 2017.
- [50] I. T. Ozbolat and M. Hospodiuk, „Current advances and future perspectives in extrusion-based bioprinting“, *Biomaterials*, vol. 76, pp. 321–343, 2016.
- [59] J. Groll *et al.*, „A definition of bioinks and their distinction from biomaterial inks“, *Biofabrication*, vol. 11, no. 1, 2019.
- [109] S. Gretzinger, N. Beckert, A. Gleadall, C. Lee-Thedieck, and J. Hubbuch, „3D bioprinting – Flow cytometry as analytical strategy for 3D cell structures“, *Bioprinting*, vol. 11, no. March, e00023, 2018.
- [188] S. V. Murphy and A. Atala, „3D bioprinting of tissues and organs“, *Nature biotechnology*, vol. 32, no. 8, pp. 773–785, 2014.
- [198] Y. Zhao, Y. Li, S. Mao, W. Sun, and R. Yao, „The influence of printing parameters on cell survival rate and printability in microextrusion-based 3D cell printing technology“, *Biofabrication*, vol. 7, no. 4, 2015.
- [201] B. Webb and B. J. Doyle, „Parameter optimization for 3D bioprinting of hydrogels“, *Bioprinting*, vol. 8, no. July, pp. 8–12, 2017.
- [227] B. V. Slaughter, S. S. Khurshid, O. Z. Fisher, A. Khademhosseini, and N. A. Peppas, „Hydrogels in Regenerative Medicine“, *Advanced Materials*, vol. 21, no. 32-33, pp. 3307–3329, 2009.
- [228] J. Thiele, Y. Ma, S. M. C. Bruekers, S. Ma, and W. T. S. Huck, „25th Anniversary Article: Designer Hydrogels for Cell Cultures: A Materials Selection Guide“, *Advanced Materials*, vol. 26, no. 1, pp. 125–148, 2014.
- [229] A. S. Theus *et al.*, „Bioprintability: Physiomechanical and Biological Requirements of Materials for 3D Bioprinting Processes“, *Polymers*, vol. 12, no. 10, p. 2262, 2020.
- [230] W. Liu *et al.*, „Extrusion Bioprinting of Shear-Thinning Gelatin Methacryloyl Bioinks“, *Advanced Healthcare Materials*, vol. 6, no. 12, pp. 1–11, 2017.
- [231] A. Erdem *et al.*, „3D Bioprinting of Oxygenated Cell-Laden Gelatin Methacryloyl Constructs“, *Advanced Healthcare Materials*, vol. 9, no. 15, pp. 1–12, 2020.
- [232] H. Jongprasitkul, S. Turunen, V. S. Parihar, and M. Kellomäki, „Two-step crosslinking to enhance the printability of methacrylated gellan gum biomaterial ink for extrusion-based 3D bioprinting“, *Bioprinting*, vol. 25, no. September 2021, 2022.
- [233] A. Habib, V. Sathish, S. Mallik, and B. Khoda, „3D printability of alginate-carboxymethyl cellulose hydrogel“, *Materials*, vol. 11, no. 3, 2018.
- [234] A. Mondal *et al.*, „Characterization and printability of Sodium alginate -Gelatin hydrogel for bioprinting NSCLC co-culture“, *Scientific Reports*, vol. 9, no. 1, pp. 1–12, 2019.
- [235] B. H. Lee, N. Lum, L. Y. Seow, P. Q. Lim, and L. P. Tan, „Synthesis and characterization of types A and B gelatin methacryloyl for bioink applications“, *Materials*, vol. 9, no. 10, pp. 1–13, 2016.
- [236] G. Gillispie *et al.*, „Assessment methodologies for extrusion-based bioink printability“, *Biofabrication*, vol. 12, no. 2, 2020.
- [237] T. Gao *et al.*, „Optimization of gelatin-alginate composite bioink printability using rheological parameters: A systematic approach“, *Biofabrication*, vol. 10, no. 3, 2018.
- [238] M. D. Giuseppe *et al.*, „Mechanical behaviour of alginate-gelatin hydrogels for 3D bioprinting“, *Journal of the Mechanical Behavior of Biomedical Materials*, vol. 79, pp. 150–157, 2018.
- [239] M. Uzun-Per *et al.*, „Automated Image Analysis Methodologies to Compute Bioink Printability“, *Advanced Engineering Materials*, vol. 2000900, pp. 1–12, 2020.
- [240] A. A. Aldana, F. Valente, R. Dilley, and B. Doyle, „Development of 3D bioprinted GelMA-alginate hydrogels with tunable mechanical properties“, *Bioprinting*, vol. 21, no. June 2020, e00105, 2021.
- [241] S. Dani *et al.*, „Homogeneous and reproducible mixing of highly viscous biomaterial inks and cell suspensions to create bioinks“, *Gels*, vol. 7, no. 4, pp. 1–17, 2021.
- [242] E. N. Malamas, E. G. Petrakis, M. Zervakis, L. Petit, and J.-D. Legat, „A survey on industrial vision systems, applications and tools“, *Image and Vision Computing*, vol. 21, no. 2, pp. 171–188, 2003.
- [243] O. Semeniuta, S. Dransfeld, K. Martinsen, and P. Falkman, „Towards increased intelligence and automatic improvement in industrial vision systems“, *Procedia CIRP*, vol. 67, pp. 256–261, 2018.

- [244] W. Schuurman *et al.*, „Gelatin-Methacrylamide Hydrogels as Potential Biomaterials for Fabrication of Tissue-Engineered Cartilage Constructs“, *Macromolecular Bioscience*, vol. 13, no. 5, pp. 551–561, 2013.
- [245] F. Koch, K. Tröndle, G. Finkenzeller, R. Zengerle, S. Zimmermann, and P. Koltay, „Generic method of printing window adjustment for extrusion-based 3D-bioprinting to maintain high viability of mesenchymal stem cells in an alginate-gelatin hydrogel“, *Bioprinting*, vol. 20, e00094, 2020.
- [246] Z. Di *et al.*, „Ultra High Content Image Analysis and Phenotype Profiling of 3D Cultured Micro-Tissues“, *PLoS ONE*, vol. 9, no. 10, R. Oshima, Ed., e109688, 2014.
- [247] S. Eggert and D. W. Huttmacher, „In vitro disease models 4.0 via automation and high-throughput processing“, *Biofabrication*, vol. 11, no. 4, 2019.
- [248] D. E. Godar, „3D Bioprinting: Surviving under Pressure“, *Tissue Regeneration*, 2018.
- [249] D. Grijalva Garces, C. P. Radtke, and J. Hubbuch, „A Novel Approach for the Manufacturing of Gelatin-Methacryloyl“, *Polymers*, vol. 14, no. 24, p. 5424, 2022.
- [250] A. F. Habeeb, „Determination of free amino groups in proteins by trinitrobenzenesulfonic acid“, *Analytical Biochemistry*, vol. 14, no. 3, pp. 328–336, 1966.
- [251] H. Münstedt and F. R. Schwarzl, *Deformation and Flow of Polymeric Materials*. Berlin, Heidelberg: Springer Berlin Heidelberg, 2014.
- [252] J. H. Chung *et al.*, „Bio-ink properties and printability for extrusion printing living cells“, *Biomaterials Science*, vol. 1, no. 7, pp. 763–773, 2013.
- [253] L. Wenger, S. Strauß, and J. Hubbuch, „Bioprinting Automated and dynamic extrusion pressure adjustment based on real-time flow rate measurements for precise ink dispensing in 3D bioprinting“, *Bioprinting*, vol. 28, no. July, pp. 1–14, 2022.
- [254] D. L. Cohen, W. Lo, A. Tsavaris, D. Peng, H. Lipson, and L. J. Bonassar, „Increased Mixing Improves Hydrogel Homogeneity and Quality of Three-Dimensional Printed Constructs“, *Tissue Engineering Part C: Methods*, vol. 17, no. 2, pp. 239–248, 2011.
- [255] Y. He, F. Yang, H. Zhao, Q. Gao, B. Xia, and J. Fu, „Research on the printability of hydrogels in 3D bioprinting“, *Scientific Reports*, vol. 6, pp. 1–13, 2016.
- [256] S. Naghieh, M. Sarker, N. K. Sharma, Z. Barhoumi, and X. Chen, „Printability of 3D Printed Hydrogel Scaffolds: Influence of Hydrogel Composition and Printing Parameters“, *Applied Sciences*, vol. 10, no. 1, p. 292, 2019.
- [257] A. G. Tabriz, M. A. Hermida, N. R. Leslie, and W. Shu, „Three-dimensional bioprinting of complex cell laden alginate hydrogel structures“, *Biofabrication*, vol. 7, no. 4, p. 045 012, 2015.
- [258] K. Nair *et al.*, „Characterization of cell viability during bioprinting processes“, *Biotechnology Journal*, vol. 4, no. 8, pp. 1168–1177, 2009.
- [259] J. Snyder, A. Rin Son, Q. Hamid, C. Wang, Y. Lui, and W. Sun, „Mesenchymal stem cell printing and process regulated cell properties“, *Biofabrication*, vol. 7, no. 4, 2015.
- [260] J. Marzi *et al.*, „Non-Invasive Three-Dimensional Cell Analysis in Bioinks by Raman Imaging“, *ACS Applied Materials & Interfaces*, vol. 14, no. 27, pp. 30 455–30 465, 2022.
- [261] H. Park, S.-W. Kang, B.-S. Kim, D. J. Mooney, and K. Y. Lee, „Shear-reversibly Crosslinked Alginate Hydrogels for Tissue Engineering“, *Macromolecular Bioscience*, vol. 9, no. 9, pp. 895–901, 2009.
- [262] F. Hafezi *et al.*, „Bioprinting and preliminary testing of highly reproducible novel bioink for potential skin regeneration“, *Pharmaceutics*, vol. 12, no. 6, pp. 1–21, 2020.

7

On the Reproducibility of extrusion-based Bioprinting: Round Robin Study on Standardization in the Field

© IOP Publishing. Reproduced with permission. All rights reserved.

David Grijalva Garces^{1,2*}, Svenja Strauß^{1,2*}, Sarah Gretzinger^{1,2}, Barbara Schmiegl^{1,2}, Tomasz Jüngst^{3,4}, Jürgen Groll^{3,4}, Lorenz Meinel⁵, Isabelle Schmidt⁶, Hanna Hartmann⁶, Katja Schenke-Layland^{6,7}, Nico Brandt⁸, Michael Selzer⁹, Stefan Zimmermann¹⁰, Peter Koltay¹⁰, Alexander Southan^{11,12}, Günter E. M. Tovar^{11,12}, Sarah Schmidt¹², Achim Weber¹², Tilman Ahlfeld¹³, Michael Gelinsky¹³, Thomas Scheibel^{14,4}, Rainer Detsch¹⁵, Aldo R. Boccaccini¹⁵, Toufik Naolou¹⁶, Cornelia Lee-Thedieck¹⁶, Christian Willems^{17, 17}, Stephan Allgeier¹⁸, Bernd Köhler¹⁸, Tiaan Friedrich¹⁹, Heiko Briesen¹⁹, Janine Buchholz²⁰, Dietrich Paulus²⁰, Anselm von Gladiss²⁰, and Jürgen Hubbuch^{1,2}

- ¹ Institute of Functional Interfaces, Karlsruhe Institute of Technology (KIT), Eggenstein-Leopoldshafen, Germany
- ² Institute of Process Engineering in Life Sciences, Section IV: Biomolecular Separation Engineering, Karlsruhe Institute of Technology (KIT), Karlsruhe, Germany
- ³ Department for Functional Materials in Medicine and Dentistry, Institute of Functional Materials and Biofabrication, University of Würzburg, Würzburg, Germany
- ⁴ Bavarian Polymer Institute, University of Bayreuth, Bayreuth, Germany
- ⁵ Institute of Pharmacy and Food Chemistry, University of Würzburg, Würzburg, Germany
- ⁶ NMI Natural and Medical Sciences Institute at the University of Tübingen, Reutlingen, Germany
- ⁷ Institute of Biomedical Engineering, Department for Medical Technologies and Regenerative Medicine, Eberhard Karls University of Tübingen, Tübingen, Germany
- ⁸ Institute for Applied Materials, Karlsruhe Institute of Technology, Karlsruhe, Germany
- ⁹ Institute for Nanotechnology, Karlsruhe Institute of Technology, Karlsruhe, Germany
- ¹⁰ Laboratory for MEMS Applications, Department of Microsystems Engineering, University of Freiburg, Freiburg, Germany
- ¹¹ Institute of Interfacial Process Engineering and Plasma Technology, University of Stuttgart, Stuttgart, Germany
- ¹² Functional Surfaces and Materials, Fraunhofer Institute for Interfacial Engineering and Biotechnology, Stuttgart, Germany
- ¹³ Center for Translational Bone, Joint, and Soft Tissue Research, Faculty of Medicine, Technische Universität Dresden, Dresden, Germany
- ¹⁴ Chair of Biomaterials, University of Bayreuth, Bayreuth, Germany
- ¹⁵ Institute of Biomaterials, Friedrich-Alexander University Erlangen-Nuremberg, Erlangen, Germany
- ¹⁶ Institute of Cell Biology and Biophysics, Leibniz University Hannover, Hannover, Germany
- ¹⁷ Department Biomedical Materials, Martin Luther University Halle-Wittenberg, Halle (Saale), Germany
- ¹⁸ Institute for Automation and Applied Informatics, Karlsruhe Institute of Technology, Eggenstein-Leopoldshafen, Germany
- ¹⁹ Process Systems Engineering, School of Life Sciences, Technical University of Munich, Freising, Germany
- ²⁰ Institute for Computational Visualistics, Active Vision Group, University of Koblenz, Koblenz, Germany
- * Contributed equally

Abstract

The outcome of three-dimensional (3D) bioprinting heavily depends, amongst others, on the interaction between the developed bioink, the printing process, and the printing equipment. However, if this interplay is ensured, bioprinting promises unmatched possibilities in the health care area. To pave the way for comparing newly developed biomaterials, clinical studies, and medical applications (i.e. printed organs, patient-specific tissues), there is a great need for standardization of manufacturing methods in order to enable technology transfers. Despite the importance of such standardization, there is currently a tremendous lack of empirical data that examines the reproducibility and robustness of production in more than one location at a time. In this work, we present data derived from a round robin test for extrusion-based 3D printing performance comprising 12 different academic laboratories throughout Germany and analyze the respective prints using automated image analysis in three independent academic groups. The fabrication of objects from polymer solutions was standardized as much as currently possible to allow studying the comparability of results from different laboratories. This study has led to the conclusion that current standardization conditions still leave room for the intervention of operators due to missing automation of the equipment. This affects significantly the reproducibility and comparability of bioprinting experiments in multiple laboratories. Nevertheless, automated image analysis proved to be a suitable methodology for quality assurance as three independently developed workflows achieved similar results. Moreover, the extracted data describing geometric features showed how the function of printers affects the quality of the printed object. A significant step toward standardization of the process was made as an infrastructure for distribution of material and methods, as well as for data transfer and storage was successfully established.

7.1 Introduction

3D bioprinting is attracting widespread interest due to the possibility to manufacture customized artificial tissues in regards to individual patient treatment, designing models for medical studies or organ-on-a-chip applications [263, 264]. For these products to be approved by authorities for medical application or clinical studies, high reproducibility and robust processes will inevitably be a challenge. The safety of the products should be guaranteed by standards and norms. In the field of bioprinting, there is still a need for universally applicable guidelines and standard operating procedures (SOPs). These should be included from the very beginning of the production of bioinks through to process analytical technology (PAT) strategies and standardized analytical methodologies. In order to be able to compare, for example, bioinks or bioprinter setups in interlaboratory tests or prepare technology transfers, standardized methodologies are a prerequisite. Due to the missing guidelines, research groups develop own expertise and there is hardly any exchange of information between groups. This said, the use of interlaboratory data bases as advocated by the research community is still in its infancy. In this regard, there have been advances in the field of bioprinting, where the Kadi4Mat infrastructure was used for process design, documentation, data storage, and exchange [265]. Looking at other related research areas such as tissue engineering, the International Organization for Standardization (ISO) has already constituted a technical committee (TC) for tissue-engineering of medical products, i.e. ISO/TC 150/SC 7, aiming to implement relevant standards for testing and manufacturing methods. Therefore, it is only a matter of time before such subcommittees for bioprinting form. At the local level, for example, policy committees have

already been formed as part of the Verein Deutscher Ingenieure (VDI), the Association of German Engineers. The VDI guidelines committee (Richtlinienausschuss 5708) aims for the definition of basic terminology, device requirements, and bioink testing methodologies. The development of robust protocols and standards is of crucial importance for a successful clinical translation of biomaterials and bioprinting as has been mentioned in literature [266].

With regard to future application in clinical studies, there are some process steps which would benefit from standardization. The first aspect is the production and characterization of newly developed bioinks which consist of biomaterials, cells, and other additives [59, 193]. It is, for example, not an easy undertaking to homogeneously introduce cells into the highly viscous solution to complete the bioink because air bubbles present a common challenge [167, 267, 268]. One suggestion is to introduce the cells above the gelation temperature of the solution [269]. The second aspect includes the printing process itself and the equipment of the bioprinters. There are different techniques for extrusion-based bioprinters, such as pneumatically operated or piston-driven methods [3, 188]. In addition, there are bioprinters where the cartridge or nozzle can be tempered including different principles, such as the use of a cooling agent or thermoelectric control. Another feature that not every bioprinter is equipped with is the automatic calibration of the coordinates of the nozzle tip which can have an influence on the printing result and thus on the reproducibility.

To ensure the quality and reproducibility of bioprinted structures, the performance of bioprinting evaluation is already being discussed [270, 271]. Filament collapse, fusion and grid tests are three commonly suggested evaluation methods. These evaluation methods are useful for both developers and users of bioprinting processes. The filament collapse test evaluates the printer's ability to deposit a filament on a platform with pillars at increasing intervals without the strand collapsing [199, 272]. This is important for the production of stable and reproducible complex structures. The yield stress of the material used can be derived here, which plays an important role in the design of bioinks as it defines the shear stress for initiating the material flow. The filament fusion test evaluates the printer's ability to deposit filaments meander-like at different distances, which can be used to determine the accuracy of the print test [273, 274]. The grid test evaluates the accuracy and precision of the printer by printing a grid pattern. The distance between the lines, pore diameter, pore geometry and the crossing point of struts are analyzed here for assessment [275]. Special attention should be given to the methodologies for quantitative analysis as the printed objects are evaluated and the outcome is translated into numbers. Image analysis (IA) is a suitable tool as it is fast, non-invasive, can be automated and, thus increases objectivity. Currently, there are still publications where 'the printability was judged by eyes' [255], or the images were cropped, and subsequently analyzed manually by a person [237]. This is a time-consuming procedure and dependent on the subjective impression of one observer only. Furthermore, acquired photographs were 'analysed in ImageJ where the width of the strand was measured at multiple locations and averaged' [240]. Hence, the number and location of measurements are variable and depend on a subjective decision by the observer. There have been advances toward automation of IA, however, the study still includes several manual steps for detection and cropping of artifacts [239]. In conclusion, the studies listed above show user-dependent methodologies based on subjective decisions which limit the overall comparison. So far, cell analytics in the field of bioprinting is also lacking standardization. Microscopy is a commonly used method for investigating cell viability and morphology, however, this method is user-dependent as well due to manual focusing and manual counting of observations [235, 244]. A more advanced

alternative for cell analytics is offered by raman imaging, which has been used for the analysis of cells within 3D printed objects [260]. Even though this topic is out of the scope of the present study, in which no cells were used, it should be standardized as well. Throughout this work, we use the term ink to refer to the applied polymeric solutions in our studies as all experiments were cell-free.

To date and to the best of our knowledge, no studies of the reproducibility and comparison of bioprinting experiments in multiple laboratories have been reported. In this round robin study, we tested how consistent printed-geometry results can be obtained with 12 laboratories cooperating. Therefore, an infrastructure for central distribution of SOPs with information regarding the preparation procedure for inks, and parameters for printing experiments was established. Additionally, the consumables and biomaterials were distributed by the organizing laboratory. A device for standardized image acquisition was developed and used within the round robin experiments. In total 10 prototypes of this so called Bioprinting Fidelity Imager (BioFI) were fabricated and used by different laboratories to record images of the printed objects. For quantitative assessment of the recorded images automated IA was included in order to extract features from the images of the printed objects. Finally, based on the experimental results, several factors that can be improved to increase reproducibility have been identified in order to make bioprinting more reliable and reproducible for future medical applications.

7.2 Materials and methods

7.2.1 Round robin workflow and design

The round robin test was designed and performed to provide a general overview of to which extent bioprinting experiments concur in different laboratories. A compact schematic of the workflow of the project is depicted in Figure 7.1. As already suggested by the name of the project SOP_BioPrint, SOPs for the individual stages were developed in advance and distributed to all participating entities by the organizing laboratory.

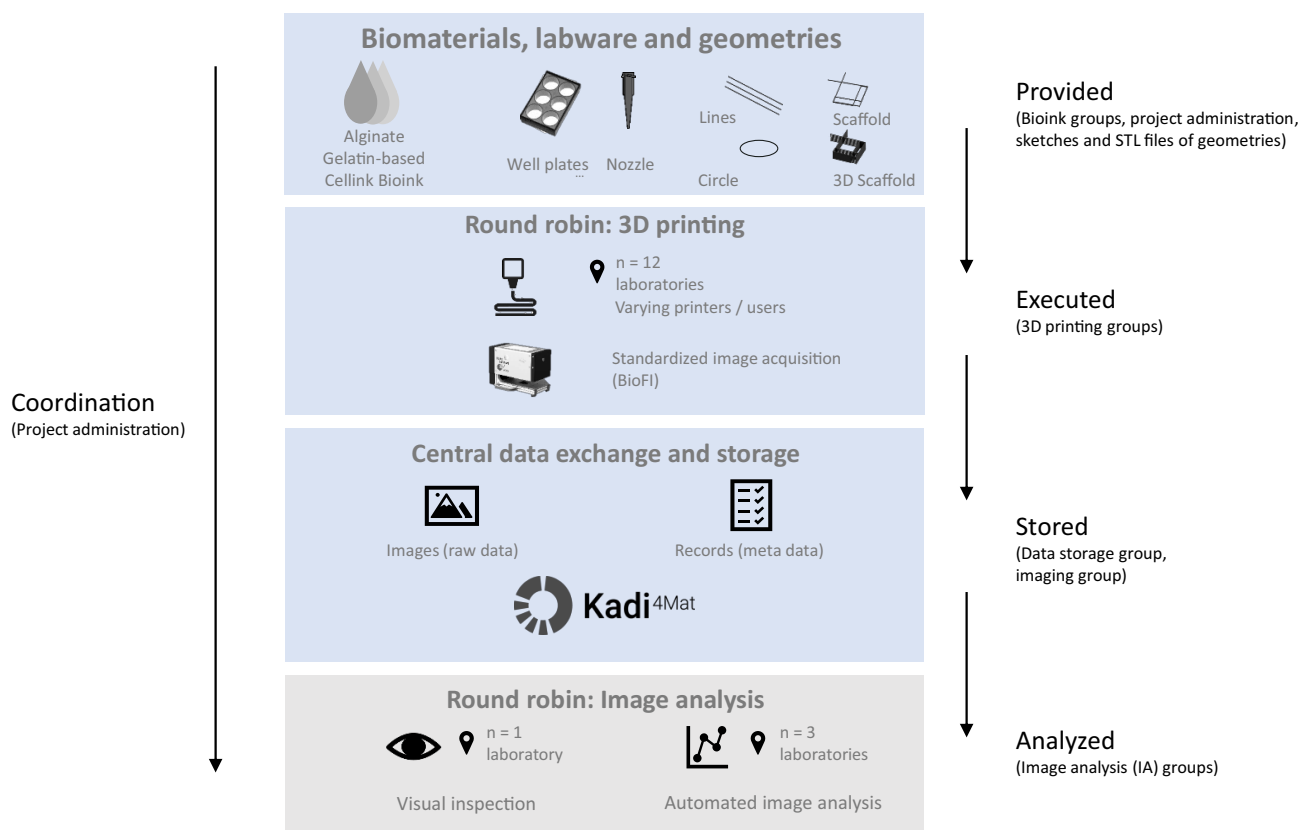


Figure 7.1 Illustrative scheme summarizing the workflow in the round robin tests. Biomaterials, labware, and geometries as well as detailed standard operation procedures (SOPs) regarding the preparation and use of materials were distributed. The Round robin - 3D printing was performed in 12 independent laboratories and comprised the 3D printing experiments and documentation. Subsequently, images of the printed geometries were acquired using the Bioprinting Fidelity Imager (BioFI) system. The Kadi4Mat platform was used for central data exchange and storage. The Round robin - Image analysis was divided into two parts. A qualitative evaluation of the images was performed by the organizing laboratory and extraction of quantitative geometric features was done individually by three image analysis groups independently. Statistical analysis and data visualization in the presented study were performed by the organizing laboratory.

7.2.2 Biomaterials, labware, and geometries

In order to achieve a high degree of standardization, the organizing laboratory provided the participating laboratories with the biomaterials, labware, and the files of the designed geometries including orientation to be printed. Three different polymeric solutions were used, two of which were provided by research institutions including preparation instructions. Alginate was provided by the Department for Functional Materials in Medicine and Dentistry from the University of Würzburg (Würzburg, Germany) with instructions for preparing a 4% (w/v) alginate ink in ultrapure water. The properties of this biomaterial in bioprinting is summarized by Karakaya *et al.* [276]. The biomaterials for the gelatin-based ink and guidelines on its preparation were provided by the Department of Functional Surfaces and Materials at Fraunhofer Institute for Interfacial Engineering and Biotechnology (Stuttgart, Germany). The methacrylation of gelatin

and its subsequent use as an ink was performed according to Wenz *et al.* [277]. Briefly, the ink consisted of 12 % (w/w) functionalized gelatin, i.e. a mixture of 7 % (w/w), and 5 % (w/w) gelatin with degrees of methacrylation of 0.62 mmol/g, 0.82 mmol/g, respectively, and 0.84 % (w/w) of LAP photo initiator dissolved in Dulbecco's phosphate-buffered saline (DPBS). The commercially available Cellink Bioink was used as a third ink and purchased from Cellink (Gothenburg, Sweden). This alginate nanocellulose bioink [137] was delivered as ready-to-use cartridges and procured from a single batch. Labware used in the printing experiment consisted of a single-use conic 25G (0.25 mm inner diameter) nozzle from Cellink and six-well glass bottom plates from iBL (Gerasdorf, Austria). An SOP specified the procurement details (part number, manufacturer, distributor) for well plates and nozzles. Additionally, the STL files, or in case of problems during slicing, the sketches of the objects were provided by the organizing laboratory. A larger sketch of the geometries is presented in the supplementary section. The first model was a pattern of three parallel 25 mm long lines with a distance of 2 mm between the lines. These were to be printed in parallel to the short edge of the well plate. The second object was a circle with a diameter of 12 mm. The first and second models both consisted of a single layer. The third model was designed as a rectangle with two layers. There were two meandering lines printed in two separate layers rotated by 90°. To create a closed square, there was a start up line with the length $l = 5$ mm in each layer. The fourth and last model was a stack of several layers of the scaffold, resulting in a total height of 1.2 mm. The start up filaments of both structures had to be printed oriented to the top left corner of each well plate.

7.2.3 Round robin - 3D printing

The experimental design in the Round robin - 3D printing test is summarized schematically in Figure 7.2. The twelve participating laboratories located in Germany are listed alphabetically below:

- Center for Translational Bone, Joint, and Soft Tissue Research, Technische Universität Dresden, Dresden
- Chair of Biomaterials, University of Bayreuth, Bayreuth
- Department of Functional Materials in Medicine and Dentistry, University of Würzburg, Würzburg
- Functional Surfaces and Materials, Fraunhofer Institute for Interfacial Engineering and Biotechnology, Stuttgart
- Institute of Biomaterials, Friedrich-Alexander University Erlangen-Nuremberg, Erlangen
- Institute of Cell Biology and Biophysics, Leibniz University Hannover, Hannover
- Institute of Functional Interfaces, Karlsruhe Institute of Technology, Eggenstein-Leopoldshafen
- Institute of Interfacial Process Engineering and Plasma Technology, University of Stuttgart, Stuttgart
- Institute of Pharmacy, Martin Luther University Halle-Wittenberg, Halle (Saale)
- Institute of Pharmacy and Food Chemistry, University of Würzburg, Würzburg
- Laboratory for MEMS Applications, Department of Microsystems Engineering, University of Freiburg, Freiburg
- NMI Natural and Medical Sciences Institute at the University of Tübingen, Reutlingen

Training of participants with respect to SOPs was executed virtually. Regarding the conception of SOPs, the 3D printing comprised the largest operational window and proved to be the most difficult to standardize. This was due to the fact that the participating entities used different printing equipment with varying specifications. Local adaptations were done by the respective lab

teams within the SOP. Table 7.1 provides relevant information of printers used in the Round robin - 3D printing test. The equipment included three custom-designed printers, five BioX™ and one Inkredible+™ (Cellink), two 3D Discovery™ (regenHU Ltd, Villaz-St-Pierre, Switzerland), and a BioScaffolder® (GeSiM mbH, Radeberg, Germany). Laboratory identification numbers were generated randomly and are used as Lab 1 to Lab 12 throughout this study for the analysis of the produced data sets.

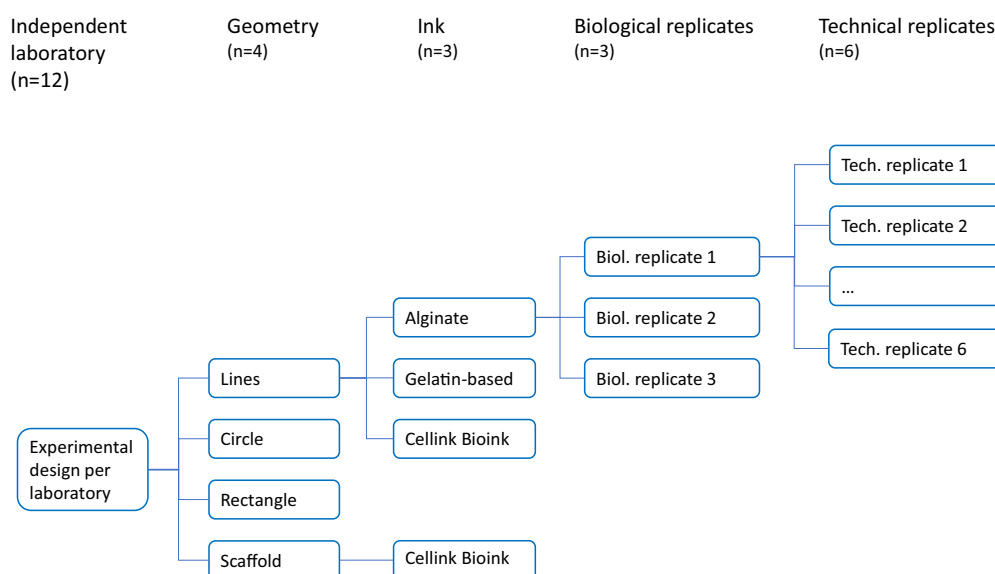


Figure 7.2 Scheme of the experimental design of the Round robin - 3D printing. Twelve different academic laboratories throughout Germany participated in the Round robin - 3D printing test ($n = 12$). Line, circle, and rectangle ($n = 3$) geometries were printed using three different inks ($n = 3$). Additionally, a three-dimensional (3D) scaffold was printed using Cellink Bioink ($n = 1$). As the experiments were performed without cells, independently prepared inks from the same batch were considered as analogs of biological replicates. In the case of Cellink Bioink, the use of an independent cartridge was considered as a biological replicate. For each biological replicate ($n = 3$), the ink was used in order to print six samples as technical replicates ($n = 6$). The resulting data sets contained 180 images for each individual laboratory. Exemplary images of the printed geometries with each ink are presented in Figure G.3.

Table 7.1 Extrusion principles and specifications of printing equipment used by the participating laboratories in the Round robin - 3D printing test. Laboratory identification numbers were generated randomly.

Lab	Extrusion principle	Temperature control	Z-height calibration
1	mechanical piston	fluid circulation	user-controlled
2	mechanical piston	none	user-controlled
3	pneumatic	electric heating	user-controlled
4	pneumatic	none	user-controlled
5	pneumatic	none	user-controlled
6	pneumatic	fluid circulation	automated
7	pneumatic	none	automated
8	pneumatic	electric heating	user-controlled
9	mechanical piston	electric heating	user-controlled
10	pneumatic	fluid circulation	automated
11	pneumatic	electric heating	user-controlled
12	pneumatic	electric heating	user-controlled

The biomaterials for gelatin-based ink and alginate were distributed as dry materials by the organizing laboratory. Both inks were prepared independently as three batches prior to the printing experiments in the laboratories of the participating entities. The commercially available Cellink Bioink was purchased as specified in the SOP. Three ready-to-use cartridges containing the ink were used. As the 3D-printing experiments were performed without cells, independently prepared inks from the same batch were considered as analogs of biological replicates. Six samples of each structure, e.g. line, circles, and rectangle, were printed using each ink (i.e. technical replicates). Additionally, a 3D scaffold was printed using Cellink Bioink as six samples of the structure (i.e. technical replicates). This resulted in a number of 180 objects per laboratory and in a total number of 2160 for the entire Round robin - 3D printing test. For the printing process, a window of operation regarding printing parameters was set by the organizing laboratory in order to print filaments in a similar metric range. These printing parameters were dependent on the used inks. They are listed in Table 7.2. For the case of the mechanically driven printers, the printing parameter was the axial speed of the piston. Therefore, a target width of 1 mm should be met. Once a parameter was set, it should not be changed over the complete series of printing experiments. Moreover, a standardized record was filled by each participating laboratory for documentation [265]. After the printing process, the well plates containing the six objects of a single structure were imaged externally. The BioFI system was specially developed for this purpose by the Laboratory for MEMS Applications, Department of Microsystems Engineering of the University of Freiburg (Freiburg, Germany) and Hahn-Schickard-Gesellschaft für Angewandte Forschung e.V. (Villingen-Schwenningen, Germany). Imaging equipment and method are specially adapted to polymeric solutions showing low contrast to the background. Simply speaking, the BioFI consisted of calibrated digital image sensor with fixed magnification optics and illumination, that enables acquisition of microscopy images in bright field and dark field mode. The whole equipment works as a stand alone device controlled by an embedded Linux system. The BioFI contained a bracket to hold the well plate in a proper position. Size scales were integrated below each single well for size determination. Imaging settings including lighting and exposure time were standardized and could not be modified by the operator. Printing records and acquired images were uploaded in the central database [265].

Table 7.2 Materials employed in the Round robin - 3D printing test with recommendations of printing parameters.

Ink	Extrusion pressure (kPa)	xy Speed (mm/sec)	Temperature (°C)
Alginate ink	50-120	20	RT
Gelatin-based ink	70-80	20	22-28
Cellink Bioink	20-30	20	RT

7.2.4 Central data exchange and storage

The distribution of SOPs and storage of documentation of the printing experiments of the Round robin test was implemented in a research data management system named Kadi4Mat [278]. Furthermore, all images were uploaded systematically so that, in combination with the relevant records, every step can be retrieved and analyzed at a later point in time. This systematic data storage was not only used for the purpose referred to, it simultaneously fulfilled the function of an electronic lab notebook (ELN) and proved to be important to the development toward digital laboratory. The detailed use of the Kadi4Mat database used in this study is described by Schmiege *et al.* [265]. After completing the experimental part in the laboratories, the analysis of the images of printed structures was divided into two parts. Hereby, the database allowed the quantitative analysis of objects using automated image analysis with the target to extract geometric features of the printed structures and to store them systematically again.

7.2.5 Round robin - Image analysis

A qualitative analysis was performed by the organizing laboratory in order to explore possible challenges which may complicate an automated evaluation and the extent of occurrence. To do so, two independent observers studied all images and classified them into categories. The categories used were offset position, orientation of structure, additional paths, non-continuous filaments, material excess, off focus, and weak contrast. In addition to the qualitative analysis, a quantitative assessment was carried out independently from the qualitative analysis. Three image analysis groups were included in the study for the quantitative assessment of the printed structures. Throughout this study, group identification numbers are used as IA Group 1, IA Group 2, and IA Group 3 regarding image analysis. The academic entities are given alphabetically in the list below:

- Chair of Process Systems Engineering, Technical University of Munich, Freising
- Institute for Automation and Applied Informatics, Karlsruhe Institute of Technology, Eggenstein-Leopoldshafen
- Institute for Computational Visualistics, University of Koblenz, Koblenz

This study was designed as a randomized and double-blinded multicenter study. The image analysis groups had access to the submitted images, and were able to freely develop a workflow to extract sets of parameters. It is noteworthy that the three groups were chosen to have different backgrounds and have not worked previously in the field of bioprinting or tissue engineering to avoid any bias. The backgrounds of the chosen groups were active vision where sensor data is processed and reacted to, application-oriented information including process automation, and development of process systems

engineering concepts, among other things, also for biological processes. The extracted geometric features include but are not limited to determinations of line width and length, circle inner and outer radius, and circle gap size. To ensure a non-biased analysis, the image analysis groups did not receive any information about the categorization performed in the qualitative analysis. All images were analyzed and the data sets were extracted using the three IA methodologies as presented below.

The first image analysis process consisted of four consecutive steps. The same general four-step process chain was used for all patterns, but the specific implementation of each step may differ between the lines, circle, and rectangle patterns. A manual preliminary step rotated all images by 0° , 90° , 180° , and 270° in order to bring them into the expected orientation as specified in the STL template. Step (I) of the automated process chain estimated the location of the printed structure based on a search for geometric primitives. For the circle and rectangle structures, the inner contours of the circle and of the large square cavity were used, respectively. A fixed ROI (region of interest) was formed around the calculated coordinates. For the lines structure, the small crosses of the substrate were used instead as lateral delimiters of the ROI. Step (II) consisted in tracing the contours of the printed structures in the estimated ROI. For the lines structure and the circle structure, both contours of each line and of the circle were extracted. For the rectangle structure, only the inner contours of the four cavities were traced. For the circle and rectangle structures, the nominal position of the extracted contours was defined by the pattern position detected in the previous step. For the lines structure, the six strongest step edges in a vertical projection profile of the ROI were used as reference contour locations. Step (III) analyzed the contour traces and removed parts that are classified as artifacts, e.g. from dust particles, rather than actual printed contours. Step (IV) calculated quantitative feature metrics. The printed line width and circle width were calculated as the distance between corresponding contour pairs, measured horizontally, and radially. For the rectangle structure, the areas of the square and rectangular cavities were calculated as numbers of pixels inside the cavity contours, if the contours were closed. Steps (I) and (II) were implemented in Visual C# 9.0 (Microsoft, Redmond, USA) using the Matrox Imaging Library MIL X 22H1 (Matrox Electronic Systems, Montreal, Canada). Steps (III) and (IV) were implemented in MATLAB[®] R2022a (TheMathWorks Inc., Natick, USA).

The second image analysis workflow started with determining the conversion factor from pixel to millimeter. Locations of the size scales which were integrated in the pictures were obtained by correlating binarized reference images and the input grayscale image. This factor was determined by summing up the rows or columns belonging to the 10 mm scale. Thereby, another reference image containing the printed geometry was drawn with the measurements of the construction sketches. The ROI for each geometry just as printing angle for lines and scaffolds were determined by rotating the reference and calculating the highest correlation to the input image. Contour detection was performed using a canny edge detector returning a binary edge image. Next up, small impurities were filtered by deleting all contours with a smaller area than a given threshold. To single out each strand of the line geometry individually, the image was subdivided. If necessary, the recognized edges were closed by active contours creating the segmentation outlines of the printed geometry, allowing images for each individual contour. A full segmentation as well as images of each scaffold hole were preserved by filling the contours with a flood fill procedure. These images enabled the calculation of different geometry characteristics such as area and line width. For the area calculation, all pixels of the filled segmentation were summed up. The first step of the line width computation

was the partition of the segment outlines into two matching contours by the medial axis of the geometry. Circle geometries were divided to an inner and outer contour whereas line geometries were separated to left and right. Scaffolds were split to multiple parts, resulting in several upper and lower as well as right and left relating contours. Afterwards, the smallest distance from each pixel of one contour to all pixels of the matching contour was computed and stored as an array. As a last step, the mean and median line widths of the complete geometry were calculated using the mean and median values of the entire array. Additionally, the results were transferred into the metric system by multiplication with the conversion factor. The program was implemented in Python 3.8.13 (Python Software Foundation, Delaware, USA) using the libraries OpenCV 4.6.0, NumPy 1.22.4, and Scikit-image 0.19.3[279].

The third image analysis approach for evaluating print quality consisted of four main steps: (I) segmentation of the printed geometry, (II) edge detection, (III) matching of the target geometry, and (IV) the evaluation of its quality. For the segmentation step (I), the scaled geometry and blank images were denoised with guided filtering [280] under self-guidance, resulting in edge-preserving noise reduction. KAZE features [281] were then computed and the blank image was aligned with the image of the printed geometry. By subtracting the aligned blank image from the image of the geometry, the marks on the plate and the backlight were removed. For edge detection (II), the gradient of the segmented geometry image is calculated. Local minima were reduced in order to be able to detect edges with the watershed algorithm. For this purpose, the 0.9 quantile of the gradient distribution was calculated. This 0.9 quantile was then used as a threshold for an H-minima transformation, where all local minima with a depth below this threshold were removed. Subsequently, the edges were extracted as watershed ridge lines, and small artifacts were removed by area opening with a minimum area of 0.25 mm^2 . The next step was to match the given geometry templates to the edge image (III). For this purpose, points on the inner and outer edges of the geometries were sampled. On the edge image, edge pixels of parallel lines with distances between 0.25 mm and 2 mm were selected. This selection was done by finding the maximum response of a Frangi filter [282]. Finally, the geometry template was aligned with the selected edge pixels by kernel correlation registration [283], and all edge pixels not connected to the region covered by the matched template were removed. Finally, for the quantitative evaluation of the printed structure (IV), the width of the detected structure was measured for the line and circle geometries. Missing segments were defined by zero width. For the rectangle and scaffold geometries, a flood fill was seeded to the expected center of the hole, and the centroid, as well as the covered area were measured. The program was implemented in MATLAB[®] R2022a used with the libraries Signal Processing Toolbox 9.0, Image Processing Toolbox 11.5, Statistics and Machine Learning Toolbox 12.3, Global Optimization Toolbox 4.7, Computer Vision Toolbox 10.2, and Parallel Computing Toolbox 7.6.

The data sets extracted by the image analysis groups were evaluated by the organizing laboratory. Outliers were detected and compared to the corresponding image. Only for the case of outliers arising from artifacts not recognized as such by the image processing workflows, the corresponding data was not used for further analysis. In terms of metrics regarding the printed structures, line and circle width were used in this study for the purpose of clarity. For the calculation of both parameters, filament width of each printed geometry were determined at several point along the complete structure. Data provided below is the mean and the corresponding standard deviation

of the mean width of single printed geometries. Both parameters were used for the calculation of the percentage coefficient of variation (CV) as the ratio of mean value to the associated standard deviation. A schematic representation of the two parameters is shown in the supplementary section.

7.2.6 Data handling and visualization

Data processing and evaluation including the calculation of mean and standard deviation as well as CV of the data sets, and data visualization were performed with MATLAB® R2022a.

7.3 Results and discussion

7.3.1 Round robin - 3D printing

The experimental part of the round robin study was conducted in twelve independent research institutions. After completion of the printing experiments, each laboratory submitted the acquired images and reports on Kadi4Mat. Thereby, support from the organizing laboratory was provided during data submission if required, as the project participants used this platform for the first time. It is noteworthy to mention that the experiments were not performed simultaneously as only a limited amount of BioFI imaging systems were used. The experimental part took place in a time frame of five months.

7.3.2 Round robin - Image analysis: qualitative

After having completed the practical part of the elaborate Round robin - 3D printing test, a visual inspection of images of printed structures was performed to get a first impression of the data quality. Some deviations from the specifications were found and sorted into five categories, and a possible root cause of the deviation was defined. However, not every deviation can be clearly traced back to a single cause, which is why there are some overlapping causes. The results are shown in Figure 7.3 by exemplary images.

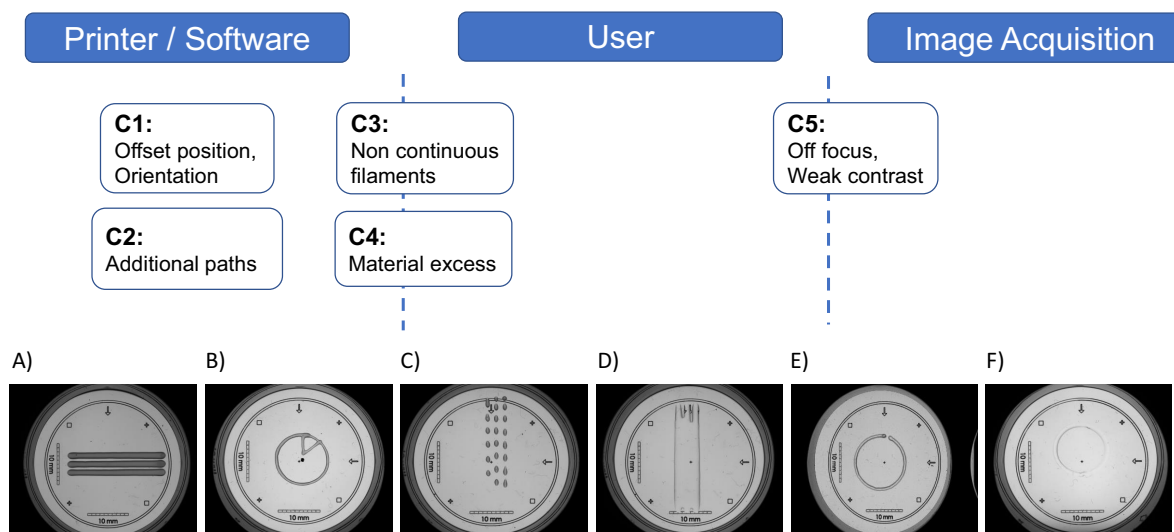


Figure 7.3 Overview of deviations with images shown as examples that occurred during the printing experiments. These can be caused by the setup (printer and software), the operator, or problems during image acquisition. Not every deviation can be traced back to a single cause. Therefore, some deviations are assigned to several causes and are in-between. A) Lines are rotated 90° compared to the original STL file, categorized as C1. B) Additional paths printed within the circle, categorized as C2. C) Discontinuous lines and simultaneously off-centered positioning, categorized as C1 and C3. D) Lines merged together due to excessive material corresponding to category C4. E) Substrate not properly placed in the BioFI imaging system, categorized as C5. F) Weak contrast between background and printed material as well as printed in an offset position, categorized as C5 and C1. Scale bars left and below printed geometries: 10 mm.

Category C1 includes samples where the orientation was different from the original STL file or samples with an offset position in relation to the center of the plate. Images that qualified for this category showed one of both of the named conditions. As can be seen in Figure 7.3 A), the line structures were deposited in a horizontal orientation, i.e. parallel to the long edge of the well plate, whereas the intended STL files contained structures aligned vertically. Category C2 contains printed structures showing additional paths other than the expected structure. Figure 7.3 B) shows the circle geometry with an excentric strand connecting the middle of the circle and the circumference. Both categories were probably produced by mistakes in the printing setup, i.e. software and printer. Category C3, and Category C4 are comprised of samples with non-continuous filaments, and material excess, respectively. Category C3 can be caused by a printing system that cannot keep the set pneumatic pressure stable or it can be the product of nozzle clogging. Corresponding to this category, Figure 7.3 C) exemplifies an intermittent line structure. Category C4 can arise due some printer equipment not having the feature to set a defined temperature leading to a lower viscosity of the ink. Similarly, a further origin of issues concerning this category can be an excessively high pneumatic pressure applied by the printer equipment. Figure 7.3 D) displays an excessive amount of material deposited on the substrate to the extent that all three intended strands fuse together to a single outspread shape without any specific geometry. Both categories C3 and C4 might also be affected by the inappropriate setting of printing parameters, which could be

originated both by the user and by the printing setup. Category C5 consists of images lacking high contrast between printed structures and structures out of focus. This can occur if the well plate is not properly placed in the bracket in the imaging system as seen in Figure 7.3 E) and F). Each image was classified into the categories of the presented challenges. The ratio of images found in each category to the total amount of images is presented in Figure 7.4 A).

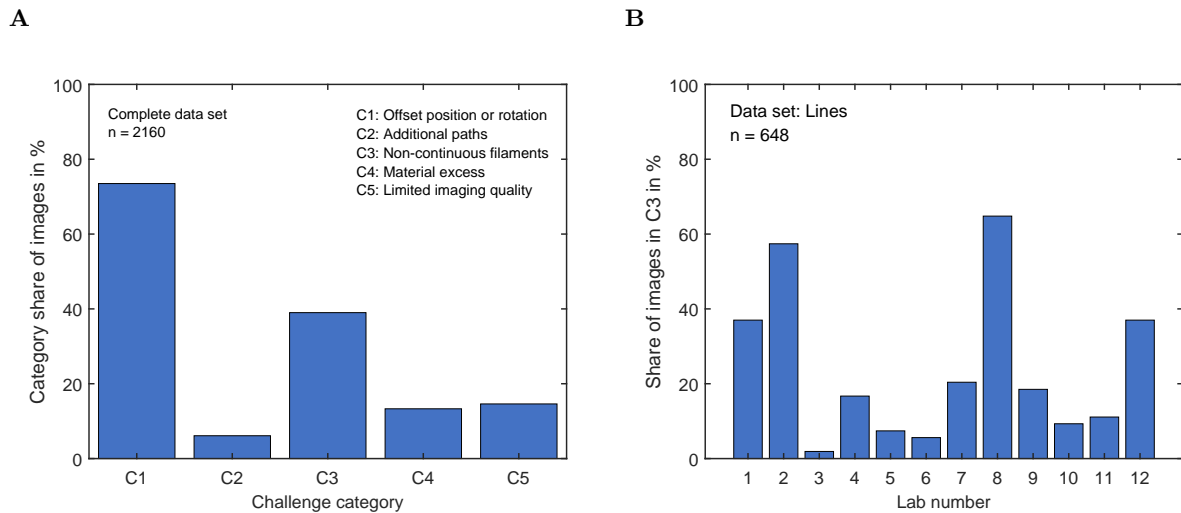


Figure 7.4 Deviations of the images from the specifications taken in the round robin test. The deviations presented in the images were divided into challenge categories. Single images could be qualify for more than one challenge category. The respective share of the total image data set is shown in A) ($n = 2160$). In B), the subset of images of printed line geometries that were classified as category 3 is shown by occurrence in the 12 laboratories ($n = 648$).

C1 with 73.1 % represents rotation and/or shifts from the origin and C2 with 6.1 % the amount of additional paths. C3 with 39 % is the percentage of non-continuous filaments, and C4 with 13.3 % shows the occurrence of material excess. The fifth category - C5 - with 14.6 % includes images of limited image quality.

At first sight, the C1 category seems to be a big issue, however, this issue could be overcome by the development of algorithms that identify ROI by matching the imaged structure to the expected structure and rotate the image as required. Similarly, the matching of the expected geometry with the binarized images enabled the selection of ROIs avoiding additional paths present in images categorized as C2. Remarkably, only a subset of images showed the geometry as it was designed regarding the intended orientation. C5 contained images of limited acquisition quality, which could also be analyzed by the developed workflows as denoising steps. Sensitive thresholding was included. These steps could overcome artifacts such as dust or scratches on the substrate. The deposition of excessive amounts of material leading to fusing of the filaments or random geometries was categorized as C4. The images in this category did not resemble the expected geometries and could therefore not be analyzed. Regarding category C3, non-continuous filaments resembled the intended structure and could therefore be analyzed by the algorithms used. It is noteworthy that even though a sequence of dots can resemble a line, the intended structure was not complete. All in all, this evaluation of the images shows what kind of issues are to be expected in the future and helps with the development of analysis methods to distinguish between the various cases and the

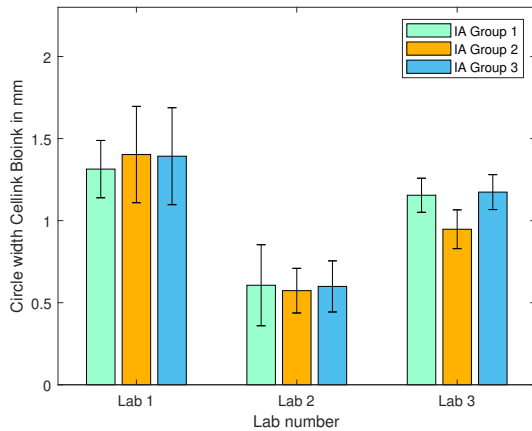
challenges to be reckoned with.

The subset of data of line geometries consisted of 648 images of line geometries, i.e. data sets of 54 images per laboratory. The share of images of printed line geometries showing broken filaments, thus classified as category C3, is presented in Figure 7.4 B). An exemplary image is shown in Figure 7.3 C). What can be clearly seen here is that there is a scatter in the laboratories between 2 to 65 %. Which leads to the conclusion that even a simple structure like a single line or circle could not be printed by any laboratory with 100 % reliability. This indicates that there are still significant challenges to be overcome regarding reliability and reproducibility of bioprinting, before medical applications with high regulatory requirements are intended. Although the entire process was standardized as much as possible, the results differ significantly between the laboratories. This large scatter might be a clear indicator of the results being nevertheless still highly dependent on the operator and printer. However, it was not feasible to determine which of both factors is the main cause of variability. After having conducted the visual qualitative analysis, the main deviations were identified and can be considered to be applied in the future development of analytics. Possible countermeasures for future round robins might be a) further improvement of the SOPs, b) training of the laboratory staff along the SOPs, and c) refinement of the IA procedures towards potential outliers.

7.3.3 Round robin - Image analysis: quantitative

Following printing and data storage, three groups specialized in image analysis developed an image processing workflow to extract the features of the objects without prior knowledge of the categorized deviations. In order to investigate whether the three methods developed by the IA groups might lead to different results, the geometric features of each group extracted per laboratory were compared. For simplification, exemplary results of one analysis parameter, i.e. the circle width (see Figure G.1) printed with Cellink Bioink and with gelatin-based ink for three laboratories, are presented in Figure 7.5.

A Cellink Bioink



B Gelatin-based ink

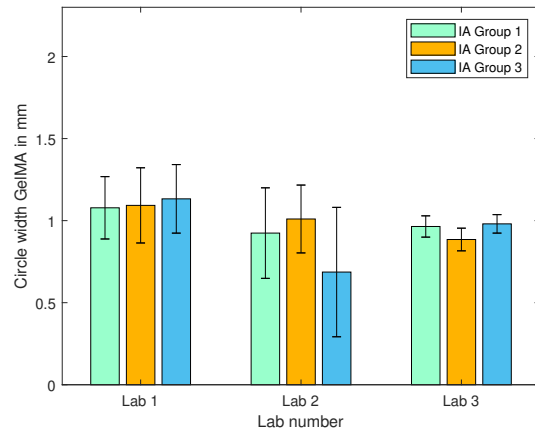


Figure 7.5 Filament width of circle geometries extracted by the three image analysis groups 1-3. In A), the circle width printed with Cellink Bioink, and in B), the circle width printed with gelatin-based ink are depicted with the respective standard deviations. The data of laboratories 1 to 3 are shown as exemplars. Each image analysis groups analyzed every single printed structure by all laboratories ($n = 108$), and the geometric parameters were determined where possible.

In Figure 7.5, the results as regards circle width and variation of the 'strand' when printing a circle and the associated standard deviations printed by three laboratories and extracted by all three IA groups are shown, Cellink Bioink in A) and the gelatin-based ink in B). For Cellink Bioink, the circle width determined by the different IA groups were: a) Lab 1 1.4 mm, b) Lab 2 0.6 mm, c) Lab 3 1.1 mm. Comparing single laboratories, the results extracted by the IA groups are in the same range. The largest difference of extracted data was observed for Lab 3 ranging from a circle width of (0.95 ± 0.10) mm, to a circle width of (1.17 ± 0.10) mm. The extracted measurements regarding filament width of line and circle structures differed slightly when comparing the data extracted by the different image analysis workflows. The deviations in the metrics might originate from the different methodologies used in the preprocessing of the images, where background noise and artifacts are removed. Similarly, the edges of the printed structures were not detected in an equal manner by all IA groups. The extraction of data was thus affected. As mentioned above, the acquired images showed issues such as weak contrast between ink and background. These issues regarding image quality also influence the extraction capability of automated image processing. Future studies should include the assessment of performance of automated image analysis including a comparison of images by determination of the Jaccard index or the Sorensen-Dice coefficient. These parameters enable quantification of the similarity between the analyzed image and the ground-truth presented as the desired geometry. This might not be an easy task, as the designed geometry is transferred as STL file between locations. The geometry to be printed is sliced by each printer software in different manner. Especially for more complex structures, this could lead to differences in the printing path and therefore in the produced geometry. It must be noted, that the image processing groups were not included in the development of the imaging setup. This can be improved in future studies. Nevertheless, all three independently developed methods delivered results in similar ranges which in turn emphasizes the suitability and robustness of automated image processing as an evaluation tool.

Here, the focus was initially placed on single-layer objects, since the first layer is crucial because all other layers are applied on top of it. Automated image processing should also be applied to three-dimensional structures in future studies.

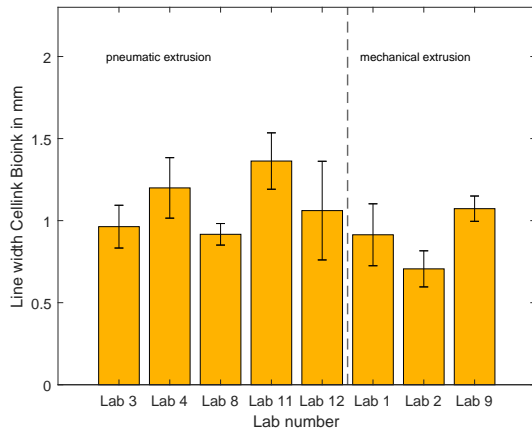
In the following, for a quantitative analysis of printed structures and the assessment of the reproducibility of printing processes, only a subset of data is presented. Several hypotheses were tested and only data of qualified laboratories were selected. Any variations in mean and standard deviations of the geometric features account for the effects proceeding from the printing process or the used ink. The exemplary data is presented in three case studies comparing extrusion mechanism, coordinate calibration, and temperature control of the printing equipment used (Chapters 7.3.4.1-7.3.4.3). Additionally, the selection of inks was also limited to Cellink Bioink and gelatin-based ink, since these differ most in terms of appearance. Furthermore, the gelatin-based ink shows a thermo-sensitive property due to the sol-gel transition of the protein solution [54].

7.3.4 Assessment of the reproducibility in 3D bioprinting

7.3.4.1 Case study 1: pneumatic vs. mechanical extrusion

In the design of the round robin test and the conception of SOPs, the utmost possible standardization was used. The printers represented the parameter with the greatest leeway, since not all laboratories had the same models available. Thus, factors influencing the reproducibility of 3D bioprinting in different laboratories were examined by grouping the data from different laboratories that presented similarities in terms of the function of the used printing equipment. A first aspect to be examined was the extrusion mechanism of the used equipment. Therefore, data sets of laboratories using the same device model were compared with those of laboratories that used custom models. The Cellink BioX printer is equipped with pneumatic powered printheads. Lab 3, Lab 4, Lab 8, Lab 11, and Lab 12 set the pneumatic pressure to 23 kPa, 25 kPa, 20 kPa, 23 kPa, and 20 kPa, respectively. In contrast, all three custom models used piston-driven extrusion using the velocity of axial movement of the piston as a printing setting. In Figure 7.6, the line and circle structures were selected and quantified in terms of filament width.

A Line width



B Circle width

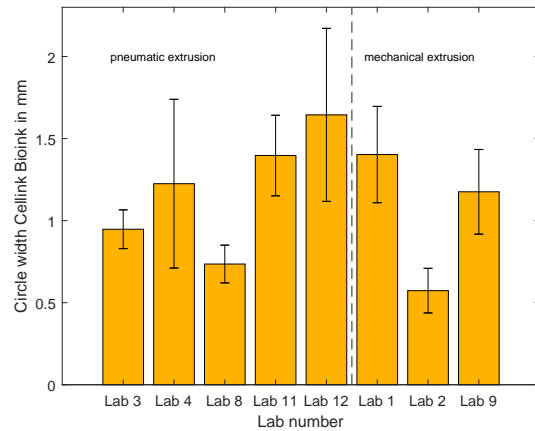


Figure 7.6 Filament width of geometries printed with Cellink Bioink. In A), the mean line width, and in B), the mean circle width are presented. The laboratories are classified according to the extrusion mechanism of the used printers. On the left side of each diagram, data is shown from laboratories using pneumatically driven printers. On the right side, data is presented from laboratories using custom-made printers based on the movement of a piston.

Table 7.3 Summary of the coefficients of variation (CV) for each laboratory regarding the examination of the effects of the extrusion mechanism on the filament width.

Lab	Pneumatic extrusion					Mechanical extrusion		
	3	4	8	11	12	1	2	9
	Line width Cellink Bioink							
CV in %	13.5	15.4	7.2	12.6	28.3	20.7	15.6	7.2
	Circle width Cellink Bioink							
CV in %	12.5	42.0	15.6	17.6	32.1	20.9	23.7	21.9

The widths of the lines and circles printed with Cellink Bioink are presented in Figure 7.6 A) and B), respectively. The printed lines by the laboratories using the pneumatically driven mechanism showed a width in the range of 0.96 to 1.36 mm with standard deviations between 0.07 mm and 0.3 mm. The line widths extracted from geometries printed with the mechanical extrusion systems were in the range of 0.71 to 1.07 mm, and the associated standard deviations showed values varying from 0.08 to 0.19 mm. The widths of printed circles by the group of laboratories using pneumatic extrusion had a minimal mean value of 0.74 mm achieved by Lab 8 with a standard deviation of 0.12 mm. The maximum mean circle width and standard deviation were produced by Lab 12 with values of 1.64 mm and 0.53 mm, respectively. The circle width extracted from the samples printed with the piston-driven devices presented mean values between 0.57 mm and 1.4 mm. The related standard deviations are within the range of 0.14 to 0.29 mm. The effect of the extrusion mechanism was compared by calculation of the CV, and the values are provided in Table 7.3. The CVs of the pneumatically driven process are in a wide range between 7.2 to 42.0%. In contrast, the CVs of the mechanical piston printers are within a clearly narrower range from 7.2 to 23.7%. The filament width should be independent of the trajectory of the printhead, as long as the printing

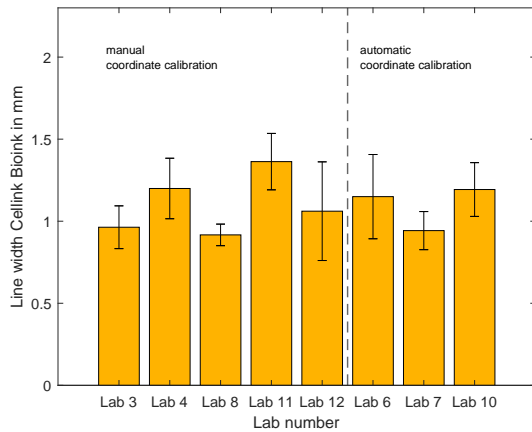
velocity is the same. Therefore, low variability should be the case in the comparison between line and circle width. The higher variabilities of the widths of lines and circles printed with all five pneumatically driven systems was shown although the same experimental setup was used using pressures within the range of 20 to 25 kPa. All five bioprinters are the same model, windows of printing parameters were the same in all laboratories, and the labware used was provided centrally by the organizing laboratory. Additionally, the ink was acquired centrally from a single batch and distributed to the participating laboratories. It is noteworthy that the biomaterial is delivered in a filled cartridge ready to use. The high inter- and intralaboratory variability of the printed structures might be related to the function of the device where the extrusion pressure is supplied by a compact, built-in compressor that might not be able to hold the set pressure over the whole processing time. Furthermore, the tubes connecting the air supply with the cartridge are loose in the housing and, depending on the tube length, might get squeezed depending on the position of the printhead in relation to the housing. Additionally, several laboratories reported occasional clogging of the nozzles when using this ink. Such deficiency can occur when the material is not homogeneously mixed, leading to an aggregation of the nanocellulose used as a thickener. Similar issues regarding heterogeneities of bioinks and the effect on printing have been shown by Chung *et al.* [252]. Regarding the mean values of the filament width produced in the laboratories, the difference can be explained by the round robin setup and the functionality of the printers. The organizing laboratory set a minimum and maximum target filament width with additional information as to which pressure values were necessary to produce these strand widths with a representative printer during the test design. As the mechanical extrusion printers used in the round robin test were custom-manufactured devices, the respective laboratories had to determine the printer parameters necessary to reach the target filament width individually with regard to the individual printer. The lower variability in the data produced by the single laboratories could be explained by the extrusion mechanism where the piston displacement pushes the ink out of the cartridge. In contrast to pneumatic extrusion, material heterogeneities do not affect the ink flow as this is defined by the chosen speed of the displacement of the piston. The presented data in this comparison demonstrated the influence of the extrusion mechanism leading to non-reproducible printing processes, and showed the advantages of piston-operated extrusions systems used in the field of bioprinting. Alternatively, further methods to increase the reproducibility of pneumatic extrusion have been presented by Armstrong *et al.* [284] and by Wenger *et al.* [253]. Both studies involve the process monitoring and adaptation of the pneumatic pressure. The first method uses a laser scanner to measure the deposited filament width and corrects the printing parameter to reach a certain width. The latter monitors the flow rate and corrects the pneumatic pressure to overcome fluctuations. A further aspect of printing systems that can highly influence the printed geometry is the calibration of coordinates, i.e. the distance between the tip of the nozzle and the surface of the used substrate used.

7.3.4.2 Case study 2: coordinate calibration

In terms of the investigation of the effect of coordinate calibration on the reproducibility of bioprinting, the five laboratories operating with the same printer were grouped again. This model requires the operator to set the z-height manually. A second group of laboratories was considered for comparison, these used printing systems equipped with optical sensors for determination of the coordinates of the nozzle tip, i.e. the process was automated. In Figure 7.7, the results of line width

A), and circle width B) are shown, both structures were printed with Cellink Bioink. The CV was also calculated for each laboratory and is given in Table 7.4.

A Line width



B Circle width

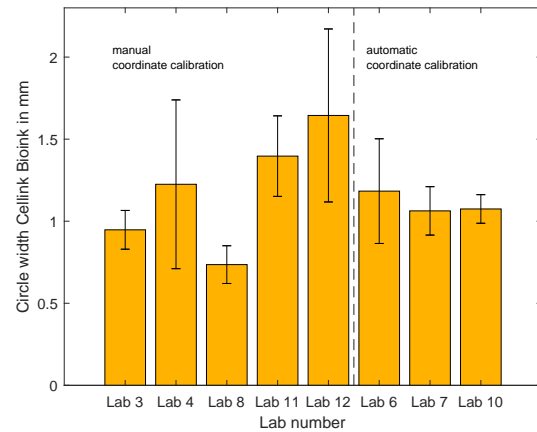


Figure 7.7 Filament width of geometries printed with Cellink Bioink. In A), the mean line width, and in B), the mean circle width are presented. The laboratories are classified according to the mechanism used for coordinate calibration. On the left side of each diagram, data is shown from laboratories using a printer where the position of the tip of the nozzle is calibrated manually by the operator. On the right side, the process of coordinate calibration is performed automatically using an optical sensor.

Table 7.4 Summary of the coefficients of variation (CV) for each laboratory regarding the examination of the effects of the method used for coordinate calibration on the filament width.

Lab	Pneumatic extrusion					Mechanical extrusion		
	3	4	8	11	12	1	2	9
	Line width Cellink Bioink							
CV in %	13.5	15.4	7.2	12.6	28.3	20.7	15.6	7.2
	Circle width Cellink Bioink							
CV in %	12.5	42.0	15.6	17.6	32.1	20.9	23.7	21.9

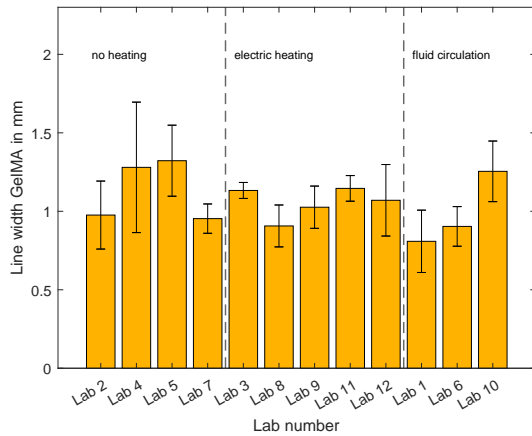
The range of the mean line width printed after manual calibration of the coordinates was 0.92 to 1.36 mm, and the line width range for the automated setting of coordinates was 0.94 to 1.19 mm. In terms of standard deviation, the highest value was 0.3 mm, shown by the data from equipment where manual coordination calibration was performed, and was generally in the range of 0.07 to 0.3 mm. For the printers equipped with automated coordinate calibration features, the standard deviation with a value of 0.26 mm was the highest. Deviations from the mean were in a lower range with 0.12 to 0.26 mm compared to the group of printers with manual calibration procedures. Regarding the data from circle mean width, the range is even larger with a range of 0.74 to 1.64 mm for the data produced with the manually calibrated printers. A smaller range was detected for automatic calibration with a range of 1.06 to 1.18 mm. Similarly to the mean width of the printed circle, the standard deviation increases as well for the first group, i.e. printers required to be manually calibrated regarding the z-height. The values of the standard deviation were in the range of 0.12

to 0.53 mm. The standard deviation of the circle width produced by the printers of the second group was in the range of 0.09 to 0.32 mm. The CVs of the line width printed with Cellink Bioink using manually calibrated printers showed a maximum value of 28.3%. The maximum value of the CVs was lower in the group of automated calibration printers with 22.3%. The difference between CVs was larger when circle geometries were printed. The first group and second group showed CVs up to 42.0% and 27%, respectively. Overall, the results regarding filament width and CVs are an indication of the fact that the operator-dependent calibration step introduces variations into the printing process as the distance between surface of the substrate and nozzle tip cannot be manually set to a standard value. The effect of varying distance between the tip of the nozzle and the surface of the substrate on the filament width has been shown by Naghieh *et al.* [256]. Therefore, the automation of the coordinate calibration enhances the robustness of the printing process. In the first and second case studies, Cellink Bioink was used. This ink shows viscoelastic properties such as shear-thinning, as reported in literature [197, 285]. A more complex rheological behavior is presented by the gelatin-based ink which was used as a third case study. The protein solution undergoes gelation under physiological temperatures [54, 230], and, therefore, the printing process using gelatin-based ink is challenged by the ability of the printer to heat and control the temperature at the cartridge.

7.3.4.3 Case study 3: temperature control

To examine the impact of the different printer configurations influencing the reproducibility of printed geometries with gelatin-based ink, the laboratories were grouped according to the types of temperature control of the respective printers. The extracted data is shown in Figure 7.8, where the line width is shown again in A), and the circle width in B) from the different laboratories. The four bioprinters on the left side have no cartridge temperature control, the five in the middle have an electric heating, and the three bioprinters on the right side are equipped with a fluid circulation heating, where the fluid temperature is set externally. In Lab 3, Lab 9, Lab 12, Lab 1, Lab 6, Lab 10 a temperature of 23 °C, 23.5 °C, 23 °C, 21 °C, 24 °C, and 22.5 °C was used respectively. Two laboratories increased the temperature during the experiments. Lab 8 performed the experiments in a range of 23 °C to 26 °C and Lab 11 in a range of 21 °C to 25 °C. The respective CVs are given in Table 7.5.

A Line width



B Circle width

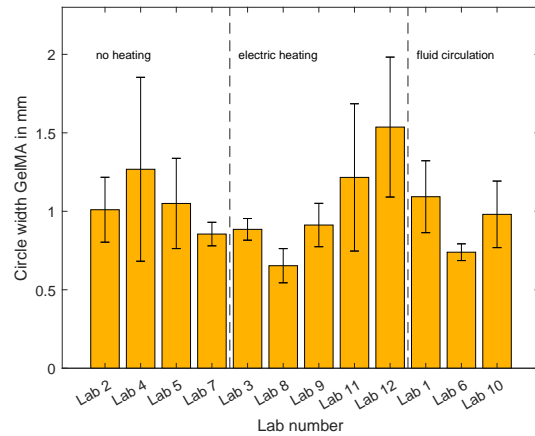


Figure 7.8 Filament width of geometries printed with gelatin-based ink. In A), the mean line width, and in B), the mean circle width are presented. The laboratories are classified according to the mechanism used for temperature control. On the left side of each diagram, data is shown from laboratories using equipment without heating elements. In the middle, data is shown from the devices equipped with electric heating in the cartridge holder. On the right side, the temperature control uses fluid circulation and an external setting of the fluid temperature.

Table 7.5 Summary of the coefficients of variation (CV) for each laboratory regarding the examination of the effects of the mechanism for temperature control on the filament width.

Lab	No heating				Electric heating					Fluid circulation		
	2	4	5	7	3	8	9	11	12	1	6	10
Line width gelatin-based ink												
CV in %	22.2	32.5	17.1	9.8	4.5	14.7	13.1	7.1	21.3	24.6	14.0	15.4
Circle width gelatin-based ink												
CV in %	20.5	46.2	27.4	8.8	7.8	16.7	15.1	38.6	29.0	21.0	7.2	21.6

The results of the mean line width of the group with no temperature control showed values in the range from 0.95 to 1.32 mm and standard deviations in a range of 0.09 to 0.42 mm. In the second group of printers, i.e. devices equipped with electric heating, the mean line widths were in the range of 0.91 to 1.15 mm with standard deviations in the range of 0.05 to 0.23 mm. The mean widths of lines printed with equipment where the temperature is controlled by fluid circulation were in the range of 0.86 to 1.27 mm with standard deviations between 0.07 mm and 0.59 mm. The results of mean circle width are in the range of 0.89 to 1.54 mm with standard deviations between 0.08 to 0.59 mm without heating, in the range of 0.65 to 1.54 mm with standard deviations between 0.07 to 0.47 mm for electric heating, and in the range of 0.74 to 1.09 mm with standard deviations between 0.05 to 0.23 mm for fluid circulation. The variability of the intralaboratory comparison is reflected in the respective coefficients of variation. The highest variability was observed in the samples produced by the group of laboratories using printers without the capability of heating the cartridge during the process, where the CVs show values in the range of 9.8 to 32.5 % regarding the line geometry, and the variability according to the CVs increased to 8.8 to 46.2 % regarding the circle geometry. The same trend was observed in the group of printers with electric heating elements. The CVs of the

printed line structures are in the range of 4.5 to 21.3%, and in the range of 7.8 to 38.6% regarding printed circles. The variability of the width of printed geometries produced with printers with temperature control over fluid circulation was lower both for lines and circles where the calculated CVs were 14.0 to 24.6%, and 7.2 to 21.6%, respectively. As solutions containing gelatin and gelatin derivatives undergo a sol-gel transition around physiological temperatures [54], the heating of the cartridge containing bioinks is essential. Without the control of temperature, the gelatin-based ink undergoes a transition into a gel state where the viscosity increases during processing time. This process has been shown to be time-dependent and to be affected by the temperature difference between solution and environment [286, 287]. A further challenge regarding the use of gelatin-based inks is the possible clogging of nozzles which is mentioned in further bioprinting studies [288, 289]. The SOPs indicated that the printing parameters should be kept constant during a printing session, i.e. printing of six technical replicates. However, it was mentioned as well that it is possible to increase the pneumatic pressure as a measure to counteract the gelation of the gelatin-based ink. The low variability of the structures, both lines and circles, produced by Lab 7 without heating can be explained by the fact that the pressure was adjusted, i.e. increased, during the printing process. In contrast, Lab 5 increased the pneumatic pressure during printing as well, which did not improve the variability of printed geometries. A second possibility to counteract gelation of the gelatin-based ink was the possibility to increase the temperature of the cartridge holder. This measure was taken by Lab 8 and Lab 11. Both groups used printers equipped with electric heating. While the CV of printed lines and circles by Lab 8 stayed in the same range, the CVs of printed lines and circles by Lab 11 differed notably. This shows the important effect of the individual operators on the printing process and printed geometries. Laboratories using printers of the third group, i.e. where the temperature is regulated over fluid circulation, completed the experimental series without the adjustment of printing parameters, both pneumatic pressure and printing temperature. Over the external setting of fluid temperature, the cooling of the cartridge is possible in contrast to the electric elements that are only able to heat the cartridge. It is noteworthy that the lowest variability was shown by the results by Lab 3. Overall, it can be stated that individual operators, and the different equipment of the printer affect the results and, thus, limit the comparability of the provided data. In order to provide robust printing processes, there is still a need for process control and higher degrees of automation in the printing equipment.

7.4 Conclusion

The presented study highlights the successful collaboration of 15 groups nationwide with the shared goal of analyzing reproducibility and introducing standards to the bioprinting field in order to accelerate the transition from laboratory practice to production for clinical applications. For this round robin study, SOPs were written containing information about material preparation, use of labware, and experimental printing setup. Materials were acquired and distributed centrally by the organizing laboratory. Identical imaging conditions were provided by use of the BioFI prototype instrument and the data was centrally managed in the Kadi4Mat platform. During the evaluation process, a distinction was made between a qualitative and a quantitative image analysis. In the qualitative investigation, it was shown that several deviations in the printing and imaging processes occur. This study provides an up-to-date overview of possible deviations and helps to analyze where the process needs to be enhanced. An important outcome was that the individual operators still have a significant impact on the resulting structure. Similarly, the recognition of

possible factors diminishing the reproducibility of the process after imaging can be differentiated and included in the development of automated image analysis. These issues were not considered by the three IA groups because the analysis was performed simultaneously and independently. Three different methods obtained results in the similar range regarding geometric features of the printed samples. This proved that automated IA is a suitable tool for the assessment of printing process reproducibility and quantitative comparability in the bioprinting field is by far not achieved, yet, due to lack in standardization in terms of bioprinting equipment. Hereby, devices equipped with pistons for mechanical extrusion, automated calibration of coordinates, especially z-height, and temperature-controlled printheads proved to be advantageous. Although target line widths were used in this study as a method for device-independent transfer, the product equivalency between locations could not be shown. In the future development of bioprinters, the above-mentioned problems need to be addressed. Ultimately, different cell types must be included in the process and the effects of cellular material on the reproducibility need to be characterized. Thereby, a significant effect is expected. The production of bioprinted structures might face requirements imposed by regulatory agencies when trying to make the leap into clinical stages. These agencies require information on the range of operating conditions that will result in the products and materials meeting certain quality criteria. This preliminary round robin test identified significant present challenges to be overcome in order to provide robust bioprinting processes. Furthermore, a nationwide infrastructure and network is now established, which can be used for material evaluation and evaluation of standards in the field of bioprinting.

Conflict of interest

The authors declare that the research was conducted in the absence of any commercial or financial relationships that could be construed as a potential conflict of interest.

Author contributions

Conceptualization: D G, S S, S G, B S, and J H; Data curation—metadata production: D G, S S, S G, B S, T J, J G, L M, I S, H H, K S L, S Z, P K, S Sc, A W, A S, G E M T, T A, M G, T S, R D, A R B, T N, C L T, C W, and T G; Data curation—interpretation of research data : D G, S S, S G, and B S; Formal analysis: D G, and S S; Funding acquisition: J H; Investigation— performance of experiments: D G, S S, S G, B S, T J, J G, L M, I S, H H, K S L, S Z, P K, S Sc, A W, A S, G E M T, T A, M G, T S, R D, A R B, T N, C L T, C W, and T G; Methodology—experimental design: D G, S S, S G and B S; Methodology—material development: T J, J G, S Z, P K, A W, S Sc, T A, and M G; Project administration: J H; Resources: J H; Software: D G, S S, N B, M S, S A, B K, T F, H B, J B, A V G, and D P; Supervision: J H; Validation: D G, and S S; Visualization: D G, and S S; Writing—original draft: D G, and S S; Writing—review & editing: S G, B S, T J, J G, L M, I S, H H, K S L, N B, M S, S Z, P K, A S, G E M T, S Sc, A W, T A, M G, T S, R D, A R B, T N, C L T, C W, T G, S A, B K, T F, H B, J B, D P, A V G, and J H.

All authors have read and agreed to the published version of the manuscript.

Funding

The organizing laboratory, Institute of Functional Interfaces of the Karlsruhe Institute of Technology received funding from the Federal Ministry of Education and Research (BMBF) as project SOP_Bioprint under contract number 13XP5071B for the Round robin - 3D printing and Round robin - image analysis tests.

The development of the Bioprinting Fidelity Imager (BioFI) imaging system by the Department of Microsystems Engineering of the University of Freiburg, Germany, and Hahn-Schickard-Gesellschaft für angewandte Forschung e.V. was supported by the Federal Ministry of Education and Research (BMBF) under the contract numbers 02P20E020 and 02P20E021.

Acknowledgments

The authors wish to express their thanks for the support the following scientists of the institutions mentioned above for the collaboration during the experimental and analysis part in this study: Nico Brandt, Ellena Fuhrmann, Markus Germann, Fritz Koch, Lukas Kornelius, Annika Lechner, Klaus-Martin Reichert, and Matthias Ruopp. We acknowledge support by the KIT-Publication Fund of the Karlsruhe Institute of Technology.

Data availability statement

The data cannot be made publicly available upon publication because no suitable repository exists for hosting data in this field of study. The data that support the findings of this study are available upon reasonable request from the authors.

Chapter references

- [3] J. Malda *et al.*, „25th anniversary article: Engineering hydrogels for biofabrication“, *Advanced Materials*, vol. 25, no. 36, pp. 5011–5028, 2013.
- [54] K. Y. Lee and D. J. Mooney, „Hydrogels for tissue engineering“, *Chemical Reviews*, vol. 101, no. 7, pp. 1869–1879, 2001.
- [59] J. Groll *et al.*, „A definition of bioinks and their distinction from biomaterial inks“, *Biofabrication*, vol. 11, no. 1, 2019.
- [137] K. Markstedt, A. Mantas, I. Tournier, H. Martínez Ávila, D. Hägg, and P. Gatenholm, „3D bioprinting human chondrocytes with nanocellulose-alginate bioink for cartilage tissue engineering applications“, *Biomacromolecules*, vol. 16, no. 5, pp. 1489–1496, 2015.
- [167] S. Seiffert and J. Sprakel, „Physical chemistry of supramolecular polymer networks“, *Chemical Society Reviews*, vol. 41, no. 2, pp. 909–930, 2012.
- [188] S. V. Murphy and A. Atala, „3D bioprinting of tissues and organs“, *Nature biotechnology*, vol. 32, no. 8, pp. 773–785, 2014.
- [193] M. Hospodiuk, M. Dey, D. Sosnoski, and I. T. Ozbolat, „The bioink: A comprehensive review on bioprintable materials“, *Biotechnology Advances*, vol. 35, no. 2, pp. 217–239, 2017.
- [197] K. Hölzl, S. Lin, L. Tytgat, S. Van Vlierberghe, L. Gu, and A. Ovsianikov, „Bioink properties before, during and after 3D bioprinting“, *Biofabrication*, vol. 8, no. 3, pp. 1–19, 2016.
- [199] A. Ribeiro *et al.*, „Assessing bioink shape fidelity to aid material development in 3D bioprinting“, *Biofabrication*, vol. 10, no. 1, 2018.
- [230] W. Liu *et al.*, „Extrusion Bioprinting of Shear-Thinning Gelatin Methacryloyl Bioinks“, *Advanced Healthcare Materials*, vol. 6, no. 12, pp. 1–11, 2017.
- [235] B. H. Lee, N. Lum, L. Y. Seow, P. Q. Lim, and L. P. Tan, „Synthesis and characterization of types A and B gelatin methacryloyl for bioink applications“, *Materials*, vol. 9, no. 10, pp. 1–13, 2016.
- [237] T. Gao *et al.*, „Optimization of gelatin-alginate composite bioink printability using rheological parameters: A systematic approach“, *Biofabrication*, vol. 10, no. 3, 2018.
- [239] M. Uzun-Per *et al.*, „Automated Image Analysis Methodologies to Compute Bioink Printability“, *Advanced Engineering Materials*, vol. 2000900, pp. 1–12, 2020.
- [240] A. A. Aldana, F. Valente, R. Dilley, and B. Doyle, „Development of 3D bioprinted GelMA-alginate hydrogels with tunable mechanical properties“, *Bioprinting*, vol. 21, no. June 2020, e00105, 2021.
- [244] W. Schuurman *et al.*, „Gelatin-Methacrylamide Hydrogels as Potential Biomaterials for Fabrication of Tissue-Engineered Cartilage Constructs“, *Macromolecular Bioscience*, vol. 13, no. 5, pp. 551–561, 2013.
- [252] J. H. Chung *et al.*, „Bio-ink properties and printability for extrusion printing living cells“, *Biomaterials Science*, vol. 1, no. 7, pp. 763–773, 2013.
- [253] L. Wenger, S. Strauß, and J. Hubbuch, „Bioprinting Automated and dynamic extrusion pressure adjustment based on real-time flow rate measurements for precise ink dispensing in 3D bioprinting“, *Bioprinting*, vol. 28, no. July, pp. 1–14, 2022.
- [255] Y. He, F. Yang, H. Zhao, Q. Gao, B. Xia, and J. Fu, „Research on the printability of hydrogels in 3D bioprinting“, *Scientific Reports*, vol. 6, pp. 1–13, 2016.
- [256] S. Naghieh, M. Sarker, N. K. Sharma, Z. Barhoumi, and X. Chen, „Printability of 3D Printed Hydrogel Scaffolds: Influence of Hydrogel Composition and Printing Parameters“, *Applied Sciences*, vol. 10, no. 1, p. 292, 2019.
- [260] J. Marzi *et al.*, „Non-Invasive Three-Dimensional Cell Analysis in Bioinks by Raman Imaging“, *ACS Applied Materials & Interfaces*, vol. 14, no. 27, pp. 30 455–30 465, 2022.
- [263] W. Sun *et al.*, „The bioprinting roadmap“, *Biofabrication*, vol. 12, no. 2, 2020.
- [264] K. Tröndle *et al.*, „Scalable fabrication of renal spheroids and nephron-like tubules by bioprinting and controlled self-assembly of epithelial cells“, *Biofabrication*, vol. 13, no. 3, 2021.
- [265] B. Schmiege *et al.*, „Structured Data Storage for Data-Driven Process Optimisation in Bioprinting“, *Applied Sciences*, 2022.
- [266] P. Bartolo, A. Malshe, E. Ferraris, and B. Koc, „3D bioprinting: Materials, processes, and applications“, *CIRP Annals*, vol. 71, no. 2, pp. 577–597, 2022.
- [267] J. Chrenek, R. Kirsch, K. Scheck, and S. M. Willerth, „Protocol for printing 3D neural tissues using the BIO X equipped with a pneumatic printhead“, *STAR Protocols*, vol. 3, no. 2, p. 101 348, 2022.
- [268] S. Strauß, D. Grijalva Garces, and J. Hubbuch, „Analytics in Extrusion-Based Bioprinting: Standardized Methods Improving Quantification and Comparability of the Performance of Bioinks“, *Polymers*, vol. 15, no. 8, p. 1829, 2023.

- [269] F. P. Melchels, W. J. Dhert, D. W. Hutmacher, and J. Malda, „Development and characterisation of a new bioink for additive tissue manufacturing“, *Journal of Materials Chemistry B*, vol. 2, no. 16, pp. 2282–2289, 2014.
- [270] L. Ouyang, R. Yao, Y. Zhao, and W. Sun, „Effect of bioink properties on printability and cell viability for 3D bioplotting of embryonic stem cells“, *Biofabrication*, vol. 8, no. 3, p. 035 020, 2016.
- [271] E. Karakaya, L. Fischer, J. Hazur, A. R. Boccaccini, I. Thievensen, and R. Detsch, „Strategies to evaluate alginate based bioinks applying extrusion printing for biofabrication“, *Transactions on Additive Manufacturing Meets Medicine*, vol. 2, no. 1, pp. 1–2, 2020.
- [272] J. M. Rodríguez-Rego, L. Mendoza-Cerezo, A. Macías-García, J. P. Carrasco-Amador, and A. C. Marcos-Romero, „Methodology for characterizing the printability of hydrogels“, *International Journal of Bioprinting*, vol. 9, no. 2, pp. 280–291, 2023.
- [273] A. Schwab, R. Levato, M. D’Este, S. Piluso, D. Eglin, and J. Malda, „Printability and Shape Fidelity of Bioinks in 3D Bioprinting“, *Chemical Reviews*, vol. 120, no. 19, pp. 11 028–11 055, 2020.
- [274] T. Kreller, T. Distler, S. Heid, S. Gerth, R. Detsch, and A. Boccaccini, „Physico-chemical modification of gelatine for the improvement of 3D printability of oxidized alginate-gelatine hydrogels towards cartilage tissue engineering“, *Materials & Design*, vol. 208, p. 109 877, 2021.
- [275] V. Bednarzig, S. Schrüfer, T. C. Schneider, D. W. Schubert, R. Detsch, and A. R. Boccaccini, „Improved 3D Printing and Cell Biology Characterization of Inorganic-Filler Containing Alginate-Based Composites for Bone Regeneration: Particle Shape and Effective Surface Area Are the Dominant Factors for Printing Performance“, *International Journal of Molecular Sciences*, vol. 23, no. 9, p. 4750, 2022.
- [276] E. Karakaya *et al.*, „How to Determine a Suitable Alginate for Biofabrication Approaches using an Extensive Alginate Library?“, *Biomacromolecules*, 2023.
- [277] A. Wenz, K. Borchers, G. E. Tovar, and P. J. Kluger, „Bone matrix production in hydroxyapatite-modified hydrogels suitable for bone bioprinting“, *Biofabrication*, vol. 9, no. 4, 2017.
- [278] N. Brandt *et al.*, „Kadi4Mat: A Research Data Infrastructure for Materials Science“, *Data Science Journal*, vol. 20, no. 1, pp. 1–14, 2021.
- [279] S. van der Walt *et al.*, „scikit-image: image processing in Python“, *PeerJ*, vol. 2, no. 1, e453, 2014.
- [280] K. He, J. Sun, and X. Tang, „Guided image filtering“, *IEEE Transactions on Pattern Analysis and Machine Intelligence*, vol. 35, no. 6, pp. 1397–1409, 2013.
- [281] P. F. Alcantarilla, A. Bartoli, and A. J. Davison, „KAZE Features“, in *Computer Vision – ECCV 2012*, Berlin, Heidelberg: Springer Berlin Heidelberg, 2012, pp. 214–227.
- [282] A. F. Frangi, W. J. Niessen, K. L. Vincken, and M. A. Viergever, „Multiscale vessel enhancement filtering“, in *Medical Image Computing and Computer-Assisted Intervention — MICCAI’98*, Berlin, Heidelberg: Springer Berlin Heidelberg, 1998, pp. 130–137.
- [283] Y. Tsin and T. Kanade, „A Correlation-Based Approach to Robust Point Set Registration“, in *Computer Vision - ECCV 2004*, Berlin, Heidelberg: Springer Berlin Heidelberg, 2004, pp. 558–569.
- [284] A. A. Armstrong, A. G. Alleyne, and A. J. Wagoner Johnson, „1D and 2D error assessment and correction for extrusion-based bioprinting using process sensing and control strategies“, *Biofabrication*, vol. 12, no. 4, 2020.
- [285] M. Kesti, P. Fisch, M. Pensalfini, E. Mazza, and M. Zenobi-Wong, „Guidelines for standardization of bioprinting: A systematic study of process parameters and their effect on bioprinted structures“, *BioNanoMaterials*, vol. 17, no. 3-4, pp. 193–204, 2016.
- [286] M. Djabourov, J. Leblond, and P. Papon, „Gelation of aqueous gelatin solutions. I. Structural investigation“, *Journal de Physique*, vol. 49, no. 2, pp. 319–332, 1988.
- [287] Y. Maki and M. Annaka, „Gelation of fish gelatin studied by multi-particle tracking method“, *Food Hydrocolloids*, vol. 101, no. October 2019, p. 105 525, 2020.
- [288] E. Hoch, T. Hirth, G. E. Tovar, and K. Borchers, „Chemical tailoring of gelatin to adjust its chemical and physical properties for functional bioprinting“, *Journal of Materials Chemistry B*, vol. 1, no. 41, pp. 5675–5685, 2013.
- [289] I. Pepelanova, K. Kruppa, T. Scheper, and A. Lavrentieva, „Gelatin-Methacryloyl (GelMA) Hydrogels with Defined Degree of Functionalization as a Versatile Toolkit for 3D Cell Culture and Extrusion Bioprinting“, *Bioengineering*, vol. 5, no. 3, p. 55, 2018.

Conclusion

Within the scope of this doctoral thesis, it was the goal to develop standardized process strategies and analytical methodologies to enable a safe, effective, and large-scale manufacturing process of customized artificial tissues for medical applications. Two major factors are already identified in literature, but no comprehensive strategy to counteract is established:

a): One is the lack of standardized bioink evaluation methods which facilitate the comparison and consequently the development of bioinks. Concerning the development of bioinks, specific formulations for each type of tissue are to be designed with proper rheological properties allowing for high printing accuracy and a biocompatibility that allows for high cell viability, proliferation and supply with nutrients. As a result, there is a wide range of bioinks, some of which have very different chemical and physical properties. As a consequence, there is a need for an automated bioink printing accuracy method which can be used for the wide range of bioinks. Image analysis was established successfully to cope with this challenge.

b): The other major factor is the control of the bioprinting process itself. 3D bioprinting is an ideal manufacturing method for personalized medicine as it offers a flexibility in geometrical design. However, production processes must be reliable and reproducible when it comes to patient treatments. Accordingly, suitable process parameters have to be found and controlled to overcome this obstacle.

In the first study (Chapter 3) an image-based analysis method for 3D printed lines and printing accuracy was established. This study served as proof of concept for IA in the bioprinting field. The cell confluency measurement of a plate reader was used as image acquisition device and the images were analyzed afterwards. This methodical approach offers the advantages of being usable for a wide range of bioinks, being non-invasive, and saves images with results permanently. This method can be used for system characterization, bioink printability evaluation and for bioprinting process optimization. The line analysis tool was successfully applied to characterize the length, width and area. In order to make measurements comparable, a new criterion for width determination within a

stable area was introduced. However, the method had a few limitations. Completely transparent materials could not be detected and the imaging process took approximately 2 min. Nonetheless, the method was feasible to detect the lines and to detect the shrinkage behavior of printed lines over time. This method was the basis for a shrinkage study for two commercially available bioinks. A statistically significant shrinkage within 10 min was observed. This needs to be considered by the creation of CAD models and highlights the need for a fast imaging acquisition with regard to quality inspection. In general, image analysis demonstrated to be an effective and reliable analysis methodology for bioinks and can contribute to the field as process development tool.

The second study (Chapter 4) focused on the increase of process robustness and reproducibility as this is of high importance for a safe application of artificial tissues. It was verified whether the flow rate as control parameter is more suitable than the conventional printing parameters. In this work, pneumatic extrusion-based bioprinters were employed. Flow rates generated by these systems are aside from the printing pressure also influenced by the material viscosity, associated therewith, by temperature, nozzle geometry, to name but a few. This is a complex network of parameters which are system related, e.g. cartridge filling level, and environmental related, e.g. temperature fluctuations. However, it is more straightforward to control for the flow rate instead of the commonly used parameters. For a proof of concept, a liquid flow meter based on a thermal principle was integrated into the bioprinter and used as calibration tool. The pressure was adjusted until a set flow rate was reached and it was tested whether this approach is superior to the conventional approach, in which a fixed pressure value is set as printing parameter. This study demonstrated that process performance of the constant flow rate approach increased reproducibility in comparison to the constant pressure approach. The reproducibility was inspected by measuring the scatter of the individual volumes of the 3D printed cylinders for both approaches. Furthermore, the sensor was employed to investigate whether the cartridge filling level has an effect on the extrusion rate. Thus, the flow rate was monitored permanently during the complete emptying of a cartridge in two bioprinter systems. The cartridge filling level turned out to be for both pneumatic systems an important factor affecting material flow.

The third study (Chapter 5) is an advancement of the results of the previous study with the aim to set the flow rate automatically. A software tool was established enabling the automated monitoring and real-time control of a target flow rate. The pressure was used as a control parameter to achieve a target flow. The setup was tested for several materials, namely Kolliphor in a concentration of 25 % (w/w) and 30 % (w/w) and another composition of 2 % (w/w) alginate with 7 % (w/w) Laponite. The sensor was calibrated beforehand for each material. After the completion, the functionality was evaluated in three use cases. In a continuous dispensing experiment, the flow rate was kept constant and even a nozzle clogging could be solved. The adaptation to ink inhomogeneities was tested by filling a cartridge with layers of different Kolliphor concentrations. The set up was able to cope with the transition from one layer to another and adapted each time the pressure. In the last case study, a system transfer was simulated by exchanging the nozzle and here, too, the controller could successfully regulate the pressure so that even cylinders could be printed.

In the fourth study (Chapter 6) standardized methods were developed to compare bioinks performance and the effect of the process on cell viability was investigated. A standardized flow rate

was realized by calculating ink specific extrusion pressures based on the individual flow behavior. Bioinks specific viscosities in dependence on shear rate were determined and fitted according to Ostwald-de Waele relationship. In combination with the Hagen-Poiseuille equation, the necessary pressure for a target flow rate in the respective system could be calculated for individual bioinks. It should be noted that this approach is not dynamically adaptable to bioink inhomogeneities or other changes occurring during the process. It also has to be recalculated for each nozzle geometry, bioink, and each process condition, since, for example, a change in temperature also changes the viscosity. Printing accuracy evaluation was covered by the extended image processing tool box. The hardware was optimized by a new vision system enabling for a fast image acquisition process and a proper illumination setup. The automated and time-saving analysis method was extended with the additional tools for circle and angle structure analysis. In this study, two in house developed bioinks were employed consisting of 3% (w/v) alginate with 3% (w/v) GelMA and 4% (w/v) alginate with 3% (w/v) GelMA. Printing performance was investigated for both polymeric solution with and without cells in order to see whether cells have an impact. All in all, the 1% (w/v) difference in alginate concentration and the bioinks with and without cells were all in a comparable range. To gain a deeper process understanding, the process workflow and its impact on cell viability was investigated. Thus, for three biological replicates cell viability was initially examined after cell harvest, after mixing the cells in both polymeric formulations and immediately after extrusion through the nozzle. Both steps led to a slight decrease in cell viability. However, interestingly, the difference of 1% (w/v) alginate in the starting formulation had a significant impact on cell viability in both process steps. The implementation of the proposed concept provides great capabilities to save time and money by eliminating user-dependent printing parameter screenings and facilitating process transfers.

In the fifth study (Chapter 7), empirical data of extrusion-based bioprinting processes in 12 academic laboratories were collected analyzing how far standardization has progressed and how reproducible same objects can be manufactured. Thus, a round robin test was successfully organized and conducted. For all laboratory steps SOPs were written, labware and materials from same producer batches ordered, an infrastructure was established for data storage and exchange. Each printed sample was documented by a picture captured with a specifically designed imaging system under same illumination conditions. Then, a qualitative and quantitative assessment was performed. In the qualitative analysis, two operators inspected all images visually and investigated what kind of and to what share deviations occurred. It could be concluded that the individual operator still has a significant influence and that the printing process would profit from further automation. In the quantitative analysis, three independent IA groups processed the images and extracted the object metrics. Here, it was shown that the equipment of the printers as well as the operators still have a strong influence on the results and that it is not yet possible to bioprint independently of location and people. Nonetheless and more important, all three imaging groups obtained equivalent results and image processing proved to be again a suitable analysis method. In addition, a nationwide infrastructure and network has now been established that can be used to evaluate materials and assess standards in the field of bioprinting. This can be used in prospective studies for further development of standards in the field of bioprinting.

In summary, this thesis contributes to the field of bioprinting by examining the current standardization and creating awareness of possible deviations. This will help to eliminate these in the future. In three studies in a constant further development of the image acquisition setup, image processing

was proven to be a suitable analysis method for bioprinted objects and printing accuracy evaluation. This in turn will accelerate bioink development, process optimization and system characterization. It was also shown, how the printer design can be increased in robustness. A flow rate as control parameter, automated coordination calibration, and a temperature control of the cartridge are beneficial if not necessary. Increased objectivity and comparability for both will help to accelerate process as well as material development. These are key elements toward making the leap from laboratory experiments to future medical applications.

Outlook

The investigation of standardization revealed that there are still challenges to be overcome. This concerns the definition of terms, defining manufacturing procedures or standardized guidelines and quality assurance methodologies. However, some committees have started to form to answer these questions. One step which would profit from standardization or further research is the mixing step of cells in the hydrogel as well as the filling in cartridges. This poses some challenges for high viscosity materials as often air bubbles are introduced and simultaneously, no high shear stresses should occur and disrupt the cell walls. Some prototypes of static mixer designs are already tested, but are not yet commercially available. During this thesis the common transfer of biomaterial between two syringes was applied, but it has the disadvantage of being highly user-dependent concerning number of forth and back movements and applied force. In order to eliminate an operator's influence, automatization can bring progress. An automated process control meaning to set a target flow rate increases objectivity and comparability. The used set up with the liquid flow meter was relatively large and unfortunately, no other equipment like nozzle heating or cure-on-dispense device could be used simultaneously. Therefore it would be beneficial to have an integrated flow meter and also to test some other measurement principle. The used flow meter was originally developed for liquids and had to be calibrated for each material specifically. The output data were partially very noisy, but a proof of concept was performed for all tested materials successfully. Another option to control the flow rate is to have a closer look on the mechanical principles for extrusion which have been a bit neglected by 3D printing manufacturers due to their more complex configuration. A further possibility is to combine image processing with the process control. It would be conceivable, as is already the case with other pick and place tasks, to use an integrated vision system and analyze the width of the extruded strand and then, if necessary, automatically regulate the pressure in a feedback loop. All in all, a flow rate based process control is promising for eliminating laborious process optimizations. Besides, there is a need for well-equipped and robust bioprinters which are able to generate a reliable flow rate at each position.

The other experimental focus of this thesis was image processing. It could be proven that it is a suitable analysis method. In this thesis, different geometries have been investigated with regard to evaluate the printing performance of bioinks. This might, however, be justified as the first layer is important to be precise to be able to build up a whole object and to evaluate the performance of a bioink. Nonetheless, the third dimension should be included in the future and best image acquisition performed online in the printer and not external. This requires to equip the bioprinter with cameras in suitable angles and with a proper illumination for low contrast materials. An additional open field of high importance is the establishment of cell analytic for 3D applications. The choice of material already has an impact on cell viability as well as functionality and should be considered for future medical application. At present it is only possible to examine the cells using invasive methods, and the method of staining must also be adapted to the matrix structure. The dyes must be able to diffuse through the hydrogel network.

To sum it up, the technical challenges are identified and now respective countermeasures can be taken. Once automated and robust printer designs, SOPs, and trained personnel are available, technical challenges are overcome. At the same time, tissue-specific inks with appropriate cell analysis need to be developed. There is still work to be done, but it is not impossible.

References

- [1] Y. Yu, Q. Wang, C. Wang, and L. Shang, „Living Materials for Regenerative Medicine“, *Engineered Regeneration*, vol. 2, no. August, pp. 96–104, 2021.
- [2] F. Berthiaume, T. J. Maguire, and M. L. Yarmush, „Tissue engineering and regenerative medicine: History, progress, and challenges“, *Annual Review of Chemical and Biomolecular Engineering*, vol. 2, pp. 403–430, 2011.
- [3] J. Malda *et al.*, „25th anniversary article: Engineering hydrogels for biofabrication“, *Advanced Materials*, vol. 25, no. 36, pp. 5011–5028, 2013.
- [4] H. G. Yi, H. Kim, J. Kwon, Y. J. Choi, J. Jang, and D. W. Cho, „Application of 3D bioprinting in the prevention and the therapy for human diseases“, *Signal Transduction and Targeted Therapy*, vol. 6, no. 1, 2021.
- [5] W. Wu, Q. Zheng, X. Guo, J. Sun, and Y. Liu, „A programmed release multi-drug implant fabricated by three-dimensional printing technology for bone tuberculosis therapy“, *Biomedical Materials*, vol. 4, no. 6, 2009.
- [6] D. G. Hwang *et al.*, „A 3D bioprinted hybrid encapsulation system for delivery of human pluripotent stem cell-derived pancreatic islet-like aggregates“, *Biofabrication*, vol. 14, no. 1, 2022.
- [7] S. Panda *et al.*, „A focused review on three-dimensional bioprinting technology for artificial organ fabrication“, *Biomaterials Science*, vol. 10, no. 18, pp. 5054–5080, 2022.
- [8] C. Mota, S. Camarero-Espinosa, M. B. Baker, P. Wieringa, and L. Moroni, „Bioprinting: From Tissue and Organ Development to in Vitro Models“, *Chemical Reviews*, vol. 120, no. 19, pp. 10 547–10 607, 2020.
- [9] S. V. Murphy and A. Atala, „3D bioprinting of tissues and organs“, *Nature Biotechnology*, vol. 32, no. 8, pp. 773–785, 2014.
- [10] S. M. Hull, L. G. Brunel, and S. C. Heilshorn, *3D Bioprinting of Cell-Laden Hydrogels for Improved Biological Functionality*, 2022.
- [11] B. V. Slaughter, S. S. Khurshid, O. Z. Fisher, A. Khademhosseini, and N. A. Peppas, „Hydrogels in regenerative medicine“, *Advanced Materials*, vol. 21, no. 32-33, pp. 3307–3329, 2009.

- [12] M. P. Sekar *et al.*, „Current standards and ethical landscape of engineered tissues—3D bioprinting perspective“, *Journal of Tissue Engineering*, vol. 12, 2021.
- [13] M. Kesti, P. Fisch, M. Pensalfini, E. Mazza, and M. Zenobi-Wong, „Guidelines for standardization of bioprinting: A systematic study of process parameters and their effect on bioprinted structures“, *BioNanoMaterials*, vol. 17, no. 3-4, pp. 193–204, 2016.
- [14] N. Paxton, W. Smolan, T. Böck, F. Melchels, J. Groll, and T. Jungst, „Proposal to assess printability of bioinks for extrusion-based bioprinting and evaluation of rheological properties governing bioprintability“, *Biofabrication*, vol. 9, no. 4, p. 44107, 2017.
- [15] K. F. Freed and S. F. Edwards, „Polymer viscosity in concentrated solutions“, *The Journal of Chemical Physics*, vol. 61, no. 9, pp. 3626–3633, 1974.
- [16] S. S and R. G, „Robot assisted sensing, control and manufacture in automobile industry“, *Journal of ISMAC*, vol. 01, no. 03, pp. 180–187, 2019.
- [17] Y. Tang *et al.*, „Recognition and Localization Methods for Vision-Based Fruit Picking Robots: A Review“, *Frontiers in Plant Science*, vol. 11, no. May, pp. 1–17, 2020.
- [18] S. Mellor, L. Hao, and D. Zhang, „Additive manufacturing: A framework for implementation“, *International Journal of Production Economics*, vol. 149, pp. 194–201, 2014.
- [19] D. Bourell *et al.*, „Materials for additive manufacturing“, *CIRP Annals - Manufacturing Technology*, vol. 66, no. 2, pp. 659–681, 2017.
- [20] M. A., R. K. Y., and K. L., „Improve the accuracy, surface smoothing and material adaption in STL file for RP medical models“, *Journal of Manufacturing Processes*, vol. 21, pp. 46–55, 2016.
- [21] I. Gibson, D. Rosen, B. Stucker, and M. Khorasani, *Additive Manufacturing Technologies*. Cham: Springer International Publishing, 2021, vol. 89, pp. 82–86.
- [22] C. Kohtala, „Addressing sustainability in research on distributed production: An integrated literature review“, *Journal of Cleaner Production*, vol. 106, pp. 654–668, 2015.
- [23] S. Ford and M. Despeisse, „Additive manufacturing and sustainability: an exploratory study of the advantages and challenges“, *Journal of Cleaner Production*, vol. 137, pp. 1573–1587, 2016.
- [24] J. Plocher and A. Panesar, „Review on design and structural optimisation in additive manufacturing: Towards next-generation lightweight structures“, *Materials and Design*, vol. 183, 2019.
- [25] B. Blakey-Milner *et al.*, „Metal additive manufacturing in aerospace: A review“, *Materials and Design*, vol. 209, p. 110 008, 2021.
- [26] R. Leal *et al.*, „Additive manufacturing tooling for the automotive industry“, *International Journal of Advanced Manufacturing Technology*, vol. 92, no. 5-8, pp. 1671–1676, 2017.
- [27] A. A. Zadpoor and J. Malda, „Additive Manufacturing of Biomaterials, Tissues, and Organs“, *Annals of Biomedical Engineering*, vol. 45, no. 1, pp. 1–11, 2017.
- [28] S. C. Ligon, R. Liska, J. Stampfl, M. Gurr, and R. Mülhaupt, „Polymers for 3D Printing and Customized Additive Manufacturing“, *Chemical Reviews*, vol. 117, no. 15, pp. 10 212–10 290, 2017.

-
- [29] E. Pei *et al.*, Eds., *Springer Handbook of Additive Manufacturing* (Springer Handbooks). Springer International Publishing, 2023.
- [30] *DIN EN ISO/ASTM 52900:2022-03, Additive Fertigung – Grundlagen – Terminologie (ISO/ASTM 52900:2021)*. Berlin: Beuth Verlag, 2022.
- [31] L. J. Tan, W. Zhu, and K. Zhou, „Recent Progress on Polymer Materials for Additive Manufacturing“, *Advanced Functional Materials*, vol. 30, no. 43, 2020.
- [32] K. V. Wong and A. Hernandez, „A Review of Additive Manufacturing“, *ISRN Mechanical Engineering*, vol. 2012, pp. 1–10, 2012.
- [33] J. Kruth, „Material Incess Manufacturing by Rapid Prototyping Techniques“, *CIRP Annals*, vol. 40, no. 2, pp. 603–614, 1991.
- [34] J. P. Kruth, X. Wang, T. Laoui, and L. Froyen, „Lasers and materials in selective laser sintering“, *Assembly Automation*, vol. 23, no. 4, pp. 357–371, 2003.
- [35] P. Nandwana, A. M. Elliott, D. Siddel, A. Merriman, W. H. Peter, and S. S. Babu, „Powder bed binder jet 3D printing of Inconel 718: Densification, microstructural evolution and challenges“, *Current Opinion in Solid State and Materials Science*, vol. 21, no. 4, pp. 207–218, 2017.
- [36] S. J. Yoo, T. Spray, E. H. Austin, T. J. Yun, and G. S. van Arsdell, „Hands-on surgical training of congenital heart surgery using 3-dimensional print models“, *Journal of Thoracic and Cardiovascular Surgery*, vol. 153, no. 6, pp. 1530–1540, 2017.
- [37] S. Amrhein, M. L. Schwab, M. Hoffmann, and J. Hubbuch, „Characterization of aqueous two phase systems by combining lab-on-a-chip technology with robotic liquid handling stations“, *Journal of Chromatography A*, vol. 1367, pp. 68–77, 2014.
- [38] L. Wenger, C. P. Radtke, J. Göpper, M. Wörner, and J. Hubbuch, „3D-Printable and Enzymatically Active Composite Materials Based on Hydrogel-Filled High Internal Phase Emulsions“, *Frontiers in Bioengineering and Biotechnology*, vol. 8, pp. 1–17, 2020.
- [39] C. Fee, „3D-printed porous bed structures“, *Current Opinion in Chemical Engineering*, vol. 18, pp. 10–15, 2017.
- [40] S. Nawada, S. Dimartino, and C. Fee, „Dispersion behavior of 3D-printed columns with homogeneous microstructures comprising differing element shapes“, *Chemical Engineering Science*, vol. 164, pp. 90–98, 2017.
- [41] B. Schmiege, A. Schimek, and M. Franzreb, „Development and performance of a 3D-printable poly(ethylene glycol) diacrylate hydrogel suitable for enzyme entrapment and long-term biocatalytic applications“, *Engineering in Life Sciences*, vol. 18, no. 9, pp. 659–667, 2018.
- [42] J. Groll *et al.*, „Biofabrication: reappraising the definition of an evolving field“, *Biofabrication*, vol. 8, no. 1, p. 013001, 2016.
- [43] V. Mironov, T. Boland, T. Trusk, G. Forgacs, and R. R. Markwald, „Organ printing: Computer-aided jet-based 3D tissue engineering“, *Trends in Biotechnology*, vol. 21, no. 4, pp. 157–161, 2003.
- [44] F. Guillemot, V. Mironov, and M. Nakamura, „Bioprinting is coming of age: Report from the International Conference on Bioprinting and Biofabrication in Bordeaux (3B’09)“, *Biofabrication*, vol. 2, no. 1, 2010.

- [45] J. P. Vacanti and R. Langer, „Tissue engineering: the design and fabrication of living replacement devices for surgical reconstruction and transplantation“, *The Lancet*, vol. 354, no. SUPPL.1, S32–S34, 1999.
- [46] W. Sun *et al.*, „The bioprinting roadmap“, *Biofabrication*, vol. 12, no. 2, 2020.
- [47] A. B. Dababneh and I. T. Ozbolat, „Bioprinting Technology: A Current State-of-the-Art Review“, *Journal of Manufacturing Science and Engineering*, vol. 136, no. 6, p. 061016, 2014.
- [48] L. Ning *et al.*, „Process-induced cell damage: pneumatic versus screw-driven bioprinting“, *Biofabrication*, vol. 12, no. 2, 2020.
- [49] L. R. Darwish, M. T. El-Wakad, and M. M. Farag, „Towards an Ultra-Affordable Three-Dimensional Bioprinter: A Heated Inductive-Enabled Syringe Pump Extrusion Multifunction Module for Open-Source Fused Deposition Modeling Three-Dimensional Printers“, *Journal of Manufacturing Science and Engineering*, vol. 143, no. 12, 2021.
- [50] I. T. Ozbolat and M. Hospodiuk, „Current advances and future perspectives in extrusion-based bioprinting“, *Biomaterials*, vol. 76, pp. 321–343, 2016.
- [51] P. Diloksumpan *et al.*, „Combining multi-scale 3D printing technologies to engineer reinforced hydrogel-ceramic interfaces“, *Biofabrication*, vol. 12, no. 2, 2020.
- [52] A. S. Hoffman, „Hydrogels for biomedical applications“, *Advanced Drug Delivery Reviews*, vol. 64, no. SUPPL. Pp. 18–23, 2012.
- [53] E. M. Ahmed, „Hydrogel: Preparation, characterization, and applications: A review“, *Journal of Advanced Research*, vol. 6, no. 2, pp. 105–121, 2015.
- [54] K. Y. Lee and D. J. Mooney, „Hydrogels for tissue engineering“, *Chemical Reviews*, vol. 101, no. 7, pp. 1869–1879, 2001.
- [55] Y. Liang, J. He, and B. Guo, „Functional Hydrogels as Wound Dressing to Enhance Wound Healing“, *ACS Nano*, vol. 15, no. 8, pp. 12687–12722, 2021.
- [56] E. Caló and V. V. Khutoryanskiy, „Biomedical applications of hydrogels: A review of patents and commercial products“, *European Polymer Journal*, vol. 65, pp. 252–267, 2015.
- [57] P. Franco and I. De Marco, „Contact Lenses as Ophthalmic Drug Delivery Systems: A Review“, *Polymers*, vol. 13, no. 7, p. 1102, 2021.
- [58] N. A. Peppas and D. S. Van Blarcom, „Hydrogel-based biosensors and sensing devices for drug delivery“, *Journal of Controlled Release*, vol. 240, pp. 142–150, 2016.
- [59] J. Groll *et al.*, „A definition of bioinks and their distinction from biomaterial inks“, *Biofabrication*, vol. 11, no. 1, 2019.
- [60] T. Ahlfeld *et al.*, „Development of a clay based bioink for 3D cell printing for skeletal application“, *Biofabrication*, vol. 9, no. 3, p. 034103, 2017.
- [61] S. Dani *et al.*, „Homogeneous and reproducible mixing of highly viscous biomaterial inks and cell suspensions to create bioinks“, *Gels*, vol. 7, no. 4, pp. 1–17, 2021.
- [62] O. Smidsrød, G. Skja, *et al.*, „Alginate as immobilization matrix for cells“, *Trends Biotech*, vol. 8, no. March, pp. 71–78, 1990.
- [63] K. Y. Lee and D. J. Mooney, „Alginate: Properties and biomedical applications“, *Progress in Polymer Science (Oxford)*, vol. 37, no. 1, pp. 106–126, 2012.

- [64] S. V. Murphy, A. Skardal, and A. Atala, „Evaluation of hydrogels for bio-printing applications“, *Journal of Biomedical Materials Research - Part A*, vol. 101 A, no. 1, pp. 272–284, 2013.
- [65] G. Kloeck *et al.*, „Biocompatibility of mannuronic acid-rich alginates“, *Biomaterials*, vol. 18, no. 10, pp. 707–713, 1997.
- [66] Y. Cao, H. Cong, B. Yu, and Y. Shen, „A review on the synthesis and development of alginate hydrogels for wound therapy“, *Journal of Materials Chemistry B*, no. 1, pp. 2801–2829, 2023.
- [67] W. Cook, „Alginate dental impression materials: Chemistry, structure, and properties“, *Journal of Biomedical Materials Research*, vol. 20, no. 1, pp. 1–24, 1986.
- [68] D. Li, Z. Wei, and C. Xue, „Alginate-based delivery systems for food bioactive ingredients: An overview of recent advances and future trends“, *Comprehensive Reviews in Food Science and Food Safety*, vol. 20, no. 6, pp. 5345–5369, 2021.
- [69] J. a. Rowley, G. Madlambayan, and D. J. Mooney, „Alginate hydrogels as synthetic extracellular matrix materials“, *Biomaterials*, vol. 20, no. 1, pp. 45–53, 1999.
- [70] A. Iglesias-Mejuto and C. A. García-González, „3D-printed alginate-hydroxyapatite aerogel scaffolds for bone tissue engineering“, *Materials Science and Engineering C*, vol. 131, no. October, 2021.
- [71] E. Y. Heo *et al.*, „Novel 3D printed alginate–BFP1 hybrid scaffolds for enhanced bone regeneration“, *Journal of Industrial and Engineering Chemistry*, vol. 45, pp. 61–67, 2017.
- [72] D. Nguyen *et al.*, „Cartilage Tissue Engineering by the 3D Bioprinting of iPS Cells in a Nanocellulose/Alginate Bioink“, *Scientific Reports*, vol. 7, no. 1, pp. 1–10, 2017.
- [73] R. Ahmad Raus, W. M. F. Wan Nawawi, and R. R. Nasaruddin, „Alginate and alginate composites for biomedical applications“, *Asian Journal of Pharmaceutical Sciences*, vol. 16, no. 3, pp. 280–306, 2021.
- [74] K. Yue, G. Trujillo-de Santiago, M. M. Alvarez, A. Tamayol, N. Annabi, and A. Khademhosseini, „Synthesis, properties, and biomedical applications of gelatin methacryloyl (GelMA) hydrogels“, *Biomaterials*, vol. 73, pp. 254–271, 2015.
- [75] S. Naahidi *et al.*, „Biocompatibility of hydrogel-based scaffolds for tissue engineering applications“, *Biotechnology Advances*, vol. 35, no. 5, pp. 530–544, 2017.
- [76] S. Chen, Y. Wang, J. Lai, S. Tan, and M. Wang, „Structure and Properties of Gelatin Methacryloyl (GelMA) Synthesized in Different Reaction Systems“, *Biomacromolecules*, vol. 24, no. 6, pp. 2928–2941, 2023.
- [77] A. G. Kurian, R. K. Singh, K. D. Patel, J. H. Lee, and H. W. Kim, „Multifunctional GelMA platforms with nanomaterials for advanced tissue therapeutics“, *Bioactive Materials*, vol. 8, no. June 2021, pp. 267–295, 2022.
- [78] M. C. Bouwmeester *et al.*, „Bioprinting of Human Liver-Derived Epithelial Organoids for Toxicity Studies“, *Macromolecular Bioscience*, vol. 21, no. 12, p. 2100327, 2021.
- [79] N. R. Barros *et al.*, „Biofabrication of endothelial cell, dermal fibroblast, and multilayered keratinocyte layers for skin tissue engineering“, *Biofabrication*, vol. 13, no. 3, p. 035030, 2021.

- [80] E. Russo and C. Villa, „Poloxamer hydrogels for biomedical applications“, *Pharmaceutics*, vol. 11, no. 12, 2019.
- [81] G. Dumortier, J. L. Grossiord, F. Agnely, and J. C. Chaumeil, „A review of poloxamer 407 pharmaceutical and pharmacological characteristics“, *Pharmaceutical Research*, vol. 23, no. 12, pp. 2709–2728, 2006.
- [82] D. B. Kolesky, R. L. Truby, A. S. Gladman, T. A. Busbee, K. A. Homan, and J. A. Lewis, „3D bioprinting of vascularized, heterogeneous cell-laden tissue constructs“, *Advanced Materials*, vol. 26, no. 19, pp. 3124–3130, 2014.
- [83] P. S. Gungor-Ozkerim, I. Inci, Y. S. Zhang, A. Khademhosseini, and M. R. Dokmeci, „Bioinks for 3D bioprinting: An overview“, *Biomaterials Science*, vol. 6, no. 5, pp. 915–946, 2018.
- [84] N. E. Fedorovich, J. R. De Wijn, A. J. Verbout, J. Alblas, and W. J. Dhert, „Three-dimensional fiber deposition of cell-laden, viable, patterned constructs for bone tissue printing“, *Tissue Engineering - Part A*, vol. 14, no. 1, pp. 127–133, 2008.
- [85] T. G. Mezger, *The Rheology Handbook*, 4th ed. Hanover: Vincentz Network GmbH & Co. KG, 2014.
- [86] T. Osswald and N. Rudolph, *Carl Hanser Verlag*. 2006, pp. 1–8.
- [87] M. Rubinstein and R. H. Colby, *Polymer Physics*. Oxford University Press, 2003.
- [88] C. Verdier, „Rheological Properties of Living Materials . From Cells to Tissues“, vol. 5, no. June 2003, pp. 67–91, 2004.
- [89] P. A. Janmey, P. C. Georges, and S. Hvidt, „Basic Rheology for Biologists“, *Methods in Cell Biology*, vol. 83, 2007.
- [90] N. R. Pal and S. K. Pal, „A review on image segmentation techniques“, *Pattern Recognition*, vol. 26, no. 9, pp. 1277–1294, 1993.
- [91] F. Perez-Sanz, P. J. Navarro, and M. Egea-Cortines, „Plant phenomics: an overview of image acquisition technologies and image data analysis algorithms“, *GigaScience*, vol. 6, no. 11, pp. 1–18, 2017.
- [92] Y.-S. Chen, *Image Processing*, Y.-S. Chen, Ed. InTech, 2009.
- [93] M. L. Giger, H.-P. Chan, and J. Boone, „Anniversary Paper: History and status of CAD and quantitative image analysis: The role of Medical Physics and AAPM“, *Medical Physics*, vol. 35, no. 12, pp. 5799–5820, 2008.
- [94] J. Beyerer, F. P. León, and C. Frese, *Automatische Sichtprüfung: Grundlagen, Methoden und Praxis der Bildgewinnung und Bildauswertung*. Springer-Verlag, 2016.
- [95] F. Pernkopf and P. O’Leary, „Image acquisition techniques for automatic visual inspection of metallic surfaces“, *NDT and E International*, vol. 36, no. 8, pp. 609–617, 2003.
- [96] B. Jähne and H. Haußecker, *Computer vision and applications*. Academic Press, 2000.
- [97] D. Casasent and X. W. Chen, „New training strategies for RBF neural networks for X-ray agricultural product inspection“, *Pattern Recognition*, vol. 36, no. 2, pp. 535–547, 2003.
- [98] O. Semeniuta, S. Dransfeld, K. Martinsen, and P. Falkman, „Towards increased intelligence and automatic improvement in industrial vision systems“, *Procedia CIRP*, vol. 67, pp. 256–261, 2018.

-
- [99] J. F. Arinez, Q. Chang, R. X. Gao, C. Xu, and J. Zhang, „Artificial Intelligence in Advanced Manufacturing: Current Status and Future Outlook“, *Journal of Manufacturing Science and Engineering*, vol. 142, no. 11, pp. 1–16, 2020.
- [100] T. Gao *et al.*, „Optimization of gelatin-alginate composite bioink printability using rheological parameters: A systematic approach“, *Biofabrication*, vol. 10, no. 3, 2018.
- [101] A. Ribeiro *et al.*, „Assessing bioink shape fidelity to aid material development in 3D bioprinting“, *Biofabrication*, vol. 10, no. 1, 2018.
- [102] Y. He, F. Yang, H. Zhao, Q. Gao, B. Xia, and J. Fu, „Research on the printability of hydrogels in 3D bioprinting“, *Scientific Reports*, vol. 6, pp. 1–13, 2016.
- [103] M. Uzun-Per *et al.*, „Automated Image Analysis Methodologies to Compute Bioink Printability“, *Advanced Engineering Materials*, vol. 2000900, pp. 1–12, 2020.
- [104] C. Riccardi and I. Nicoletti, „Analysis of apoptosis by propidium iodide staining and flow cytometry“, *Nature Protocols*, vol. 1, no. 3, pp. 1458–1461, 2006.
- [105] N. Grigoryeva, *Fluorescence Methods for Investigation of Living Cells and Microorganisms*. BoD–Books on Demand, 2020.
- [106] N. G. Papadopoulos, G. V. Dedoussis, G. Spanakos, A. D. Gritzapis, C. N. Baxevanis, and M. Papamichail, „An improved fluorescence assay for the determination of lymphocyte-mediated cytotoxicity using flow cytometry“, *Journal of Immunological Methods*, vol. 177, no. 1-2, pp. 101–111, 1994.
- [107] A. Adan, G. Alizada, Y. Kiraz, Y. Baran, and A. Nalbant, *Flow cytometry: basic principles and applications*. 2017, vol. 37, pp. 163–176.
- [108] C. Ortolani, *Flow Cytometry Today*. Springer Nature, 2022.
- [109] S. Gretzinger, N. Beckert, A. Gleadall, C. Lee-Thedieck, and J. Hubbuch, „3D bioprinting – Flow cytometry as analytical strategy for 3D cell structures“, *Bioprinting*, vol. 11, no. March, e00023, 2018.
- [110] J. Groll *et al.*, „Biofabrication: Reappraising the definition of an evolving field“, *Biofabrication*, vol. 8, no. 1, p. 013001, 2016.
- [111] S. Duin *et al.*, „3d bioprinting of functional islets of langerhans in an alginate/methylcellulose hydrogel blend“, *Advanced Healthcare Materials*, vol. 8, no. 7, p. 1 801 631, 2019.
- [112] J. Malda *et al.*, „25th anniversary article: Engineering hydrogels for biofabrication“, *Advanced Materials*, vol. 25, no. 36, pp. 5011–5028, 2013.
- [113] A. Atala, „Engineering organs“, *Current Opinion in Biotechnology*, vol. 20, no. 5, pp. 575–592, 2009.
- [114] S. Murphy and A. Atala, „3d bioprinting of tissues and organs“, *Nature biotechnology*, vol. 32, 2014.
- [115] F. Groeber, M. Holeiter, M. Hampel, S. Hinderer, and K. Schenke-Layland, „Skin tissue engineering — in vivo and in vitro applications“, *Advanced Drug Delivery Reviews*, vol. 63, no. 4, pp. 352–366, 2011.
- [116] T. Jungst, W. Smolan, K. Schacht, T. Scheibel, and J. Groll, „Strategies and molecular design criteria for 3d printable hydrogels“, *Chemical Reviews*, vol. 116, no. 3, pp. 1496–1539, 2016.

- [117] A. S. Hoffman, „Hydrogels for biomedical applications“, *Advanced Drug Delivery Reviews*, vol. 64, pp. 18–23, 2012.
- [118] S. Krishnamoorthi, A. Banerjee, and A. Roychoudhury, „Immobilized enzyme technology: Potentiality and prospects“, *J Enzymol Metabol*, vol. 1, no. 1, pp. 010–104, 2015.
- [119] B. Schmiege, A. Schimek, and M. Franzreb, „Development and performance of a 3d-printable poly(ethylene glycol) diacrylate hydrogel suitable for enzyme entrapment and long-term biocatalytic applications“, *Engineering in Life Sciences*, vol. 18, no. 9, pp. 659–667, 2018.
- [120] B. Schmiege, M. Nguyen, and M. Franzreb, „Simulative minimization of mass transfer limitations within hydrogel-based 3d-printed enzyme carriers“, *Frontiers in Bioengineering and Biotechnology*, vol. 8, p. 365, 2020.
- [121] K. Y. Lee and D. J. Mooney, „Hydrogels for tissue engineering“, *Chemical Reviews*, vol. 101, no. 7, pp. 1869–1879, 2001.
- [122] J. Zhu, „Bioactive modification of poly(ethylene glycol) hydrogels for tissue engineering“, *Biomaterials*, vol. 31, no. 17, pp. 4639–4656, 2010.
- [123] T. Vermonden, R. Censi, and W. E. Hennink, „Hydrogels for protein delivery“, *Chemical Reviews*, vol. 112, pp. 2853–2888, 2012.
- [124] A. G. Tabriz, M. A. Hermida, N. R. Leslie, and W. Shu, „Three-dimensional bioprinting of complex cell laden alginate hydrogel structures“, *Biofabrication*, vol. 7, no. 4, p. 045 012, 2015.
- [125] T. T. Demirtaş, G. Irmak, and M. Gümüşderelioğlu, „A bioprintable form of chitosan hydrogel for bone tissue engineering“, *Biofabrication*, vol. 9, no. 3, p. 035 003, 2017.
- [126] J. Y. Park *et al.*, „A comparative study on collagen type i and hyaluronic acid dependent cell behavior for osteochondral tissue bioprinting“, *Biofabrication*, vol. 6, no. 3, p. 035 004, 2014.
- [127] J. D. Kosmala, D. B. Henthorn, and L. Brannon-Peppas, „Preparation of interpenetrating networks of gelatin and dextran as degradable biomaterials“, *Biomaterials*, vol. 21, no. 20, pp. 2019–2023, 2000.
- [128] B. V. Slaughter, S. S. Khurshid, O. Z. Fisher, A. Khademhosseini, and N. A. Peppas, „Hydrogels in regenerative medicine“, *Advanced Materials*, vol. 21, no. 32-33, pp. 3307–3329, 2009.
- [129] M. Du *et al.*, „3d bioprinting of BMSC-laden methacrylamide gelatin scaffolds with CBD-BMP2-collagen microfibers“, *Biofabrication*, vol. 7, no. 4, p. 044 104, 2015.
- [130] S. Naahidi *et al.*, „Biocompatibility of hydrogel-based scaffolds for tissue engineering applications“, *Biotechnology Advances*, vol. 35, no. 5, pp. 530–544, 2017.
- [131] R. A. Scott and N. A. Peppas, „Highly crosslinked, peg-containing copolymers for sustained solute delivery“, *Biomaterials*, vol. 20, no. 15, pp. 1371–1380, 1999.
- [132] S. Bertlein *et al.*, „Thiol–ene clickable gelatin: A platform bioink for multiple 3d biofabrication technologies“, *Advanced Materials*, vol. 29, no. 44, p. 1 703 404, 2017.
- [133] A. C. Jen, M. C. Wake, and A. G. Mikos, „Review: Hydrogels for cell immobilization“, *Biotechnology and Bioengineering*, vol. 50, no. 4, pp. 357–364, 1996.

- [134] K. Yue, G. [-d. Santiago], M. M. Alvarez, A. Tamayol, N. Annabi, and A. Khademhosseini, „Synthesis, properties, and biomedical applications of gelatin methacryloyl (gelma) hydrogels“, *Biomaterials*, vol. 73, pp. 254–271, 2015.
- [135] L. Wenger, C. Radtke, J. Göpper, M. Wörner, and J. Hubbuch, „3d-printable and enzymatically active composite materials based on hydrogel-filled high internal phase emulsions“, *Frontiers in Bioengineering and Biotechnology*, vol. 8, p. 713, 2020.
- [136] T. Gao *et al.*, „Optimization of gelatin–alginate composite bioink printability using rheological parameters: A systematic approach“, *Biofabrication*, vol. 10, no. 3, p. 034 106, 2018.
- [137] K. Markstedt, A. Mantas, I. Tournier, H. Martínez Ávila, D. Hägg, and P. Gatenholm, „3D bioprinting human chondrocytes with nanocellulose-alginate bioink for cartilage tissue engineering applications“, *Biomacromolecules*, vol. 16, no. 5, pp. 1489–1496, 2015.
- [138] T. Lorson *et al.*, „A Thermogelling Supramolecular Hydrogel with Sponge-Like Morphology as a Cytocompatible Bioink“, *Biomacromolecules*, vol. 18, no. 7, pp. 2161–2171, 2017.
- [139] N. Soltan, L. Ning, F. Mohabatpour, P. Papagerakis, and X. Chen, „Printability and Cell Viability in Bioprinting Alginate Dialdehyde-Gelatin Scaffolds“, *ACS Biomaterials Science and Engineering*, vol. 5, no. 6, pp. 2976–2987, 2019.
- [140] B. Webb and B. J. Doyle, „Parameter optimization for 3d bioprinting of hydrogels“, *Bioprinting*, vol. 8, pp. 8–12, 2017.
- [141] A. Ribeiro *et al.*, „Assessing bioink shape fidelity to aid material development in 3d bioprinting“, *Biofabrication*, vol. 10, no. 1, p. 014 102, 2017.
- [142] E. N. Malamas, E. G. Petrakis, M. Zervakis, L. Petit, and J.-D. Legat, „A survey on industrial vision systems, applications and tools“, *Image and Vision Computing*, vol. 21, no. 2, pp. 171–188, 2003.
- [143] L. S. Chow and R. Paramesran, „Review of medical image quality assessment“, *Biomedical Signal Processing and Control*, vol. 27, pp. 145–154, 2016.
- [144] F. M. Wunner *et al.*, „Printomics: The high-throughput analysis of printing parameters applied to melt electrowriting“, *Biofabrication*, vol. 11, 2019.
- [145] F. Yang, H. Zhao, Q. Gao, B. Xia, and F. Jianzhong, „Research on the printability of hydrogels in 3d bioprinting“, *Scientific Reports*, vol. 6, p. 29 977, 2016.
- [146] Q. Gao *et al.*, „3d printing of complex GelMA-based scaffolds with nanoclay“, *Biofabrication*, vol. 11, no. 3, p. 035 006, 2019.
- [147] M. Alonzo *et al.*, „A comparative study in the printability of a bioink and 3d models across two bioprinting platforms“, *Materials Letters*, vol. 264, p. 127 382, 2020.
- [148] M. K. Włodarczyk-Biegun, J. I. Paez, M. Villiou, J. Feng, and A. del Campo, „Printability study of metal ion crosslinked peg-catechol based inks“, *bioRxiv*, 2019.
- [149] C. P. Radtke, N. Hillebrandt, and J. Hubbuch, „The biomaker: An entry-level bioprinting device for biotechnological applications“, *Journal of Chemical Technology & Biotechnology*, vol. 93, no. 3, pp. 792–799, 2018.
- [150] T. Billiet, M. Vandenhaute, J. Schelfhout, S. [Vlierberghe], and P. Dubruel, „A review of trends and limitations in hydrogel-rapid prototyping for tissue engineering“, *Biomaterials*, vol. 33, no. 26, pp. 6020–6041, 2012.

- [151] A. S. Mao and D. J. Mooney, „Regenerative medicine: Current therapies and future directions“, *Proceedings of the National Academy of Sciences of the United States of America*, vol. 112, no. 47, pp. 14 452–14 459, 2015.
- [152] H. R. Culver, J. R. Clegg, and N. A. Peppas, „Analyte-Responsive Hydrogels: Intelligent Materials for Biosensing and Drug Delivery“, *Accounts of Chemical Research*, vol. 50, no. 2, pp. 170–178, 2017.
- [153] S. Caddeo, M. Boffito, and S. Sartori, „Tissue engineering approaches in the design of healthy and pathological in vitro tissue models“, *Frontiers in Bioengineering and Biotechnology*, vol. 5, no. AUG, pp. 1–22, 2017.
- [154] Y. Chen *et al.*, „Noninvasive in vivo 3d bioprinting“, *Science Advances*, vol. 6, no. 23, 2020.
- [155] K. A. Smeds and M. W. Grinstaff, „Photocrosslinkable polysaccharides for in situ hydrogel formation“, *Journal of Biomedical Materials Research*, vol. 54, no. 1, pp. 115–121, 2001.
- [156] K. Yue, G. Trujillo-de Santiago, M. M. Alvarez, A. Tamayol, N. Annabi, and A. Khademhosseini, „Synthesis, properties, and biomedical applications of gelatin methacryloyl (GelMA) hydrogels“, *Biomaterials*, vol. 73, pp. 254–271, 2015.
- [157] N. Paxton, W. Smolan, T. Böck, F. Melchels, J. Groll, and T. Jungst, „Proposal to assess printability of bioinks for extrusion-based bioprinting and evaluation of rheological properties governing bioprintability“, *Biofabrication*, vol. 9, no. 4, p. 044 107, 2017.
- [158] C. P. Radtke, N. Hillebrandt, and J. Hubbuch, „The biomaker: An entry-level bioprinting device for biotechnological applications“, *Journal of Chemical Technology & Biotechnology*, vol. 93, no. 3, pp. 792–799, 2018.
- [159] J. A. Rowley, G. Madlambayan, and D. J. Mooney, „Alginate hydrogels as synthetic extracellular matrix materials“, *Biomaterials*, vol. 20, no. 1, pp. 45–53, 1999.
- [160] E. Axpe and M. L. Oyen, „Applications of alginate-based bioinks in 3d bioprinting“, *International journal of molecular sciences*, vol. 17, no. 12, p. 1976, 2016.
- [161] A. F. Bonatti, I. Chiesa, G. Vozzi, and C. De Maria, „Open-source cad-cam simulator of the extrusion-based bioprinting process“, *Bioprinting*, vol. 24, e00172, 2021.
- [162] T. G. Mezger, *Das Rheologie Handbuch*, 5th ed. Vincentz Network, 2016.
- [163] T. Jungst, W. Smolan, K. Schacht, T. Scheibel, and J. Groll, „Strategies and Molecular Design Criteria for 3D Printable Hydrogels“, *Chemical Reviews*, vol. 116, no. 3, pp. 1496–1539, 2016.
- [164] Y. Zhao, Y. Li, S. Mao, W. Sun, and R. Yao, „The influence of printing parameters on cell survival rate and printability in microextrusion-based 3d cell printing technology“, *Biofabrication*, vol. 7, no. 4, p. 045 002, 2015.
- [165] T. Osswald and N. Rudolph, *Polymer rheology : fundamentals and applications* (Hanser eLibrary). München: Hanser, 2014.
- [166] P. Fisch, M. Holub, and M. Zenobi-Wong, „Improved accuracy and precision of bioprinting through progressive cavity pump-controlled extrusion“, *bioRxiv*, 2020.
- [167] S. Seiffert and J. Sprakel, „Physical chemistry of supramolecular polymer networks“, *Chemical Society Reviews*, vol. 41, no. 2, pp. 909–930, 2012.

- [168] M. Matamoros *et al.*, „Temperature and humidity pid controller for a bioprinter atmospheric enclosure system“, *Micromachines*, vol. 11, no. 11, 2020.
- [169] A. Rasmussen and M. Zaghoul, „The design and fabrication of microfluidic flow sensors“, in *1999 IEEE International Symposium on Circuits and Systems (ISCAS)*, vol. 5, 1999, 136–139 vol.5.
- [170] W. J. Fleming, „Overview of automotive sensors“, *IEEE Sensors Journal*, vol. 1, no. 4, pp. 296–308, 2001.
- [171] N. Nguyen, „Micromachined flow sensors—a review“, *Flow Measurement and Instrumentation*, vol. 8, no. 1, pp. 7–16, 1997.
- [172] G. Schnell and R. Schäfer, „Ein thermischer Durchflußsensor.für die Infusionstechnik“, *Biomedizinische Technik*, vol. 40, no. 3, pp. 50–53, 1995.
- [173] L. Banović and B. Vihar, „Development of an extruder for open source 3d bioprinting“, *Journal of Open Hardware*, vol. 2, no. 1, 2018.
- [174] C. Yan, M. E. Mackay, K. Czymmek, R. P. Nagarkar, J. P. Schneider, and D. J. Pochan, „Injectable solid peptide hydrogel as a cell carrier: Effects of shear flow on hydrogels and cell payload“, *Langmuir*, vol. 28, no. 14, pp. 6076–6087, 2012.
- [175] R. V. Opel, W. Hynes, M. Moya, *et al.*, „Flow sensor integration for precision dispensing of visco-elastic biomaterials“, 2017.
- [176] P. Blainey, M. Krzywinski, and N. Altman, „Replication: Quality is often more important than quantity“, *Nature Methods*, vol. 11, no. 9, pp. 879–881, 2014.
- [177] J. T. Kuo, L. Yu, and E. Meng, „Micromachined thermal flow sensors—a review“, *Micromachines*, vol. 3, no. 3, pp. 550–573, 2012.
- [178] M. Kesti, P. Fisch, M. Pensalfini, E. Mazza, and M. Zenobi-Wong, „Guidelines for standardization of bioprinting: A systematic study of process parameters and their effect on bioprinted structures“, *BioNanoMaterials*, vol. 17, no. 3-4, pp. 193–204, 2016.
- [179] Z.-Y. Wang, Q.-Z. Zhang, M. Konno, and S. Saito, „Sol–Gel transition of alginate solution by the addition of various divalent cations: A rheological study“, *Biopolymers*, vol. 34, no. 6, pp. 737–746, 1994.
- [180] S. V. Murphy and A. Atala, „3d bioprinting of tissues and organs“, *Nature biotechnology*, vol. 32, no. 8, pp. 773–785, 2014.
- [181] L. Ning *et al.*, „Process-induced cell damage: Pneumatic versus screw-driven bioprinting“, *Biofabrication*, vol. 12, no. 2, p. 025 011, 2020.
- [182] L. Ning and X. Chen, „A brief review of extrusion-based tissue scaffold bio-printing“, *Biotechnology journal*, vol. 12, no. 8, p. 1 600 671, 2017.
- [183] I. Barratt, Y. Yan, B. Byrne, and M. Bradley, „Mass flow measurement of pneumatically conveyed solids using radiometric sensors“, *Flow Measurement and Instrumentation*, vol. 11, no. 3, pp. 223–235, 2000.
- [184] I. Gibson, D. Rosen, B. Stucker, and M. Khorasani, *Additive Manufacturing Technologies*, 3rd ed. Springer, 2021.
- [185] E. Kroll and D. Artzi, „Enhancing aerospace engineering students’ learning with 3D printing wind-tunnel models“, *Rapid Prototyping Journal*, vol. 17, no. 5, pp. 393–402, 2011.

- [186] C. Parra-Cabrera, C. Achille, S. Kuhn, and R. Ameloot, „3D printing in chemical engineering and catalytic technology: structured catalysts, mixers and reactors“, *Chemical Society Reviews*, vol. 47, no. 1, pp. 209–230, 2018.
- [187] K. V. Wong and A. Hernandez, „A Review of Additive Manufacturing“, *ISRN Mechanical Engineering*, vol. 2012, pp. 1–10, 2012.
- [188] S. V. Murphy and A. Atala, „3D bioprinting of tissues and organs“, *Nature biotechnology*, vol. 32, no. 8, pp. 773–785, 2014.
- [189] N. J. Castro, C. Meinert, P. Levett, and D. W. Hutmacher, „Current developments in multifunctional smart materials for 3D/4D bioprinting“, *Current Opinion in Biomedical Engineering*, vol. 2, pp. 67–75, 2017.
- [190] B. Schmieg, J. Döbber, F. Kirschhöfer, M. Pohl, and M. Franzreb, „Advantages of Hydrogel-Based 3D-Printed Enzyme Reactors and Their Limitations for Biocatalysis“, *Frontiers in Bioengineering and Biotechnology*, vol. 6, no. JAN, pp. 1–12, 2019.
- [191] R. Langer and J. P. Vacanti, „Tissue Engineering“, *Science*, vol. 260, no. 5110, pp. 920–926, 1993.
- [192] S. Krishnamoorthi, A. Banerjee, and A. Roychoudhury, „Immobilized Enzyme Technology: Potentiality and Prospects“, *Journal of Enzymology and Metabolism*, vol. 1, no. 1, pp. 1–11, 2015.
- [193] M. Hospodiuk, M. Dey, D. Sosnoski, and I. T. Ozbolat, „The bioink: A comprehensive review on bioprintable materials“, *Biotechnology Advances*, vol. 35, no. 2, pp. 217–239, 2017.
- [194] C. P. Radtke, N. Hillebrandt, and J. Hubbuch, „The Biomaker: an entry-level bioprinting device for biotechnological applications“, *Journal of Chemical Technology and Biotechnology*, vol. 93, no. 3, pp. 792–799, 2018.
- [195] D. Bociaga, M. Bartniak, K. Sobczak, and K. Rosinska, „An Integration of a Peristaltic Pump-Based Extruder Into a 3D Bioprinter Dedicated to Hydrogels“, *Materials*, vol. 13, no. 19, 2020.
- [196] L. Ning *et al.*, „Process-induced cell damage: pneumatic versus screw-driven bioprinting“, *Biofabrication*, vol. 12, no. 2, 2020.
- [197] K. Hölzl, S. Lin, L. Tytgat, S. Van Vlierberghe, L. Gu, and A. Ovsianikov, „Bioink properties before, during and after 3D bioprinting“, *Biofabrication*, vol. 8, no. 3, pp. 1–19, 2016.
- [198] Y. Zhao, Y. Li, S. Mao, W. Sun, and R. Yao, „The influence of printing parameters on cell survival rate and printability in microextrusion-based 3D cell printing technology“, *Biofabrication*, vol. 7, no. 4, 2015.
- [199] A. Ribeiro *et al.*, „Assessing bioink shape fidelity to aid material development in 3D bioprinting“, *Biofabrication*, vol. 10, no. 1, 2018.
- [200] V. H. M. Mouser, F. P. W. Melchels, J. Visser, W. J. A. Dhert, D. Gawlitta, and J. Malda, „Yield stress determines bioprintability of hydrogels based on gelatin-methacryloyl and gellan gum for cartilage bioprinting“, *Biofabrication*, vol. 8, no. 3, p. 035 003, 2016.
- [201] B. Webb and B. J. Doyle, „Parameter optimization for 3D bioprinting of hydrogels“, *Bioprinting*, vol. 8, no. July, pp. 8–12, 2017.

- [202] R. Opel, W. ” Hynes, and M. Moya, *Flow Sensor Integration for Precision Dispensing of Visco-Elastic Biomaterials*, 2017.
- [203] S. Strauß, B. Schroth, and J. Hubbuch, „Evaluation of the Reproducibility and Robustness of Extrusion-Based Bioprinting Processes Applying a Flow Sensor“, *Frontiers in Bioengineering and Biotechnology*, vol. 10, pp. 1–14, 2022.
- [204] W. J. Fleming, „Overview of Automotive Sensors“, *IEEE Sensors Journal*, vol. 1, no. 4, pp. 296–308, 2001.
- [205] U. Schmid, G. Krötz, and D. Schmitt-Landsiedel, „A volumetric flow sensor for automotive injection systems“, *Journal of Micromechanics and Microengineering*, vol. 18, no. 4, 2008.
- [206] Y. Li *et al.*, „Gas/oil/water flow measurement by electrical capacitance tomography“, *Measurement Science and Technology*, vol. 24, no. 7, 2013.
- [207] R. Thorn, G. A. Johansen, and B. T. Hjertaker, „Three-phase flow measurement in the petroleum industry“, *Measurement Science and Technology*, vol. 24, no. 1, 2013.
- [208] D. L. Polla *et al.*, „Microdevices in Medicine“, *Annual Review of Biomedical Engineering*, vol. 2, no. 1, pp. 551–576, 2000.
- [209] C. J. Okereke, O. A. Lasode, and I. O. Ohijeagbon, „Exergoeconomic analysis of an industrial beverage mixer system: Process data“, *Data in Brief*, vol. 32, p. 106 125, 2020.
- [210] L. D. Pedersen, „Assessment of sensors used in the food industry“, *Food Control*, vol. 2, no. 2, pp. 87–98, 1991.
- [211] N. T. Nguyen, „Micromachined flow sensors - A review“, *Flow Measurement and Instrumentation*, vol. 8, no. 1, pp. 7–16, 1997.
- [212] J. T. Kuo, L. Yu, and E. Meng, „Micromachined Thermal Flow Sensors - A Review“, *Micromachines*, vol. 3, no. 3, pp. 550–573, 2012.
- [213] S. Silvestri and E. Schena, „Micromachined Flow Sensors in Biomedical Applications“, *Micromachines*, vol. 3, no. 2, pp. 225–243, 2012.
- [214] C. Li *et al.*, „Smart catheter flow sensor for real-time continuous regional cerebral blood flow monitoring“, *Applied Physics Letters*, vol. 99, no. 23, pp. 10–14, 2011.
- [215] A. D. Augst, H. J. Kong, and D. J. Mooney, „Alginate hydrogels as biomaterials“, *Macromolecular Bioscience*, vol. 6, no. 8, pp. 623–633, 2006.
- [216] F. Pahlevanzadeh *et al.*, „Recent Trends in Three-Dimensional Bioinks Based on Alginate for Biomedical Applications“, *Materials*, vol. 13, no. 18, p. 3980, 2020.
- [217] S. Duin *et al.*, „3D Bioprinting of Functional Islets of Langerhans in an Alginate/Methylcellulose Hydrogel Blend“, *Advanced Healthcare Materials*, vol. 8, no. 7, pp. 1–14, 2019.
- [218] F. F. Cai, S. Heid, and A. R. Boccaccini, *Potential of Laponite® incorporated oxidized alginate-gelatin (ADA-GEL) composite hydrogels for extrusion-based 3D printing*, 2021.
- [219] M. Shen, Y. Sun, J. Xu, X. Guo, and R. K. Prud’Homme, „Rheology and Adhesion of Poly(acrylic acid)/Laponite Nanocomposite Hydrogels as Biocompatible Adhesives“, *Langmuir*, vol. 30, no. 6, pp. 1636–1642, 2014.
- [220] Sensirion, *STEP file Sensirion SLI*, <https://sensirion.com/resource/cad/sli>, Accessed: 2022-01-26, 2021.

- [221] V. Dubey, H. Goud, and P. C. Sharma, „Role of PID Control Techniques in Process Control System: A Review“, in *Data Engineering for Smart Systems*, P. Nanda, V. K. Verma, S. Srivastava, R. K. Gupta, and A. P. Mazumdar, Eds., Singapore: Springer, 2022, pp. 659–670.
- [222] R. A. Paz, „The Design of the PID Controller“, Ph.D. dissertation, Klipsch School of Electrical and Computer Engineering, 2001.
- [223] G. Wolterink, A. Umrani, M. Schouten, R. Sanders, and G. Krijnen, „3D-Printed Calorimetric Flow Sensor“, *2020 IEEE Sensors*, pp. 1–4, 2020.
- [224] I. R. Schmolka, „Physical Basis for Poloxamer Interactions“, *Annals of the New York Academy of Sciences*, vol. 720, no. 1, pp. 92–97, 1994.
- [225] H. Seki and T. Shigemasa, „Retuning oscillatory PID control loops based on plant operation data“, *Journal of Process Control*, vol. 20, no. 2, pp. 217–227, 2010.
- [226] H. O. Bansal, R. Sharma, and P. R. Shreeraman, „PID Controller Tuning Techniques: A Review“, *Journal of Control Engineering and Technology*, vol. 2, no. 4, pp. 168–176, 2012.
- [227] B. V. Slaughter, S. S. Khurshid, O. Z. Fisher, A. Khademhosseini, and N. A. Peppas, „Hydrogels in Regenerative Medicine“, *Advanced Materials*, vol. 21, no. 32-33, pp. 3307–3329, 2009.
- [228] J. Thiele, Y. Ma, S. M. C. Bruekers, S. Ma, and W. T. S. Huck, „25th Anniversary Article: Designer Hydrogels for Cell Cultures: A Materials Selection Guide“, *Advanced Materials*, vol. 26, no. 1, pp. 125–148, 2014.
- [229] A. S. Theus *et al.*, „Bioprintability: Physiomechanical and Biological Requirements of Materials for 3D Bioprinting Processes“, *Polymers*, vol. 12, no. 10, p. 2262, 2020.
- [230] W. Liu *et al.*, „Extrusion Bioprinting of Shear-Thinning Gelatin Methacryloyl Bioinks“, *Advanced Healthcare Materials*, vol. 6, no. 12, pp. 1–11, 2017.
- [231] A. Erdem *et al.*, „3D Bioprinting of Oxygenated Cell-Laden Gelatin Methacryloyl Constructs“, *Advanced Healthcare Materials*, vol. 9, no. 15, pp. 1–12, 2020.
- [232] H. Jongprasitkul, S. Turunen, V. S. Parihar, and M. Kellomäki, „Two-step crosslinking to enhance the printability of methacrylated gellan gum biomaterial ink for extrusion-based 3D bioprinting“, *Bioprinting*, vol. 25, no. September 2021, 2022.
- [233] A. Habib, V. Sathish, S. Mallik, and B. Khoda, „3D printability of alginate-carboxymethyl cellulose hydrogel“, *Materials*, vol. 11, no. 3, 2018.
- [234] A. Mondal *et al.*, „Characterization and printability of Sodium alginate -Gelatin hydrogel for bioprinting NSCLC co-culture“, *Scientific Reports*, vol. 9, no. 1, pp. 1–12, 2019.
- [235] B. H. Lee, N. Lum, L. Y. Seow, P. Q. Lim, and L. P. Tan, „Synthesis and characterization of types A and B gelatin methacryloyl for bioink applications“, *Materials*, vol. 9, no. 10, pp. 1–13, 2016.
- [236] G. Gillispie *et al.*, „Assessment methodologies for extrusion-based bioink printability“, *Biofabrication*, vol. 12, no. 2, 2020.
- [237] T. Gao *et al.*, „Optimization of gelatin-alginate composite bioink printability using rheological parameters: A systematic approach“, *Biofabrication*, vol. 10, no. 3, 2018.
- [238] M. D. Giuseppe *et al.*, „Mechanical behaviour of alginate-gelatin hydrogels for 3D bioprinting“, *Journal of the Mechanical Behavior of Biomedical Materials*, vol. 79, pp. 150–157, 2018.

- [239] M. Uzun-Per *et al.*, „Automated Image Analysis Methodologies to Compute Bioink Printability“, *Advanced Engineering Materials*, vol. 2000900, pp. 1–12, 2020.
- [240] A. A. Aldana, F. Valente, R. Dilley, and B. Doyle, „Development of 3D bioprinted GelMA-alginate hydrogels with tunable mechanical properties“, *Bioprinting*, vol. 21, no. June 2020, e00105, 2021.
- [241] S. Dani *et al.*, „Homogeneous and reproducible mixing of highly viscous biomaterial inks and cell suspensions to create bioinks“, *Gels*, vol. 7, no. 4, pp. 1–17, 2021.
- [242] E. N. Malamas, E. G. Petrakis, M. Zervakis, L. Petit, and J.-D. Legat, „A survey on industrial vision systems, applications and tools“, *Image and Vision Computing*, vol. 21, no. 2, pp. 171–188, 2003.
- [243] O. Semeniuta, S. Dransfeld, K. Martinsen, and P. Falkman, „Towards increased intelligence and automatic improvement in industrial vision systems“, *Procedia CIRP*, vol. 67, pp. 256–261, 2018.
- [244] W. Schuurman *et al.*, „Gelatin-Methacrylamide Hydrogels as Potential Biomaterials for Fabrication of Tissue-Engineered Cartilage Constructs“, *Macromolecular Bioscience*, vol. 13, no. 5, pp. 551–561, 2013.
- [245] F. Koch, K. Tröndle, G. Finkenzeller, R. Zengerle, S. Zimmermann, and P. Koltay, „Generic method of printing window adjustment for extrusion-based 3D-bioprinting to maintain high viability of mesenchymal stem cells in an alginate-gelatin hydrogel“, *Bioprinting*, vol. 20, e00094, 2020.
- [246] Z. Di *et al.*, „Ultra High Content Image Analysis and Phenotype Profiling of 3D Cultured Micro-Tissues“, *PLoS ONE*, vol. 9, no. 10, R. Oshima, Ed., e109688, 2014.
- [247] S. Eggert and D. W. Huttmacher, „In vitro disease models 4.0 via automation and high-throughput processing“, *Biofabrication*, vol. 11, no. 4, 2019.
- [248] D. E. Godar, „3D Bioprinting: Surviving under Pressure“, *Tissue Regeneration*, 2018.
- [249] D. Grijalva Garces, C. P. Radtke, and J. Hubbuch, „A Novel Approach for the Manufacturing of Gelatin-Methacryloyl“, *Polymers*, vol. 14, no. 24, p. 5424, 2022.
- [250] A. F. Habeeb, „Determination of free amino groups in proteins by trinitrobenzenesulfonic acid“, *Analytical Biochemistry*, vol. 14, no. 3, pp. 328–336, 1966.
- [251] H. Münstedt and F. R. Schwarzl, *Deformation and Flow of Polymeric Materials*. Berlin, Heidelberg: Springer Berlin Heidelberg, 2014.
- [252] J. H. Chung *et al.*, „Bio-ink properties and printability for extrusion printing living cells“, *Biomaterials Science*, vol. 1, no. 7, pp. 763–773, 2013.
- [253] L. Wenger, S. Strauß, and J. Hubbuch, „Bioprinting Automated and dynamic extrusion pressure adjustment based on real-time flow rate measurements for precise ink dispensing in 3D bioprinting“, *Bioprinting*, vol. 28, no. July, pp. 1–14, 2022.
- [254] D. L. Cohen, W. Lo, A. Tsavaris, D. Peng, H. Lipson, and L. J. Bonassar, „Increased Mixing Improves Hydrogel Homogeneity and Quality of Three-Dimensional Printed Constructs“, *Tissue Engineering Part C: Methods*, vol. 17, no. 2, pp. 239–248, 2011.
- [255] Y. He, F. Yang, H. Zhao, Q. Gao, B. Xia, and J. Fu, „Research on the printability of hydrogels in 3D bioprinting“, *Scientific Reports*, vol. 6, pp. 1–13, 2016.

- [256] S. Naghieh, M. Sarker, N. K. Sharma, Z. Barhoumi, and X. Chen, „Printability of 3D Printed Hydrogel Scaffolds: Influence of Hydrogel Composition and Printing Parameters“, *Applied Sciences*, vol. 10, no. 1, p. 292, 2019.
- [257] A. G. Tabriz, M. A. Hermida, N. R. Leslie, and W. Shu, „Three-dimensional bioprinting of complex cell laden alginate hydrogel structures“, *Biofabrication*, vol. 7, no. 4, p. 045 012, 2015.
- [258] K. Nair *et al.*, „Characterization of cell viability during bioprinting processes“, *Biotechnology Journal*, vol. 4, no. 8, pp. 1168–1177, 2009.
- [259] J. Snyder, A. Rin Son, Q. Hamid, C. Wang, Y. Lui, and W. Sun, „Mesenchymal stem cell printing and process regulated cell properties“, *Biofabrication*, vol. 7, no. 4, 2015.
- [260] J. Marzi *et al.*, „Non-Invasive Three-Dimensional Cell Analysis in Bioinks by Raman Imaging“, *ACS Applied Materials & Interfaces*, vol. 14, no. 27, pp. 30 455–30 465, 2022.
- [261] H. Park, S.-W. Kang, B.-S. Kim, D. J. Mooney, and K. Y. Lee, „Shear-reversibly Crosslinked Alginate Hydrogels for Tissue Engineering“, *Macromolecular Bioscience*, vol. 9, no. 9, pp. 895–901, 2009.
- [262] F. Hafezi *et al.*, „Bioprinting and preliminary testing of highly reproducible novel bioink for potential skin regeneration“, *Pharmaceutics*, vol. 12, no. 6, pp. 1–21, 2020.
- [263] W. Sun *et al.*, „The bioprinting roadmap“, *Biofabrication*, vol. 12, no. 2, 2020.
- [264] K. Tröndle *et al.*, „Scalable fabrication of renal spheroids and nephron-like tubules by bioprinting and controlled self-assembly of epithelial cells“, *Biofabrication*, vol. 13, no. 3, 2021.
- [265] B. Schmieg *et al.*, „Structured Data Storage for Data-Driven Process Optimisation in Bioprinting“, *Applied Sciences*, 2022.
- [266] P. Bartolo, A. Malshe, E. Ferraris, and B. Koc, „3D bioprinting: Materials, processes, and applications“, *CIRP Annals*, vol. 71, no. 2, pp. 577–597, 2022.
- [267] J. Chrenek, R. Kirsch, K. Scheck, and S. M. Willerth, „Protocol for printing 3D neural tissues using the BIO X equipped with a pneumatic printhead“, *STAR Protocols*, vol. 3, no. 2, p. 101 348, 2022.
- [268] S. Strauß, D. Grijalva Garces, and J. Hubbuch, „Analytics in Extrusion-Based Bioprinting: Standardized Methods Improving Quantification and Comparability of the Performance of Bioinks“, *Polymers*, vol. 15, no. 8, p. 1829, 2023.
- [269] F. P. Melchels, W. J. Dhert, D. W. Hutmacher, and J. Malda, „Development and characterisation of a new bioink for additive tissue manufacturing“, *Journal of Materials Chemistry B*, vol. 2, no. 16, pp. 2282–2289, 2014.
- [270] L. Ouyang, R. Yao, Y. Zhao, and W. Sun, „Effect of bioink properties on printability and cell viability for 3D bioplotting of embryonic stem cells“, *Biofabrication*, vol. 8, no. 3, p. 035 020, 2016.
- [271] E. Karakaya, L. Fischer, J. Hazur, A. R. Boccaccini, I. Thievensen, and R. Detsch, „Strategies to evaluate alginate based bioinks applying extrusion printing for biofabrication“, *Transactions on Additive Manufacturing Meets Medicine*, vol. 2, no. 1, pp. 1–2, 2020.

- [272] J. M. Rodríguez-Rego, L. Mendoza-Cerezo, A. Macías-García, J. P. Carrasco-Amador, and A. C. Marcos-Romero, „Methodology for characterizing the printability of hydrogels“, *International Journal of Bioprinting*, vol. 9, no. 2, pp. 280–291, 2023.
- [273] A. Schwab, R. Levato, M. D’Este, S. Piluso, D. Eglin, and J. Malda, „Printability and Shape Fidelity of Bioinks in 3D Bioprinting“, *Chemical Reviews*, vol. 120, no. 19, pp. 11 028–11 055, 2020.
- [274] T. Kreller, T. Distler, S. Heid, S. Gerth, R. Detsch, and A. Boccaccini, „Physico-chemical modification of gelatine for the improvement of 3D printability of oxidized alginate-gelatine hydrogels towards cartilage tissue engineering“, *Materials & Design*, vol. 208, p. 109 877, 2021.
- [275] V. Bednarzig, S. Schrüfer, T. C. Schneider, D. W. Schubert, R. Detsch, and A. R. Boccaccini, „Improved 3D Printing and Cell Biology Characterization of Inorganic-Filler Containing Alginate-Based Composites for Bone Regeneration: Particle Shape and Effective Surface Area Are the Dominant Factors for Printing Performance“, *International Journal of Molecular Sciences*, vol. 23, no. 9, p. 4750, 2022.
- [276] E. Karakaya *et al.*, „How to Determine a Suitable Alginate for Biofabrication Approaches using an Extensive Alginate Library?“, *Biomacromolecules*, 2023.
- [277] A. Wenz, K. Borchers, G. E. Tovar, and P. J. Kluger, „Bone matrix production in hydroxyapatite-modified hydrogels suitable for bone bioprinting“, *Biofabrication*, vol. 9, no. 4, 2017.
- [278] N. Brandt *et al.*, „Kadi4Mat: A Research Data Infrastructure for Materials Science“, *Data Science Journal*, vol. 20, no. 1, pp. 1–14, 2021.
- [279] S. van der Walt *et al.*, „scikit-image: image processing in Python“, *PeerJ*, vol. 2, no. 1, e453, 2014.
- [280] K. He, J. Sun, and X. Tang, „Guided image filtering“, *IEEE Transactions on Pattern Analysis and Machine Intelligence*, vol. 35, no. 6, pp. 1397–1409, 2013.
- [281] P. F. Alcantarilla, A. Bartoli, and A. J. Davison, „KAZE Features“, in *Computer Vision – ECCV 2011*, Berlin, Heidelberg: Springer Berlin Heidelberg, 2012, pp. 214–227.
- [282] A. F. Frangi, W. J. Niessen, K. L. Vincken, and M. A. Viergever, „Multiscale vessel enhancement filtering“, in *Medical Image Computing and Computer-Assisted Intervention — MICCAI’98*, Berlin, Heidelberg: Springer Berlin Heidelberg, 1998, pp. 130–137.
- [283] Y. Tsin and T. Kanade, „A Correlation-Based Approach to Robust Point Set Registration“, in *Computer Vision - ECCV 2004*, Berlin, Heidelberg: Springer Berlin Heidelberg, 2004, pp. 558–569.
- [284] A. A. Armstrong, A. G. Alleyne, and A. J. Wagoner Johnson, „1D and 2D error assessment and correction for extrusion-based bioprinting using process sensing and control strategies“, *Biofabrication*, vol. 12, no. 4, 2020.
- [285] M. Kesti, P. Fisch, M. Pensalfini, E. Mazza, and M. Zenobi-Wong, „Guidelines for standardization of bioprinting: A systematic study of process parameters and their effect on bioprinted structures“, *BioNanoMaterials*, vol. 17, no. 3-4, pp. 193–204, 2016.
- [286] M. Djabourov, J. Leblond, and P. Papon, „Gelation of aqueous gelatin solutions. I. Structural investigation“, *Journal de Physique*, vol. 49, no. 2, pp. 319–332, 1988.

- [287] Y. Maki and M. Annaka, „Gelation of fish gelatin studied by multi-particle tracking method“, *Food Hydrocolloids*, vol. 101, no. October 2019, p. 105 525, 2020.
- [288] E. Hoch, T. Hirth, G. E. Tovar, and K. Borchers, „Chemical tailoring of gelatin to adjust its chemical and physical properties for functional bioprinting“, *Journal of Materials Chemistry B*, vol. 1, no. 41, pp. 5675–5685, 2013.
- [289] I. Pepelanova, K. Kruppa, T. Scheper, and A. Lavrentieva, „Gelatin-Methacryloyl (GelMA) Hydrogels with Defined Degree of Functionalization as a Versatile Toolkit for 3D Cell Culture and Extrusion Bioprinting“, *Bioengineering*, vol. 5, no. 3, p. 55, 2018.

List of Figures

1.1	Different manufacturing techniques in bioprinting.	5
1.2	Typical flow curves of fluids showing shear stress as a function of shear rate.	9
3.1	Overview of the data and image processing for line analysis.	37
3.2	Schematic process of the shrinkage study.	38
3.3	Results of printed Nivea® lines.	39
3.4	Results of printed lines directly after printing.	41
3.5	Results of shrinkage study employing Cellink® Bioink.	43
3.6	Results of shrinkage study employing Biogelx™-ink-RGD.	44
4.1	Hierarchical overview the experiment design for evaluation of the reproducibility.	54
4.2	Incorporation setups for the flow sensor.	56
4.3	Illustration of the sensor's thermal based measuring principle.	57
4.4	Results of the sensor accuracy for alginate and Kolliphor.	61
4.5	Results of filling level influence investigation for Kolliphor based inks.	62
4.6	Results of filling level influence investigation for alginate based inks.	64
4.7	Results of the reproducibility tests.	66
4.8	Results of reproducibility tests shown in boxplots.	68
5.1	Schematic of the workflow applied in the study.	79
5.2	Schematic representation of the thermal measuring principle of the liquid flow meter, 3D visualization of the arrangement of the hardware components of the PID control setup, printer cartridge filled with alternating layers of P30 and P25 and dispensing tips used in the study.	81
5.3	Schematic of the interactions between the components of the PID control setup.	82
5.4	Screenshot of the graphical user interface of the Python-based PID control tool.	83
5.5	Schematic block diagram of the employed PID feedback loop showing the interaction between printer, flow sensor and PID controller.	84
5.6	Shear stress-controlled oscillatory measurements showing the storage modulus G' and loss modulus G'' for all prepared inks.	87
5.7	Yield stress, as determined from rotational measurements, and loss factor $\tan \delta$, as determined from oscillatory measurements, for all evaluated inks.	88
5.8	Continuous dispensing runs of P30.	89

5.9	Overview of all performed continuous dispensing runs depicted as swarm plots.	91
5.10	Initial phase of hollow cylinder printing with an inhomogeneous ink.	92
5.11	Printing of hollow cylinders with an inhomogeneous ink.	93
5.12	Hollow cylinders printed with different inks and nozzles.	95
6.1	Representation of the process for object recognition.	109
6.2	Schematic of the workflow for the investigation of processing effects on cell viability. . .	111
6.3	Viscosities of biomaterial inks.	112
6.4	Results of printing accuracy for the line structure.	114
6.5	Exemplary raw images.	114
6.6	Results of printing accuracy for the circle structure.	115
6.7	Results of printing accuracy for the angle structure.	116
6.8	Results of cell viability investigation.	119
7.1	Workflow design of the round robin test.	130
7.2	Scheme of the experimental design of the Round robin - 3D printing.	132
7.3	Depiction of occurring deviations.	138
7.4	Proportion of deviation of the total image data set.	139
7.5	Filament width of circle geometries determined by three IA groups.	141
7.6	Line and circle width compared by extrusion mechanism.	143
7.7	Line and circle width in dependence on coordinate calibration.	145
7.8	Line and circle width in dependence on temperature control.	147
E.1	Calibration curves of all inks employed in the present study.	196
E.2	Photograph of the employed experimental setup while printing a hydrogel cylinder. . . .	197
E.3	Continuous dispensing runs of P25.	198
E.4	Continuous dispensing runs of A2L7.	199
G.1	Designed models used during the Round robin - 3D printing test.	203
G.2	Schematic draft of line and circle width.	203
G.3	Exemplary raw images of each printed geometry and bioink.	204

List of Tables

3.1	Printing parameters of materials for investigating line analysis tool.	36
3.2	Results of the line detection feasibility study.	40
4.1	Printing parameters for sensor accuracy testing.	58
4.2	Overview of all experiments carried out for investigating the influence of cartridge filling level.	58
4.3	Set pressures applied during filling level investigations.	59
4.4	Overview of setups for reproducibility experiments.	59
4.5	Printing parameters for the investigation of reproducibility.	59
4.6	Boxplot key figures of Kolliphor.	69
4.7	Boxplot key figures of alginate.	69
5.1	Ink compositions with the corresponding extrusion pressure, as employed for printing runs with a constant pressure setting.	80
5.2	Proportional, integral and derivative gain, as applied for all experiments involving the PID control for automatic pressure adjustment.	84
6.1	Composition of biomaterial inks.	106
6.2	Representation of the printed objects with respective parameters that have been determined.	108
7.1	Overview of bioprinters used with the respective equipment.	133
7.2	Overview of materials with respective printing parameters.	134
7.3	Coefficients of variation (CV) for each laboratory regarding line and circle widths for different extrusion mechanisms.	143
7.4	Coefficients of variation (CV) for each laboratory regarding line and circle widths for coordinate calibration.	145
7.5	Coefficients of variation (CV) for each laboratory regarding line and circle widths for different temperature controls.	147
C.1	Comparison of original images with the detected objects of 3D-printed lines.	186
D.1	Results of the density calibration for sodium alginate and Kolliphor.	190
D.2	Results of the flow sensor SLI-1000 FMK calibration.	190

Abbreviations

Acronym	Meaning
2D	two-dimensional
3D	three-dimensional
AM	additive manufacturing
ANOVA	analysis of variance
CAD	computer aided design
CAM	calcein-acetoxymethyl ester
cFR	constant flow rate
CLIP	continuous liquid interface production
CSR	controlled shear rate
CSS	controlled shear stress
cP	constant pressure
DLP	digital light processing
DMA	dynamic mechanical analysis
DNA	deoxyribonucleic acid
DoF	degree of functionalization
EBB	extrusion-based bioprinting
EBM	electron beam melting
ECM	extracellular matrix
ELN	electronic laboratory notebook
FDA	Food and drug administration
FDM	fused deposit modeling
FSC	forward scatter
G	α -L-gulonate
GelMA	gelatine-methacrylate
GRAS	generally recognized as safe
GUI	graphical user interface
IA	image analysis

Continued on next page

Development of standardization strategies

Acronym	Meaning
LAP	lithium-phenyl-2,4,6-trimethylbenzoylphosphinate
LIFT	laser-induced forward transfer
LOM	laminated object manufacturing
LVE	linear viscoelastic
M	β -D-mannuronate
MA	methacrylic anhydride
NIH	National Institute of Health
PAT	process analytical technology
PEG	poly(ethylene glycol)
PEO	poly(ethylene oxide)
PI	propidium iodide
PID	proportional-integral-derivative
PLA	polylactid acid
PMT	photomultiplier
PPO	poly(propylene oxide)
RGD	arginine-glycine-aspartic acid
RP	Rapid prototyping
RM	regenerative medicine
SLA	stereolithography apparatus
SLS	selective laser sintering
SOP	standard operating procedure
SSC	side scatter
STL	standard triangle language or standard tessellation language
TE	tissue engineering
UV	ultraviolet light

Symbols

Symbol	Meaning
$\dot{\gamma}$	shear rate
E	modulus of elasticity
ϵ	elongation
η	viscosity
G'	storage modulus
G''	loss modulus
K	consistency index
l	length
n	power law exponent
p	pressure
\dot{Q}	flow rate
R	radius
ρ	density
τ	shear stress
ω	angular velocity
V	volume
\bar{v}	mean velocity



Appendix Chapter 3

Image Analysis as PAT-Tool for Use in Extrusion-Based Bioprinting





Svenja Strauß¹, Rafaela Meutelet¹, Luka Radosevic¹, Sarah Gretzinger^{1,2} and Jürgen Hubbuch^{1,2}

¹ Institute of Engineering in Life Sciences, Section IV: Biomolecular Separation Engineering, Karlsruhe Institute of Technology (KIT), Karlsruhe, Germany





² Institute of Functional Interfaces, Karlsruhe Institute of Technology (KIT), Eggenstein-Leopoldshafen, Germany

C.1

Table C.1 Comparison of original images with the detected objects of 3D-printed lines using different materials. Images were generated using the microplate reader Spark[®] from Tecan Group AG (Männedorf, Switzerland) and each well was measured using the cell confluence method. Afterwards, images were imported into Matlab and have been analyzed automated by the line analysis tool via image processing. On the left side is the original image and on the right side the isolated, detected object.

Material	Example for original image and detected object	
Nivea		
Pure Kolliphor solution		

Kolliphor with food coloring powder		
Kolliphor with food coloring paste		
Kolliphor with Cochineal Red		

Cellink Bioink	 A dark, rectangular micrograph showing a single, smooth filament of Cellink Bioink. The filament is uniform in thickness and has a slightly irregular, natural-looking edge.	 A bright, rectangular micrograph showing a single filament of Cellink Bioink. The filament is very uniform in thickness and has a very smooth, consistent edge.
Biogelx-ink-RGD	 A dark, rectangular micrograph showing a single filament of Biogelx-ink-RGD. The filament is uniform in thickness and has a slightly irregular, natural-looking edge.	 A bright, rectangular micrograph showing a single filament of Biogelx-ink-RGD. The filament is very uniform in thickness and has a very smooth, consistent edge.

D

Appendix Chapter 4

Evaluation of the Reproducibility and Robustness of Extrusion-based Bioprinting Processes applying a Flow Sensor

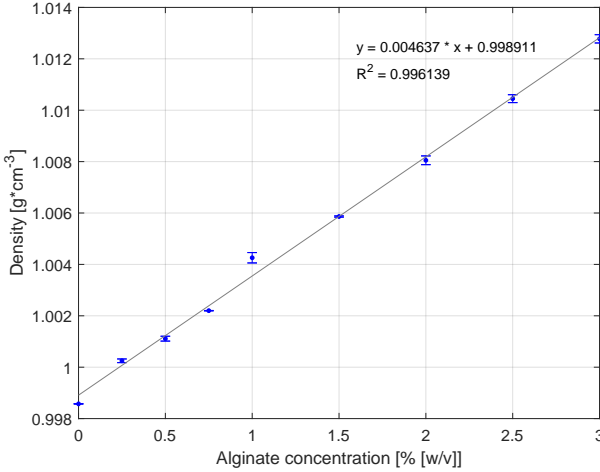
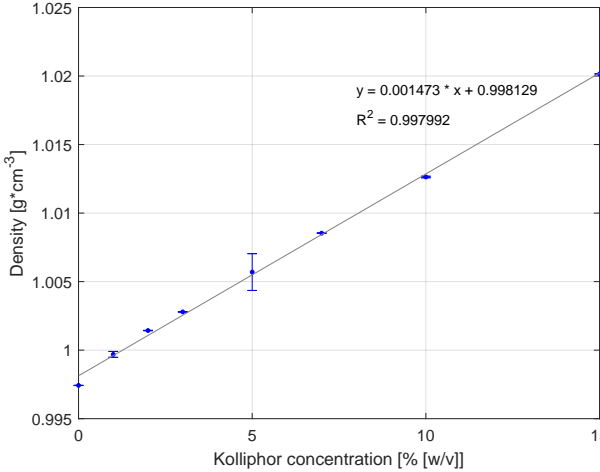
Svenja Strauß¹, Bianca Schroth¹, and Jürgen Hubbuch^{1,2}

¹ Institute of Process Engineering in Life Sciences, Section IV: Biomolecular Separation Engineering, Karlsruhe Institute of Technology (KIT), Karlsruhe, Germany

² Institute of Functional Interfaces, Karlsruhe Institute of Technology (KIT), Eggenstein-Leopoldshafen, Germany

D.1 Density calibration curves

Table D.1 Results of the density calibration for sodium alginate and Kolliphor using a micro liquid density sensor. For sodium alginate the concentrations of 0.25, 0.5, 0.75, 1, 1.5, 2, 2.5, 3 % (w/v) and Kolliphor concentrations of 1, 2, 3, 5, 10, 15 % (w/v) were measured in triplicate.

Hydrogel	Density calibration graph
Sodium alginate	 <p>Density calibration graph for Sodium alginate. The y-axis represents Density [g*cm⁻³] and the x-axis represents Alginate concentration [% w/v]. The regression equation is $y = 0.004637 \cdot x + 0.998911$ and the coefficient of determination is $R^2 = 0.996139$.</p>
Kolliphor P 407	 <p>Density calibration graph for Kolliphor P 407. The y-axis represents Density [g*cm⁻³] and the x-axis represents Kolliphor concentration [% w/v]. The regression equation is $y = 0.001473 \cdot x + 0.998129$ and the coefficient of determination is $R^2 = 0.997992$.</p>

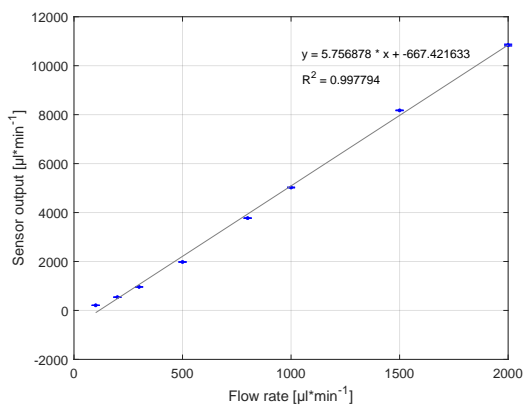
D.2 Flow sensor calibration curves

Table D.2 Results of the flow sensor SLI-1000 FMK calibration for alginate concentrations of 8, 10, 12 and 15 % (w/v) and for Kolliphor concentrations of 15, 20, 25, 28 and 30 % (w/v). The flow sensor was connected via luer lock to a syringe pump and each flow rate was measured in triplicate.

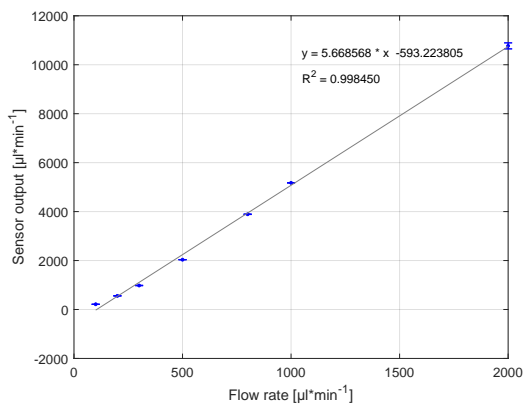
Hydrogel and concentration

Flow sensor SLI-1000 FMK calibration graph

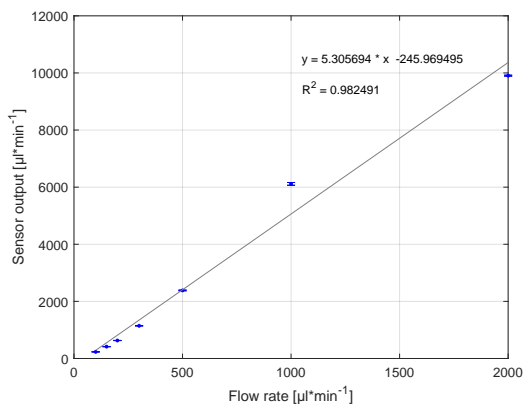
8 % (w/v) sodium alginate



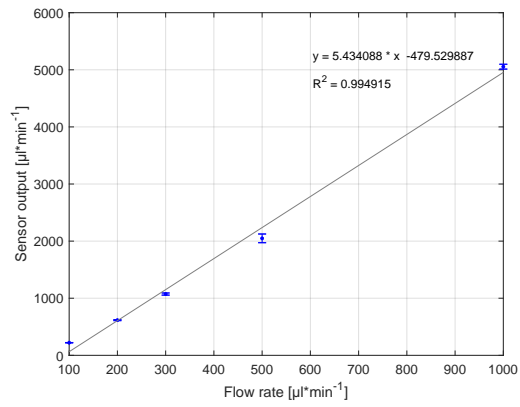
10 % (w/v) sodium alginate



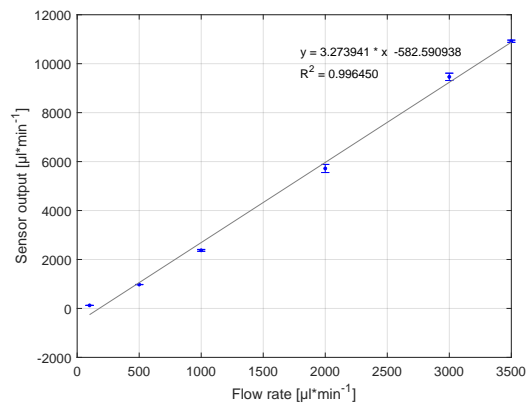
12 % (w/v) sodium alginate



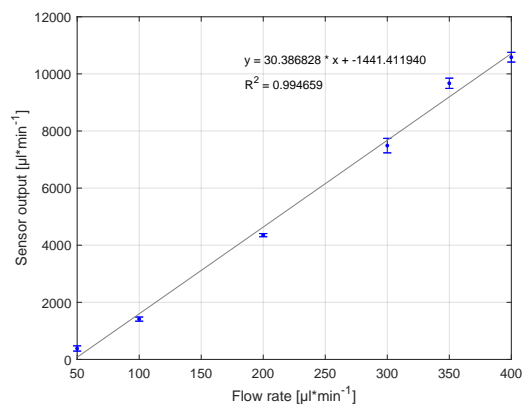
15% (w/v) sodium alginate



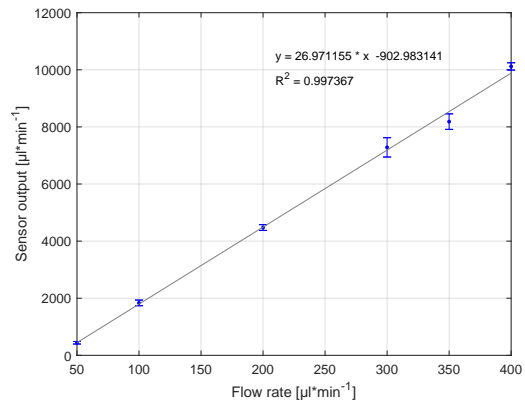
15% (w/v) kolliphor P 407



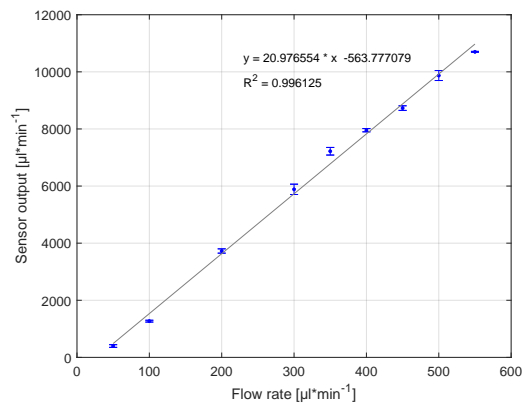
20% (w/v) kolliphor P 407



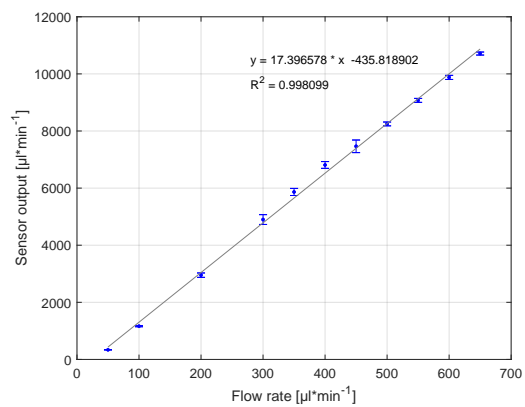
25 % (w/v) kolliphor P 407



28 % (w/v) kolliphor P 407



30 % (w/v) kolliphor P 407





Appendix Chapter 5
Automated and Dynamic Extrusion Pressure Adjustment
Based on Real-Time Flow Rate Measurements for Precise
Ink Dispensing in 3D Bioprinting

Lukas Wenger^{1*}, Svenja Strauß^{2*} and Jürgen Hubbuch^{1,2}

¹ Institute of Process Engineering in Life Sciences, Section IV: Biomolecular Separation Engineering, Karlsruhe Institute of Technology (KIT), Karlsruhe, Germany

² Institute of Functional Interfaces, Karlsruhe Institute of Technology (KIT), Eggenstein-Leopoldshafen, Germany

* Contributed equally

E.1 Sensor calibration curves

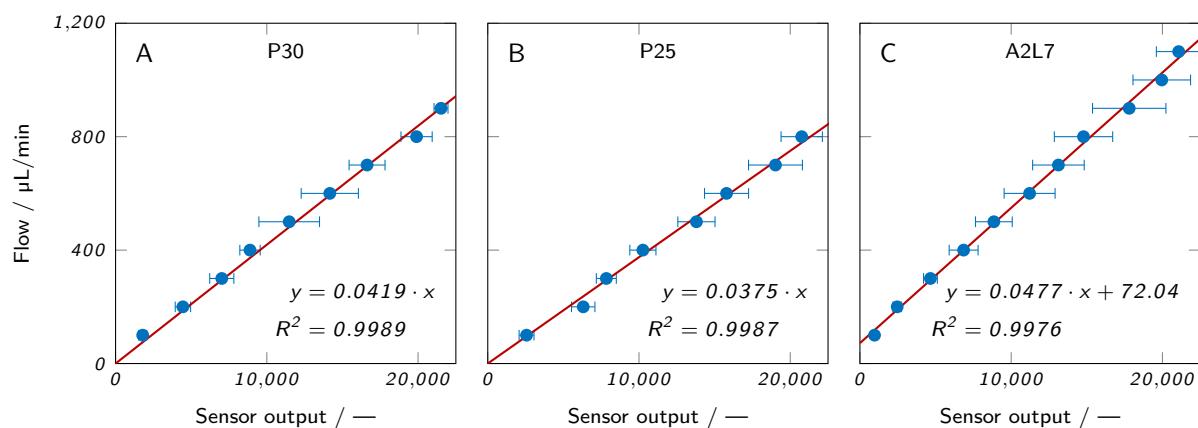


Figure E.1 Calibration curves of all inks employed in the present study. The calibration data was stored in an Excel file and imported by the Python-based software tool to convert sensor output data to flow rate values.

E.2 Experimental setup

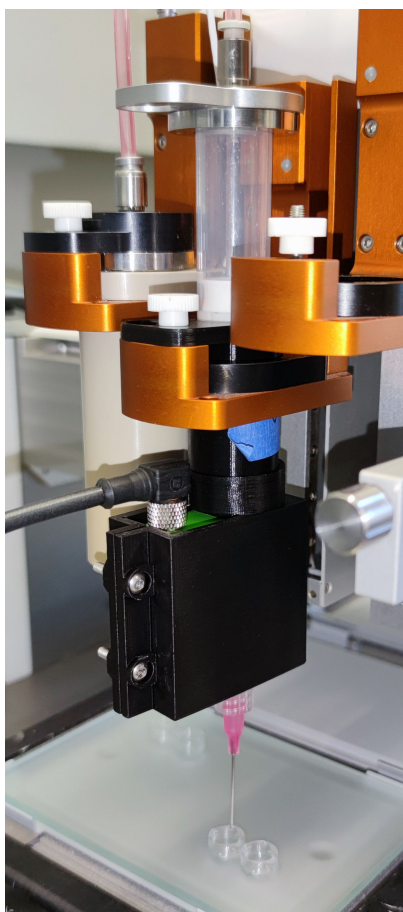


Figure E.2 Photograph of the employed experimental setup while printing a hollow hydrogel cylinder.

E.3 Continuous dispensing P25

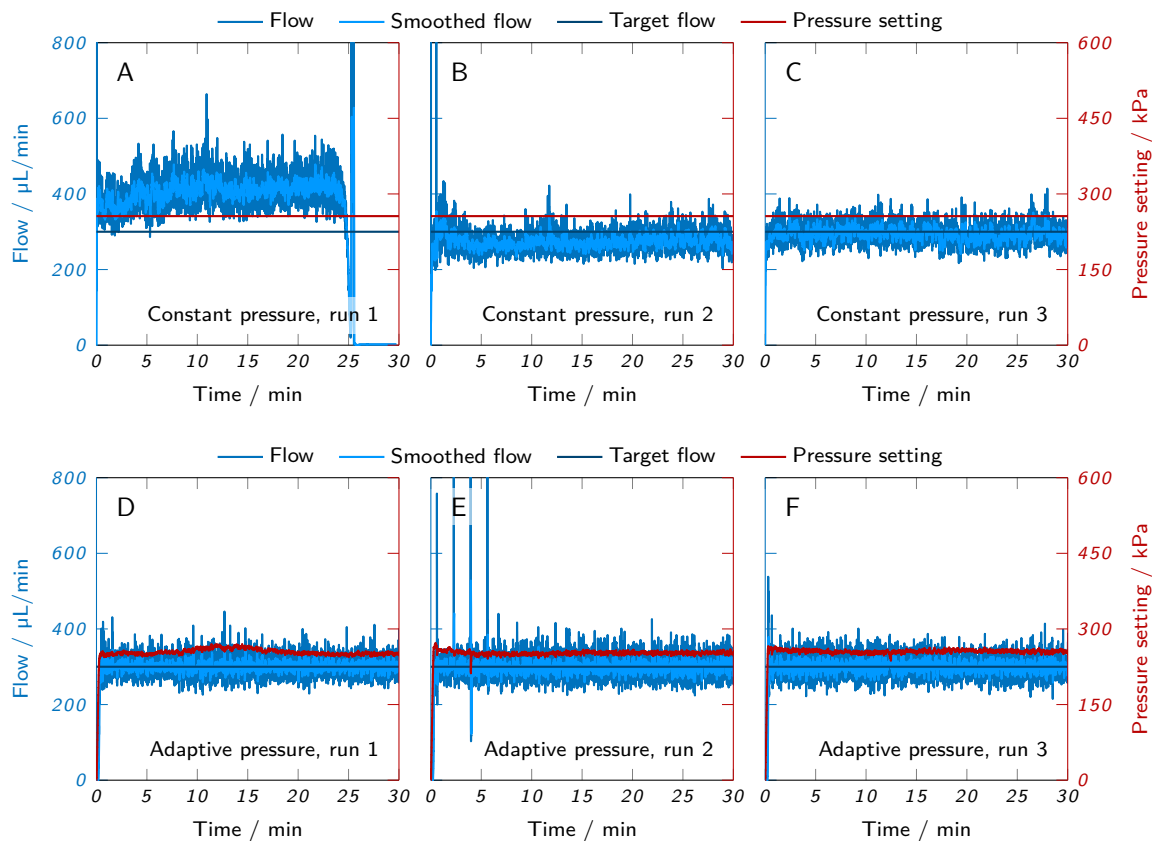


Figure E.3 Continuous dispensing runs of P25. The measured flow and the pressure setting are plotted over time. (A-C) Runs with constant pressure setting are compared to (D-F) runs with adaptive PID pressure control and a target flow rate of 300 $\mu\text{L}/\text{min}$.

E.4 Continuous dispensing A2L7

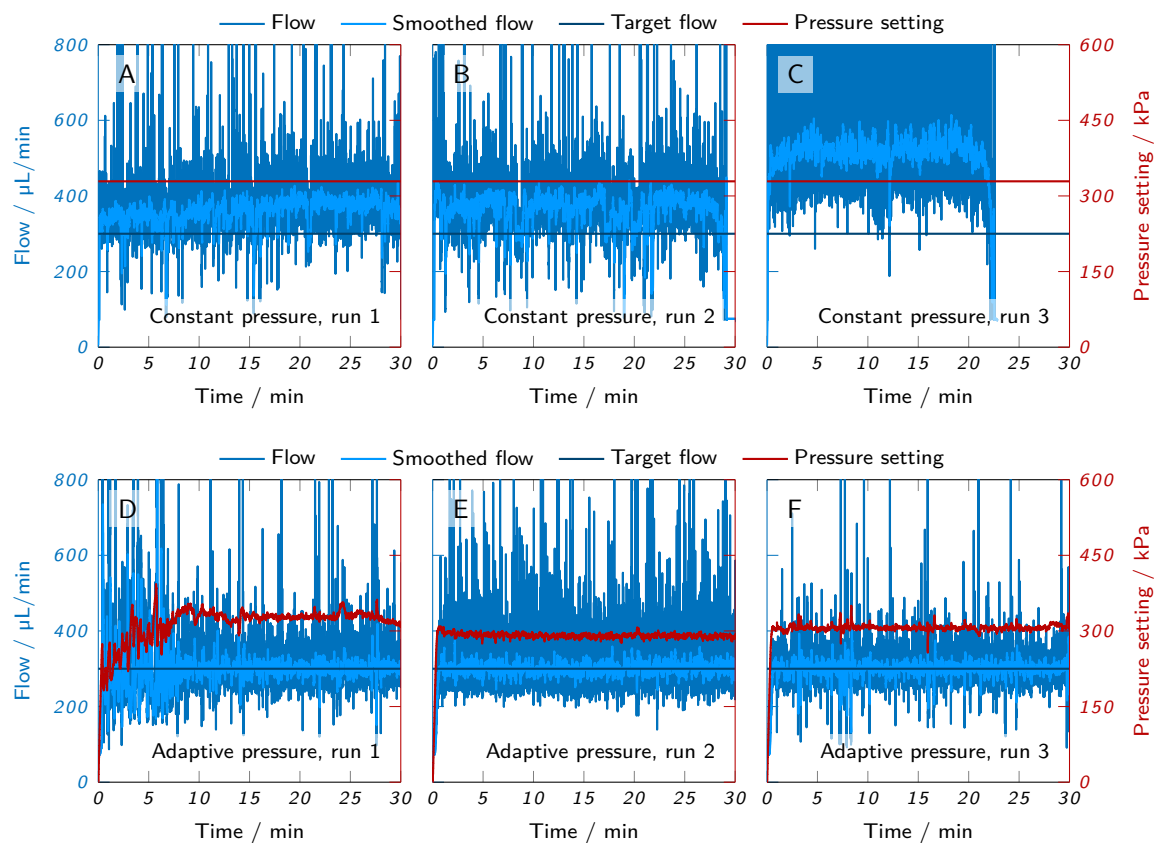


Figure E.4 Continuous dispensing runs of A2L7. The measured flow and the pressure setting are plotted over time. (A-C) Runs with constant pressure setting are compared to (D-F) runs with adaptive PID pressure control and a target flow rate of 300 $\mu\text{L}/\text{min}$.



Appendix Chapter 7

On the Reproducibility of extrusion-based Bioprinting: Round Robin Study on Standardization in the Field

David Grijalva^{1,2*}, Svenja Strauß Garces^{1,2*}, Sarah Gretzinger^{1,2}, Barbara Schmiege^{1,2}, Tomasz Jüngst^{3,4}, Jürgen Groll^{3,4}, Lorenz Meinel⁵, Isabelle Schmidt⁶, Hanna Hartmann⁶, Katja Schenke-Layland^{6,7}, Nico Brandt⁸, Michael Selzer⁹, Stefan Zimmermann¹⁰, Peter Koltay¹⁰, Alexander Southan^{11,12}, Günter E. M. Tovar^{11,12}, Sarah Schmidt¹², Achim Weber¹², Tilman Ahlfeld¹³, Michael Gelinsky¹³, Thomas Scheibel^{14,4}, Rainer Detsch¹⁵, Aldo R. Boccaccini¹⁵, Toufik Naolou¹⁶, Cornelia Lee-Thedieck¹⁶, Christian Willems^{17, 17}, Stephan Allgeier¹⁸, Bernd Köhler¹⁸, Tiaan Friedrich¹⁹, Heiko Briesen¹⁹, Janine Buchholz²⁰, Dietrich Paulus²⁰, Anselm von Gladiss²⁰, and Jürgen Hubbuch^{1,2}

- ¹ Institute of Functional Interfaces, Karlsruhe Institute of Technology (KIT), Eggenstein-Leopoldshafen, Germany
- ² Institute of Process Engineering in Life Sciences, Section IV: Biomolecular Separation Engineering, Karlsruhe Institute of Technology (KIT), Karlsruhe, Germany
- ³ Department for Functional Materials in Medicine and Dentistry, Institute of Functional Materials and Biofabrication, University of Würzburg, Würzburg, Germany
- ⁴ Bavarian Polymer Institute, University of Bayreuth, Bayreuth, Germany
- ⁵ Institute of Pharmacy and Food Chemistry, University of Würzburg, Würzburg, Germany
- ⁶ NMI Natural and Medical Sciences Institute at the University of Tübingen, Reutlingen, Germany
- ⁷ Institute of Biomedical Engineering, Department for Medical Technologies and Regenerative Medicine, Eberhard Karls University of Tübingen, Tübingen, Germany
- ⁸ Institute for Applied Materials, Karlsruhe Institute of Technology, Karlsruhe, Germany
- ⁹ Institute for Nanotechnology, Karlsruhe Institute of Technology, Karlsruhe, Germany
- ¹⁰ Laboratory for MEMS Applications, Department of Microsystems Engineering, University of Freiburg, Freiburg, Germany
- ¹¹ Institute of Interfacial Process Engineering and Plasma Technology, University of Stuttgart, Stuttgart, Germany
- ¹² Functional Surfaces and Materials, Fraunhofer Institute for Interfacial Engineering and Biotechnology, Stuttgart, Germany
- ¹³ Center for Translational Bone, Joint, and Soft Tissue Research, Faculty of Medicine, Technische Universität Dresden, Dresden, Germany
- ¹⁴ Chair of Biomaterials, University of Bayreuth, Bayreuth, Germany
- ¹⁵ Institute of Biomaterials, Friedrich-Alexander University Erlangen-Nuremberg, Erlangen, Germany
- ¹⁶ Institute of Cell Biology and Biophysics, Leibniz University Hannover, Hannover, Germany
- ¹⁷ Department Biomedical Materials, Martin Luther University Halle-Wittenberg, Halle (Saale), Germany
- ¹⁸ Institute for Automation and Applied Informatics, Karlsruhe Institute of Technology, Eggenstein-Leopoldshafen, Germany
- ¹⁹ Process Systems Engineering, School of Life Sciences, Technical University of Munich, Freising, Germany
- ²⁰ Institute for Computational Visualistics, Active Vision Group, University of Koblenz, Koblenz, Germany
- * Contributed equally

G.1 CAD models used during the Round robin - 3D printing test

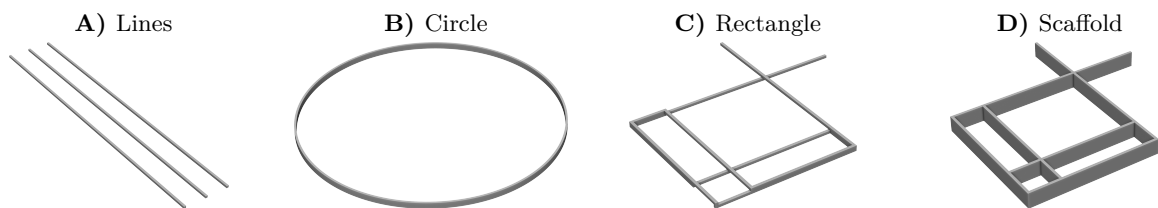


Figure G.1 Designed models used during the Round robin - 3D printing test. A) single layer line, B) single layer circle, C) two layer rectangle geometries, and D) scaffold which equaled the rectangle geometry with several printed layers.

G.2 Schematic draft of line and circle width

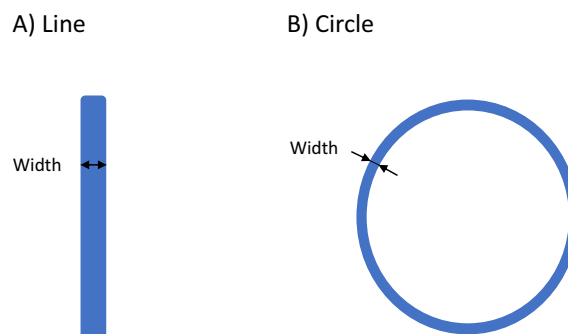


Figure G.2 Schematic draft of features describing the geometries used in the results from the Round robin - Image analysis study, namely line width A) and circle width B).

G.3 Exemplary raw images

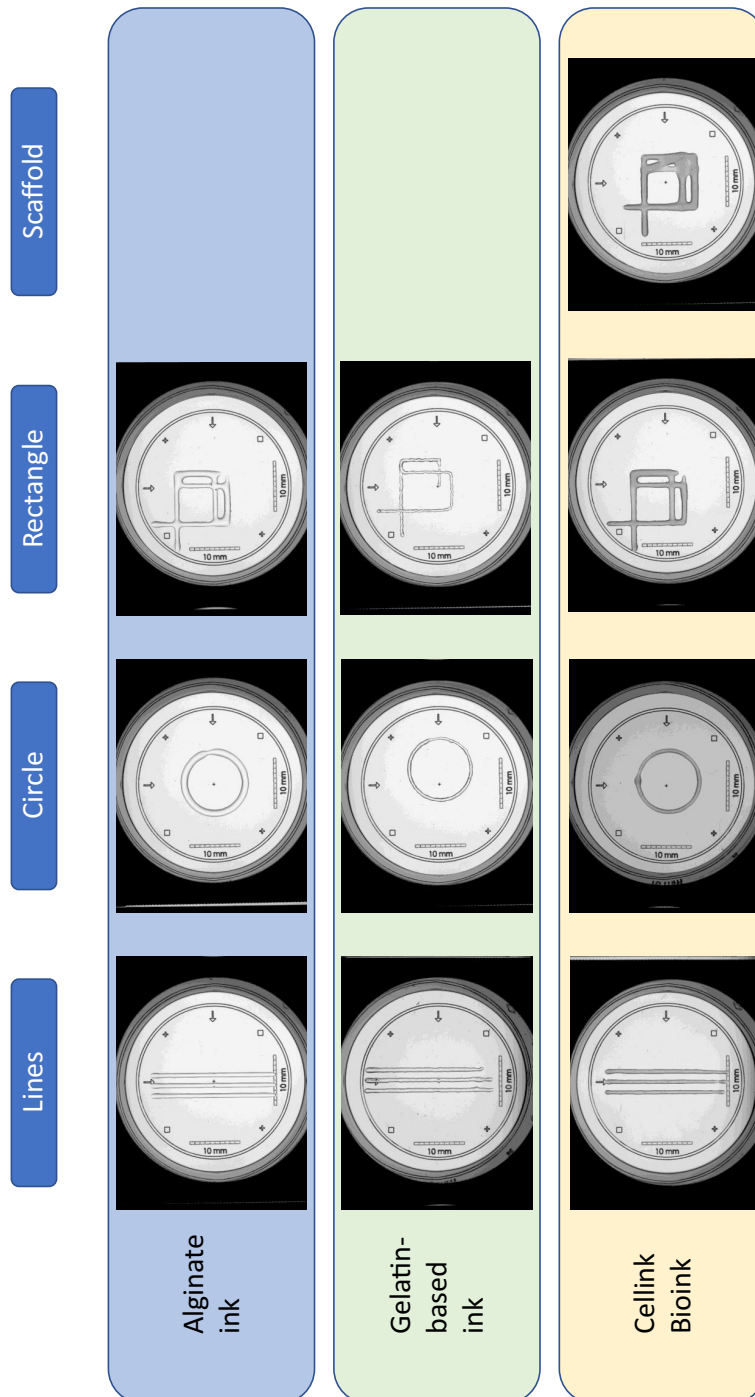


Figure G.3 Exemplary raw images of each printed geometry and bioink during the Round robin - 3D printing test. Scale bars left and below printed geometries: 10 mm